13/1/04

SPATIO-TEMPORAL ORGANIZATION OF CYTOSOLIC CA^{2+} SIGNALS

A modelling approach to the molecular mechanisms and physiological implications of Ca^{2+} oscillations and waves

Geneviève Dupont

Thèse présentée en vue de l'obtention du grade d'agrégé de l'enseignement supérieur de la Faculté des Sciences de l'Université Libre de Bruxelles

Janvier 2005

Acknowledgement

I first wish to thank Albert Goldbeter. I constantly enjoy my chance of working in his group. After having communicated to me his knowledge and enthusiasm for the modelling study of biological rhythms, he provides me a stimulating and nice environment to develop my own research interests.

I wish to express my special thanks to Philippe Champeil, Laurent Combettes and Stéphane Swillens. Our many years collaboration lie at the heart of this research. Through our never-ending discussions, I have discovered the fruitfulness and the invaluable pleasure of an interdisciplinary teamwork.

If this was allowed, this thesis would have many co-authors. Besides my colleagues mentioned above, I have indeed benefited from collaborations with Christophe Erneux, Rémi Dumollard, Thierry Tordjmann, Paul De Koninck, Gérald Houart, David Gall, Franck Borgese, José Borghans and Erika Baus. I wish to express here my gratitude to all of them. I am also especially thankful to Michael Berridge who has welcomed me in his laboratory in Cambridge. I have particularly appreciated the opportunity he gave me to do experiments as well as his always clear-cut advices.

Other people have enlightened or motivated my research work through informal discussions. I wish to thank more especially Martin Falcke, Ursula Kummer, Luc Leybaert, Jean-Pierre Ozil, Jan Parys, Christian Sardet and James Sneyd.

For discussions of all kinds, friendship and technical matters, I would like to thank the past and present members of the 'Service de Chimie Physique'. I am particularly grateful to Jean-Christophe Leloup, Didier Gonze, Gérald Houart and José Halloy.

My husband Benoît and my children, Isabelle, Vincent and Pierre often show a great patience and support for my work. For this, and much more, I would like to express them once again my thankfulness.

This work was financially supported by the Belgian 'Fonds National de la Recherche Scientifique'.

Contents

CHAPTER I

Introduction

I.1. Oscillations and waves of cytosolic Ca^{2+} : a prototypic example of self-organized system in cell biology.

The first observation of sustained oscillations of cytosolic Ca^{2+} in non-excitable cells has been performed about 20 yeas ago (Cuthbertson and Cobbold, 1985). Given the many roles of Ca^{2+} as an universal second messenger, this discovery has influenced a great number of concepts in the field of cellular physiology. Not only are these oscillations observed in nearly all cell types, but they often play a key role in vital phenomena such as, for example, fertilization or gene expression. Moreover, these repetitive Ca^{2+} spikes also possesses a well-defined spatial organization.

Cytosolic Ca^{2+} oscillations in fact provide one example of rhythmic phenomenon occurring in living systems. The latter's are present at all levels of biological organization and play a fundamental role in the maintenance of life (Goldbeter, 1996 ; Goldbeter, 2002). Many of them are very familiar to all of us, as for example the cardiac rhythm, the cell cycle, the circadian rhythms or the reproduction cycle. Although very widespread, rhythmic phenomena have long been observed without being really understood from a molecular point of view. A definitive step towards their understanding has been made with the discovery of dissipative structures, when Prigogine and Balescu (1956) showed that sustained oscillations can occur far from thermodynamic equilibrium in open systems governed by laws characterized by well-defined non-linear relations. Although not specifically aimed at understanding biological systems –rhythmic phenomena are indeed far from being restricted to living systems–, this discovery has shed a new light on many biological phenomena (Prigogine *et al.*, 1969) and, many years later, has certainly played a key role in the uncovering of the mechanism underlying Ca^{2+} oscillations.

Many biological oscillators rely on a specific type of non-linear regulation known as 'autocatalysis' : in this case, the stationary state is destabilized by a positive feedback exerted by one compound on its own production. Thus, glycolytic oscillations, observed in yeast and muscle cells for a given range of substrate injection rates, can be ascribed to a peculiarity of the phosphofructokinase (PFK) . This allosteric enzyme, which catalyses the transformation of fructose monophosphate and ATP into fructose bisphosphate and ADP, is indeed activated by its own product (Goldbeter and Lefever, 1972 ; Goldbeter and Nicolis ; 1976). In the same manner, the positive feedback exerted by cAMP on its own production is at the origin of the periodic generation of cAMP signals that control the aggregation of *Dictyostelium discoideum* amoebae after starvation (Goldbeter and Segel, 1977 ; Martiel and Goldbeter, 1987). In this latter case, as for Ca^{2+} dynamics, temporal and spatial organization are closely linked. When amoebae are placed on an solid support such as agar, they periodically move towards aggregation centres emitting cAMP pulses, thus creating a phenomenon of wave propagation. Cytosolic Ca^{2+} oscillations are also based on a positive feedback, namely the amplification of Ca^{2+} release from the internal Ca^{2+} stores (sarco- or endoplasmic reticulum) by cytosolic Ca^{2+} itself. This regulation is well known under the acronym 'CICR' for 'Ca^{2+}-induced Ca^{2+} release'. Interestingly, the existence of such a regulation was first predicted theoretically (Dupont and Goldbeter, 1989 ; Goldbeter *et al.*, 1990) before being confirmed experimentally (Bezprozvanny *et al.*, 1991 ; Finch *et al.*, 1991). As expected theoretically (Nicolis and Prigogine, 1977), Ca^{2+} waves can be ascribed to the same regulatory mechanisms as oscillations (Dupont and Goldbeter, 1992a).

Although it is now well established that CICR lies at the core of Ca^{2+} oscillations and waves, many other factors need to be taken into account to apprehend more detailed and cell-specific aspects of Ca^{2+} signalling. There is thus a real need for the elaboration of more sophisticated models. The latter's are however still adequately studied in the framework of dynamical systems (Goldbeter, 1996 ; Keener and Sneyd, 1998; Dupont *et al.*, 1999; 2003b; Schuster *et al.*, 2002).

I.2. Hierarchical organization of Ca^{2+} signals

The concentration of free Ca^{2+} in the cytosol is actively kept much lower (100-200 nM) than extracellular (1-2 mM) and intrareticular (0.5 mM) Ca^{2+} concentrations (Berridge, 1997). The cytosol, with its very low concentration of free calcium, is thus located at the interface between these 2 calcium-rich environments. This results in the cytosol being a site of major, rapid variations in Ca^{2+} concentration in response to the transfer of small quantities of Ca^{2+} from the extracellular medium or intracellular storage compartments. As we shall see here below, the detailed study of Ca^{2+} dynamics will lead us to consider dynamical events ranging from the sub-micron scale (elementary events) to centimetres (organ). It is interesting to remind here however that an organism like a human being possesses about 1300 g of Ca^{2+} , which are mainly localized in bones. Only a few grams of free Ca^{2+} are distributed in the extra- and intracellular media. Their regulation, which is the focus of so many studies, is however crucial for the proper functioning of all living organisms.

In non-excitable cells, cytosolic **Ca^{2+} oscillations** in response to hormonal stimuli were the first type of Ca^{2+} signal to be reported (Cuthbertson and Cobbold, 1985; Woods *et al.*, 1987). These oscillations result from a periodic exchange of Ca^{2+} between the cytosol and the internal stores (endoplasmic reticulum, ER or sarcoplasmic reticulum, SR). Their period ranges from less than one second to tens of minutes, depending on the cell type and on the dose of external agonist. The frequency of Ca^{2+} oscillations indeed always increases with the level of stimulation. This phenomenon, known as 'frequency-encoding of Ca^{2+} oscillations', plays a key role in many physiological processes (Berridge, 1997; Berridge *et al.*, 2000). Vital phenomena such as secretion, gene expression or neuronal differentiation (Berridge *et al.*, 1998) are thus regulated by the frequency rather than by the amplitude of Ca^{2+} oscillations. The link between Ca^{2+} oscillations and their physiological implications is also much investigated, both experimentally and with models. Although Ca^{2+} oscillations generally take the form of regular spikes, **complex Ca^{2+} oscillations** have also been observed (Dixon *et al.*, 1993; 1995). Such complex oscillations are reminiscent of the bursting-type behaviour displayed by electrically excitable cells.

Intracellular waves of Ca^{2+} often accompany Ca^{2+} oscillations (Berridge, 1993); in most cases, the Ca^{2+} concentration indeed first increases locally, and the increase then propagates in the whole cell as a wave, travelling at a speed of 10-50 μms^{-1} (Berridge and Dupont, 1995). The appearance of the Ca^{2+} waves much varies from one cell type to another. The front can be planar as in cardiac or smooth muscle cells, elliptical as in hepatocytes or in eggs, or even adopt a spiral shape as in immature *Xenopus* oocytes or in cardiac cells after overloading of the Ca^{2+} stores (see Jaffe, 1993 and Berridge and Dupont, 1995 for reviews). Moreover, in some cells, the front is very narrow as compared to the cell dimension, in which case several fronts can even be observed simultaneously. In other cells, the Ca^{2+} front is so large that it invades the whole cell before a homogeneous return to the basal level: such waves, observed for example in hepatocytes or in eggs at fertilization, are often referred to as 'Ca^{2+} tides' (see Dupont and Goldbeter, 1992a and McDougall and Sardet, 1995 for reviews).

Spatial propagation of the repetitive Ca^{2+} rises from cell to cell has also been observed as, for example, in the liver, in epithelia or in insect salivary glands (Sanderson *et al.*, 1994). The significance of such **intercellular Ca^{2+} waves** may be to optimize the physiological response at the organ level. In the brain, Ca^{2+} waves are even seen to propagate from one cell type to another, namely from glial cells to neurons (Nedergaard, 1994; Braet *et al.*, 2004).

Oscillations, intra- and intercellular waves all tightly depend on the subcellular properties of the Ca^{2+} releasing entities, namely the $InsP_3$-sensitive Ca^{2+} channels (see below). The arrangement of these channels on the surface of the ER appears to considerably affect the resulting Ca^{2+} signal. Advances in the Ca^{2+} imaging techniques have allowed the visualization of the Ca^{2+} increase caused by a single Ca^{2+} channel (a Ca^{2+} event known as a 'Ca^{2+} blip') or by a small group of channels (a Ca^{2+} event known as a 'Ca^{2+} puff'). These **elementary Ca^{2+} signals** (Parker *et al.*, 1996) of course involve much smaller time-

and space-scales than oscillations and waves. Moreover, given the small number of Ca^{2+}-releasing channels involved in their generation, their description requires a stochastic approach.

I.3. Regulatory mechanisms of cytoplasmic Ca^{2+} increases and related theoretical models

The mechanism of Ca^{2+} oscillations relies on the feedback processes that regulate Ca^{2+} levels within the cell. Upon binding to a specific membrane receptor, the external stimulus (hormone or neurotransmitter) triggers the synthesis of inositol 1,4,5-trisphosphate ($InsP_3$), which binds to the $InsP_3$ receptor ($InsP_3R$). This receptor, located on the membrane of the intracellular Ca^{2+} stores (endoplasmic or sarcoplasmic reticulum), behaves as a Ca^{2+} channel. Upon $InsP_3$ binding, Ca^{2+} is released from the stores into the cytosol (Fig. I.1). Moreover, as Ca^{2+} stimulates the activity of the $InsP_3$ receptor/channel, this release is progressively enhanced in a process known as $InsP_3$-sensitive Ca^{2+}-induced Ca^{2+} release (CICR). This self-activation process represents a key element in the instability mechanism that generates repetitive Ca^{2+} spiking.

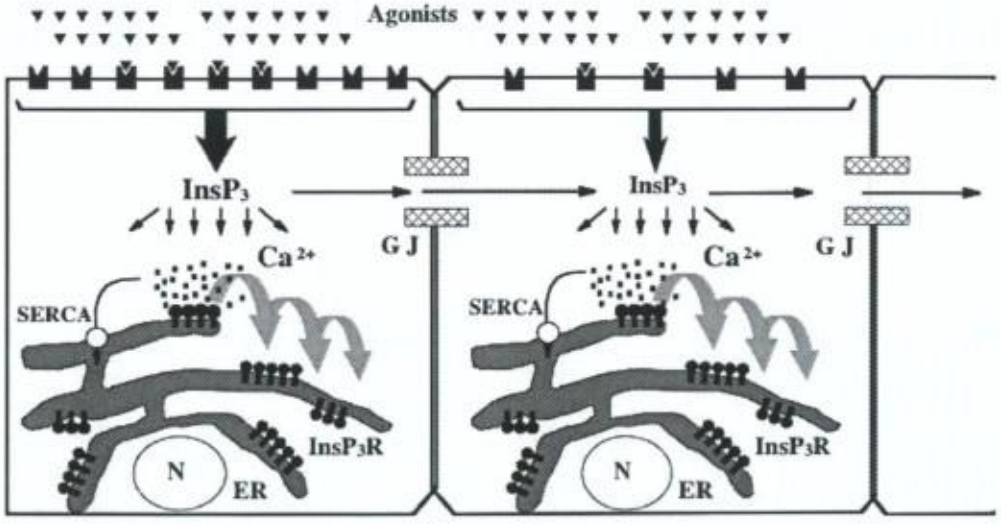

Fig. I.1. Schematic representation of the spatio-temporal organization of calcium signals in a group of connected cells: from Ca^{2+} blips to intercellular waves. The different levels of organization are discussed in section I.2. ER, endoplasmic reticulum; GJ, gap junctions; $InsP_3R$, $InsP_3$ receptor-Ca^{2+} channel; N, nucleus, SERCA, specific Ca^{2+} ATPases.

However, Ca^{2+} oscillations are regulated by a variety of other processes that could play an active role in the oscillatory mechanism itself or in the shaping of Ca^{2+} spikes. A non-exhaustive list of such Ca^{2+}-regulatory processes is given in Table I.1. On the basis of these regulatory processes, a variety of theoretical models have been developed to account for Ca^{2+} oscillations.

I.3.1. Ca^{2+}-induced Ca^{2+} release

This regulation, known as CICR, plays a primary role in the origin of Ca^{2+} oscillations (see above). Activation by cytosolic Ca^{2+} of the release of Ca^{2+} from the intracellular stores into the cytosol has first been proposed for the ryanodine receptor (RyR). This receptor, which shares many structural and functional similarities with the $InsP_3R$ (Berridge, 1993), is responsible for Ca^{2+} release in muscle and cardiac cells, as well as in neurons (Endo *et al.*, 1970; Fabiato and Fabiato, 1975; Kuba and Takeshita, 1981). Following its incorporation into theoretical models for $InsP_3$-induced Ca^{2+} oscillations (Goldbeter *et al.*, 1990; Dupont and Goldbeter, 1993), $InsP_3$-sensitive CICR has been experimentally demonstrated (Wakui *et al.*, 1990). A minimal model based on CICR (Goldbeter *et al.*, 1990; Dupont

and Goldbeter, 1993) qualitatively reproduces Ca^{2+} oscillations. The equations governing the minimal model are given in Table I.2. As shown in Fig. I.2, this model accounts for (1) the existence of a range of stimulation levels producing Ca^{2+} oscillations, (2) the rise in frequency with both the level of stimulation and the concentration of extracellular Ca^{2+}, and (3) the progressive rise in cytosolic Ca^{2+} preceding the onset of the Ca^{2+} spike (see, e.g. Jacob, 1990).

Ca^{2+} signalling: multiple regulatory mechanisms	
1.	Ca^{2+}-induced Ca^{2+} release
2.	PLC activation by Ca^{2+}
3.	Biphasic regulation of $InsP_3R$ by Ca^{2+}
4.	Capacitative Ca^{2+} entry
5.	$InsP_3$ 3-kinase activation by Ca^{2+}
6.	Mitochondrial control of Ca^{2+}
7.	G-protein regulation
8.	Phosphorylation of the $InsP_3R$

Table I.1: Main regulatory processes that bear on the origin and properties of Ca^{2+} oscillations (see text).

The CICR regulation, first established for type I $InsP_3Rs$ (Bezprozvanny and Ehrlich, 1994), extends to the other sub-types, although in different Ca^{2+} ranges. It is by now clear that this variety in CICR regulation contributes to the diversity of temporal patterns of Ca^{2+} signals observed in different cell types (Taylor *et al.*, 1999; Miyakawa *et al.*, 1999; Haberichter *et al.*, 2002; Hattori *et al.*, 2004). Nearly all models for Ca^{2+} oscillations rely on $InsP_3$-sensitive CICR. These models mainly differ by the degree of detail in the description of $InsP_3R$ kinetics and by the incorporation of one or the other regulatory process considered below (for review, see Sneyd *et al.*, 1995; Tang *et al.*, 1996; Dupont, 1999; Schuster *et al.*, 2002).

I.3.2. PLC activation by Ca^{2+}

The first mathematical model for $InsP_3$-induced Ca^{2+} oscillations assumed that this phenomenon relies on an oscillating level of $InsP_3$. The periodic variation of the $InsP_3$ level was based on a positive feedback loop arising from the assumed activation by Ca^{2+} of $InsP_3$ synthesis catalyzed by phospholipase C (PLC) (Meyer and Stryer, 1988 and 1991; De Young and Keizer, 1992). That such positive feedback occurs for Ca^{2+} concentrations in the physiological range of 0.1-1 μM has been demonstrated for isoforms of the enzyme that have been detected only in a few cell types.

Although many early experimental studies indicated that Ca^{2+} oscillations can be observed in the presence of a constant level of $InsP_3$ (Wakui *et al.*, 1990; Hajnoczky and Thomas, 1997), some recent experiments suggest that Ca^{2+} oscillations are accompanied by $InsP_3$ variations (Hirose *et al.*, 1999; Nash *et al.*, 2001a and 2001b). However, as will be emphasized below, $InsP_3$ oscillations could result from the well-characterized stimulation of $InsP_3$ degradation by Ca^{2+} (Takazawa *et al.*, 1990a; Sims and Allbritton, 1998), in which case they do not really participate in the core oscillatory mechanism. Moreover, the above-mentioned suppression of Ca^{2+} oscillations in DT40 cells expressing $InsP_3Rs$ with a decreased sensitivity to cytosolic Ca^{2+} (Miyakawa *et al.*, 2001) also argue against a primary role of the stimulation of PLC activity by Ca^{2+} in the generation of Ca^{2+} oscillations.

Minimal model based on CICR

Z : cytosolic Ca^{2+}

Y : Ca^{2+} in the endoplasmic reticulum

$$\frac{dZ}{dt} = v_0 + v_1\beta - V_2 + V_3 + k_f Y - kZ \qquad \text{(I.1)}$$

$$\frac{dY}{dt} = V_2 - V_3 - k_f Y \qquad \text{(I.2)}$$

with v_0: basal Ca^{2+} influx from the extracellular medium

β : level of external stimulation

$v_1\beta$: agonist-stimulated Ca^{2+} entry

$$V_2 = V_{M2}\frac{Z^2}{K_2^2 + Z^2} : Ca^{2+} \text{ pumping from the cytosol into the ER} \qquad \text{(I.3)}$$

$$V_3 = \beta V_{M3}\frac{Y^2}{K_R^2 + Y^2}\frac{Z^4}{K_A^4 + Z^4} : Ca^{2+} \text{ release from the ER into the cytosol,} \qquad \text{(I.4)}$$

activated by cytosolic Ca^{2+} (CICR)

$k_f Y$: passive efflux of Ca^{2+} from the stores into the cytosol

$k Z$: passive efflux of Ca^{2+} from the cytosol into the extracellular medium

Table I.2 : One-pool model for Ca^{2+} oscillations based on CICR (Dupont and Goldbeter, 1993). Formally similar kinetic equations are obtained in the two-pool model based on CICR (Dupont and Goldbeter, 1989; Goldbeter *et al.*, 1990).

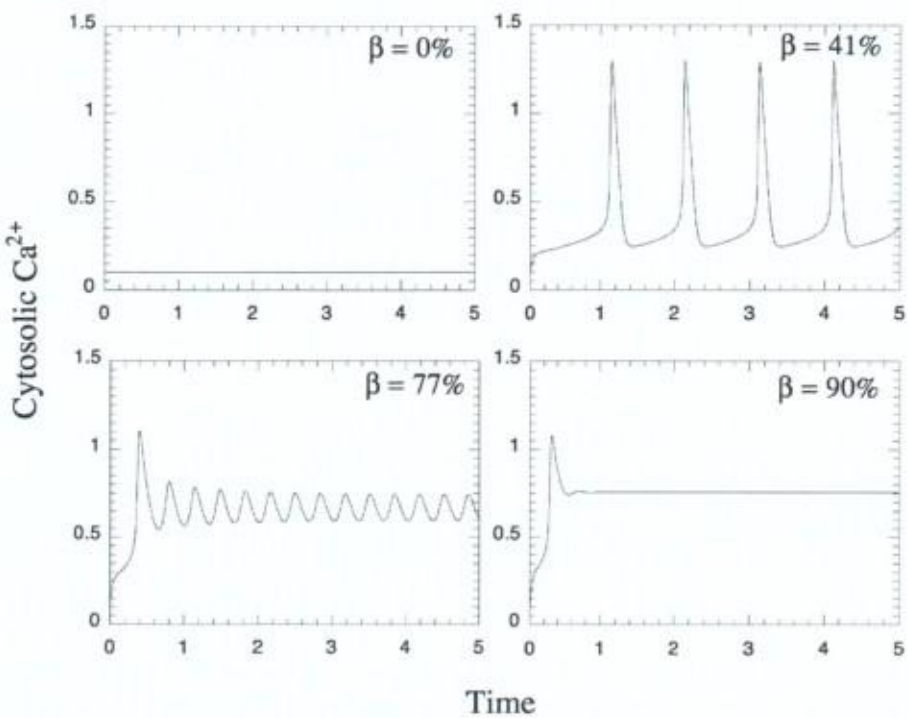

Fig. I.2. Different patterns of cytosolic Ca^{2+} oscillations generated by the model based on CICR (Table I.2) as a function of the increasing level of external stimulation. The level of $InsP_3$ is measured by parameter β that gives the saturation function of the $InsP_3R$. A low (high) steady state of cytosolic Ca^{2+} concentration is obtained for lower (higher) values of β.

I.3.3. Biphasic regulation of the $InsP_3$ receptor by Ca^{2+}

The steady-state open probability of the $InsP_3R/Ca^{2+}$ channel presents a bell-shaped dependence on cytosolic Ca^{2+} concentration (Bezprozvanny and Ehrlich, 1995). Thus, besides CICR, slower, Ca^{2+}-induced inhibition of Ca^{2+} release does also take place. From a theoretical point of view, fast activation and slower inhibition are well known to be sufficient to generate an oscillatory behavior (Goldbeter, 1996). Comprehensive overviews of models based on a detailed description of the transitions between the different states of the $InsP_3R$ are given in many reviews (see, for example, Sneyd *et al.*, 1995; Tang *et al.*, 1996; Schuster *et al.*, 2002). These models reproduce both the oscillations and the equilibrium bell-shaped Ca^{2+} dependence of the $InsP_3R$. One of these models, that will be largely used in the following chapters of this thesis, is given in Table I.3. A recent variant of this type of models is based on the intriguing possibilities that Ca^{2+} binds to the different states of the receptor with nonlinear kinetics and that Ca^{2+} binding to the receptor both decreases the rate of $InsP_3$ binding and increases the sensitivity of the receptor to $InsP_3$ (Sneyd and Dufour, 2002). These assumptions greatly enhance the agreement between the observed dynamical behaviour of the channel and the predictions of the model.

Model based on the biphasic regulation of the $InsP_3R$ by Ca^{2+}

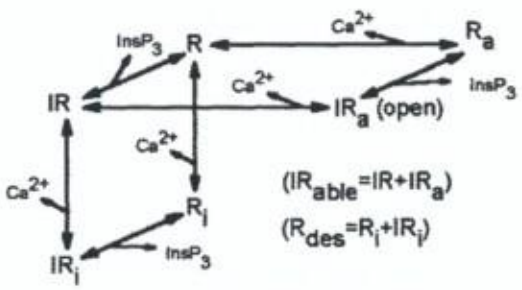

R_{des}: fraction of Ca^{2+}-desensitized $InsP_3$ receptor
C_{cyto}: cytosolic Ca^{2+}

$$\frac{dR_{des}}{dt} = k_+ C_{cyto}^{n_i} \frac{1 - R_{des}}{1 + \left(\frac{C_{cyto}}{K_{act}}\right)^{n_a}} - k_- R_{des} \qquad \text{(I.5)}$$

$$\frac{dC_{cyto}}{dt} = k_1\left(b + IR_a\right)\left(Ca_{tot} - C_{cyto}\left(\alpha + 1\right)\right) - V_{MP}\frac{C_{cyto}^{n_p}}{K_p^{n_p} + C_{cyto}^{n_p}} \qquad \text{(I.6)}$$

with IR_a: fraction of active channels $= IR_{able}\dfrac{1}{1 + \left(\frac{K_{act}}{C_{cyto}}\right)^{n_a}}$ (I.7)

IR_{able}: fraction of 'activable' channels $= \left(1 - R_{des}\right)\dfrac{IP_3}{K_{IP} + IP_3}$ (I.8)

$k_1 b$: small basal leak of Ca^{2+} through the $InsP_3R$

Ca_{tot}: total cell Ca^{2+} concentration $(= \alpha C_{ER} + C_{cyto})$

α: ratio between the ER volume and the cytosolic volume

Table I.3. Model for Ca^{2+} oscillations based on the biphasic (activation-inhibition) regulation of the $InsP_3R$ by Ca^{2+} (Swillens *et al.*, 1994; Dupont and Swillens, 1996).

The main difference between the model based on a detailed description of the transitions between the different states of the $InsP_3R$ and those simply based on $InsP_3$-sensitive CICR pertains to the mechanism responsible for the termination of the Ca^{2+} spike. In the models incorporating the inhibition of the $InsP_3R$ by Ca^{2+}, the latter regulation shuts the channel. In contrast, in models based on simple CICR, the decrease of the Ca^{2+} content of the ER leads to a decrease in cytosolic Ca^{2+} as soon as the rate of release from the ER becomes smaller than the rate of pumping into the ER.

I.3.4. Capacitative Ca^{2+} entry

During Ca^{2+} oscillations, entry of external Ca^{2+} is somehow controlled by the state of filling of the ER. Indeed, Ca^{2+} entry is prevented when Ca^{2+} stores are charged up, but store depletion immediately promotes Ca^{2+} entry into the cytosol. The mechanism of Ca^{2+} entry into the cytosol is still not totally understood and probably differs from one cell type to the other (Berridge, 1995; Lewis, 2001; Putney *et al.*, 2001). By regulating the level of Ca^{2+} inside the cells, capacitative Ca^{2+} entry (CCE) has a profound effect on the overall intracellular Ca^{2+} dynamics. Incorporated into theoretical models, this regulation has been shown to mitigate the depletion of intracellular stores and favor a stable, high steady-state level of cytosolic Ca^{2+} (Wiesner *et al.*, 1996).

I.3.5. $InsP_3$ 3-kinase activation by Ca^{2+}

The metabolism of $InsP_3$ by Ins-1,4,5-P_3 3-kinase and 5-phosphatase has been well characterized. It has been shown that the Ca^{2+} /calmodulin complex stimulates 3-kinase activity (Takazawa *et al.*, 1990a; Sims and Allbritton, 1998). Thus, each Ca^{2+} spike provokes a temporary increase in $InsP_3$ degradation, a phenomenon that leads to $InsP_3$ oscillations (Borghans *et al.*, 1997; Houart *et al.*, 1999). Thus, it is not necessary to invoke the stimulation of $InsP_3$ synthesis by Ca^{2+} to explain the experimentally observed oscillations in $InsP_3$ (Hirose *et al.*, 1999; Nash *et al.*, 2001a and 2001b). If PLC activation was the driving force of $InsP_3$ and Ca^{2+} oscillations, the peak in $InsP_3$ should precede the peak of Ca^{2+}. The opposite should be true if $InsP_3$ oscillations were passively following Ca^{2+} oscillations through stimulation of $InsP_3$ 3-kinase activity by Ca^{2+}. Current experimental techniques do not allow to discriminate between the two situations. The observation that Ca^{2+} oscillations can be induced by large amounts of $InsP_3$ analogs (Wakui *et al.*, 1990; Dumollard *et al.*, 2002) favors the view that $InsP_3$ oscillations originate from the regulation of $InsP_3$ degradation by Ca^{2+}.

I.3.6. Mitochondrial control of Ca^{2+}

Mitochondria play an important role in controlling intracellular Ca^{2+} dynamics. Mitochondrial membranes contain many Ca^{2+} transporters, such as the permeability transition pore (PTP), the Ca^{2+} uniporter and the Na^+/ Ca^{2+} and H^+/ Ca^{2+} exchangers. Through these channels, mitochondria behave as high capacity, low affinity Ca^{2+} buffers (Jouaville *et al.*, 1995) and could also play a more active role in releasing their Ca^{2+} content when overloaded, in a process called mitochondrial Ca^{2+}-induced Ca^{2+} release (Ichas *et al.*, 1997). Also, as a consequence of cytosolic Ca^{2+} oscillations, the level of Ca^{2+} inside mitochondria varies, allowing for the frequency-encoding of intramitochondrial reactions such as those based on pyruvate dehydrogenase activity (Robb-Gaspers *et al.*, 1998).

Mitochondria have been taken into account in several models for Ca^{2+} dynamics (Marhl *et al.*, 2000; Falcke *et al.*, 1999). These models predict that mitochondria can regulate the amplitude and the frequency of cytosolic Ca^{2+} spikes, and influence the transition from simple to complex Ca^{2+} oscillations.

I.3.7. G-protein regulation

G-proteins are involved in the transduction signal cascade between the external hormonal receptor and $InsP_3$ synthesis through the PLC isoform, PLCß. Possible regulations of G-protein by $InsP_3$, Ca^{2+} or diacyl-glycerol (DAG) have been incorporated into various theoretical models (Cuthbertson and Chay, 1991; Kummer *et al.*, 2000; Läer *et al.*, 2001). In these models, which often display complex Ca^{2+} oscillations, the level of $InsP_3$ oscillates together with Ca^{2+}. However, solid experimental evidence for the regulation of G-protein by Ca^{2+} or $InsP_3$ is still lacking.

I.3.8. Phosphorylation of the $InsP_3$ receptor

Phosphorylation of the $InsP_3$ receptor by protein kinases A, C and calmodulin-dependent kinase II has been demonstrated (see Bezprozvanny and Ehrlich, 1995 for review). Type III $InsP_3R$, most abundant in pancreatic acinar cells, has been shown to be largely phosphorylated in response to stimulation by cholecystokinin (Hagar and Ehrlich, 2000). Phosphorylation is not observed in response to other agonists such as acetylcholine. If it is assumed that the phosphorylated receptor does not pass Ca^{2+} current, the rate of $InsP_3R$ recovery from inactivation crucially depends on the nature of the agonist. This mechanism might explain the long-period Ca^{2+} spiking observed in these cells after stimulation by cholecystokinin (LeBeau *et al.*, 1999).

I.4. Aim of the thesis

In the following, we focus on the spatio-temporal organization of calcium signals in non-excitable cells, from the subcellular to the multicellular level. The general idea of our research work is to use the synergy provided by a combined theoretical and experimental approach to apprehend complex phenomena, such as oscillations, waves and gradients from a clear and robust point of view. Thus, the subjects related to Ca^{2+} dynamics that we have investigated, have been selected on the basis of both their physiological relevance and the possible gain provided by a theoretical approach. This procedure, clearly coming under the field nowadays referred to as 'Computational Biology' (Fall and Keizer, 2002; Goldbeter, 2002; 2004), has often allowed us and many others to grasp the molecular mechanisms and functions of Ca^{2+} oscillations and waves. Besides the classical field of neurophysiology, it can be positively stated that Ca^{2+} dynamics is one of the field of biology for which the interplay between theory and experiments has been the most fruitful.

Chapters II and III are devoted to a detailed study of Ca^{2+} oscillations. We first extend the models initially developed to account for Ca^{2+} oscillations –and presented in Tables I.2 and I.3– to take into account the metabolism of $InsP_3$. As $InsP_3$ is responsible for the release of Ca^{2+} from the internal stores, its synthesis and degradation clearly affect Ca^{2+} dynamics. In particular, as the activity of one of the enzymes responsible for $InsP_3$ degradation is stimulated by Ca^{2+} itself, there is a mechanism of signal self-modulation which is expected to lead to complex behaviours. Moreover, this model allows us to provide some simple explanation to experimental results related to the overexpression of the $InsP_3$-catabolizing enzymes. It also provides a framework allowing us to test the hypothesis that Ca^{2+} oscillations could be accompanied by $InsP_3$ oscillations. In a second step, we extend the simple model based on the biphasic regulation of the $InsP_3$ receptor by Ca^{2+} to consider the existence of three isoforms of the $InsP_3$ receptor. It is known from electrophysiological experiments that the latter's are differently regulated by Ca^{2+} and $InsP_3$. Taking these data into account, we analyse the effects of changing the respective amounts of the 3 isoforms in a model for the Ca^{2+} dynamics. The level of expression of the 3 types of $InsP_3R$ indeed depends on the cell type and on the developmental stage of the cell.

Oscillations of cytosolic Ca^{2+} are assumed to result from the periodic, coordinated opening of the whole population of $InsP_3Rs$ present in a cell. However, for weak levels of stimulation ($InsP_3$), one can

observe some other types of Ca^{2+} increases, of short durations and small amplitudes, that seem to occur randomly throughout the cell. These elementary Ca^{2+} signals are supposed to result from the opening of one or a few Ca^{2+} channels. They are modelled in **Chapter IV**, by means of stochastic simulations. The aim of this study is to make the link between the characteristics of the $InsP_3R/Ca^{2+}$ channels which have been reported in *in vitro* studies, and these small increases in Ca^{2+} observed in the cytosol.

If elementary Ca^{2+} events are considered as the smallest phenomena in the hierarchy of Ca^{2+} events, intercellular Ca^{2+} waves lie at the opposite side. In some tissues, Ca^{2+} oscillations between adjacent cells are indeed coordinated. In **Chapter V**, we focus on the case of hepatocytes. The mechanism responsible for the propagation of Ca^{2+} waves through the whole liver can indeed be apprehended on a much simpler system, consisting of a few hepatocytes connected by gap junctions. In a combined theoretical and experimental approach, we have investigated the mechanism of this intercellular propagation of Ca^{2+} waves, and more specifically the nature of the key messenger flowing through gap junctions.

The periodic propagation of Ca^{2+} waves is also observed in many eggs after fertilization. As these waves play a fundamental role in the development of the egg into an embryo, it is crucial to grasp with many details the mechanisms responsible for this early spatio-temporal organization. Focussing again on one model system, namely the ascidian egg, we start in **Chapter VI** by modelling some experimental results that have been obtained by artificially stimulating these eggs in well-defined conditions. These experiments indeed allow us to validate our model, which can then in a second step be used to provide some plausible explanations and predictions about phenomena responsible for egg activation at fertilization.

Finally, the role of Ca^{2+} as second messenger is most emphasized in **Chapter VII**. More specifically, we focus on three situations where the oscillatory nature of the Ca^{2+} signal seems to play a predominant role in its physiological implications. We thus first envisage the problem of the stimulation by Ca^{2+} of glycogenolysis in the liver, to try to theoretically uncover the possible advantage of an oscillatory Ca^{2+} signal with respect to a constant one. Second, we focus on the only enzyme that has been shown, in isolation, to be sensitive to the frequency of Ca^{2+} oscillations, namely the Ca^{2+}-calmoduline sensitive kinase II. We propose a simple model for this very peculiar enzyme. This model could serve as a 'plug-in' element in elaborated models of cell signalling in the various systems in which this kinase is involved. Finally, in a rather speculative manner, we make the link between the Ca^{2+} oscillations observed at fertilization and the early development of the egg, by considering the effect of periodic Ca^{2+} increases on a previously proposed model for the cell cycle.

PART 1 : OSCILLATIONS

CHAPTER II

Effect of $InsP_3$ metabolism on cellular Ca^{2+} oscillations

II.1. Introduction

As $InsP_3$ is directly responsible for the release of Ca^{2+} from the ER into the cytoplasm, $InsP_3$ metabolism appears as a key process that may reshape Ca^{2+} oscillations. $InsP_3$ is produced by activation of phosphoinositide-specific phospholipase C (PLC), which catalyzes the hydrolysis of phosphatidyl-inositol 4,5-bisphosphate (PIP_2) to generate $InsP_3$ and 1,2-diacylglycerol (DAG). To date, five classes of PLC have been identified : β, γ, δ, ε and ζ (Rhee, 2001; Kouchi *et al.*; 2004). The dependence of PLC activity on Ca^{2+} has been recognized for quite a long time. However, in most cases, this stimulation of PLC activity by Ca^{2+} occurs for non-physiological Ca^{2+} levels. That such positive feedback may occur for Ca^{2+} concentration in the range of 0.1-1 μM has been shown for the γ (Renard *et al.*, 1987), δ (Allen *et al.*, 1997) and ζ isoforms (Kouchi *et al.*, 2004).

Stimulation of $InsP_3$ synthesis by Ca^{2+} represents a cross-catalytic mechanism that could provide an alternative to CICR to generate Ca^{2+} oscillations. In fact, the first mathematical model for $InsP_3$-induced Ca^{2+} oscillations was based on this regulation (Meyer and Stryer, 1988; 1991). In this case, $InsP_3$ oscillations accompany Ca^{2+} oscillations. This hypothesis was rather rapidly put aside as many experiments indicated that Ca^{2+} oscillations can be observed in the presence of a constant level of $InsP_3$ (Wakui *et al.*, 1990; Hajnoczky and Thomas, 1997; Dumollard and Sardet, 2001). Some other, recent experiments however suggest that periodic $InsP_3$ variations can be observed during the course of Ca^{2+} oscillations (Hirose *et al.*, 1999; Nash *et al.*, 2001a and 2002b). These observations have reawakened enthousiasm for models based on an oscillatory production of $InsP_3$ (Taylor and Thorn, 2001). However, as will be emphasized below, $InsP_3$ oscillations could result from the well-characterized stimulation of $InsP_3$ degradation by Ca^{2+} (Takazawa *et al.*, 1990; Sims and Allbritton, 1998), in which case they do not really participate in the core oscillatory mechanism. Moreover, the suppression of Ca^{2+} oscillations in DT40 cells expressing $InsP_3Rs$ with a decreased sensitivity to cytosolic Ca^{2+} (Miyakawa *et al.*, 2001) also argue against a primary role of the stimulation of PLC activity by Ca^{2+} in the generation of Ca^{2+} oscillations.

In this chapter, we focus on the process of $InsP_3$ degradation and on its possible effect on the existence, frequency and shape of Ca^{2+} oscillations. We thus extend our model for Ca^{2+} oscillations presented in Table I.3 to consider the evolution of $InsP_3$ concentration (section II.2). We then use this model to investigate the respective importance of the two $Ins(1,4,5)P_3$ degradation pathways (section II.3; Dupont and Erneux, 1997); this allows us to propose an explanation to the counter-intuitive experimental observations performed in CHO cells overexpressing one or the other $InsP_3$-degrading enzyme (De Smedt *et al.*, 1997). Then, using a combined theoretical and experimental approach, we examine the possible physiological relevance of $InsP_3$ oscillations due to Ca^{2+}-stimulation of $InsP_3$ degradation (section II.4; Dupont *et al.*, 2003c). Finally, we use a somewhat simplified version of the model for Ca^{2+} oscillations taking $InsP_3$ degradation into account to theoretically explore the properties of the complex Ca^{2+} oscillations that may occur when two oscillatory loops (CICR and self-modulation of the $InsP_3$ signal) are concomitantly active (section II.5; Borghans *et al.*, 1997; Houart *et al.*, 1999).

II.2. Model for Ca^{2+} oscillations involving Ca^{2+}-activated $InsP_3$ degradation

II.2.1. Experimental data concerning the catabolism of Ins1,4,5-P_3

Ins1,4,5-P_3 can be inactivated in two distinct ways; it can be either dephosphorylated by the Ins1,4,5-P_3 5-phosphatase to produce inositol 1,4-bisphosphate or phosphorylated by the Ins1,4,5-P_3 3-kinase to yield inositol 1,3,4,5-tetrakisphosphate (Erneux and Takazawa, 1991; Shears, 1992). The latter Ins1,3,4,5-P_4 might regulate Ca^{2+} concentration either by potentiating Ins1,4,5-P_3-evoked Ca^{2+} release by activating Ca^{2+} entry (for review, see Hughes and Putney, 1990; Irvine, 1992; Wilcox and Nahorski, 1994) or by inhibiting Ins1,4,5-P_3-induced Ca^{2+} release (Bird and Putney, 1996). cDNAs

encoding various isoforms of Ins1,4,5-P_3 5-phosphatase and Ins1,4,5-P_3 3-kinase have been cloned (see e.g. Choi *et al.*, 1990; Takazawa *et al.*, 1990a; Takazawa *et al.*, 1991a; Takazawa *et al.*, 1991b). Type I Ins1,4,5-P_3 5-phosphatase (also designated as 43kDa 5-phosphatase) is the most widespread inositol phosphate 5-phosphatase; it can use both Ins1,4,5-P_3 and Ins1,3,4,5-P_4 as substrates. The apparent Km values of this enzyme, as reported in bovine brain, are equal to 10μM for Ins1,4,5-P_3 and 1μM for Ins1,3,4,5-P_4; the Vmax is about 10 times larger for Ins1,4,5-P_3 as substrate as compared to Ins1,3,4,5-P_4 (Verjans *et al.*, 1994). The Vmax of bovine brain Ins1,4,5-P_3 5-phosphatase was estimated to be about 500 μmol/mg/min (Erneux *et al.*, 1989). High Vmax values for Ins1,4,5-P_3 5-phosphatase have also been reported in human placenta or in porcine skeletal muscle (Verjans *et al.*, 1992; Laxminarayan *et al.*, 1993). The two major isoforms of Ins1,4,5-P_3 3-kinases, known as 3-kinases A and B, are tissue-specific (Takazawa *et al.*, 1990a; 1990b; Takazawa *et al.*, 1991a; Foster *et al.*, 1994). Both isoenzymes have a higher affinity for Ins1,4,5-P_3 than 5-phosphatase, but a lower Vmax. The Vmax of the bovine and rat brain 3-kinases are about 5-10 μmol/mg/min (Foster *et al.*, 1994; Vanweynberg *et al.*, 1995). A major qualitative difference between 3-kinase and 5-phosphatase is that most, if not all, Ins1,4,5-P_3 3-kinase activities of mammalian cells could be stimulated *in vitro* by the Ca^{2+}/calmodulin (CaM) complex. The activation factor ranges form 2 (Foster *et al.*, 1994; Takazawa *et al.*, 1990b; Takazawa *et al.*, 1989) to 17 (Takazawa *et al.*, 1988; Communi *et al.*, 1994). Moreover, Ins1,4,5-P_3 3-kinase A can be phosphorylated by CaM-kinase II, resulting in a 8-10 fold stimulation of enzyme activity (Li *et al.*, 1989). Thus, upon combination of the two latter stimulation pathways, the effective degree of stimulation of Ins1,4,5-P_3 3-kinase by Ca^{2+} is probably very high in many cell types.

II.2.2. Model for $InsP_3$ metabolism

Here, we will start from the model for Ca^{2+} dynamics that has been presented in Table I.3, and defined by eqs. (I.5)-(I.8). In this model, the concentration of $InsP_3$ was considered as a constant parameter (IP3). In order to consider the various effects of Ins1,4,5-P_3 metabolism on Ca^{2+} oscillations, we now assume that the time course of Ins1,4,5-P_3 concentration (*IP3*) obeys the following differential equation:

$$\frac{dIP3}{dt} = \gamma V_{plc} - V_k \frac{IP3}{K_k + IP3} \frac{Ccyto^{n_d}}{K_d^{n_d} + Ccyto^{n_d}} - V_{p1} \frac{IP3}{K_{p1}\left(1 + \frac{IP4}{K_{p2}}\right) + IP3} \qquad \text{(II.1)}$$

where γ represents the level of external stimulation and *Vplc* the maximal velocity of Ins1,4,5-P_3 synthesis by PLC. For the sake of simplicity, the possible stimulation of PLC activity by Ca^{2+} is not taken into account in eq. (II.1) although it can affect the temporal pattern of Ins1,4,5-P_3 accumulation; it has been checked, however, that the results presented below with respect to the respective effects of 3-kinase and 5-phosphatase on Ca^{2+} oscillations, remain qualitatively unchanged if such a feedback is incorporated in the model. Degradation of Ins1,4,5-P_3 by 5-phosphatase occurs with a maximal velocity V_{p1} and a Michaelis constant denoted by K_{p1} . K_{p2} characterizes the competitive inhibition of Ins1,4,5-P_3 5-phosphatase by Ins1,3,4,5-P_4. The maximal velocity of Ins1,4,5-P_3 3-kinase is represented by V_k while K_k stands for the Michaelis constant of the same enzyme for Ins1,4,5-P_3. Activation of Ins1,4,5-P_3 3-kinase by Ca^{2+} is characterized by a threshold constant K_d and a Hill coefficient n_d. Calmodulin is not explicitely considered as it can be assumed to be in large excess and because Ca^{2+} binding to calmodulin is not a kinetically limiting step.

In the same manner, the evolution of the concentration of Ins1,3,4,5-P_4 (*IP4*) is given by:

$$\frac{dIP4}{dt} = V_k \frac{IP3}{K_k + IP3} \frac{Ccyto^{n_d}}{K_d^{n_d} + Ccyto^{n_d}} - V_{p2} \frac{IP4}{K_{p2}\left(1 + \frac{IP3}{K_{p1}}\right) + IP4} - kIP4 \qquad \text{(II.2)}$$

in which V_{p2} is the maximal velocity of Ins1,4,5-P_3 5-phosphatase with Ins1,3,4,5-P_4 as substrate. The last term refers to a small, linear degradation of Ins1,3,4,5-P_4; for most parameter values, the latter does not play any significant role, but it ensures the existence of a steady-state level of Ins1,4,5-P_3 and Ins1,3,4,5-P_4 when the velocity of Ins1,4,5-P_3 production *($\gamma Vplc$)* becomes very large. This small degradation term could correspond to other 5-phosphatase activities as, e.g. the 75kDa 5-phosphatase (Mitchell *et al.*, 1989) or to SHIP (SH2-containing inositol phosphatase) (Damen *et al.*, 1996; Kavanaugh *et al.*, 1996).

Parameter values

For Ca^{2+} oscillations, we have considered parameter values previously used in the model defined by eqs. (I.5)-(I.8) (Dupont and Swillens, 1996). The latters do not affect the results of the present study, as long as the temporal relationship between Ca^{2+} spiking and Ins1,4,5-P_3 metabolism is not drastically changed. Thus, to keep internal consistency, we have considered parameter values leading to period of Ca^{2+} oscillations of a few seconds together with parameter values for Ins1,4,5-P_3 metabolism issued from studies performed in brain tissues. A standard set of values for the parameters characterizing the Ins1,4,5-P_3 synthesis and metabolism is given in Table II.1. Michaelis constants of 3-kinase and 5-phosphatase are directly issued from the litterature; the latter reports also provide values for the maximal velocities of the purified enzymes. However, we need to consider, in the model, apparent values for the Vmax that take into account the enzymatic concentrations. These apparent maximal velocities of Ins1,4,5-P_3 3-kinase and 5-phosphatase have thus been evaluated on the basis of total activities of crude extracts of bovine brain. The values reported in (Verjans *et al.*, 1994a) were used for Ins1,4,5-P_3 5-phosphatase, keeping in mind that, in the brain, soluble 5-phosphatase activity represents about 20% of total 5-phosphatase activity; for 3-kinase, we used the values reported in (Takazawa *et al.*, 1990b). Thus, assuming a tissular density equal to 1, the apparent Vmax for total 5-phosphatase can be estimated to be about 15 μMs^{-1}, while that of 3-kinase is of the order of 0.17 μMs^{-1}. In the simulations, we used 5μMs^{-1} and 0.5 μMs^{-1} for 5-phosphatase and 3-kinase, respectively, such as to get a ratio of 10 between the two maximal velocities; this value would represent a minimal value in brain tissues and equals that measured in Chinese hamster ovary cells in which overexpression experiments have been carried out. The detailed effect of varying this ratio will be further investigated in the present study.

Ins1,4,5-P_3 3-kinase stimulation by the Ca^{2+}-calmodulin complex is a cooperative process; thus the Hill coefficient n_d is larger than 1. The precise value of this coefficient, as well as the threshold K_d characterizing the stimulation (eqs (II.1) and (II.2)), have been chosen, in an empirical manner, such as to get appropriate stimulation levels of the Ins1,4,5-P_3 3-kinase by Ca^{2+}. In the model, indeed, the stimulation factor is given by the ratio of the third factor of the second term of the right hand side of equ. (II.1), evaluated, respectively, at the maximal and minimal levels of Ca^{2+} reached during oscillations. In that respect, it should be noted also that the value of V_k (maximal velocity of Ins1,4,5-P_3 3-kinase) that has to be incorporated in the model must be evaluated from experimental data obtained at high Ca^{2+} concentration. Finally, the maximal velocity of PLC has been chosen such as to get a physiolocial value for the resting level of Ins1,4,5-P_3 (about 0.1 μM).

Ins1,4,5-P_3 metabolism			
Symbol	**Definition**	**Standard value**	**References**
V_{plc}	Maximal velocity of IP3 synthesis	1.3 μMs^{-1}	
V_k	Maximal velocity of IP3 3-kinase	0.5 μMs^{-1}	[1,2,3,4]
K_k	Michaelis constant of IP3 3-kinase	1 μM	[1,2,3,4]
K_d	Threshold for IP3 3-kinase activation by Ca^{2+}	0.3 μM	
n_d	Hill coefficient for IP3 3-kinase activation by Ca^{2+}	2	
V_{p1}	Maximal velocity of 5-phosphatase (IP3 substrate)	5 μMs^{-1}	[2,5,6,7]
K_{p1}	Michaelis constant of 5-phosphatase (IP3 substrate)	10μM	[2,5,6,7]
V_{p2}	Maximal velocity of 5-phosphatase (IP4 substrate)	0.2 μM	[2,5,6,7]
K_{p2}	Michaelis constant of 5-phosphatase (IP4 substrate)	2μM	[2,5,6,7]
k_{ns}	Rate constant of linear degradation of IP4	$0.01s^{-1}$	

Table II.1 Standard values of the parameters characterizing Ins1,4,5-P_3 synthesis and metabolism used in the model for Ca^{2+} oscillations and Ins1,4,5-P_3 metabolism. For the references: 1: Takazawa *et al.*, 1991b; 2: Erneux *et al.*, 1989; 3: Takazawa *et al.*, 1989; 4: Takazawa *et al.*, 1988; 5: Verjans *et al.*, 1992; 6: Verjans *et al.*, 1994; 7: Laxminarayan *et al.*, 1993.

Typical behaviour of the model for Ca^{2+} *oscillations and Ins1,4,5-P_3 metabolism*

Equations (I.5)-(I.8), (II.1) and (II.2) represent a system of four ordinary differential equations that can be numerically integrated. A typical behaviour exhibited by the model is shown in Fig. II.1. It appears that cytosolic Ca^{2+} oscillations (Fig. II.1.A) drive small amplitude variations of the Ins1,4,5-P_3 (Fig. II.1.B) and Ins1,3,4,5-P_4 (Fig. II.1.C) concentrations because each Ca^{2+} spike activates Ins1,4,5-P_3 3-kinase, which provokes an increased transformation of Ins1,4,5-P_3 into Ins1,3,4,5-P_4.

Oscillations in the levels of Ins1,4,5-P_3 have been reported in some experimental studies (Harootunian *et al.*, 1991; Raha *et al.*, 1993; Hirose *et al.*, 1999; Nash *et al.*, 2001a; 2001b). The amplitude of the Ins1,4,5-P_3 and Ins1,3,4,5-P_4 variations depends on the stimulation level (larger variations are obtained for smaller values of γ), as well as on the maximal velocity and threshold constant of the Ins1,4,5-P_3 3-kinase. In the limit case where the maximal velocity of 3-kinase would be very low, as in some cell types where the activity of 5-phosphatase very much exceeds the activity of 3-kinase, these oscillations in the level of Ins1,4,5-P_3 would disappear. Importantly, the degree of Ins1,4,5-P_3 3-kinase activation by Ca^{2+} also plays a crucial role in that respect; for the simulation presented in Fig. II.1, parameters values (K_d and n_d) are such that when the level of cytosolic Ca^{2+} rises from its minimal (91 nM) to its maximal (510 nM) value, the stimulation factor is equal to about 9. Cytosolic Ca^{2+} oscillations are barely affected by these small Ins1,4,5-P_3 variations. If Ins1,4,5-P_3 is assumed to be fixed at the mean value corresponding to panel B, simulations of the model defined by eqs(I.5)-(I.8) lead to a nearly unchanged pattern of Ca^{2+} oscillations as compared to Fig. II.1.A (not shown). When external stimulation is maximal ($\gamma = 1$), oscillations of cytosolic Ca^{2+} disappear and a high steady-state level of Ca^{2+} (0.32 μM), Ins1,4,5-P_3 (18.01 μM) and Ins1,3,4,5-P_4 (11.56 μM) is established. It is also interesting to note that, in these non-oscillatory conditions, the increase in Ins1,4,5-P_3 concentration after stimulation is biphasic; when the level of Ins1,4,5-P_3 has become high enough to release Ca^{2+} from internal stores, Ins1,3,4,5-P_4 is produced, resulting in a decreased rate of net Ins1,4,5-P_3 accumulation (not shown). Finally, it should be mentioned that for some set of

parameter values, the model can display complex, bursting-like oscillations in agreement with other theoretical results (Borghans *et al.*, 1997; Houart *et al.*, 1999; see section II.4).

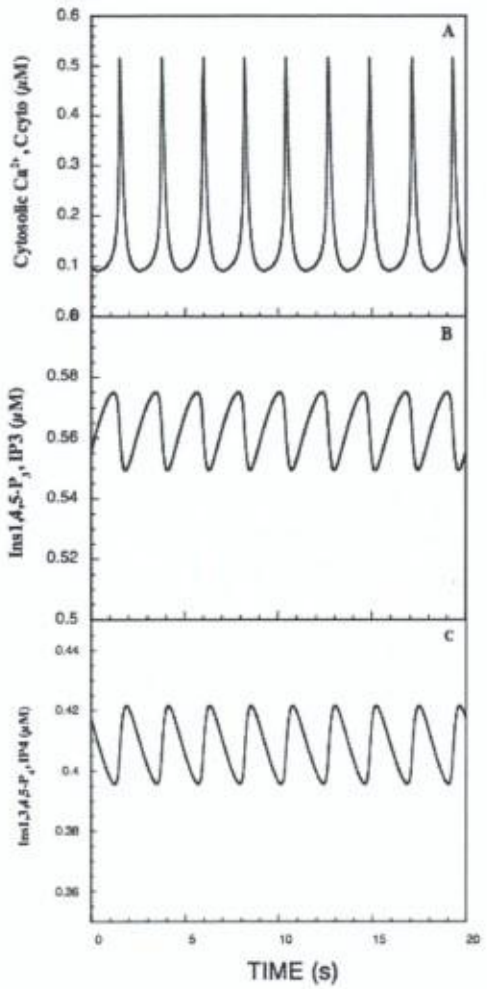

Fig. II.1. Typical oscillations obtained with the model for Ca^{2+} oscillations and Ins1,4,5-P_3 metabolism. Ins1,4,5-P_3 and Ins1,3,4,5-P_4 oscillations are passively driven by oscillations in cytosolic Ca^{2+}, occurring due to the feedback regulation of cytosolic Ca^{2+} on the Ins1,4,5-P_3 receptor. The successive panels show the evolution of cytosolic Ca^{2+} (panel A), of Ins1,4,5-P_3 (panel B) and of Ins1,3,4,5-P_4 (panel C). Results have been obtained by numerical integration of equations (I.5)-(I.8), (II.1), (II.2), with the parameters values listed in Table II.1. for Ins1,4,5-P_3 metabolism and $\gamma = 0.2$, $\alpha = 0.1$, $Catot = 80$ μM, $V_{MP} = 4$ μMs^{-1}, $K_P = 0.35$ μM, $n_P = 2$, $K_{act} = 0.56$ μM, $K_{inh} = 0.15$ μM, $n_a = 3$, $n_i = 4$, $k\text{-} = 0.5$ s^{-1}, $b = 7\ 10^{-4}$ s^{-1}, $k_f = 2.57$ s^{-1} and $K_{IP} = 1$ μM. Initial conditions correspond to a point of the limit cycle.

II.3. Theoretical study of the effect of Ins1,4,5-P_3 3-kinase and Ins1,4,5-P_3 5-phosphatase overexpression

II.3.1. Simulations

To investigate the respective roles of Ins1,4,5-P_3 3-kinase and 5-phosphatase in Ins1,4,5-P_3 metabolism, it is interesting to simulate situations that would correspond to enzymatic over- or underexpression. Different cell types indeed display different ratios of activities of the two Ins1,4,5-P_3-metabolizing enzymes. For example, Ins1,4,5-P_3 3-kinase activity is particularly low in rat

pancreatoma cells AR42J or these cells may overexpress the 5-phosphatase which degrades Ins1,4,5-P_3 into Ins1,4-P_2 (Menniti and Putney, 1990). On the other hand, the latter approach provides theoretical predictions that can be tested experimentally. The role of 3-kinase and 5-phosphatase activities on the pattern of Ca^{2+} responses has indeed been appreciated by under- or overexpressing one or two of these enzymes in fibroblasts (Balla *et al.*, 1991), *Xenopus* oocytes (Verjans *et al.*, 1994), rat kidney cells (Speed *et al.*, 1996) and Chinese hamster ovary cells (De Smedt *et al.*, 1997). It was shown that 3-kinase overexpresssion has very little –if no– effect on internal Ca^{2+} mobilization in response to external stimulation (Verjans *et al.*, 1994a; De Smedt *et al.*, 1997). In contrast 5-phosphatase underexpression significantly increases the level of resting Ca^{2+} (1.9 fold) in rat kidney cells, an effect which is triggered by an increase in the level of Ins1,4,5-P_3 (Speed *et al.*, 1996). In Chinese hamster ovary cells, overexpression of the native 5-phosphatase clearly abolishes any oscillatory Ca^{2+} activity in response to stimulation (De Smedt *et al.*, 1997).

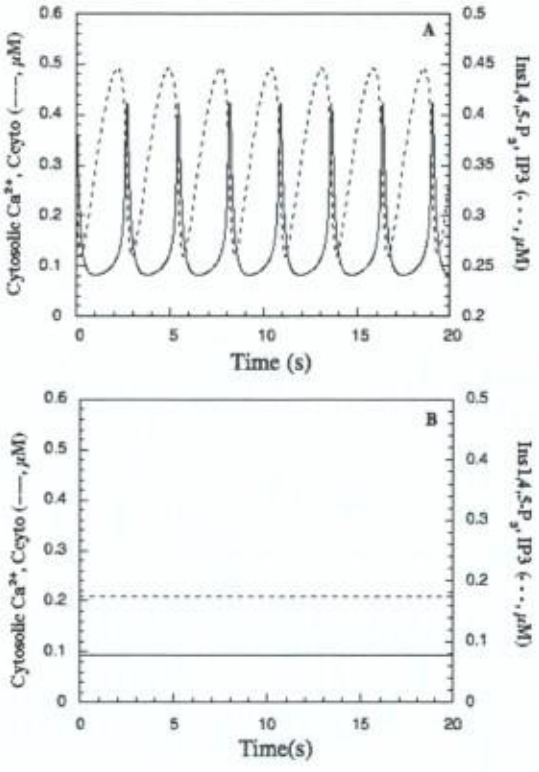

Fig. II.2. Effect of a 10-fold overexpression of Ins1,4,5-P_3 3-kinase (panel A) and of a 3-fold overexpression of Ins1,4,5-P_3 5-phosphatase (panel B) on Ca^{2+} oscillations. Overexpression of 5-phosphatase has a much more drastic effect on Ca^{2+} oscillations. Both panels have been obtained as in Fig. II.1, except for $V_{kin} = 5\ \mu Ms^{-1}$ in panel A, and $V_{p1} = 15\ \mu Ms^{-1}$ and $V_{p2} = 0.6\ \mu Ms^{-1}$ in panel B.

Overexpression is simulated in the model by increasing the appropriate maximal velocity. The effect of a 10-fold increase in the maximal velocity of Ins1,4,5-P_3 3-kinase is shown in Fig. II.2.A., in which all parameters –except the maximal velocity of 3-kinase– have been kept the same as in Fig. II.1. Sustained cytosolic Ca^{2+} oscillations still occur, with a decrease in both frequency and amplitude, due to a lower mean level of Ins1,4,5-P_3. In fact, for the situation considered in Fig. II.1, sustained oscillations disappear for a ~16 fold increase of Ins1,4,5-P_3 3-kinase maximal velocity. In contrast, a 3 fold increase in the maximal velocity of Ins1,4,5-P_3 5-phosphatase (with both Ins1,4,5-P_3 and

Ins1,3,4,5-P_4 as substrates) already leads to the disappearance of Ca^{2+} oscillations (Fig. II.2.B). The occurrence of an oscillatory pattern of Ca^{2+} response is therefore very much depending on the maximal velocity of Ins1,4,5-P_3 5-phosphatase. It also suggests that non competitive inhibitors of the 5-phosphatase would have pronounced effect on the pattern of Ca^{2+} oscillations.

II.3.2. Explanation based on the modulation of enzymatic activities

The reason why overexpressing Ins1,4,5-P_3 3-kinase or 5-phosphatase has different effects on Ca^{2+} oscillations can be understood by looking at Fig. II.3., which shows the enzymatic activities of the non-overexpressed (A) and overexpressed (B) enzymes. In a situation assumed to correspond to an intact cell (Fig. II.3.A), the activity of 5-phosphatase always exceeds that of 3-kinase, as shown by measurements performed in total brain tissues (Erneux *et al.*, 1989; Vanweyenberg *et al.*, 1995; Takazawa *et al.*, 1989) in which it has been shown that this ratio can vary from 10 to 100. Moreover, in the simulations, it clearly appears that 3-kinase only plays a significant role at the peak of a Ca^{2+} spike. A 10-fold overexpression of 3-kinase has two consequences (Fig. II.3.B). First, the activity of the latter enzyme is increased; due to the stimulation of enzymatic activity by Ca^{2+}, this effect is fully pronounced only at the peak of the Ca^{2+} spike which means that, in average, the increase in activity is smaller than for a non-regulated enzyme. Secondly, 5-phosphatase activity is considerably decreased; this is due to the competitive inhibition by Ins1,3,4,5-P_4 –the mean level of which here equals 6.56 μM– on Ins1,4,5-P_3 degradation by 5-phosphatase. Thus, interestingly, the overall effect of an overexpression of 3-kinase on the global Ins1,4,5-P_3 metabolism remains relatively small. In contrast, the assumed overexpression of 5-phosphatase has a direct effect as to increase its enzymatic activity.

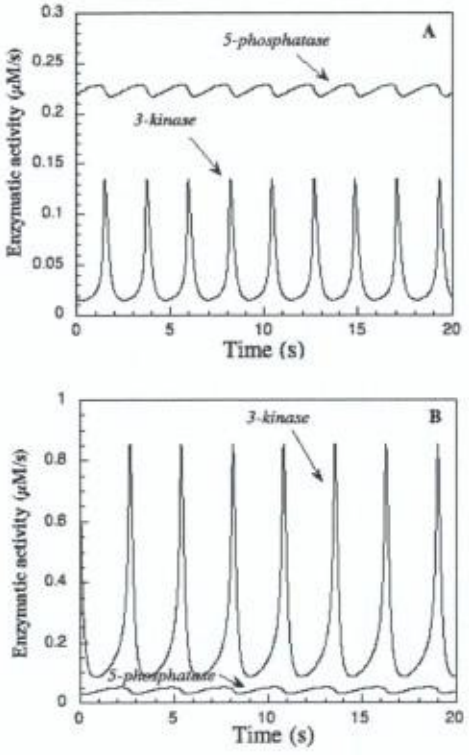

Fig. II.3. Effect of the overexpression of Ins1,4,5-P_3 3-kinase on enzymatic activities. Panel A represents the enzymatic activity of 3-kinase and of 5-phosphatase in standard conditions supposed to correspond to an intact cell (Table II.1.; Fig. II.1.). Panel B shows the same enzymatic activities when 3-kinase is overexpressed 10 times ($V_4 = 5\ \mu Ms^{-1}$; Fig. II.2.). The effect on the overall Ins1,4,5-P_3 metabolism is twofold: first, 3-kinase activity is increased (note that this effect is more

pronounced at the peak of a Ca^{2+} spike as well as the difference in scale as compared to panel A) and second the 5-phosphatase activity (in Ins1,4,5-P_3 degradation) is much decreased due to competitive inhibition by Ins1,3,4,5-P_4.

A more exhaustive view of this phenomenon can be obtained by looking at the dependence of the average levels of Ins1,4,5-P_3 and Ca^{2+} on the maximal velocity of both 3-kinase and 5-phosphatase (Fig. II.4.). The two curves of Fig. II.4.A represent the changes in average Ins1,4,5-P_3 concentrations when varying one of the maximal velocity while keeping the other one identical to the standard conditions (Table II.2.). In this view, the situation illustated in Fig. II.1 corresponds to the arrows indicated (1) in Fig. II.4.A, while (2) corresponds to 3-kinase overexpression (Fig. II.2.A) and (3) to 5-phosphatase overexpression (Fig. II.2.B). It clearly appears again that the Ins1,4,5-P_3 5-phosphatase primarily controls the mean level of Ins1,4,5-P_3 and thereby the existence of Ca^{2+} oscillations, occurring for Ins1,4,5-P_3 levels comprised between both horizontal lines of Fig. II.3.A (<Ins1,4,5-P_3> = 0.239 μM and <Ins1,4,5-P_3> = 4.32 μM). It is interesting to mention that the increase in Ins1,4,5-P_3 associated with a decrease in 5-phosphatase maximal velocity –that could be associated with 5-phosphatase underexpression– results in an increase in the cytosolic Ca^{2+} level (Fig. II.4.B.), in agreement with experimental results obtained in rat kidney cells transfected with the cDNA encoding

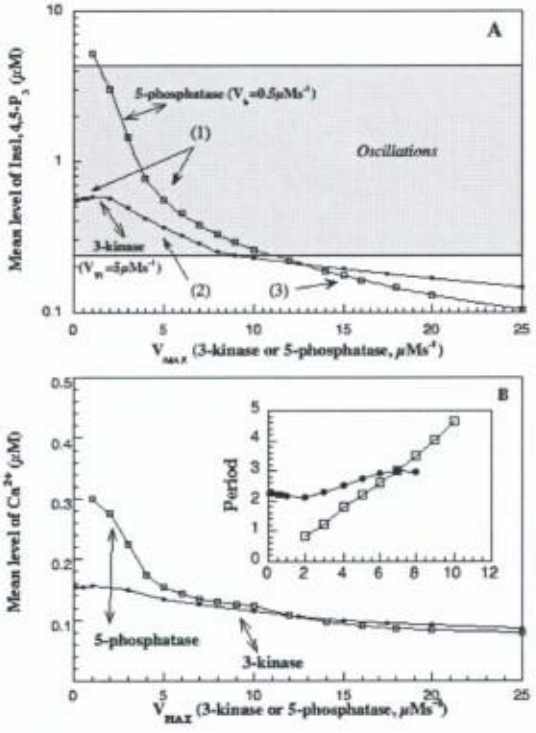

Fig. II.4. Effects of varying the maximal velocity of Ins1,4,5-P_3 3-kinase (filled dots) and Ins1,4,5-P_3 5-phosphatase (open squares) on the mean Ins1,4,5-P_3 (A) and Ca^{2+} (B) levels. Results have been obtained by numerical integration of eqs. (I.5)-(I.8), (II.1) and (II.2) with the same parameter values as in Fig. II.1., except for the values of maximal velocities indicated on the horizontal axe. Each curve represents a situation where the maximal velocity of one of both enzymes is varied while the maximal velocity of the other enzyme is taken as in Fig. II.1. Sustained Ca^{2+} oscillations exist for average Ins1,4,5-P_3 concentrations comprised between the two horizontal lines indicated on the graph A. Fig. II.1 corresponds to the points marked (1), while Fig. II.2.A and II.2.B correspond to the points marked (2) and (3), respectively. The inset in panel B indicates the period of cytosolic Ca^{2+} oscillations (in seconds) when varying the maximal velocity of Ins1,4,5-P_3 3-kinase (filled dots) and Ins1,4,5-P_3 5-phosphatase (open squares).

the 5-phosphatase cloned in the antisense orientation (Speed *et al.*, 1996). In contrast, changes in the maximal velocity of 3-kinase barely affect the resting Ca^{2+} concentration (Fig. II.4.B), in agreement with experimental results obtained in Chinese hamster ovary cells (De Smedt *et al.*, 1997). Finally, the present results suggest that the very high level of cytosolic Ca^{2+} observed after tetanic stimulation of hippocampal CA1 pyramidal cells (Petrozzino *et al.*, 1995) could be partly ascribed to the fact that, in these cells, Ins1,4,5-P_3 metabolism is principally carried out by Ins1,4,5-P_3 3-kinase (Mailleux *et al.*, 1991); in that case, the ratio of the maximal velocities of 5-phosphatase over that of 3-kinase would be low and the level of Ca^{2+} would be high (Fig. II.4.B).

II.3.3. Theoretical predictions

A first prediction relates to the change in period of Ca^{2+} oscillations for different levels of overexpression of both Ins1,4,5-P_3-metabolizing enzymes. In the range of Vmax values in which oscillations do occur, the period of oscillations increases when the maximal velocity of any of both Ins1,4,5-P_3 metabolizing enzymes is increased; however, the effect on the period is much more pronounced for 5-phosphatase than for 3-kinase (inset to Fig. II.4.B).

The quantitative aspect of the curves shown in Fig. II.4 as well as the precise values of the overexpression factor leading to the disappearance of Ca^{2+} oscillations depend on a given choice of parameter values. Clearly, two quantities play a primary role in the control of Ca^{2+} oscillations: the stimulation factor of Ins1,4,5-P_3 3-kinase by Ca^{2+}, and, second, the ratio between the maximal velocities of 3-kinase and 5-phosphatase supposed to correspond to the situation of an intact cell. Increasing any of these two quantities reinforces the dissimilarity between 3-kinase and 5-phosphatase in regulating the mean level of Ins1,4,5-P_3, and thereby the existence of Ca^{2+} oscillations. As a direct corollary of that, it is clear that results qualitatively similar to the ones presented above using parameter values corresponding to the brain (Fig. II.2) can be obtained for a large range of values of the stimulation factor and of the ratio between the maximal velocities, as long as one of these two quantities is large enough. A low stimulation factor can be compensated by a large gap between Ins1,4,5-P_3 3-kinase and 5-phosphatase and *vice-versa*. Such a variety of situations most probably occurs in the different cell types. The stimulation factor of the Ins1,4,5-P_3 3-kinase indeed varies among its three known isoenzymes, differently expressed in various tissues (Vanweyenberg *et al.*, 1995; Communi *et al.*, 1997). The ratio between the maximal velocities of 3-kinase and 5-phosphatase also much varies between cell types; in the rat hippocampus, for example, the Ins1,4,5-P_3 3-kinase activity is particularly high and this contrasts to the activity that is detected in rat liver cells (Erneux, unpublished data).

II.3.4. Discussion

In the present study, we have adressed the problem of the effect of Ins1,4,5-P_3 metabolism by Ins1,4,5-P_3 3-kinase and 5-phosphatase on Ca^{2+} oscillations. To that end, we have extended a model for Ca^{2+} oscillations to incorporate the evolution of Ins1,4,5-P_3 and Ins1,3,4,5-P_4 concentrations. As a prototype, the kinetic constants associated with these new equations have been taken from experimental data in brain tissues. Thus, the two main differences between both Ins1,4,5-P_3 metabolizing enzymes appear to be their rates of Ins1,4,5-P_3 conversion as well as the level of stimulation of 3-kinase activity by the Ca^{2+}-CaM complex, much documented by *in vitro* studies (Takazawa *et al.*, 1988; 1989; 1990b; Communi *et al.*, 1997; Li *et al.*, 1989). Moreover, in mouse thymocytes, the rate of phosphorylation of Ins1,4,5-P_3 to Ins1,3,4,5-P_4 is increased 7 fold when the free Ca^{2+} in the lysate is increased from 0.1 to 1 μM (Zilberman *et al.*, 1987). The rate of phosphorylation of Ins1,4,5-P_3 to Ins1,3,4,5-P_4 has been also shown to be Ca^{2+}-sensitive in rat aortic smooth muscle (Rossier *et al.*, 1987). Finally, another indication that this stimulation effectively occurs in *vivo* conditions is corroborated by experiments on cytosolic extracts of *Xenopus* oocytes

reporting a 4 fold activation of 3-kinase activity upon increasing cytosolic Ca^{2+} concentration from less than 100 nM to more than 1μM (Sims and Allbritton, 1998).

However, it is clear that the present model is oversimplified at least in two respects. First, we have not considered any role for Ins1,3,4,5-P_4 in Ca^{2+} mobilization, in disagreement with experimental results in some cell types. Though, this simplified model proved to be sufficient to recover experimental observations and to make predictions on the basis of well-identified parameters and regulations. In addition, preliminary theoretical results indicate that, if Ins1,3,4,5-P_4 is supposed to act as a positive feedback on Ca^{2+} influx into the cytosol, 3-kinase overexpression has a much more pronounced effect on Ca^{2+} oscillations; in that case indeed, although the Ins1,4,5-P_3 level remains primarily controlled by the Ins1,4,5-P_3 5-phosphatase, Ins1,3,4,5-P_4 much affects the mean level of Ca^{2+} which becomes high and inhibits the Ins1,4,5-P_3 receptor when 3-kinase is overexpressed. Thus, preliminary simulations suggest that Ins1,4,5-P_3 3-kinase overexpression would have different effects depending on whether or not Ins1,3,4,5-P_4 stimulates Ca^{2+} entry.

The second simplification comes from the fact that we have neglected the spatial aspects concerning the distibution of enzymatic activities. De Smedt *et al.* (1997) have clearly shown that the intracellular distribution of Ins1,4,5-P_3 5-phosphatase plays a crucial role in the observed pattern of Ca^{2+} oscillations in cells overexpressing the latter enzyme. In particular, isoprenylation of the Ins1,4,5-P_3 5-phosphatase and its targeting to the plasma membrane (De Smedt *et al.*, 1996) appears to be important in that respect. Moreover, the competitive inhibition of Ins1,4,5-P_3 5-phosphatase by Ins1,3,4,5-P_4, which plays an important role as to decrease the effect of an overexpression of Ins1,4,5-P_3 3-kinase on Ca^{2+} oscillations in the present theoretical results, also depends on the respective localization of Ins1,4,5-P_3 and Ins1,3,4,5-P_4 production. However, the present theoretical study has allowed us to gain a different, complementary understanding of the role played by the Ins1,4,5-P_3 3-kinase and 5-phosphatase activities on Ca^{2+} oscillations, on the sole basis of their intrinsic, temporal enzymatic properties.

The most straighforward prediction of the model is that, due to the stimulation of Ins1,4,5-P_3 3-kinase activity by Ca^{2+}, Ca^{2+} oscillations are accompanied by in-phase, small amplitude oscillations in the levels of Ins1,4,5-P_3 and Ins1,3,4,5-P_4. Although the experimental confirmation would require further technical progress, some indications in favour of such an oscillatory level of messengers already exist (Harootunian *et al.*, 1991; Raha *et al.*, 1993; Hirose *et al.*, 1999; Nash *et al.*, 2001a; 2001b). Moreover, it should be mentioned that, theoretically, oscillations in Ins1,4,5-P_3 –due to various mechanisms– have been obtained in other models for Ca^{2+} oscillations (see, e.g. Schuster *et al.*, 2002 for review).

The model also predicts that the mean level of Ins1,4,5-P_3, and thereby the existence of Ca^{2+} oscillations and their frequency, is primarily controlled by the Ins1,4,5-P_3 5-phosphatase. In that respect, we recover experimental results over 3-kinase and 5-phosphatase overexpression in different cell types. In particular, the recent study by De Smedt *et al.* (1997) in which 3-kinase and 5-phosphatase have been overexpressed in cells wherein the pattern of Ca^{2+} oscillations was observed by fura-2 imaging, is very clear in showing that the temporal pattern of Ca^{2+} response is much more affected by 5-phosphatase overexpression than by 3-kinase overexpression. We predict, moreover, that this behaviour can be ascribed to a combined effect of dissimilar maximal velocities of these two enzymes and to 3-kinase stimulation by Ca^{2+}. This could be tested by overexpressing to different levels the various isoforms of Ins1,4,5-P_3 3-kinases and comparing their Ca^{2+} activities. Theoretical simulations can moreover provide a useful tool to predict how these two effects might counterbalance in various cells as well as to understand how the maximal velocities of both Ins1,4,5-P_3 3-kinase and 5-phosphatase reported in the different cell types can generate various modes of enzymatic control of the temporal pattern of Ca^{2+} oscillations.

II.4. Possible role of the modulation of $InsP_3$ 3-kinase activity by Ca^{2+} on Ca^{2+} oscillations : theoretical and experimental investigation in hepatocytes

II.4.1.Introduction

It has recently become possible to detect changes in $InsP_3$ levels in single cells (Hirose *et al.*, 1999; Nash *et al.*, 2001a and 2001b). The observation that Ca^{2+} and $InsP_3$ oscillate in synchrony suggests that feedbacks at the level of $InsP_3$ synthesis or/and catabolism might play a key role in the regulation of Ca^{2+} dynamics. As presented in sections II.2 and II.3., pathways of $InsP_3$ synthesis and degradation have been well characterized. To summarize (Fig. II.5), upon binding to its specific membrane receptor, the external stimulus (A) triggers the activation of receptor-associated G-proteins. This in turn stimulates a phospholipase C (PLC) which catalyses the hydrolysis of membrane-bound phosphatidyl inositol-4,5-bisphosphate (PIP_2) to form $InsP_3$ and diacylglycerol (DAG). Already at this level, $InsP_3$ oscillations could arise either through regulation of protein kinase C (PKC), a Ca^{2+}- and DAG-dependent kinase that could exert a negative feedback on the receptor-G protein complex (Woods *et al.*, 1987; Kummer *et al.*, 2000), or through a Ca^{2+}-stimulation of PLC activity (Meyer and Stryer, 1988; Harootunian *et al.*, 1991; Kummer *et al.*, 2000). Note that this effect does not seem to occur in hepatocytes (Renard *et al.*, 1987). These 2 mechanisms could generate $InsP_3$ oscillations due to negative or positive regulation of $InsP_3$ synthesis; Ca^{2+} oscillations would thus be driven by $InsP_3$ oscillations.

In contrast, if Ca^{2+} regulates $InsP_3$ catabolism, $InsP_3$ oscillations would follow Ca^{2+} oscillations, themselves produced by the above mentioned biphasic regulation of the $InsP_3R$. $InsP_3$ can be transformed either by Ins 1,4,5-P_3 5-phosphatase-mediated dephosphorylation to yield inositol 1,4 bisphosphate, or by Ins 1,4,5-P_3 3-kinase-mediated phosphorylation to yield inositol 1,3,4,5 tetrakisphosphate ($InsP_4$) (Shears, 1992). $InsP_4$ is also a substrate for 5-phosphatase and thus acts as a competitive inhibitor of the $InsP_3$ dephosphorylation. The binding of Ca^{2+}/calmodulin (CaM) to the 3-kinase enhances its activity at variable extents: the A isoform of the enzyme is stimulated 2- to 3 fold by Ca^{2+}/CaM, whereas the B isoform is stimulated up to 10 fold (Takazawa *et al.*, 1990a; Sims and Allbritton, 1998b).

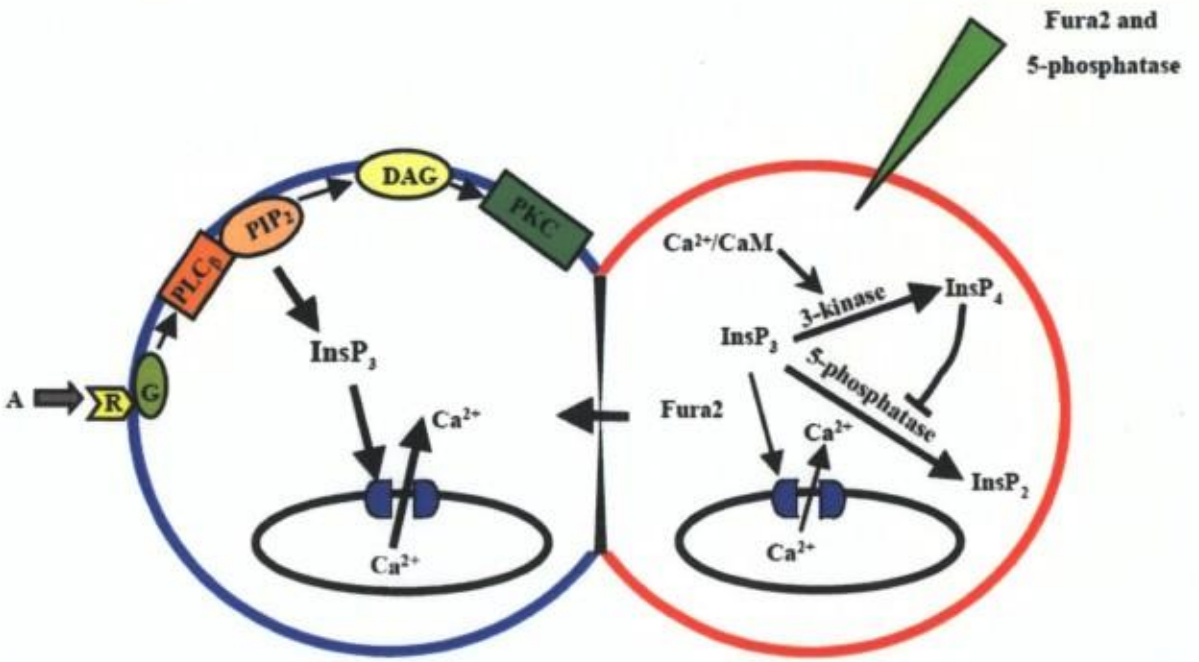

Fig. II.5. Schematic representation of the intracellular Ca^{2+} dynamics and of the $InsP_3$ signalling pathway in a doublet of connected hepatocytes.

Mathematical modelling (Kummer *et al.*, 2000; Dupont and Erneux, 1997; Mishra and Bhalla, 2002) has confirmed the intuitive prediction that this well-characterized Ca^{2+} stimulation of $InsP_3$ catabolism can generate $InsP_3$ oscillations. However, the physiological significance of these $InsP_3$ oscillations can be questioned. Basically, one could conceive 2 effects of these catabolism-induced $InsP_3$ oscillations. First, an active role of these oscillations in the pacemaker mechanism of Ca^{2+} oscillations is suggested by studies performed in hepatocytes (Chatton *et al.*, 1998) and smooth muscle cells (Fink *et al.*, 1999). It is there shown that the Ca^{2+} signal following uncaging of poorly-metabolized $InsP_3$ analogs decays more slowly than the signal following $InsP_3$ uncaging. The interpretation of Fink *et al.* (1999) is that $InsP_3$ degradation is a prerequisite for Ca^{2+} recovery. The control of $InsP_3$ removal by a Ca^{2+}-stimulated 3-kinase would provide an ideal mechanism to fulfill this requirement. Second, even if $InsP_3$ oscillations are not required for Ca^{2+} oscillations, one could argue that the enhanced degradation of $InsP_3$ following a Ca^{2+} spike plays a role in determining the relatively low frequency of Ca^{2+} oscillations, which cannot be explained on the basis of the kinetic properties of the $InsP_3R$ (Dupont and Swillens, 1996). In this view, each Ca^{2+} spike would provoke a decrease in $InsP_3$ so that the level of this messenger becomes too low to allow Ca^{2+} release through the $InsP_3R$. Consequently, the long period would correspond to the time necessary to rebuild the level of $InsP_3$ necessary to activate Ca^{2+} release through the receptor.

In the following (Dupont *et al.*, 2003c), we eliminate both hypotheses and show that the Ca^{2+}-controlled catabolism of $InsP_3$ does not play any significant role in the triggering of Ca^{2+} oscillations in hepatocytes nor in their characteristics.

II.4.2. Material and Method

Preparation of hepatocytes

Isolated rat hepatocytes were prepared from fed female Wistar rats by limited collagenase (from Boehringher) digestion of rat liver, as previously described (Combettes *et al.*, 1994). In these conditions, about 20% cells were associated by two (doublet) or three (triplet) and were distinguished from aggregates of non-connected cells in conventional light microscopy by screening for dilated bile canaliculi, indicators of maintained functional polarity [26]. After isolation, rat hepatocytes were maintained (5.10^5 cells/ml) at 4 °C in Williams' medium E (GIBCO) supplemented with 10% foetal calf serum, penicillin (100,000 units/ml) and streptomycin (100 μg/ml). Cell viability, assessed by trypan blue exclusion, remained greater than 96%, during 4 to 5 hours.

Measurement of intracellular Ca^{2+} in individual cells

Loading of hepatocytes with fura2

Hepatocytes were loaded with fura2 (Molecular Probes Inc.) by injection (see below). Small aliquots of the suspended hepatocytes ($5x10^5$ cells) were diluted in 2 ml of Williams' medium E modified as described above, then plated onto dish glass coverslips coated with collagen I, and incubated for 60 minutes at 37°C under an atmosphere containing 5% CO_2. After cell plating, the coverslips were then washed twice with a saline solution (20 mM HEPES, 116 mM NaCl, 5.4 mM KCl, 1.8 mM $CaCl_2$, 0.8 mM $MgCl_2$, 0.96 mM NaH_2PO_4, 5 mM $NaHCO_3$, and glucose 1g/l, pH 7.4). Dish coverslips were put onto a thermostated holder (36°C) on the stage of a Zeiss Axiovert 35 microscope set up for epifluorescence microscopy.

Microinjection

Microinjection was performed using an Eppendorf microinjector (5242), as described previously (Combettes *et al.*, 1994). Micropipettes with an internal tip diameter of 0.5 μm (Femtotips, Eppendorf) were filled with test agents together with 5 mM fura2 in a buffer solution containing 100 mM KCl, 20 mM NaCl, 10 mM Hepes adjusted to pH 7.1. After microinjection, cells were allowed to recover for at

least 10 minutes. The success of microinjection was assessed by monitoring the morphology of cells before and after manipulation and checking the ability of the cell to retain injected fura2 and low $[Ca^{2+}]_i$. Purification and determination of activity of the recombinant type I $InsP_3$ 5-phosphatase (19μmol/min/ml in this study) was performed as described previously (Tordjmann *et al.*, 2000; Dupont *et al.*, 2000a). $InsP_3$ 5-phosphatase was inactivated at 90°C for 20 minutes. Cells were microinjected either with inactivated $InsP_3$ 5-phosphatase or with $InsP_3$ 5-phosphatase (activity : 120nmol/min/ml in the pipette) as described above.
Ca^{2+} imaging was as described previously (Tordjmann *et al.*, 1997).

II.4.3. Theoretical prediction as to the role of the Ca^{2+}-stimulated $InsP_3$ catabolism

The model for Ca^{2+} oscillations (section II.2; Dupont and Swillens, 1996; Dupont and Erneux, 1997) relies on the biphasic regulation of the $InsP_3R$ by Ca^{2+}, with $InsP_3$ synthesized at a constant rate (proportional to the level of stimulation) and degraded by both 3-kinase and 5-phosphatase. The 3-kinase is stimulated by Ca^{2+}, and its product, $InsP_4$ competes with $InsP_3$ for 5-phosphatase (Fig. II.5). When the concentration of agonist (and thus of $InsP_3$) increases, cells typically display: (1) low constant levels of Ca^{2+}, (2) sustained Ca^{2+} oscillations, the frequency of which increases with the agonist concentration and (3) high sustained levels of Ca^{2+}.

Numerical simulations also show that the level of $InsP_3$ oscillates in phase with Ca^{2+} (Fig. II.6.A). As these oscillations rely on the Ca^{2+}-stimulation of $InsP_3$ catabolism by 3-kinase, it can be expected that their amplitude would be much reduced if the relative importance of the other degradation pathway was increased. Thus, we simulated the effect of 5-phosphatase injection and assumed that the concentration of this enzyme is increased by a factor of 25. If all the other parameters of the model are kept constant, oscillations are abolished and a low constant level of Ca^{2+} is predicted, consistent with the observed reduction in the level of $InsP_3$ (Fig. II.6.B). If the external stimulation is then increased, Ca^{2+} oscillations are recovered, but now occur in the presence of a nearly constant level of $InsP_3$ (Fig. II.6.C). In this case, the average activity of the phosphatase exceeds that of the kinase by a factor of 30, while both activities were roughly the same in the normal situation corresponding to Fig. II.6.A.

Interestingly, these results predict that the characteristics of the repetitive Ca^{2+} spikes (shape, amplitude and order of magnitude of the period) remain similar to those obtained in response to sub-maximal stimulation of a cell that was not supposed to be injected with the enzyme. Thus, the model suggests that $InsP_3$ oscillations driven by Ca^{2+}-activated $InsP_3$ degradation are not essential for $InsP_3$-induced Ca^{2+} oscillations. Detailed examination of the behavior of the model shows that this lack of effect is due to (1) receptor inactivation being much faster than $InsP_3$ removal, and (2) minimal levels of $InsP_3$ during the course of oscillations being still above the threshold required for an oscillatory behavior.

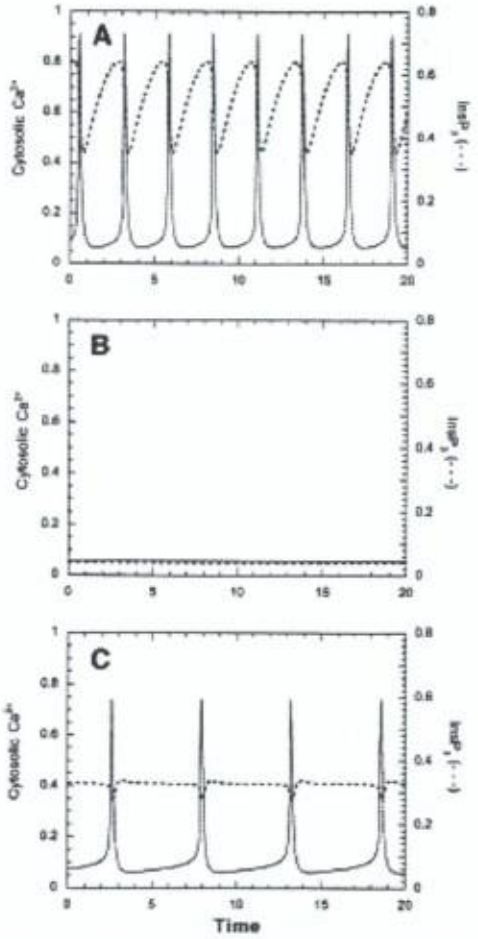

Fig. II.6 Theoretical prediction as to the possible role of the Ca^{2+}-stimulated $InsP_3$ catabolism. Panel A: oscillations of Ca^{2+} *and* $InsP_3$ in a cell stimulated with a submaximal dose of agonist. Panel B: the amount of 5-phosphatase in the simulated cell has been multiplied by 25 as compared to its value in A. Panel C: Ca^{2+} oscillations can reappear if the cell is stimulated with a high dose of agonist.

Curves have been obtained by numerical simulations of the model definded by eqs. (I.5)-(I.8), (II.1), (II.2) with: K_{act}= 0.5 μM, n_a=3, K_{inh}=0.17μM, n_i=4, k=0.5 s^{-1}, k_1=2.57 s^{-1}, b=0.0007 s^{-1}, K_{IP}=1μM, V_{MP}=6 μMs^{-1}, K_p=0.35 μM , α=0.1, Catot=80 μM, V_{PLC}=4 μMs^{-1}, V_k=5 μMs^{-1}, K_k=1 μM, K_d=0.3 μM, n_d=2. For panel A: γ=0.12, V_{p1}=5 μMs^{-1}, V_{p2}=0.2 μMs^{-1}, for panel B: γ=0.12, V_{p1}=125 μMs^{-1}, V_{p2}=5 μMs^{-1}, and for panel C: γ=1, V_{p1}=125 μMs^{-1}, V_{p2}=5 μMs^{-1}. These parameters only aim at qualitatively representing the situation encountered in hepatocytes, as most parameters are experimentally unknown. Scales are in seconds and μM.

II.4.4. Experimental results: effect of injecting $InsP_3$ 5-phosphatase into one cell of an hepatocyte doublet

In liver, hepatocytes are tightly coupled by gap junctions (Spray *et al.*, 1994). Ca^{2+} increases induced by agonists activating the $InsP_3$ cascade, such as vasopressin or noradrenaline, are highly coordinated within multiplets when gap junctions are functional (e.g. Fig. II.7.A and see (Tordjmann *et al.*, 2000) for review). Previous work suggests that calcium spikes are coordinated by the diffusion of small amounts of $InsP_3$ between cells that slightly differ in their sensitivity to the hormonal stimulus (Dupont *et al.*, 2000a) (but see also (Höfer, 1999)).

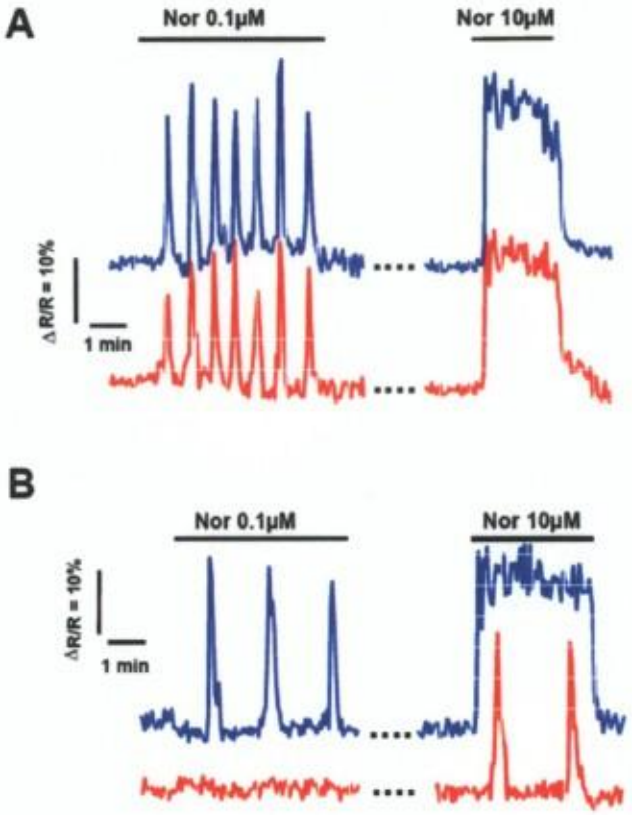

Fig. II.7. Effect of 5-phosphatase on $InsP_3$ dependent agonists induced $[Ca^{2+}]_i$ oscillations. One cell of the doublet (indicated in red) was microinjected with Fura2 and either with inactivate (A) or active $InsP_3$ 5-phosphatase (B). Then, hepatocytes doublets were challenged with noradrenaline (Nor, 0.1µM or 10 μM) for the time shown by the horizontal bar. Results are representative of those obtained using 4 (A) and 5 (B) doublets. For technical convenience, tracings were interrupted (the gap represents 3 minutes).

The fact that these coupled cells show very similar Ca^{2+} oscillations provides an ideal tool to evaluate the role of $InsP_3$ metabolism in the regulation of Ca^{2+} dynamics (see Fig. II.5 for a schematic representation of the experiments). Indeed, injection of an enzyme that acts specifically on $InsP_3$ catabolism in the injected cell but cannot diffuse through gap junctions makes it possible to observe the effect of $InsP_3$ metabolism on Ca^{2+} oscillations, while the non-injected cell provides a natural control for unperturbed Ca^{2+} oscillations. Moreover, 3-kinase B has been isolated from rat hepatocytes (Thomas *et al.*, 1994) and shown to be stimulated by Ca^{2+} (Biden *et al.*, 1988), while the activity of $InsP_3$ 5-phosphatase has been shown to be unaffected by changes in $[Ca^{2+}]$ in this cell type (Conigrave *et al.*, 1992). Thus, we have injected Type I $InsP_3$ 5-phosphatase in only one cell of hepatocyte doublets. This isoform is the most widespread of $InsP_3$ 5-phosphatases and it is not stimulated by Ca^{2+} (Verjans *et al.*, 1994a).

Together with $InsP_3$ 5-phosphatase, fura2 was microinjected; diffusion of this dye via gap junctions revealed that the two cells were indeed coupled. As shown in Fig. II.7.A, control injection in one cell of $InsP_3$ 5-phosphatase that had been previously inactivated did not result in any difference between the two cells as regards noradrenaline induced Ca^{2+} oscillations. The two cells showed similar Ca^{2+} responses both at low (0.1μM) and maximal (10μM) noradrenaline concentration. In contrast, Ca^{2+} signals in the two cells were different when active $InsP_3$ 5-phosphatase had been injected into one cell of the doublet, whatever the concentration of the agonist (Fig. II.7.B), consistent with the reduction of the $InsP_3$ concentration in the injected cell anticipated by the model (Fig. II.6.B).

In contrast, at supra-maximal concentrations of noradrenaline (10 μM), the non-injected cell shows a high sustained level of Ca^{2+}, reflecting a very high level of $InsP_3$, but the injected cell displays low-frequency Ca^{2+} oscillations, typical of an intermediate level of $InsP_3$ (Fig. II.7.B, right panel). Thus, as predicted by the model (Fig. II.6.C), an hepatocyte that has been made silent by injection of 5-phosphatase can become responsive again by increasing the concentration of the agonist. The critical observation is that oscillatory Ca^{2+} signals can be observed at high enough agonist concentrations, despite the massive Ca^{2+}-independent $InsP_3$ catabolism induced by the injection of 5-phosphatase.

II.4.5. Discussion

The present results show that, although $InsP_3$ oscillations probably arise in intact cells due to the stimulation of 3-kinase activity by Ca^{2+}, these oscillations do not play a predominant role neither in the triggering nor in the main characterisitcs of Ca^{2+} oscillations. However, they do not exclude the possibility that $InsP_3$ oscillations generated by another mechanism, for example by a PKC-mediated feedback at the level of the receptor-coupled G-protein, might play a crucial role for hepatic Ca^{2+} oscillations (Kummer *et al.*, 2000). Yet the observation (Hajnoczky and Thomas, 1997) that $InsP_3$-dependent cycles of Ca^{2+} release and re-uptake can be reproduced in permeabilized hepatocytes with $InsP_3$ clamped at submaximal concentration, suggests that the Ca^{2+} feedback on the $InsP_3R$ might well be the central oscillatory mechanism in this cell type. This suggestion is corroborated in a more indirect manner by 2 other studies. The first one shows that type 2 $InsP_3R$, which is the most abundant in hepatocytes (Wojcikiewicz, 1995), is required for the normal Ca^{2+} oscillations, while types 1 and 3 do not sustain Ca^{2+} oscillations on their own (Miyakawa *et al.*, 1999). Although both type 1 and type 2 display a bell-shaped dependence on Ca^{2+}, type 2 is known to be more sensitive to cytosolic Ca^{2+}, which may explain its observed predominant role in the generation of Ca^{2+} oscillations (see also Chapter III). The other study also strongly suggests that the $InsP_3R$ is the driving force of Ca^{2+} oscillations: it shows that Ca^{2+} oscillations (but not Ca^{2+} release) are abolished in DT40 cells in which the sensitivity of the $InsP_3Rs$ to cytosolic Ca^{2+} has been decreased by substitution of the appropriate residues (Miyakawa *et al.*, 2001).

Nevertheless, even in the hypothesis of a primary role of the $InsP_3R$ in the generation of Ca^{2+} oscillations, the origin of the long periods observed in hepatocytes and other cells still remains unsolved. The present study demonstrates that the clue for these long periods can probably not be found in the Ca^{2+}-dependence of $InsP_3$ catabolism, and thus emphasizes the necessity for investigating alternative mechanisms.

II.5. Complex Ca^{2+} oscillations originating from the self-modulation of the inositol 1,4,5-trisphosphate signal

II.5.1. Introduction

In some cell types, particularly in hepatocytes, complex Ca^{2+} oscillations reminiscent of the bursting-like behavior displayed by many electrically excitable cells have been observed in response to stimulation by specific agonists (Green *et al.*, 1993; Marrero *et al.*, 1994). As these cells are not electrically excitable, it is likely that these complex Ca^{2+} oscillations rely on the interplay between two intracellular mechanisms capable of destabilizing the steady state. Some theoretical models have been proposed to account for such complex Ca^{2+} oscillations (Chay *et al.*, 1995; Shen and Larter, 1995; Borghans *et al.*, 1997). Among these models, the one based on the interplay between CICR at the level of the $InsP_3$ receptor and the Ca^{2+}-stimulated $InsP_3$ degradation (Borghans *et al.*, 1997) appears to be of particular interest. First, this model is based on the well-characterized stimulation by Ca^{2+} of the activity of inositol 1,4,5-trisphosphate 3-kinase, one of the $InsP_3$ metabolizing enzymes (Takazawa *et al.*, 1989; Takazawa *et al.*, 1990a). Second, this model can generate a large variety of dynamical

behaviors, including deterministic chaos and Ca^{2+} oscillations of the bursting type that much resemble experimental observations (see Figs. 1 and 8 of Borghans *et al.* (1997) for a comparison between experimental and theoretical oscillations).

II.5.2. Simple model for Ca^{2+} oscillations involving Ca^{2+}-activated $InsP_3$ degradation

The model used in the present study (Houart *et al.*, 1999) is an extension of the minimal model proposed by Dupont and Goldbeter (1993) to account for the existence of simple Ca^{2+} oscillations in response to extracellular stimulation. The original model only involves two variables, namely cytosolic and intravesicular Ca^{2+} concentrations. The release of Ca^{2+} from the internal stores into the cytosol is activated by $InsP_3$ and cytosolic Ca^{2+}; such an autocatalytic process of $InsP_3$-sensitive CICR is at the core of the oscillatory mechanism. Oscillations of Ca^{2+} in this basic model do not require and are not accompanied by a periodic variation in $InsP_3$, in agreement with observations which show that repetitive Ca^{2+} spikes may occur in the presence of a constant level of $InsP_3$ (Wakui *et al.*, 1990; Berridge, 1993). However, although it is highly plausible that CICR is the primary oscillatory mechanism, the concentration of $InsP_3$ most probably evolves non-monotonously in the course of time. $InsP_3$, which is a second messenger, is synthesized by phospholipase C (PLC) in response to external stimulation and metabolized into $InsP_2$ by a 5-phosphatase and into $InsP_4$ by a 3-kinase (Takazawa *et al.*, 1990a; Berridge, 1993). An oscillatory variation of $InsP_3$ could result from the control of any of these three enzymes by Ca^{2+}. In support of such a possibility, some experiments report that the activity of PLC is stimulated by Ca^{2+} (Renard *et al.*, 1987); the activation of the 3-kinase by Ca^{2+} is even better documented (Takazawa *et al.*, 1989; Takazawa *et al.*, 1990a).

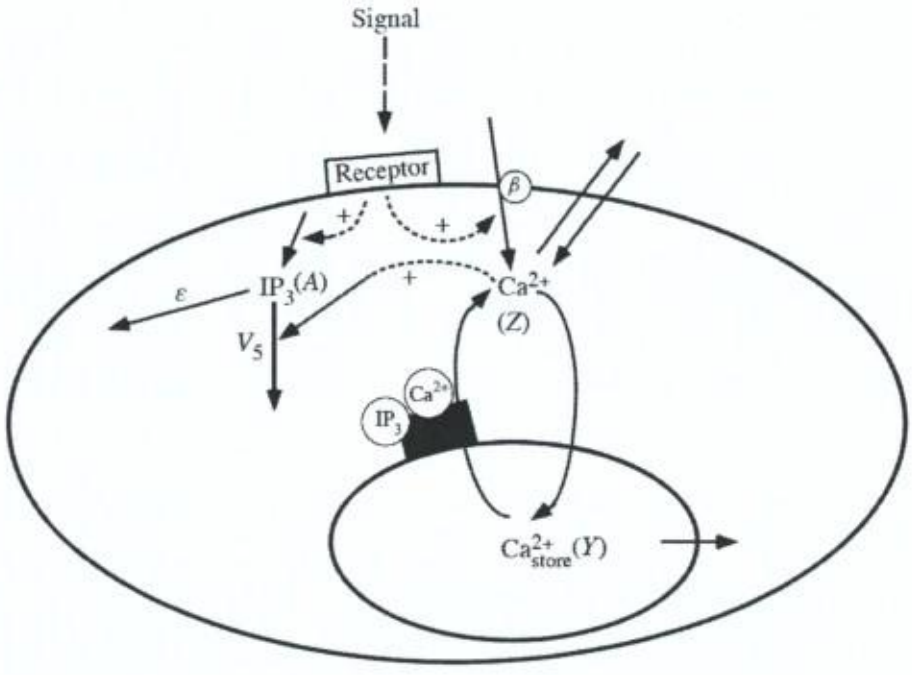

Fig. II.8. Schematic representation of the model based on the interplay between CICR and the Ca^{2+}-stimulated degradation of $InsP_3$ (see text for details). Besides simple periodic oscillations, this model can produce complex Ca^{2+} oscillations including bursting, chaos, quasiperiodic behavior, as well as birhythmicity.

Stimulation of PLC activity by Ca^{2+} has been taken into account in some theoretical models (Meyer and Stryer, 1988; Keizer and De Young, 1992; Shen and Larter, 1995). One of these models (Shen and Larter, 1995) can exhibit bursting-type oscillations (also called mixed-mode oscillations) as well as

chaos; the level of cytosolic Ca^{2+} returns in both cases to its basal value between successive Ca^{2+} spikes. Such a temporal pattern does not resemble the behavior seen in hepatocytes stimulated by various agonists such as cAMP (Capiod *et al.*, 1991), taurolithocholate 3-sulfate (Marrero *et al.*, 1994), diadenosine 5',5'''-P^1P^4-tetraphosphate (Green *et al.*, 1993), ATP or both ATP and cAMP (Dixon *et al.*, 1993, 1995; Green *et al.*, 1994). With these agonists, bursting in hepatocytes takes the form of a switch between a silent phase and an active phase made of small-amplitude Ca^{2+} oscillations around an elevated Ca^{2+} level. The latter type of complex oscillations can be obtained in numerical simulations when extending the model based on CICR to take into account the stimulation of $InsP_3$ 3-kinase activity by the Ca^{2+}/calmodulin complex, as shown by Borghans *et al.* (1997). The present paper aims at investigating in further detail the occurrence of complex oscillations in this extended model, which also incorporates Ca^{2+} pumping into the stores, Ca^{2+} exchange with the external medium, as well as stimulus-activated Ca^{2+} entry (Dupont and Goldbeter, 1993; Borghans *et al.*, 1997).

The model, schematized in Fig. II.8, contains three variables, namely the concentrations of free Ca^{2+} in the cytosol (Z) and in the internal pool (Y), and the $InsP_3$ concentration (A). The time evolution of these variables is governed by the following ordinary differential equations:

$$\frac{dZ}{dt} = V_{in} - V_2 + V_3 + k_f Y - kZ \tag{II.3}$$

$$\frac{dY}{dt} = V_2 - V_3 - k_f Y \tag{II.4}$$

$$\frac{dA}{dt} = \beta V_4 - V_5 - \varepsilon A \tag{II.5}$$

where

$$V_{in} = V_0 + V_1 \beta \tag{II.6}$$

$$V_2 = V_{M2} \frac{Z^2}{K_2^2 + Z^2} \tag{II.7}$$

$$V_3 = V_{M3} \frac{Z^m}{K_Z^m + Z^m} \frac{Y^2}{K_Y^2 + Y^2} \frac{A^4}{K_A^4 + A^4} \tag{II.8}$$

$$V_5 = V_{M5} \frac{A^p}{K_5^p + A^p} \frac{Z^n}{K_d^n + Z^n} \tag{II.9}$$

Equations (II.3)-(II.4) are the same as in the original one-pool model (see Table I.2). In contrast to the model used in sections (II.3)-(II.4), $InsP_3$ metabolism is considered in a simplified manner. The fact that the 3-kinase is stimulated by Ca^{2+} is taken into account through a term of the Hill form, with a threshold Ca^{2+} level equal to K_d. That $InsP_3$ can also be metabolized in a Ca^{2+}-independent manner by the 5-phosphatase is reflected by the term $-\varepsilon A$, which can be assumed to be of the first-order given that the latter enzyme has a low affinity for its substrate, of the order of 10 μM (Verjans *et al.*, 1992). This term is significant when the level of cytosolic Ca^{2+} is very low, i.e. when the term V_5 becomes negligible in equation (II.5). Equations (II.7)-(II.9) allow for cooperativity in the kinetics of Ca^{2+} release, Ca^{2+} pumping and $InsP_3$ phosphorylation by the 3-kinase; m, n and p are Hill coefficients related to these cooperative processes. Experimental evidence indicates that the 3-kinase behaves as a Michaelian enzyme with respect to its substrate $InsP_3$, hence p=1 (Takazawa *et al.*, 1989). The results indicate that complex oscillations, including chaos, can occur both in the presence (p>1) or absence (p=1) of cooperativity in the kinetics of 3-kinase.

II.5.3. Dependence of the frequency of simple periodic Ca^{2+} oscillations on the degree of stimulation

Intracellular Ca^{2+} oscillations take the form of abrupt spikes, sometimes preceded by a gradual increase in cytosolic Ca^{2+}. They only occur in a range bounded by two critical values of the stimulation level, with the frequency of the spikes increasing with the intensity of the stimulus. These properties are well accounted for by the model, as illustrated in Fig II.9. Panel (a) shows typical Ca^{2+} oscillations generated by the model. Here, in contrast to the original model (Dupont and Goldbeter, 1993), these oscillations are necessarily accompanied by periodic variations in the level of $InsP_3$. As can be expected from the regulations considered, the peak in $InsP_3$ slightly precedes the peak in cytosolic Ca^{2+}. The bifurcation diagram (panel b) shows the steady state value of cytosolic Ca^{2+} (Z), when it is stable, or the maxima and minima reached during oscillations when it is unstable. As in the minimal model for Ca^{2+} oscillations (Dupont and Goldbeter, 1993), the steady state value of cytosolic Ca^{2+} increases with the level of stimulation, β, and the amplitude of the oscillations remains practically constant over the whole oscillatory domain bounded by two supercritical Hopf bifurcation points. The frequency of oscillations increases with the level of external stimulation (panel c).

The relationship between the level of stimulation and the frequency of Ca^{2+} oscillations shown in Fig. II.9 (panel c) is in good qualitative agreement with experimental observations. However, numerical simulations of the model defined by equations (II.3)-(II.9) show that this is not always the case. For example, depending on the maximal rate of phosphorylation of $InsP_3$ by the 3-kinase (V_{M5}), we observe that the frequency of the oscillations increases monotonously with the degree of stimulation β (as in Fig. II.9 and in Fig. II.10, curve a, where the value of V_{M5} is small) or may pass through a minimum as a function of β (as in Fig. II.10, curve b, in which V_{M5} is larger). In the model, increasing the level of stimulation triggers a rise first in the rate of synthesis and then in the rate of degradation of $InsP_3$ (due to the enhanced stimulation of the 3-kinase by Ca^{2+}). This explains why, depending on relative parameter values, qualitatively distinct relationships between the degree of stimulation and the frequency of Ca^{2+} oscillations can be obtained.

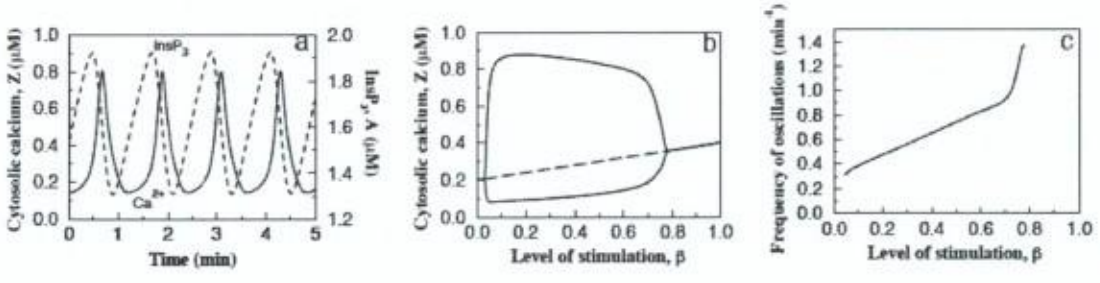

Fig. II.9. Simple oscillations of Ca^{2+} and $InsP_3$ in the model based on the interplay between CICR and the Ca^{2+}-stimulated degradation of $InsP_3$. Panel (a) shows the temporal evolution of the concentrations of cytosolic calcium (Z, solid line) and $InsP_3$ (A, dashed line). They have been obtained by numerical integration of the model defined by eqns. (II.3)-(II.9) with the following parameter values: β=0.6, ε=0.1min^{-1}, k=10min^{-1}, K_2=0.1μM, K_A=0.2μM, K_d=0.4μM, k_f=1min^{-1}, K_5=1μM, K_Y=0.2μM, K_Z=0.5μM, V_0=V_1=2μM/min, V_{M5}=5μM/min, V_{M2}=6μM/min, V_{M3}=20μM/min, V_4=2μM/min, m=p=2, n=4. Panel (b) shows the bifurcation diagram giving the steady state (stable or unstable) and the envelope of the oscillations in Z as a function of β for the same set of parameter values. Panel (c) shows the relationship between the frequency of Ca^{2+} oscillations and the level of stimulation in the same conditions.

These different relationships are illustrated in Fig. II.10, for distinct values of parameter V_{M5} which represents the maximum rate of $InsP_3$ degradation by 3-kinase. For high values of V_{M5} (curve b), the latter enzyme significantly regulates the level of $InsP_3$ which does not vary much with the level of stimulation (β). The Ca^{2+} concentration indeed rises as a function of β, and thus $InsP_3$ metabolism is

enhanced (through the activation of $InsP_3$ 3-kinase). Thus, at the beginning of the oscillatory domain, the increase in cytosolic Ca^{2+} due to the rise in β produces a slight decrease in $InsP_3$: the rate of Ca^{2+} release then decreases as β rises and, as a consequence, the frequency decreases. Beyond β=0.16, however, a switch occurs: the synthesis of $InsP_3$ rises more with β than the Ca^{2+}-induced degradation of $InsP_3$, so that the frequency of oscillations rises as β increases. For another set of parameter values, the frequency can even decrease in the entirety of the oscillatory domain as the level of stimulation increases (data not shown). In contrast, for lower values of V_{M5} (curve a), the rate of $InsP_3$ synthesis by PLC exceeds the activity of 3-kinase in the whole oscillatory domain. Thus, even at low stimulation level, the frequency always increases with β, in agreement with experimental observations. As an inverse relationship between the frequency of Ca^{2+} oscillations and the level of stimulation has never been experimentally reported, the present theoretical results suggest that Ca^{2+} oscillations are not primarily affected by variations in the level of $InsP_3$ due to the stimulation of 3-kinase activity by Ca^{2+}. This result corroborates the view that in most cell types (except some cells like hippocampal neurons – see Mailleux *et al.*, 1991), in physiological conditions, $InsP_3$ metabolism is mainly carried out by the $InsP_3$ 5-phosphatase - the action of which is reflected by the term $-\varepsilon A$ in equation (II.5) - because of the high maximum activity of this enzyme relative to that of the 3-kinase (De Smedt *et al.*, 1997; Dupont and Erneux, 1997). The present results suggest, however, that unusual relationships between the level of stimulation and the frequency of Ca^{2+} oscillations could be observed in cells overexpressing $InsP_3$ 3-kinase.

II.5.4. Complex Ca^{2+} oscillations: bursting, quasiperiodicity and chaos

Although simple Ca^{2+} oscillations resembling those shown in Fig. II.9 are usually observed in response to external stimulation, complex oscillations have also been reported in experiments performed with hepatocytes responding to a variety of agonists (Green *et al.*, 1993; Marrero *et al.*, 1994). A detailed investigation of the dynamic behavior of the model in parameter space allowed us to uncover regions of complex Ca^{2+} oscillations, including bursting, chaos and quasiperiodicity. Three sets of parameter values corresponding to these modes of complex oscillatory behavior are listed in Table II.2.

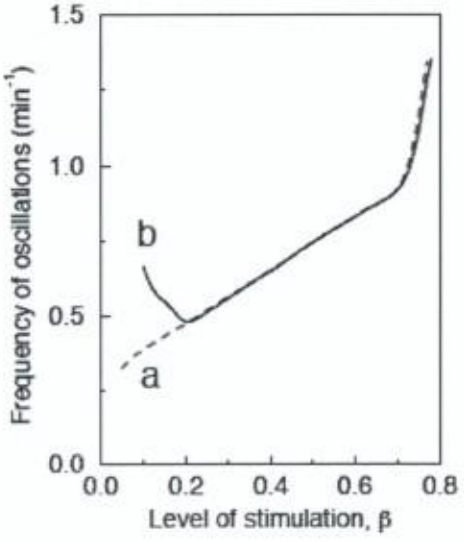

Fig. II.10 Different relationships between the frequency of Ca^{2+} oscillations and the level of stimulation in the model based on the interplay between CICR and the Ca^{2+}-stimulated degradation of $InsP_3$. Parameter values are the same as in Fig. II.9, except for V_{M5} which is equal to 5μM/min in (a) – as in Fig. II.9c - and 15μM/min in (b).

The different types of oscillations are illustrated in Fig. II.11, both as a function of time (left column) and in the phase space (right column). For oscillations of the bursting type, a large-amplitude Ca^{2+} spike is followed by smaller Ca^{2+} variations around a plateau level (Fig. II.11.a). The corresponding attractor is plotted in Fig. II.11.d. After a first, large Ca^{2+} spike, $InsP_3$ is metabolized by the 3-kinase which has been massively activated by Ca^{2+}; enough $InsP_3$, however, remains to allow for some repetitive Ca^{2+}-releasing activity through CICR, producing small-amplitude spikes, up to a point where the levels of cytosolic and intravesicular Ca^{2+} are both too low to activate Ca^{2+} release.

As illustrated in Fig. II.11, aperiodic, chaotic oscillations are usually of reduced amplitude and never undergo large excursions in the phase space (see Fig. II.11e), as compared to the case of bursting (Fig. II.11a,d). The irregularity of the oscillations shows up both in the amplitude and in the time interval between successive Ca^{2+} spikes. From a practical point of view, these intrinsically irregular oscillations might be hard to distinguish from a noisy experimental record of low-amplitude periodic Ca^{2+} oscillations. In this respect, it is of interest that an analysis of experimentally obtained time series of Ca^{2+} oscillations showed that in some cases the Ca^{2+} dynamics can be casted into low-dimensional chaos (Strizhak *et al.*, 1995). A typical strange attractor corresponding to the chaotic dynamics of Fig. II.11b is shown in Fig. II.11e. Finally, Fig. II.11c shows an example of quasiperiodic oscillations obtained with the model. Such a kind of oscillatory behavior, characterized by the existence of multiple frequencies (Bergé *et al.*, 1984), has been less often reported for biochemical systems. Although the time series much resemble the chaotic one, quasiperiodicity is easily recognizable in phase space in which all trajectories are concentrated on a torus (Fig. II.11f).

The domains in which the various modes of complex oscillatory behavior occur in the model are illustrated in Fig. II.12 by the stability diagrams established as a function of parameters ε and β which measure, respectively, the degradation of $InsP_3$ by the 5-phosphatase and the degree of cell stimulation. The three panels (a)-(c) correspond to the three sets of parameter values listed in Table II.2. In panel (a), a domain of bursting is nested within the domain of simple periodic behavior. In panel (b), a small domain of quasiperiodicity is nested within a domain of simple periodic oscillations. In panel (c), multiple nested domains are found in which, from the center to the periphery, simple periodic oscillations exhibiting a small shoulder (see thin curve in the left panel of Fig. II.15) are followed, successively, by birhythmicity, chaos, period-doublings, simple periodic oscillations, and stable steady states.

In the next section, we will discuss from a dynamical point of view the origin of these various modes of complex oscillatory behavior. To this end, we have chosen to use the particular sets of parameter values listed in Table II.2 for each mode of complex oscillations, keeping β free to vary as bifurcation parameter.

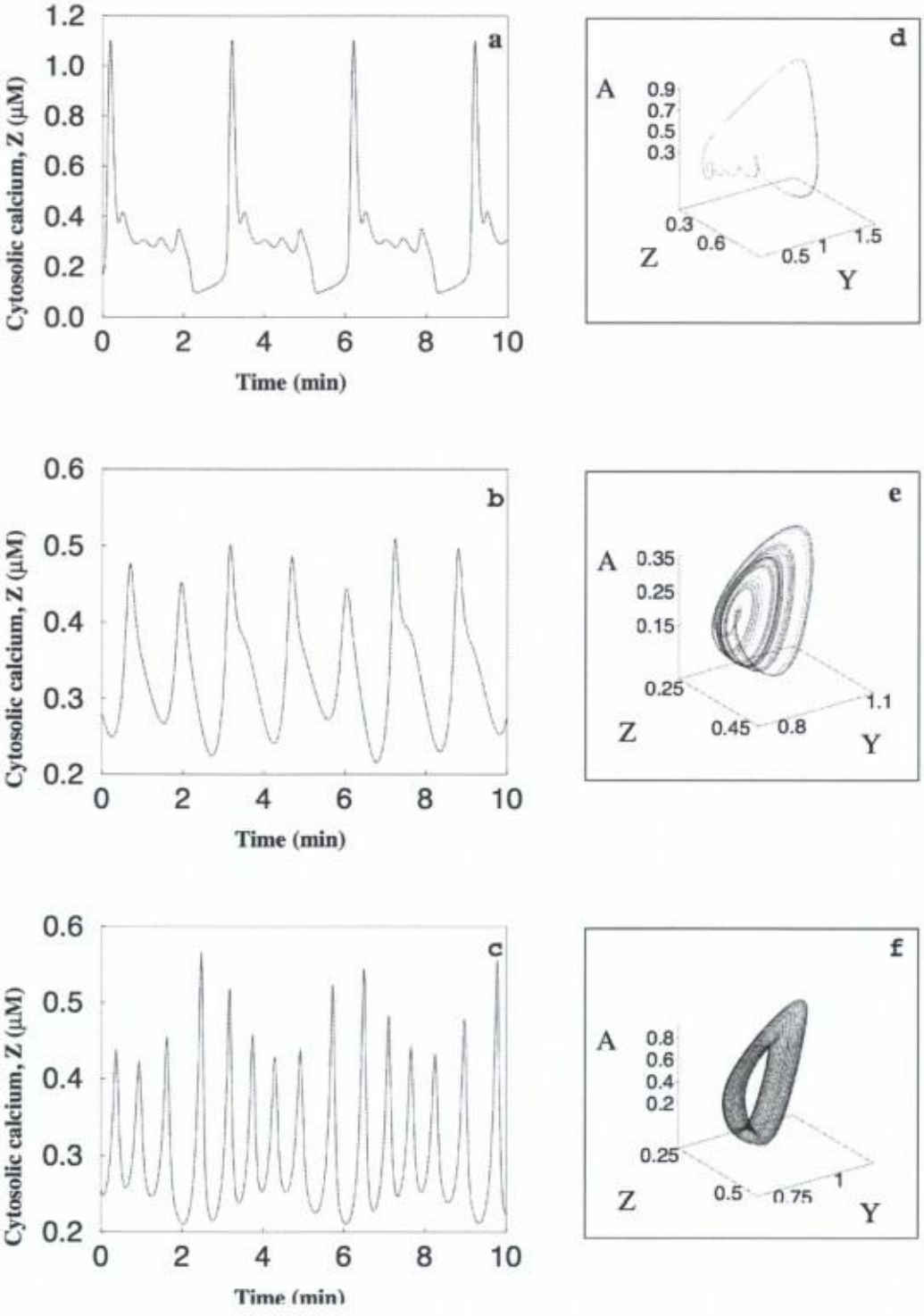

Fig. II.11. Various types of complex Ca^{2+} oscillations that can be obtained in the model based on the interplay between CICR and the Ca^{2+}-stimulated degradation of $InsP_3$. From top to bottom, these complex behaviors correspond to bursting, chaos and quasiperiodicity. The panels on the left show the evolution of cytosolic Ca^{2+} concentration while the right panels show the corresponding attractors in the phase space. Results have been obtained by numerical integration of the model defined by eqns. (II.3)-(II.9) for the three sets of parameter values listed in Table II.2, where the first column refers to panels (a) and (d), the second column to panels (b) and (e), and the third column to panels (c) and (f).

II.5.5. Bifurcation diagrams for the three types of complex oscillations

Bursting

Fig. II.13 shows a typical bifurcation diagram illustrating the origin of bursting in the model based on the interplay between CICR and Ca^{2+}-stimulated degradation of $InsP_3$. This bifurcation diagram represents a horizontal section (dashed line) through the diagram of Fig. II.12a. The level of stimulation, β, is considered as the most relevant bifurcation parameter since it is more readily amenable to experimental manipulation. Shown are the steady state, if stable, and the maxima and minima of cytosolic Ca^{2+} (Z) reached during oscillations when the steady state is unstable. The first limit cycle arises through a Hopf bifurcation at β=0.153 and loses its stability at β=0.369. A rapid sequence of bursting states can be seen for increasing stimulation levels; in this region of the bifurcation diagram, the number of peaks during the active phase of bursting increases with β. The complex oscillations disappear abruptly, and the steady state becomes stable again at β=0.483. Fig. II.14 shows that, at this critical point, the period of oscillations tends to infinity, a feature characteristic of a homoclinic bifurcation. Also noticeable in Fig. II.14 is the fact that the period increases in a stepwise manner with β, because the number of spikes in the plateau phase increases at each step.

Fig. II.13a and subsequent bifurcation diagrams have been obtained by numerical integration of eqns. (II.3)-(II.9). Similar results have also been obtained in part using the program AUTO (Doedel, 1981), but only the first bifurcations were found with this method.

Parameters	Bursting	Chaos	Quasiperiodicity
β	0.46	0.65	0.51
K_2 (μM)	0.1	0.1	0.1
K_5 (μM)	1	0.3194	0.3000
K_A (μM)	0.1	0.1	0.2
K_d (μM)	0.6	1	0.5
K_Y (μM)	0.2	0.3	0.2
K_Z (μM)	0.3	0.6	0.5
k (min^{-1})	10	10	10
k_f (min^{-1})	1	1	1
ε (min^{-1})	1	13	0.1
n	2	4	4
m	4	2	2
p	1	1	2
V_0 ($\mu Mmin^{-1}$)	2	2	2
V_1 ($\mu Mmin^{-1}$)	2	2	2
V_{M2} ($\mu Mmin^{-1}$)	6	6	6
V_{M3} ($\mu Mmin^{-1}$)	20	30	20
V_{M4} ($\mu Mmin^{-1}$)	2.5	3	5
V_{M5} ($\mu Mmin^{-1}$)	30	50	30

Table II.2. Parameter values corresponding to the various types of complex oscillatory behavior observed in the model defined by eqs. (II.3)-(II.9)

Chaos

In the bifurcation diagram shown in Fig. II.13b, representing a horizontal section for ε=13 min^{-1} in the diagram of Fig. II.12c, complex Ca^{2+} oscillations both appear and disappear by period-doubling, following the Feigenbaum sequence which is one of the best known routes leading to chaos (Bergé *et al.*, 1984). The chaotic region contains narrow windows of periodicity. This bifurcation diagram is

qualitatively similar to the one obtained by Shen and Larter (1995) in a different model for complex Ca^{2+} oscillations. However, a major quantitative difference between the two diagrams pertains to the range of stimulation levels in which complex oscillations occur: this range, which here extends from $\beta = 0.61$ to 0.68, is at least ten times larger in the present model. For some other parameter values, regions of bursting and chaos can both be observed in the same bifurcation diagram established as a function of β (data not shown).

Birhythmicity

With the same set of parameter values as in Fig. II.13b, except for ε which is slightly smaller (ε =11 min^{-1} instead of 13 min^{-1}), one can observe birhythmicity in the bifurcation diagram (Fig. II.13c, see also Fig.II.12c). This behavior corresponds to the coexistence of two stable limit cycles for the same values of the parameters. Birhythmicity here arises by a phenomenon of hysteresis involving multiple branches of oscillatory behavior separated by an unstable limit cycle, between the two limit points in β=0.509 and β=0.521 (see inset to Fig. II.13c, illustrating for the maxima of Z the coexistence between the two types of stable oscillations). For stimulation levels between β=0.509 and β=0.518, oscillations coexist with a chaotic regime. Between β=0.518 and β=0.521, two stable limit cycles coexist. These two limit cycles are represented simultaneously in Fig. II.15 where panel (a) represents the temporal evolution of cytosolic calcium and panel (b) the two limit cycles in the phase plane (Z,Y). The two stable cycles are shown for β=0.520 in Fig. II.15b, together with the corresponding oscillations in Z (Fig. II.15a).

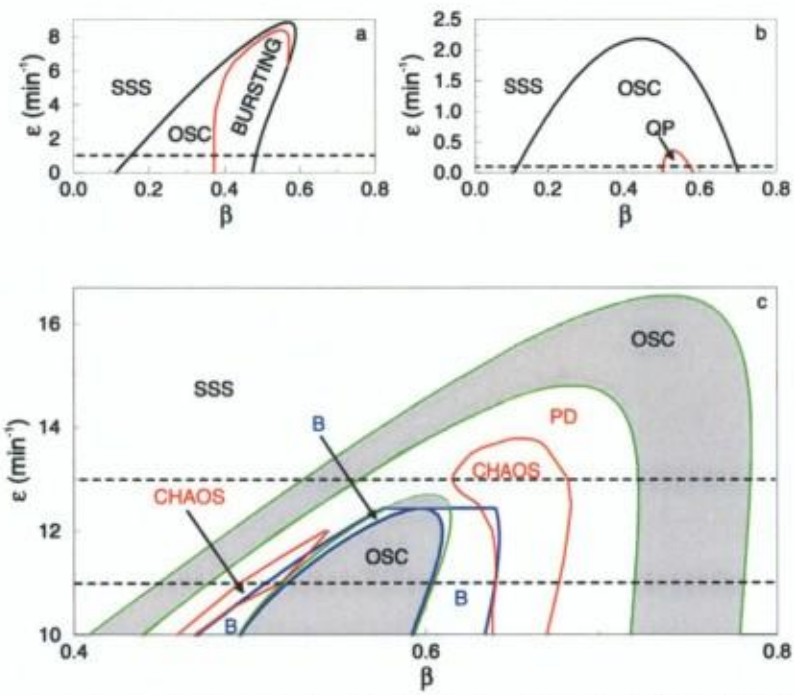

Fig. II.12. Stability diagrams showing the domains of bursting (panel a), quasiperiodicity (panel b), and chaos as well as other modes of complex oscillatory behavior (panel c). Notations are: SSS for stable steady state, OSC for simple periodic oscillations, QP for quasiperiodicity, PD for the beginning of the period-doubling sequences, CHAOS for areas of chaotic dynamics, and B for regions of birhythmicity. The diagrams have been established by numerical integration of eqns. (II.3)-(II.9) with the parameter values listed in the first, second and third columns of Table II.2 for panels (a), (c) and (b) respectively. The four horizontal dashed lines represent sections through the domains of distinct dynamic behaviors, which correspond to the bifurcation diagrams presented in Fig. II.13.

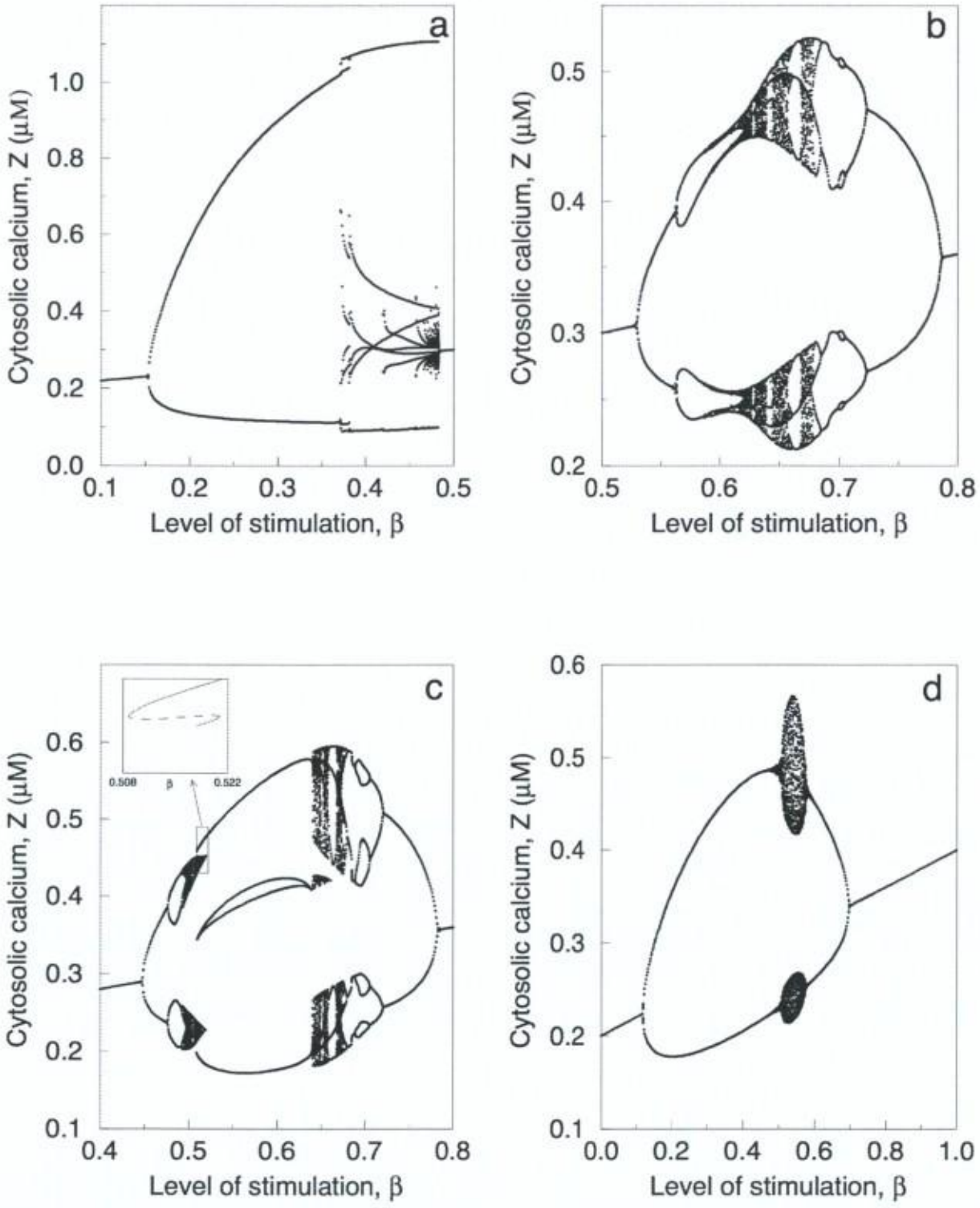

Fig.II.13 Bifurcation diagrams showing the appearance and disappearance of bursting (panel a), chaos (panel b), chaos and birhythmicity (panel c), and quasiperiodicity (panel d) as a function of β. These diagrams have been established by numerical integration of eqns. (II.3)-(II.9) for the same parameter values as in Fig. (II.11) and Fig. (II.12). Panel (a) corresponds to the section (dashed line) shown in Fig. II.12a. Panels (b) and (c) correspond to the sections (dashed lines) shown in Fig. II.12c for ε=13 min^{-1} and ε=11 min^{-1}, respectively. Panel (d) corresponds to the section (dashed line) shown in Fig. II.12b.

The unstable cycle (dashed line in the inset to Fig. II.13c) separates the attraction basins of the two stable oscillatory regimes. Thus, as illustrated in Fig. II.16, when starting from the simple periodic oscillations in the case of Fig. II.15, a perturbation in the form of a small increase in cytosolic Ca^{2+} (Z) will cause a transition to the periodic oscillations with a small shoulder. Numerical simulations indicate that the attraction basin of the small cycle is much more reduced than that of the larger cycle.

Furthermore, a phenomenon of period-adding is also seen in β=0.509 in the bifurcation diagram shown in Fig. II.13c: periodic Ca^{2+} oscillations with a small shoulder (corresponding to the appearance of an additional intermediate pair of maxima and minima in Z) can be observed from β=0.509 (where they coexist with chaotic oscillations) to 0.640, at which value another domain of chaotic oscillations begins.

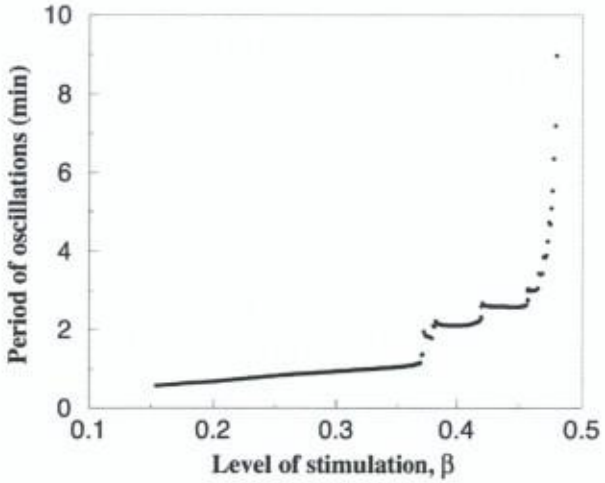

Fig. II.14. Relationship between the period of Ca^{2+} oscillations and the level of stimulation for a set of parameter values corresponding to oscillations of the bursting type. Parameter values are the same as in Fig. II.11a,d and Fig.II.12a. At the right extremity of the oscillatory domain (β=0.483), the period tends to infinity, which denotes the existence of a homoclinic bifurcation.

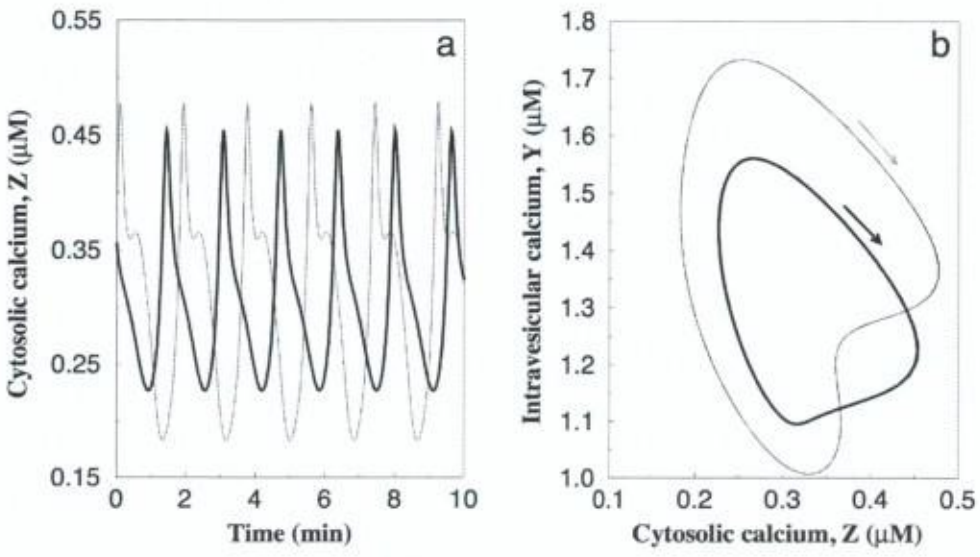

Fig. II.15. Temporal evolution of cytosolic Ca^{2+} (panel a) and limit cycles (panel b) in the (Z,Y) phase plane for the two stable coexisting cycles in the region of birhythmicity. The curves are obtained by numerical integration of eqns. (II.3)-(II.9),

starting from different initial conditions. Parameter values are those listed in the second column of Table.II.2, except for β which is equal to 0.52 and ε which is equal to 11 min^{-1}.

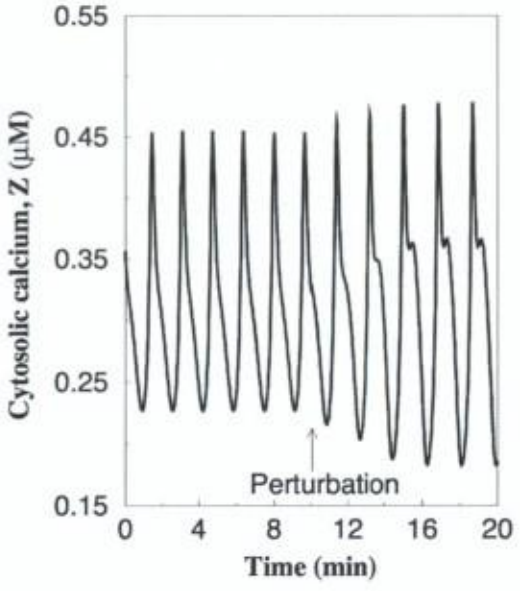

Fig. II.16. Transition between two types of coexisting, periodic oscillations following a small increase in the cytosolic Ca^{2+} level from 0.322 μM to 0.330 μM in the conditions of birhythmicity. Parameter values are the same as in Fig. II.15.

Quasiperiodicity

Quasiperiodic oscillations appear and disappear through a torus bifurcation in which the limit cycle undergoes a secondary Hopf bifurcation, as shown in Fig. II.13d which represents a section (dashed line) through the diagram of Fig. II.12b. For this reason, the system now possesses two natural incommensurable frequencies. Thus, the trajectories in the phase space tend to cover a torus, as can be seen in Fig. II.11f.

II.5.6. Characterization of complex oscillations

The various types of complex oscillations are hardly distinguishable from the sole examination of the time series and the associated phase space attractors. Several methods have been developed to characterize these behaviors (Bergé *et al.*, 1984). Here, we have characterized bursting, chaos and quasiperiodic oscillations by use of Poincaré sections. This has been done for the three cases listed in Table II.2, corresponding to the examples of bursting, chaos, and quasiperiodicity illustrated in Fig. II.11.

To build first return maps, we plot the maximum value of one variable of the system (here Z, the cytosolic Ca^{2+} concentration) as a function of the value of its preceding maximum. We have performed such an analysis and have plotted in Fig. II.17 the results obtained when considering various numbers of successive maxima in cytosolic Ca^{2+}: 5 (first row), 10 (second row), 20 (third row) and 100 (fourth row). In the case of simple, regular oscillations, such a map consists of a single point. For complex oscillations, as can be seen in Fig. II.17, there is a clear distinction between the three return maps corresponding to bursting, chaos or quasiperiodicity in the model considered for complex Ca^{2+} dynamics. In the case of bursting (Fig. II.17, first column), the map consists of five points, reflecting the number of peaks per period obtained for the particular set of parameter values considered. In the case of chaos (Fig. II.17, second column), the map tends to be continuous, with an inverted bell-shaped form, resembling that found for a large variety of chaotic systems. Finally, for the

quasiperiodic oscillations (Fig. II.17, third column), the map takes the form of a closed curve. The use of first return maps thus appears to be most appropriate for distinguishing between the different types of complex oscillatory behavior. Fig. II.17 indicates, however, that a minimum number of successive maxima must be used to reach unambiguous conclusions. Thus, in Fig. II.17, the asymptotic shape (bottom row) of the return map for chaos and quasiperiodicity begins to be distinguishable for a time series containing 10 peaks, but the picture becomes clearer when 20 maxima are considered.

II.5.7. Discussion

The study presented in the section II.5 was devoted to a thorough analysis of a model previously proposed for complex Ca^{2+} oscillations, which takes into account both CICR and stimulation by Ca^{2+} of $InsP_3$ degradation by 3-kinase (Borghans *et al.*, 1997). This model is realistic as the two types of regulation by Ca^{2+} have been well characterized. The model predicts that although simple periodic Ca^{2+} spiking is expected to be the most commonly observed behavior, complex Ca^{2+} oscillations in the form of bursting or chaos should also be seen in some non-excitable cell types under appropriate circumstances. Until now, bursting in Ca^{2+} oscillations has only been reported in experimental studies in hepatocytes responding to appropriate stimuli (Capiod *et al.*, 1991; Green *et al.*, 1993; Dixon *et al.*, 1993, 1995; Marrero *et al.*, 1994). That there exists a high variability in the propensity of different hepatocytes from the same line to display complex oscillations holds with the property of the model that the regions of bursting and chaos in parameter space are relatively small. The fact that these regions are much smaller than those of simple regular Ca^{2+} spiking furthermore agrees with the experimental observation that simple, periodic Ca^{2+} spiking is much more common than complex Ca^{2+} oscillations.

In the present model, an increase in cytosolic Ca^{2+} has two opposite effects. On one hand, due to CICR, it enhances the release of Ca^{2+} from internal stores. On the other hand, due to 3-kinase stimulation by Ca^{2+}, it brings about a decrease in $InsP_3$, which in turn reduces the rate of Ca^{2+} release into the cytosol. These counteracting effects of Ca^{2+} are the source of bursting and chaos in the present model, because the system somehow behaves as a periodically forced oscillator, for which complex oscillations are well known to occur (see, e.g., Goldbeter, 1996). Indeed, CICR, which can proceed in the presence of a constant level of $InsP_3$, provides a mechanism for autonomous oscillations, while the signal ($InsP_3$) that triggers oscillations is self-modulated, since $InsP_3$ raises the level of cytosolic Ca^{2+} which in turn decreases that of $InsP_3$ through the action of the Ca^{2+}-activated 3-kinase.

Other mechanisms generating complex Ca^{2+} oscillations have been proposed. Thus, as shown by Shen and Larter (1995), the interplay between CICR and the stimulation of phospholipase C activity by Ca^{2+} might also provide a realistic source for bursting and chaos in Ca^{2+} signaling. However, in that model, complex Ca^{2+} oscillations only arise in a very small region of the parameter space, for example between β=0.600 and β=0.628 (chaos occurs over an even smaller range of β values). Moreover, in contrast to the present results and to what is seen in hepatocytes, the pattern of Ca^{2+} bursting obtained by Shen and Larter predicts that Ca^{2+} always returns to it basal level between successive spikes. Bursting was also theoretically predicted in models involving the Ca^{2+}-induced inactivation of the $InsP_3R$ or the interplay between distinct Ca^{2+}- and $InsP_3$-sensitive Ca^{2+} pools (Borghans *et al.*, 1997). An inhibitory role of protein kinase C (PKC) in the origin of bursting in hepatocytes has been stressed by Dixon *et al.* (1993, 1995) on the basis of their experimental observations. According to these authors, this variety in temporal patterns could arise because of differences in the negative feedback exerted by PKC or G proteins coupled to the receptors. Such a regulation was incorporated in a model for Ca^{2+} bursting (Chay *et al.*, 1995) based on the activation of PLC by Ca^{2+} coupled to both the indirect inhibition of the enzyme by PKC (itself activated by Ca^{2+}) and the Ca^{2+}-induced inactivation of the $InsP_3$-sensitive Ca^{2+} channel.

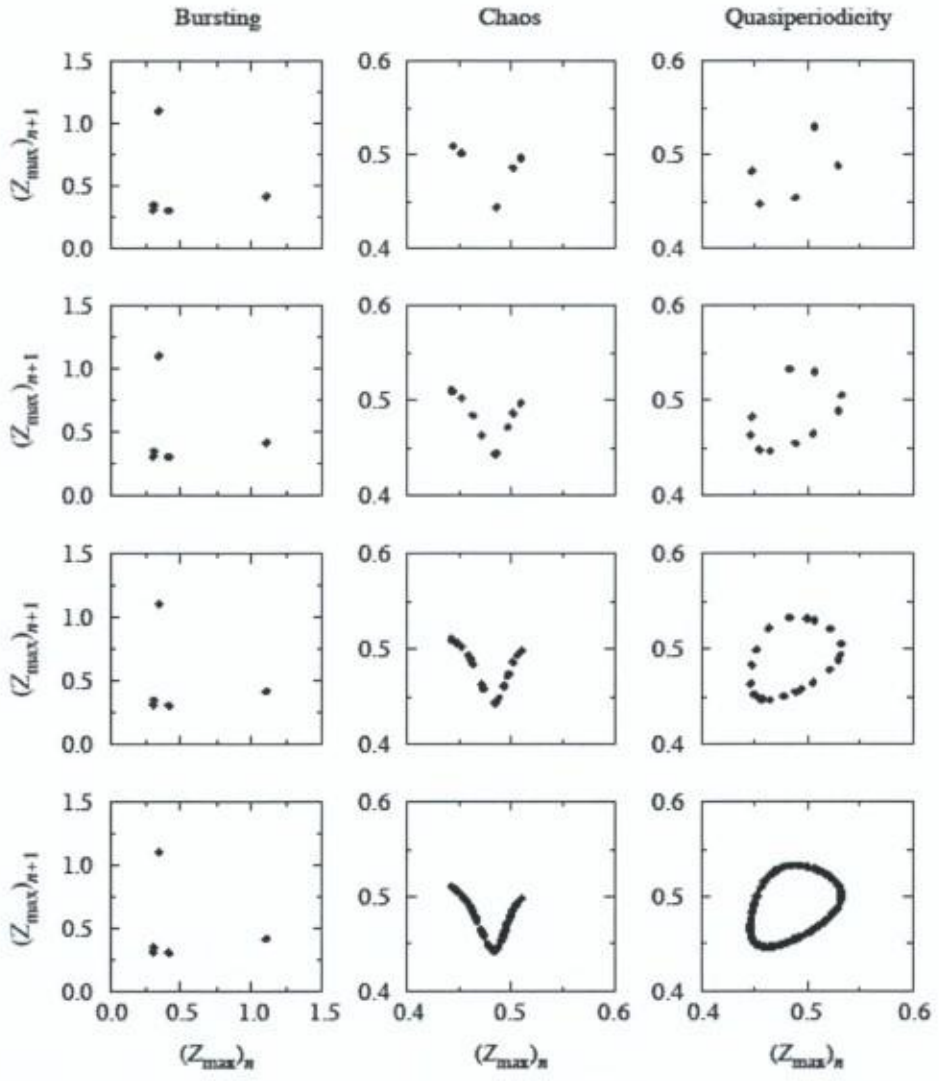

Fig. II.17 Characterization of complex Ca^{2+} oscillations by means of first return maps. Shown are the return maps obtained for bursting (column 1); chaos (column 2); and quasiperiodicity (column 3) for time series containing 5 (row 1), 10 (row 2), 20 (row 3) and 100 (row 4) successive maxima in cytosolic Ca^{2+} (Z). For each return map, the value of the $(n+1)^{th}$ peak in Z is plotted versus the n^{th} peak value. Results have been obtained numerically in the same conditions as in the corresponding panels (a)-(c) in Fig. II.11.

Complex Ca^{2+} oscillations of the bursting type are easily recognizable by the very appearance of the time evolution of the cytosolic Ca^{2+} level. In contrast, chaotic dynamics could be harder to distinguish from simple, periodic oscillations. The analysis performed here suggests that, provided that the available time series is sufficiently long, the construction of first return maps should be a straightforward method to distinguish periodic oscillations from aperiodic ones. Based on such return maps, preliminary analysis of some experimental time series of Ca^{2+} oscillations obtained in pancreatic acinar cells and hepatocytes led to the conclusion that these time series could result from chaotic dynamics (Strizhak *et al.*, 1995). However, it should be kept in mind that to perform such an analysis based on return maps, sufficiently long experimental time series must be obtained in constant conditions, with a short sampling time and a low standard deviation. Our results indicate (see Fig. II.17) that a time series containing from 10 to 20 successive maxima already allows one to distinguish between the various types of oscillatory behavior, but the longer the time series, the more unambiguous are the conlusions.

The physiological significance of aperiodic Ca^{2+} oscillations such as those shown in Fig. II.11 might be rather weak, both because they do not differ much from simple periodic oscillations and because they would be rather unstable with respect to small variations in the cellular parameters, given that the domain of chaos is much smaller than that of periodic oscillations in parameter space. The present results as well as those obtained in related models show, however, that well-known properties of intracellular Ca^{2+} signaling can readily generate complex Ca^{2+} oscillations, including chaos.

As to Ca^{2+} oscillations of the bursting type, the plateau phase during which Ca^{2+} remains elevated for a rather long period of time could serve to activate slower, Ca^{2+}-dependent processes. The possible physiological significance of oscillations of the bursting type is supported by the fact that such oscillations are reminiscent of those seen in electrically excitable cells, in which complex oscillations arise from the interplay between a plasma-membrane oscillator and the $InsP_3R$ (Chay, 1993; Keizer and De Young, 1993; Chay *et al.*, 1995; Chay, 1997). In such cells, it is known that cellular processes are differently activated by Ca^{2+} spiking or bursting; thus, in pancreatic β cells, granular exocytosis is optimized by long-duration Ca^{2+} bursting (Rorsman and Trube, 1986; Pipeleers, 1987).

Further experimental investigation of complex Ca^{2+} oscillatory dynamics would be of much value, both because it might reveal important features about the regulatory mechanisms underlying such Ca^{2+} oscillations, and because of the potential physiological significance of the phenomenon. Together with the theoretical results obtained in other models, the present work suggests that complex Ca^{2+} oscillations should be more widespread than usually thought. Our results point to self-modulation of the $InsP_3$ stimulus as a potential mechanism for generating bursting and chaos in Ca^{2+} signaling.

CHAPTER III

Modelling the effect of specific $InsP_3$ receptor isoforms on cellular Ca^{2+} signals

III.1. Introduction

As mentioned in the first Chapter, and emphasized in Chapter VII, $InsP_3$-induced Ca^{2+} oscillations control a vast array of cellular functions such as fertilization, gene expression, synaptic transmission or secretion (Berridge *et al.*, 2003 ; Combettes *et al.*, 2004). It is often assumed that the potency of the cell to control so diverse physiological processes with a compound as simple as Ca^{2+} ions results from the large versatility of the signal-induced Ca^{2+} changes (Berridge *et al.*, 2000). The existence of different $InsP_3R$ isoforms is probably an important factor allowing such diversity of responses (Ramos-Franco *et al.*, 1998 ; Miyakawa *et al.*, 1999 ; Haberichter *et al.*, 2002 ; Yule *et al.*, 2003 ; Hattori *et al.*, 2004 ; Morita *et al.*, 2004 ; see Vermassen *et al.*, 2004 for review).

In mammalian cells, three $InsP_3R$ subtypes have been identified : $InsP_3R1$, $InsP_3R2$ and $InsP_3R3$. In all cell types, functional channels result from the assemblage of receptors into homo- or hetero-tetrameric structures. The 3 isoforms are co-expressed within cells, but their respective levels of expression are largely tissue- and development specific (De Smedt *et al.*, 1997; see Taylor *et al.*, 1999 and Vermassen *et al.*, 2004 for review). Although all the $InsP_3R$ subtypes display similar ion permeation properties, they significantly differ in their regulatory properties. These dissimilarities are not only the direct consequence of slight intrinsic differences in their amino-acid sequences, but mainly rely on other factors like the interplay with accessory proteins, various modes of regulation by ATP or phosphorylation (Kaftan *et al.*, 1997 ; Hagar *et al.*, 1998 ; Wojcikiewicz and Luo, 1998 ; Moraru *et al.*, 1999 ; Hagar and Ehrlich, 2000 ; Mak *et al.*, 2001a ; 2001b ; Nadif Kasri *et al.*, 2004 ; Patterson *et al.*, 2004). The exact nature of these differences as well as their molecular origin however remain controversial and are sitll a subject of active investigation (see Taylor and Laude, 2002 and Patterson *et al.*, 2004 for reviews).

In a cellular environment, the respective proportions of the 3 $InsP_3Rs$ affect the time course of cytosolic Ca^{2+} concentration after agonist stimulation. Thus, in DT40 B cells expressing a single $InsP_3R$ subtype, the Ca^{2+} signals in response to BCR stimulation drastically depend on the receptor subtype (Miyakawa *et al.*, 1999). Strikingly, only $InsP_3R2$ isoform appears to be able to generate long-lasting, regular Ca^{2+} oscillations in this cell type. Similar results were obtained in myocytes (Morel *et al.*, 2003). In other experiments (Hattori *et al.*, 2004), $InsP_3R1$ or $InsP_3R3$ were knockdown by RNA interference in HeLa and COS-7 cells. In both cell types, knockdown of $InsP_3R1$ tends to decrease the number of Ca^{2+} spikes while knockdown of $InsP_3R3$ has the opposite effect and tends to favour long-lasting Ca^{2+} oscillations. Altogether, these experiments thus demonstrate a close correlation between the types of $InsP_3Rs$ present in a cell and the existence (and characteristics) of $InsP_3$-induced Ca^{2+} oscillations.

From a modelling point of view, it has already been suggested that variable ratios between Type 1 and Type 3 $InsP_3Rs$ may explain why the airway smooth muscle cells stemming from a presumably homogeneous population do not all display Ca^{2+} oscillations in response to the same stimulus (Haberichter *et al.*, 2002). It is proposed in the latter study that slight, random, interindividual variations in the ratios of $InsP_3R1$ to $InsP_3R3$ suffice to account for the different sensitivities of these cells to agonist stimulation. Other models have considered only one isoform but have evoked the specificity of the major $InsP_3R$ subtype present in a given cell type to explain some detailed, cell-specific characteristics of Ca^{2+} oscillations. For example, the PKA-induced phosphorylation of the $InsP_3R3$ has been theoretically suggested to be responsible for the typical shape of the CCK-induced Ca^{2+} oscillations in pancreatic acinar cells (Le Beau *et al.*, 1999). Specific modelling of the $InsP_3R2$ has also been developed to account for both oscillatory and monophasic Ca^{2+} transients in rat adrenal chromaffin cells (Inoue *et al.*, 2003).

Here, we theoretically test the hypothesis that the distinct regulations by Ca^{2+} and $InsP_3$ of the three $InsP_3R$ subtypes reported in the literature may explain their experimentally observed distinct roles in cellular Ca^{2+} signalling. To this end, we first develop phenomenological models accounting for the distinct steady-state behaviours reported for the 3 subtypes. Our models are phenomenological in the

sense that they are not based on the underlying molecular processes related to $InsP_3$ and Ca^{2+} binding, but are rather mathematical expressions fitting the observed behaviours. We then incorporate these different descriptions of the $InsP_3Rs$ into a dynamical model for the cellular Ca^{2+} signalling. We find that slight differences in the Ca^{2+} regulatory properties of these $InsP_3Rs/Ca^{2+}$ channels can lead to drastically distinct Ca^{2+} signalling patterns when they are expressed in a cell. We thus recover the experimental results obtained in myocytes (Morel *et al.*, 2003), DT40 B-cells (Miyakawa *et al.*, 1999), HeLa and COS-7 cells (Hattori *et al.*, 2004) as to the effect of selectively expressing or down-regulating $InsP_3R$ isoforms.

III.2. Mathematical model

As far as the direct effects of Ca^{2+} and $InsP_3$ on the Ca^{2+} releasing activity of the $InsP_3Rs$ are concerned, the $InsP_3R$ isoforms differ by 2 factors : their sensitivity to $InsP_3$ and their mode of regulation by Ca^{2+}. As to the former difference, it is clear by now that the 3 isoforms bind $InsP_3$ with different affinities and that these differences influence the potency of $InsP_3$ to release Ca^{2+} (Missiaen *et al.*, 1998 ; Wojcikiewicz and Luo, 1998 ; Miyakawa *et al.*, 1999 ; Dyer and Michelangeli, 2001). The sequence of Ca^{2+} sensitivity reported in the literature is in the order : $InsP_3R2 \geq InsP_3R1 > InsP_3R3$. In our model, these differences are reflected by distinct half-saturation constants for $InsP_3R$ activation by $InsP_3$. Thus, we choose $K_1 = 0.5\ \mu M$, $K_2 = 0.2\ \mu M$ and $K_3 = 2\ \mu M$ for sub-types 1, 2 and 3 respectively.

As to the regulation of the three $InsP_3R$ isoforms by Ca^{2+}, the available data are controversial, although it is widely accepted that such regulation plays a fundamental role for the generation of Ca^{2+} oscillations. In trying to classify the behaviours reported in the literature, one can distinguish the three following cases :

(1) a classical fast activation-slow inhibition of the Ca^{2+}-releasing activity of the $InsP_3R$ by Ca^{2+}, with apparently no interplay between the regulations by Ca^{2+} and by $InsP_3$ (Champeil *et al.*, 1989 ; Dufour *et al.*, 1997 ; Ramos-Franco *et al.*, 1998). As this type of behaviour has mainly been reported for receptors isolated from hepatocytes, which are known to predominantly express the type 2 receptor, we associate the 'classical bell-shaped curve' with $InsP_3R2$. Many mathematical models have already been proposed to account for such a behaviour (for reviews, see : Sneyd *et al.*, 1995a ; Tang *et al.*, 1996 ; Dupont, 1999 ; Schuster *et al.*, 2002). Here, we use the simple description for this type of receptor dynamics that has been presented in Table I.3 (Dupont and Swillens, 1996). In this model, the evolution equation for $R_{i,2}$, defined as the fraction of $InsP_3R2$ that has been inhibited by Ca^{2+}, is given by :

$$\frac{dR_{i2}}{dt} = k_{+,2}\left(1 - R_{i2}\right)\frac{C_c^{n_i}}{1+\left(\frac{C_c}{K_{act}}\right)^{n_a}} - k_{-,2}R_{i2} \qquad \text{(III.1)}$$

where $k_{+,2}$ is the rate of inhibition of the $InsP_3R2$ by cytosolic Ca^{2+} and $k_{-,2}$ the rate of relief from this inhibition. Activation of the receptor by Ca^{2+} is assumed to be instantaneous and characterized by a threshold constant K_{act}. Inactivation is assumed to occur only on receptors that have been activated by Ca^{2+}. Parameters n_a and n_i are the Hill coefficients characterizing the cooperativity of the activation and inhibition processes. The fraction of active (i.e. open) type 2 receptors is then given by :

$$IR_{a,2} = (1 - R_{i2})\frac{IP_3}{K_2 + IP_3}\frac{C_c^{n_a}}{C_c^{n_a} + K_{act}^{n_a}} \qquad \text{(III.2)}$$

where K_2 is the half-saturation constant of the $InsP_3R2$ for $InsP_3$. Following the data of Miyakawa *et al.* (1999), the $InsP_3$ dependence of Ca^{2+} release is supposed to be non-cooperative. The fraction of open $InsP_3R2$ at steady-state as a function of Ca^{2+} concentration is illustrated in the middle panel of Fig. III.1 for 3 values of the $InsP_3$ concentration. As expected from equ. (III.2), an increase in $InsP_3$ simply shifts the bell-shaped curve towards higher opening levels (but not horizontally).

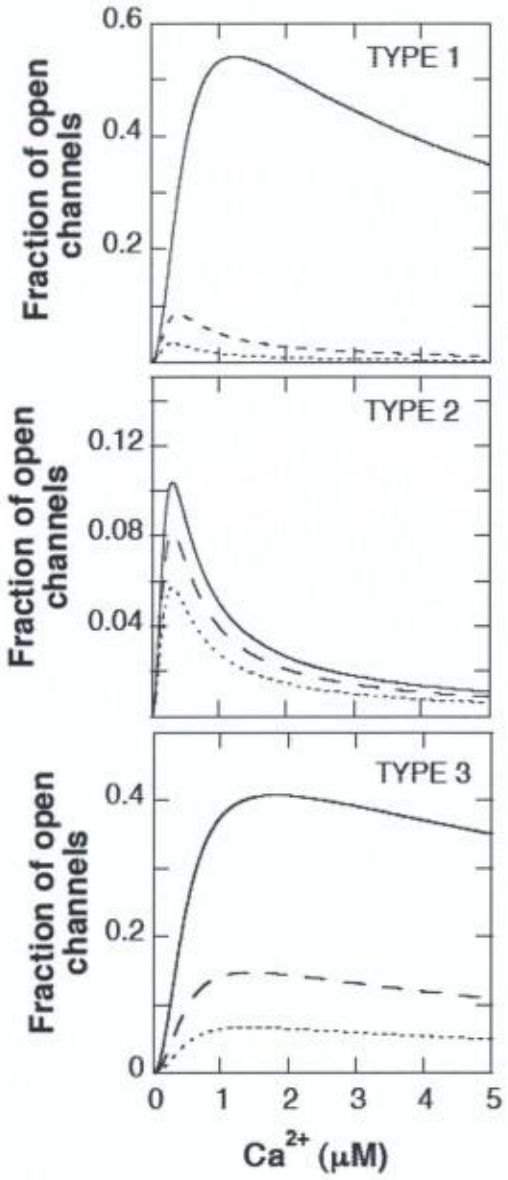

Fig. III.1. Steady-state open probabilities of the different types of $InsP_3Rs$ as a function of the concentration of Ca^{2+} at the cytosolic side of the channel, for three levels of $InsP_3$: 0.2 μM (dotted curve), 0.5 μM (dashed curve) and 2 μM (plain curve). Type 1 : curves have been obtained by solving eqs (III.3) and (III.4) at steady-state, with the following parameter values : $k_{+,1} = 14.4606\ \mu M^{-3}s^{-1}$, $k_{-1} = 0.217\ s^{-1}$, $K_{act} = 0.5\ \mu M$, $K_{i,1} = 0.5\ \mu M$, $K_1 = 0.5\ \mu M$, $n_i = 3$, $n = 3$, $n_a = 2$. The inhibition constant of the receptor by Ca^{2+} ($K_{inh,1}$) thus equals 0.247 μM. Type 2 : curves have been obtained by solving equs (III.1) and (III.2) at steady-state, with the same parameter values as for type 1 except for: $K_2 = 0.2\ \mu M$. Type 3 : curves have been obtained by solving equs (III.1) and (III.2) at steady-state, with the same parameter values as for type 1 except for: $k_{-3} = 21.7\ s^{-1}$, $K_3 = K_{i,3} = 2\ \mu M$. Thus, $K_{inh,2} = 1.145\ \mu M$.

(2) In other experiments, an interplay between the regulations by Ca^{2+} and $InsP_3$ have been reported in addition to the biphasic regulation of the receptor activity by Ca^{2+}. In some instances indeed, the

threshold Ca^{2+} concentration leading to $InsP_3R/Ca^{2+}$ channel inactivation increases with the $InsP_3$ concentration (Kaftan *et al.*, 1997 ; Mak *et al.*, 1998 ; Moraru *et al.*, 1999). This behaviour has mainly been reported for $InsP_3R1$. Sophisticated models based for example on the existence of 2 $InsP_3$ binding sites characterized by different affinities have been proposed (Kaftan *et al.*, 1997). Here, we simply assume that the inhibition of the $InsP_3R1$ by Ca^{2+} is reduced when the level of $InsP_3$ increases. This approach is in fact similar to that of Mak *et al.* (1998) where the half-saturation constant for inhibition of the $InsP_3R1$ by Ca^{2+} increases with $InsP_3$ (equation (2) in Mak *et al.*, 1998). A plausible molecular explanation would be that the Ca^{2+} inhibition of the $InsP_3R1$ is mediated by calmodulin. Following this hypothesis, the ability of IP_3 to protect receptors from Ca^{2+} inhibition would reflect its ability to regulate the interplay between calmodulin and the inhibitory Ca^{2+} binding sites (Taylor and Laude, 2002). In this context, the evolution equation for R_1, defined as the fraction of $InsP_3R_1$ that has been inhibited by Ca^{2+}, is given by :

$$\frac{dR_{i1}}{dt} = k_{+,1}\left(1 - R_{i1}\right)\frac{C_c^{n_i}}{1+\left(\frac{C_c}{K_{act}}\right)^{n_a}}\frac{K_{i,1}^n}{K_{i,1}^n + IP_3^n} - k_{-,1}R_{i2} \qquad \text{(III.3)}$$

where $k_{+,1}$ is the rate of inhibition of the $InsP_3R1$ by cytosolic Ca^{2+} and $k_{-,1}$ the rate of relief from this inhibition. $K_{i,1}$ and n are the threshold constant and Hill coefficient characterizing the inhibitory effect of $InsP_3$ on the Ca^{2+}-induced inactivation of the receptor. As in the case of type 2 receptors, the fraction of active type 1 receptors is given by :

$$IR_{a,1} = (1 - R_{i1})\frac{IP_3}{K_1 + IP_3}\frac{C_c^{n_a}}{C_c^{n_a} + K_{act}^{n_a}} \qquad \text{(III.4)}$$

As shown in the first panel of Fig. III.1, the fraction of open type 1 $InsP_3R$ first increases and then decreases when increasing the level of Ca^{2+} at the cytosolic side of the channel, with a shift of the maximum of the curve to the right when increasing $InsP_3$ concentration. The maximum open probability also much depends on the $InsP_3$ concentration ; this is due to the decreased level of inhibition by Ca^{2+} at high $InsP_3$ concentration. When comparing types 1 and 2, it is noticeable that for a given $InsP_3$ concentration, the steady-state curve for type 1 is much broader than for type 2. Thus, type 1 appears to be less sensitive to Ca^{2+} changes. Receptor inactivation by Ca^{2+} is indeed less effective for type 1 than for type 2, because of the inhibition by $InsP_3$ of this inactivation by Ca^{2+} for $InsP_3R1$.

(3) A third type of behaviour that has often been reported in the literature is that of an $InsP_3R$ that is activated by Ca^{2+}, but not inhibited by this compound, or, at non-physiologically high Ca^{2+} concentrations. This possible behaviour has mainly been reported for the type 3 $InsP_3R$ (Hagar *et al.*, 1998 ; Miyakawa *et al.*, 1999). Thus, we consider the same evolution equation for the fraction of $InsP_3R_3$ that has been inhibited by Ca^{2+} (R_3) as for R_1 (Equ. III.3 where the indexes '1' have to be replaced by '3'), but change the value of the kinetic constant k_- so that $k_{-,3}$ is 10 times larger that $k_{-,1}$. In such conditions, inactivation by Ca^{2+} is much less effective. Thus, when plotting the fraction of open $InsP_3R3$ as a function of the cytosolic Ca^{2+} concentration, the biphasic character or the curve nearly disappears (see the third panel of Fig. III.1). Note that the difference between the curves aimed at modelling types 1 and 3 is mainly visible at low $InsP_3$ concentrations. Indeed, when $InsP_3$ is high, the inactivation by Ca^{2+} plays a minor role in both cases.

It should be emphasized that the above description of the regulations of the various $InsP_3R$ subtypes is much simplified. Moreover, we have associated a given regulatory behaviour with a specific receptor type mainly on the basis of the results reported for differentially-expressed $InsP_3Rs$ in DT40 cells (Miyakawa *et al.*, 1999), as they are directly related to the Ca^{2+} signalling data. The main

purpose of this initial approach is indeed to test the effect of realistic variations in the mode of regulation of the $InsP_3Rs$ on the global Ca^{2+} dynamics in a cell.

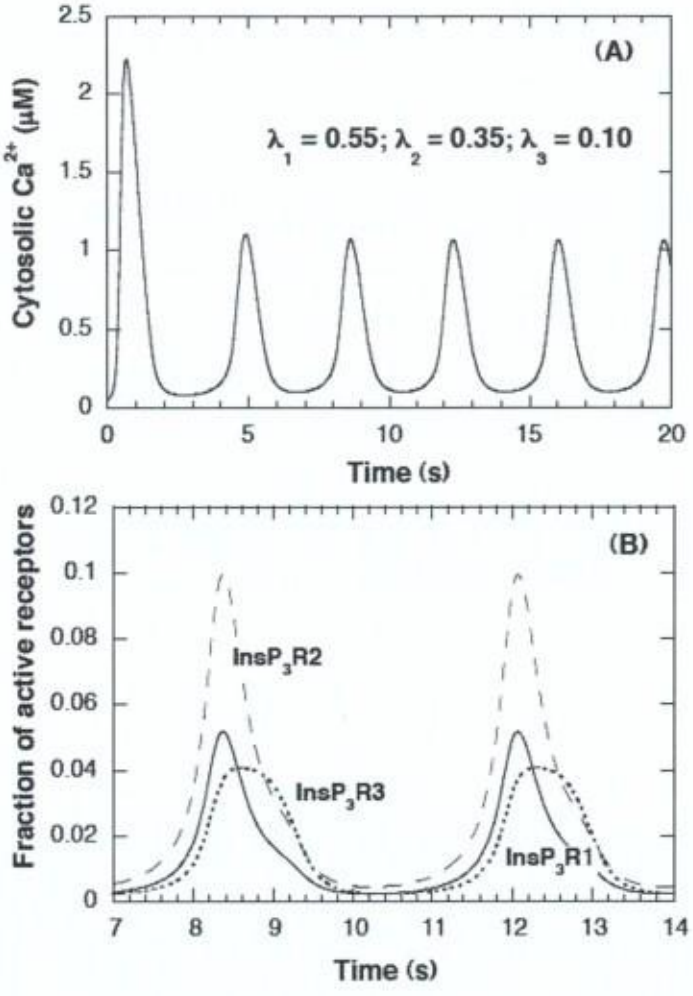

Fig. III.2. Oscillations in the concentration of cytosolic Ca^{2+} (A) and in the fraction of open $InsP_3Rs$ (B) in a simulated cell assumed to co-express all 3 $InsP_3R$ isoforms. Note that the time scale in panel (B) has been enlarged for clarity. Curves have been obtained by numerical integration of eqs. (III.1) to (III.5), with the parameter values given in Fig. III.1 and $IP_3 = 0.12$ μM, $C_T = 80$ μM, $\alpha = 0.1$, $b = 7\ 10^{-4}$, $k_1 = k_2 = k_3 = 1\ s^{-1}$, $V_{MP} = 4\ \mu Ms^{-1}$, $K_p = 0.35$ μM, $n_p = 2$. The proportions of the various $InsP_3Rs$ used in this simulation are 0.55 (λ_1), 0.35 (λ_2) and 0.1 (λ_3) for types 1, 2 and 3, respectively.

To do so, we have to incorporate our equations describing the dynamics of the 3 receptor subtypes (eqs. (III.1)-(III.4)) into a global description of the Ca^{2+} exchange processes between the cytosol and the ER. Thus, Ca^{2+} is released from the ER by 3 different types of $InsP_3R$ that can possess different maximal fluxes (k_i) and are present in various proportions (λ_i, with $\lambda_1 + \lambda_2 + \lambda_3 \leq 1$). The pumping of Ca^{2+} back into the ER is represented by the usual kinetic expression for a Ca^{2+}-ATPase. Thus, the evolution of the concentration of cytosolic Ca^{2+} in a cell reads :

$$\frac{dC_c}{dt} = \sum_{i=1}^{3} \lambda_i k_i \left(b + IR_{a,i}\right)\left(C_T - C_c(\alpha + 1)\right) - V_{MP} \frac{C_c^{n_p}}{C_c^{n_p} + K_p^{n_p}} \qquad \text{(III.5)}$$

where C_T stands for the total concentration of free Ca^{2+} in the cell, α for the volume ratio between the ER and the cytosol ; $k_i b$ represents a small leak term through the different receptor types.

III.3. Simulations of the effect of changing the amounts of the different $InsP_3Rs$ subtypes

We first simulate the Ca^{2+} dynamics in a cell expressing the 3 types of $InsP_3Rs$ in well-defined proportions (Fig. III.2A). As expected, sustained Ca^{2+} oscillations can be observed in a given range of $InsP_3$ concentrations ; this range extends from 50 to 210 nM for the parameter values considered in Fig. III.2. The proportions of the 3 isoforms correspond to 55% of type 1 ($\lambda_1 = 0.55$), 35% of type 2 ($\lambda_2 = 0.35$) and 10% of type 3 ($\lambda_3 = 0.10$).

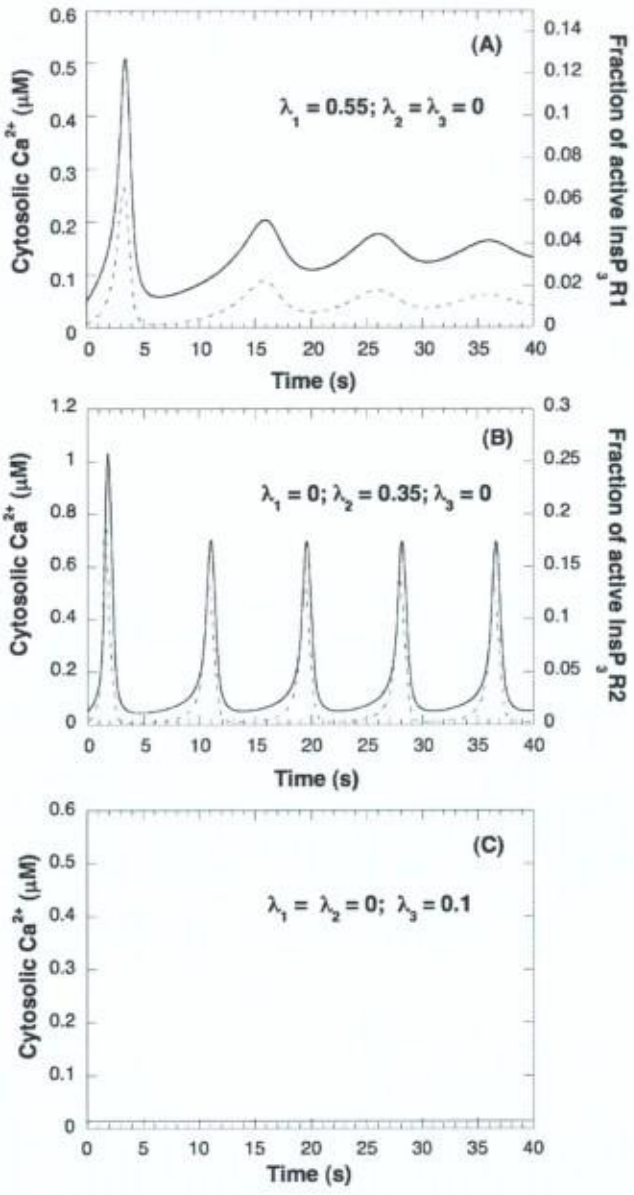

Fig. III.3. Effect of selectively expressing one $InsP_3R$ isoform on Ca^{2+} oscillations. All equations and parameters are the same as in Fig. III.2, except for the proportions of receptors, which are indicated in the different panels. In panels A and B, the plain line shows the evolution of the cytosolic Ca^{2+} concentration, while the dashed curve shows the fraction of active $InsP_3R1$ or $InsP_3R2$, respectively.

These values could represent the distribution of the 3 types of receptors in a wild-type DT40 cell, where the 3 isoforms are known to coexist. In the absence of any other quantitative data, these values have been roughly estimated from Northern blot analysis of the level of $InsP_3Rs$ transcript observed in

wild-type DT40 cells (Sugawara *et al.*, 1997). Results of the model are not highly sensitive to these proportions.

It is clear from Fig. III.2B that the 3 isoforms exhibit different behaviours in the course of Ca^{2+} oscillations. The highest fraction of open receptor is reached by type 2 (dashed line) because it possesses the highest affinity for $InsP_3$. Type 2 is also the first one to become stimulated by Ca^{2+}, i.e. it is sensitive to lower Ca^{2+} concentrations than the other 2 types. This is in agreement with the steady-state behaviours shown in Fig. III.1. $InsP_3R1$ (plain line) is always less active than $InsP_3R2$, as it has a lower affinity for $InsP_3$. Moreover, as receptor inactivation is reduced by $InsP_3$, the peaks are broader, which means that type 1 is less sensitive to Ca^{2+} changes than type 2. Finally, concerning type 3 (dotted line), it is clear from the shape of the spike that the fraction of open $InsP_3R3$ decreases because Ca^{2+} decreases, but that inhibition of the $InsP_3R_3$ by Ca^{2+} does not play any significant role in this diminishing phase.

We then test the effect of expressing only one receptor type in a simulated cell. Thus, we consider that 2 out of the 3 isoforms have been suppressed, but that the amount of the last isoform remains the same. Results of these simulations are shown in Fig. III.3. When all $InsP_3R2$ and $InsP_3R3$ are suppressed, a first peak followed by damped Ca^{2+} oscillations is obtained with the model (Fig. III.3A). Thus, in these conditions, $InsP_3R1$ alone cannot sustain Ca^{2+} oscillations, even if the latter's represent more than half the $InsP_3Rs$ present in the wild type cell. In contrast, a lower proportion (35%) of type 2 $InsP_3Rs$ sustains Ca^{2+} spiking (Fig. III.3B). The frequency of oscillations is however lower than that of the wild type cell. Finally, $InsP_3R3$ isoforms alone seem to be insensitive to a stimulation by the same dose of $InsP_3$, as shown in Fig. III.3C. In fact, for this choice of parameter values, type 3 $InsP_3$ receptors alone can never display Ca^{2+} oscillations, whatever the $InsP_3$ concentration. This can be understood because in a closed cell (i.e. when the Ca^{2+} exchanges with the extracellular medium are neglected), sustain Ca^{2+} oscillations cannot occur only on the base of a positive feedback of Ca^{2+} on the activity of the $InsP_3R$; an effective inhibitory mechanism is also required (Sneyd *et al.*, 1995). In our simulated $InsP_3R3$, the negative feedback, although present in the equations, is not strong enough (see Fig. III.1C) because of the choice of parameter values.

To try to understand the contrasting behaviours of types 1 and 2 $InsP_3Rs$, it is useful to resort to bifurcation diagrams. Such type of diagrams allows to illustrate the behaviour of the system for a large range of $InsP_3$ concentrations. Shown in Fig. III.4A and III.4B are the bifurcation diagrams corresponding to a cell expressing only type 1 (Fig. III.4A) or type 2 (Fig. III.4B) receptors : in both figures, the plain line shows the steady-state Ca^{2+} level as a function of the $InsP_3$ concentration, and the dashed line shows the maximum of Ca^{2+} oscillations when they occur. Note the different scales in both diagrams. The dotted line represents the unstable steady state during oscillations ; this state –that is not observed– corresponds to the Ca^{2+} concentration around which oscillations occur. The shape of the curve showing the steady state Ca^{2+} level (stable or unstable) as a function of $InsP_3$ (thin lines) much differs between types 1 and 2. For type 2, this level rises because the fraction of open receptors increases with the level of $InsP_3$ (Equ. III.2), for which $InsP_3R2$ has a high affinity ($K_2 = 0.2\ \mu M$). Once Ca^{2+} becomes high, inhibition by Ca^{2+} becomes predominant and the level of Ca^{2+} does not depend on the level of $InsP_3$ anymore.

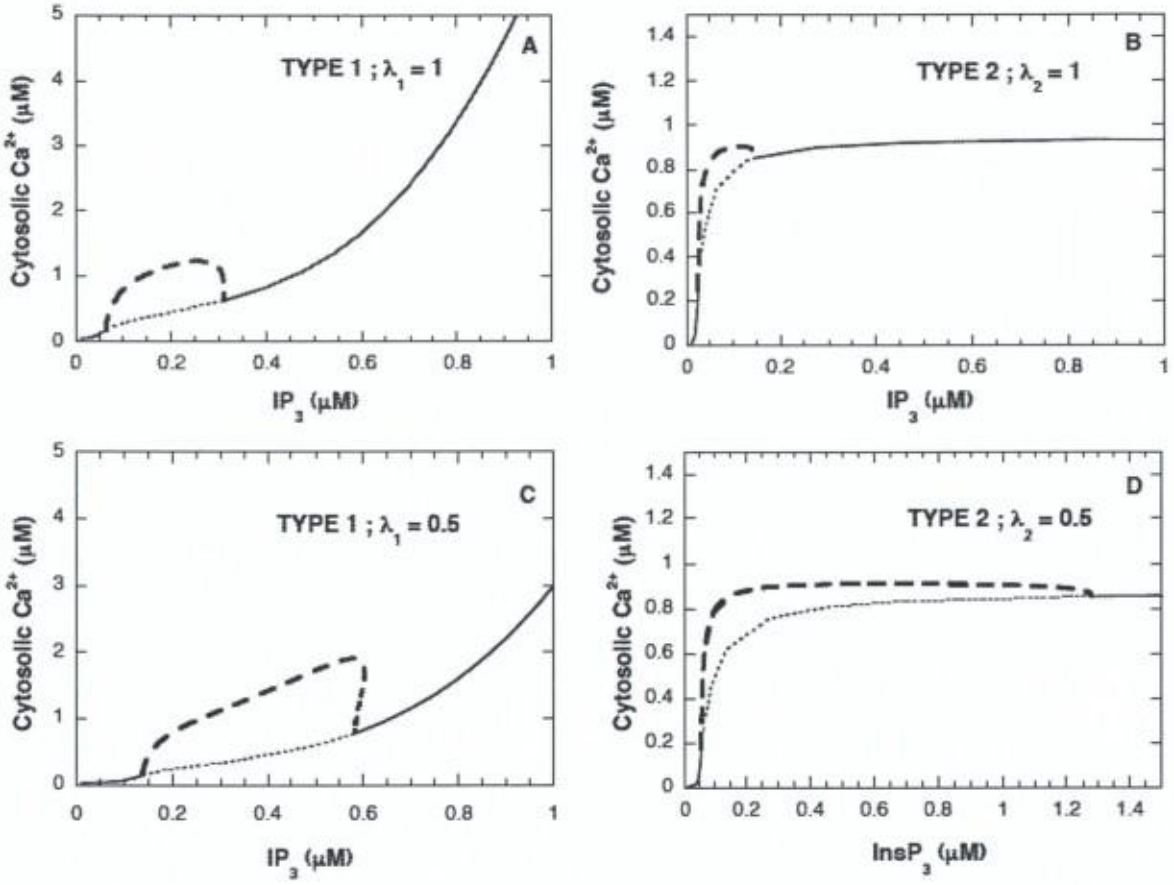

Fig. III.4. Bifurcation diagrams showing the effect of changing the receptor density (λ_i) on the occurrence of Ca^{2+} oscillations. These diagrams show the steady state Ca^{2+} levels as a function of the $InsP_3$ concentration. When the steady state is stable, it is indicated by a plain curve. When it is unstable, it is indicated by a dotted line ; in this case, the steady state is not observed but oscillations around this steady state occur. In this case, the maximum value of the Ca^{2+} concentration reached during the oscillations is indicated by a dashed line. Thus, in these diagrams, oscillations are observed for domains of $InsP_3$ values in which there is no plain line. Panels A and B correspond to cells possessing only one type of $InsP_3R$. The shapes of the curves are very different for type 1 (A) or type 2 (B). When the density of receptors (λ_i) is decreased, it leads in both cases to an increase of the oscillatory domain. This increase is however much larger for type 2 (D) than for type 1 (C). See text for details. Results have been obtained using AUTO (Doedel, 1981), as implemented by *xppaut* (Ermentrout, 2002). Equations and parameters are the same as in Figs. III.2 and III.3, except for the values for the λ_i

In contrast, for type 1, the steady-state level of Ca^{2+} first smoothly increases with $InsP_3$ because of the lower affinity of $InsP_3R1$ for $InsP_3$ ($K_1 = 0.5$ μM). When $InsP_3$ further increases, the rise of Ca^{2+} as a function of $InsP_3$ becomes very fast because receptor deactivation by Ca^{2+} occurs progressively less. For both isoforms, oscillations roughly occur when the (unstable) steady state level of Ca^{2+} is in the range of the activation and inhibition constants of the receptors ($K_{act} = 0.5$ μM and $K_{inh} = 0.247$ μM for types 1 and 2) ; thus, one observes that oscillations occur for ~0.2 μM < C_c < ~0.8 μM.

The diagrams shown in Fig. III.4A and B would correspond to cases where all $InsP_3Rs$ in a given cell are the same (as $\lambda_i = 1$). To understand why the suppression of one or the other type of $InsP_3Rs$ does differently affect the Ca^{2+} dynamics of the cell, we redraw the same bifurcation diagram for lower values of λ_i (Fig. III.4C & D). In contrast to what would be expected intuitively, the oscillatory domain increases in both cases. This is due to the fact that, as there are less channels, there is less Ca^{2+} released, which postpones the inhibition for higher values of $InsP_3$. Interestingly, the increase in the oscillatory domain is much larger for type 2 than for type 1. Again, this can be explained by the facts

that the steady-state level of Ca^{2+} does not change much with $InsP_3$ for type 2 (but well for type 1) and that oscillations of Ca^{2+} can only occur when the steady state level of Ca^{2+} is in the range of the activation and inhibition constants of the receptors (the value of the steady Ca^{2+} level at which oscillations disappear is roughly the same for both isoforms). Not shown in Fig. III.4 is the fact that if λ_i becomes too small, oscillations are no longer possible whatever the $InsP_3$ concentration, just because there is not enough Ca^{2+} released. In this case, the bifurcation diagram appears as a nearly flat line on the x axis. Thus, both for type 1 and type 2 receptors, the size of the oscillatory domain first increases and later decreases when decreasing λ_i (not shown).

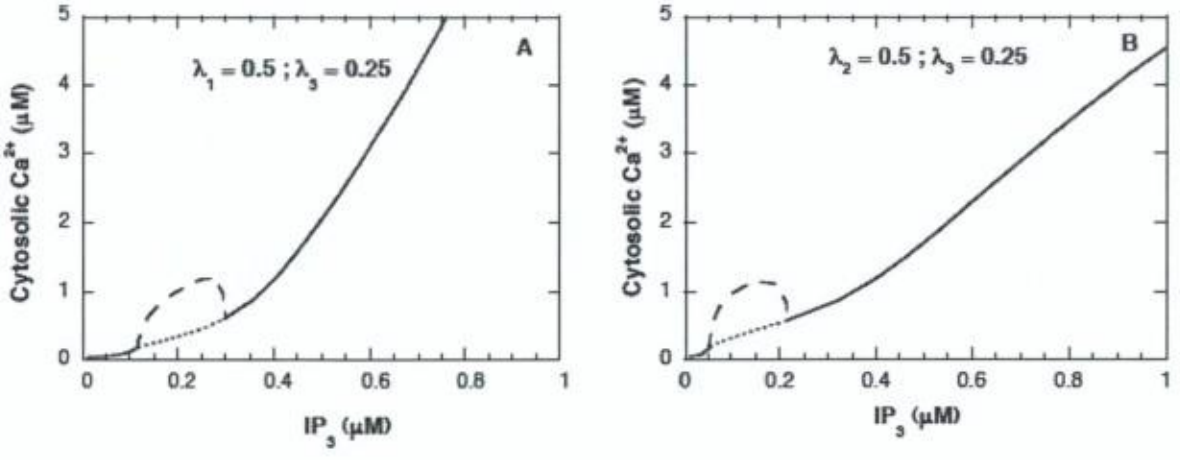

Fig. III.5. Bifurcation diagrams showing the effect of adding some amount of type 3 receptors to an homogeneous population of type 1 (A) or type 2 (B) receptors. These curves have to be compared with Figs. III.4C and III.4D, respectively. In both cases, the oscillatory domain is much reduced when adding a small proportion of type 3. Results have been obtained as in Fig. III.4.

The behaviour of type 3 is different, as oscillations cannot be obtained in this range of parameter values (Fig. III.3C). Moreover, for the situation shown in Fig. III.3, $InsP_3R3$s even tend to suppress the Ca^{2+} oscillations generated by $InsP_3R1$ and/or $InsP_3R2$. This is shown in Fig. III.5 : Fig. III.5A is the bifurcation diagram of a system characterized by twice more $InsP_3R1$ than $InsP_3R3$. Thus, by comparison of Fig. III.4C and Fig. III.5A, one can directly see the effect of type 3 receptors on $InsP_3R1$. Clearly, the oscillatory domain is much reduced. The flux of Ca^{2+} through the $InsP_3Rs$ indeed increases the Ca^{2+} level for all values of $InsP_3$ concentrations, without providing the feedbacks necessary for oscillations to occur. The effect of type 3 on type 2 receptors is even more pronounced (compare Figs. III.4D and III.5B).

Although in the situations encountered above, type 3 isoforms have an inhibitory effect on $InsP_3R2$ and $InsP_3R1$-induced Ca^{2+} oscillations, simulations predict that this is not always the case. An example of such a situation is shown in Fig. III.6. The upper panel shows damped oscillations obtained in the absence of $InsP_3R3$ with a low density of both type 1 and 2 receptors. In this case, oscillations cannot be sustained, because the global flux of Ca^{2+} is too small to reach the typical Ca^{2+} concentration in which activation/inhibition by Ca^{2+} may occur. Sustained Ca^{2+} oscillations can be obtained in this case by the addition of $InsP_3R3$ (Fig. III.6B), which increases the total Ca^{2+} release from the ER. It is interesting to note that starting from a situation as that shown in Fig. III.6B (i.e. when the overall receptor density is low), the suppression of *any* type of receptors provokes the disappearance of Ca^{2+} oscillations. In the same manner, for slightly higher values of receptor densities, one can get situations where 2 out of the 3 isoforms are enough to get oscillations, whatever the nature of these receptors (for example, for $\lambda_1 = 0.35$, $\lambda_2 = 0.25$ and $\lambda_3 = 0.15$ in the same conditions as in Fig. III.6, not shown).

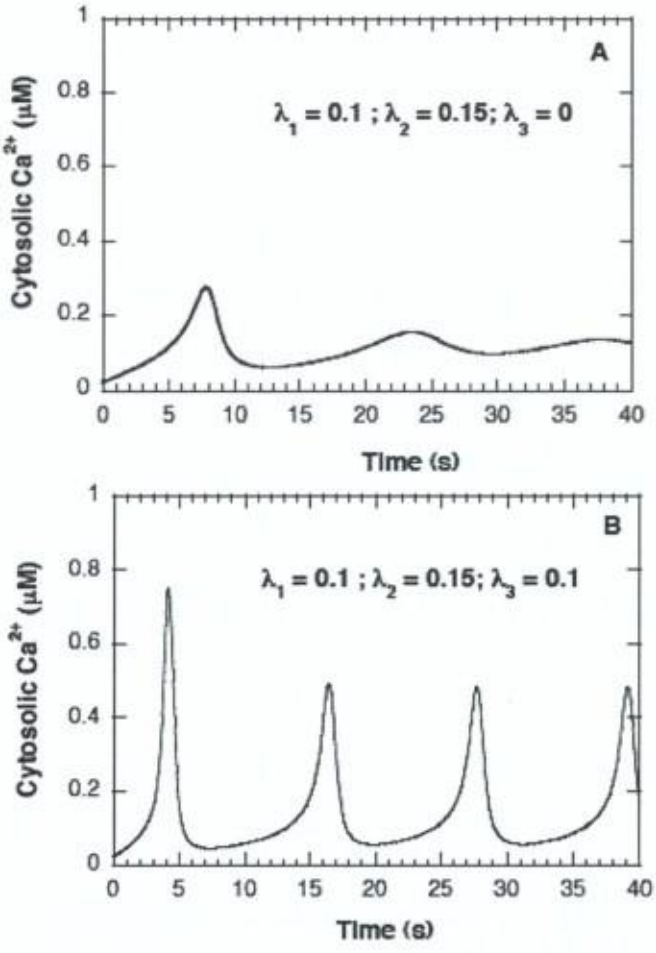

Fig. III.6. Addition of $InsP_3R3$ can restore oscillation in a simulated cell in which the population of type 1 and type 2 receptors is too low. Panel A : damped Ca^{2+} oscillations obtained in a cell characterised by a low density of type 1 and type 2 receptors. Panel B : when adding a small amount of type 3 receptors to the same simulated cells, oscillations become sustained (see text). Results have been obtained as in Figs. III.2 and III.3 except for the values of the λ_i, which are indicated, and for $IP_3 = 0.2$ µM.

III.4. Discussion

Multiple isoforms of the $InsP_3R$ have been identified. They are differently expressed in different cell types, with different cellular locations and at distinct developmental stages (Vermassen *et al.*, 2004). However, our understanding of the functional significance of this receptor diversity remains rather limited. The detailed investigation of the effect of specific $InsP_3$ receptor isoforms on cellular Ca^{2+} signals is indeed a delicate problem. Its full understanding involves electrophysiological and biochemical characterizations of the 3 isoforms, as well as the detailed analysis of Ca^{2+} signals in cells either characterized by different sub-populations of receptors, or artificially expressing one or the other isoform. A modelling approach can thus help to make the link between these various data and suggest some conclusions about the respective role of each isoform.

It is clear that our description of the regulatory properties of the $InsP_3R$ subtypes as well as the assignment of these properties to a given subtype provides a much simplified description of the reality. One oversimplification is, for instance, that we have not considered the heterotetrameric nature of most $InsP_3Rs$ complexes. We have also adopted the point of view that the $InsP_3R3$ is not (or nearly not) inhibited by Ca^{2+}, an hypothesis that is far from being widely acknowledged (see, for example, Missiaen *et al.*, 1998 ; Swatton *et al.*, 1999). In the same manner, the displacement of the bell-shaped

dependence of the fraction of open $InsP_3Rs$ on Ca^{2+} has been often reported for other types than for type 1 (see, for example, Mak *et al.*, 2001b). Our aim here was of course not to validate or invalidate any study of this sort but rather to make the link between well-defined regulations of the $InsP_3Rs$ by Ca^{2+} and $InsP_3$ and their possible effect on the robustness of Ca^{2+} oscillations at the cellular level.

We have thus shown that if one assumes that $InsP_3R2$ is the most sensitive to $InsP_3$ and to Ca^{2+} changes (reflected by a sharp bell-shaped curve, Fig. III.1), one theoretically recovers the experimental conclusion that this type is the major Ca^{2+} oscillator. It is interesting to stress that both characteristics of this subtype (high $InsP_3$ sensitivity and sharp bell-shaped curve) both favour the existence of Ca^{2+} oscillations upon an extended range of $InsP_3$ concentration and receptor density.

A smoother bell-shaped steady-state dependence of the open probability of the $InsP_3R$ on Ca^{2+} is obtained when assuming that $InsP_3$ affects the Ca^{2+}-induced inhibition of the channel. Although this regulation was deduced from the observation that the bell-shaped curve is shifted to the right when increasing the $InsP_3$ concentration, it led to the theoretical conclusion that Ca^{2+} oscillations based on this mechanism are less robust and easily transformed into damped oscillations. When considering that the interplay between $InsP_3$ and Ca^{2+}-induced inhibition typifies $InsP_3R1$, one recovers the experimental observations performed in DT40, myocytes, COS and HeLa cells as to the effect of selectively expressing type 1 $InsP_3R$ or down-regulating types 2 and 3 (Miyakawa *et al.*, 1999 ; Morel *et al.*, 2003 and Hattori *et al.*, 2004). It is interesting to stress that, again, the observed behaviour is also reinforced by a reduced sensitivity of this $InsP_3R$ to $InsP_3$ (as compared to type 2).

When the steady-state dependence of the open probability of the $InsP_3R$ is assumed to be a monotonous function of Ca^{2+} (as we did for $InsP_3R3$), no oscillations can be obtained considering this isoform only. In fact, this conclusion is similar to the results obtained with the 'Ca^{2+}-induced Ca^{2+} release' models of first generation (Dupont and Goldbeter, 1993) where Ca^{2+} oscillations required some Ca^{2+} exchange with the extracellular medium. As we have considered here the situation of a closed cell, the $InsP_3R3$ can only provide a constant influx into the cytoplasm. However, as its sensitivity to $InsP_3$ is weak, this constant Ca^{2+} flux is most of the time rather low. Moreover, the modelling assumption that the cytoplasm does not exchange Ca^{2+} with the external medium is likely responsible for the discrepancy between the experimental and theoretical results visible in Fig. III.3C. In the model, when a cell is assumed to contain only $InsP_3R3$, stimulation by a relatively low dose of $InsP_3$ does not produce any visible Ca^{2+} increase. In contrast, one large Ca^{2+} peak is seen in the experiments (Miyakawa *et al.*, 1999 ; Hattori *et al.*, 2004). The latter behaviour could be reproduced by the model (not shown) if one considers that BCR stimulation of DT40 cells elicits Ca^{2+} entry from the external medium in a manner that is dependent on the expression of the $InsP_3R3$ isoform, as proposed by Morita *et al.* (2004) (see also Guillemette *et al.*, 2005).

Following the available experimental data, we have focused on the effect of changing the $InsP_3R$ density on Ca^{2+} oscillations. The analysis shows that, both for types 1 and 2, oscillations occur for a larger range of $InsP_3$ concentrations when the receptor density is reduced up to a certain limit. The resulting reduced Ca^{2+} flux indeed postpones the inhibitory effect of Ca^{2+} on its own release. The effect is however much more pronounced for type 2 where $InsP_3$ does not interfere with Ca^{2+}-induced inhibition (see Fig. III.4 and section III.3). In contrast to the effect of reducing type 1 or 2 receptor density, the effect of the addition of type 3 receptor can both suppress and induce Ca^{2+} oscillations depending on the conditions. In most cases, the constant Ca^{2+} influx provided by $InsP_3R3$ tends to suppress type1 and/or type 2-induced Ca^{2+} oscillations by providing a constant inhibitory input of Ca^{2+}. However, when the overall density of $InsP_3R1$ and $InsP_3R2$ in a cell is too low for sustained Ca^{2+} oscillations to occur, addition of a small amount of $InsP_3R3$ can boost up Ca^{2+} oscillations, exactly as the combination of a sub-threshold stimulation and Ca^{2+} entry can provoke oscillations (Rooney *et al.*, 1991). These theoretical conclusions thus suggest that the present experimental results might not apply to all cell types, and that the $InsP_3R3$ is not always an 'anti-oscillatory unit'.

In the future, this approach needs to be pursued to investigate the spatial aspects related to the spatially inhomogeneous distribution of receptor sub-types. It is clear indeed that the functional

interactions between the 3 subtypes will be affected by their possible spatial clustering. The regulations by accessory proteins, which clearly differ from one $InsP_3R$ isoform to the other, is another point that deserves to be further explored and that might help to improve our understanding of the origin of the impressive variety of $InsP_3$-mediated intracellular Ca^{2+} signals.

PART 2: STOCHASTIC SIMULATIONS

CHAPTER IV

Stochastic simulations of the Ca^{2+} dynamics around small clusters of $InsP_3$-sensitive Ca^{2+} channels

IV.1. Introduction

We have seen that the Ca^{2+}-dependence of the opening of $InsP_3$-sensitive Ca^{2+} channels in the endoplasmic reticulum is believed to play a major role in both elementary and global aspects of Ca^{2+} signalling in a variety of cell types (see Chapter I and Berridge, 1993; 1997 for reviews). The dual effect of Ca^{2+} on channel opening, i.e. fast activation and slower inhibition, has been well characterized in *in vitro* systems by $^{45}Ca^{2+}$ flux measurements and electophysiological measurements in lipid bilayers (Bezprozvanny *et al.*, 1991; Finch *et al.*, 1991). On the other hand, *in vivo* observations of the behaviour of these channels suggest that the bell-shaped dependence of their activity on cytosolic Ca^{2+} plays a major role in the regulation of Ca^{2+} in intact cells (Berridge, 1997), presumably because the activities of the $InsP_3$-sensitive Ca^{2+} channels distributed throughout the cytoplasm may be co-ordinated through Ca^{2+} diffusion. For sufficient stimulatory levels, oscillations and waves can develop. From a theoretical point of view, this feedback effect of Ca^{2+} on the Ca^{2+} releasing activity has been incorporated in many different models, and has accounted for a variety of experimental facts, e.g. oscillations of cytosolic Ca^{2+} and intracellular propagation of waves (see Sneyd *et al.*, 1995; Tang *et al.*, 1996; Dupont, 1999 and Schuster *et al.*, 2002 for reviews).

Independently, the potential implications of the fact that the local Ca^{2+} concentration is much higher at the mouth of an open channel than in the bulk cytoplasm gained wide recognition (Stern, 1992; Neher, 1995; Kasai and Petersen, 1994). The spatial and dynamic characteristics of these intermediate Ca^{2+} domains were studied for several types of channels (Sherman *et al.*, 1990; Neher and Augustine, 1992; Imredy and Yue, 1992; Rizzuto *et al.*, 1993; Kargacin, 1994; Monck *et al.*, 1994; Llinas *et al.*, 1995; Smith *et al.*, 1996; Rios and Stern, 1997). Previously, we suggested that these intermediate domains could be responsible for interesting properties of the $InsP_3$-sensitive channel, such as the possibility to generate an incremental detection-like behaviour (Swillens *et al.*, 1994) or long-period Ca^{2+} oscillations (Dupont and Swillens, 1996). The critical role of endogenous or exogenous Ca^{2+} buffers for such local Ca^{2+} signalling was also recognized (Zhou and Neher, 1993; Gabso *et al.*, 1997).

Since most models are interested in describing the behaviour of a cell which contains a large population of channels, they are generally based on deterministic kinetic equations. However, it is not clear how the idea of intermediate domains with a high concentration of Ca^{2+} can withstand the explicit consideration of both the stochastic nature of the channel opening and the relatively fast Ca^{2+} diffusion: indeed, it is not unreasonable to anticipate intuitively that such a domain would be washed away by passive diffusion very rapidly after channel closure.

In this chapter, we have therefore attempted to describe in stochastic terms the behaviour first of a single (sections IV.2 and IV.3) and than of a group (section IV.4) of $InsP_3$-sensitive channel inserted in a cytosolic-like medium with realistic diffusion characteristics. Interestingly, we found that under these conditions, and with minimal hypotheses about the parameters to be used, our simulated single channel exhibited bursts of activity, i.e. repetitive openings due to re-activation of the channel by the Ca^{2+} ions flowing through it. The resulting simulated rises in the average Ca^{2+} concentration in a macroscopic volume around the channel were reminiscent of experimentally observed fundamental events in Ca^{2+} release, the so-called 'blips' (Parker and Yao, 1996), whose duration had not been understood previously and for which our simulaton might thus provide a realistic explanation. Besides these true elementary events resulting from transient activation of a single channel, other types of small-scale Ca^{2+} increases, called 'Ca^{2+} puffs', have been reported. These puffs, exhibiting amplitudes about 5 times higher than blips, are thought to result from the concerted opening of a few clustered channels. Thus, in the second part of this chapter (section IV.4), we go a step further and aim at understanding how clusters of $InsP_3$-sensitive channels could generate blips and puffs forming a continuum of events of graded size and variable time courses.

IV.2. Stochastic model of an isolated $InsP_3$-sensitive Ca^{2+} channel

IV.2.1. Operational model for the $InsP_3$-sensitive Ca^{2+} channel

Our aim (Swillens *et al.*, 1998) was to develop an operational model which could account for the following properties of the $InsP_3$-sensitive Ca^{2+} channel : (i) the open probability of the channel exhibits a bell-shaped dependence on cytosolic Ca^{2+} concentration, with a slight positive cooperativity (Bezprozvanny *et al.*, 1991); and (ii) the mean open time of the channel decreases as the Ca^{2+} flux increases (Bezprozvanny and Ehrlich, 1994).

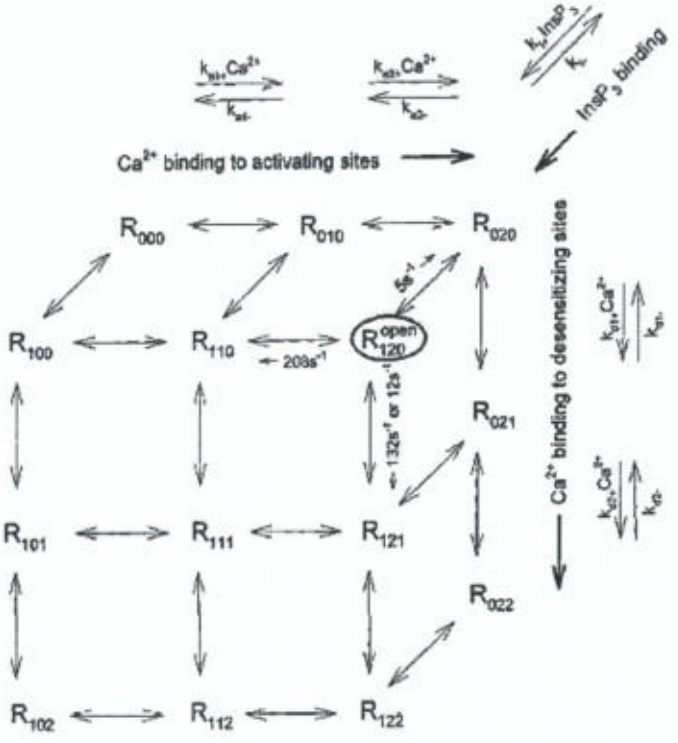

Fig. IV.1. Model for the $InsP_3$-sensitive Ca^{2+} channel. The channel exhibits different states, defined by the absence or the presence of $InsP_3$ and Ca^{2+} in the respective specific binding sites: the symbol R_{ijk} refers to the state of the channel, to which i (0 or 1) $InsP_3$ molecule, j (0, 1 or 2) Ca^{2+} ions (at the activating sites) and k (0, 1 or 2) Ca^{2+} ions (at the desensitizing sites) are bound. The transitions between the different states may be described by a cubic scheme, partially represented in this figure. Ca^{2+} binding to activating and desensitizing sites are shown as horizontal and vertical transitions, respectively. $InsP_3$ binding is represented by transitions between back and front faces of the cube. The life time of the open state (encircled) depends on the kinetics of the three events, which, in this scheme, are quantitatively characterized by their first order (for $InsP_3$ dissociation or Ca^{2+} dissociation from the activating site) or pseudo first order (for Ca^{2+} binding to the desensitizing site) rate constants. In the latter case, the value is proportional to the Ca^{2+} concentration at the mouth of the channel: the high and the low values shown correspond to an unitary current of 1.1 pA or 0.1 pA, respectively, under bilayer experimental conditions. The values of the kinetic constants used in the following simulations are given in Table IV.2.

Our basic model is shown in Fig. IV.1. It is based on the existence of a single $InsP_3$ binding site (for simplicity, it is assumed here that $InsP_3$ binding is not cooperative (Watras *et al.*, 1991), two activating Ca^{2+} binding sites and two inhibitory or 'desensitizing' Ca^{2+} binding sites. It is assumed that $InsP_3$ binding does not depend on Ca^{2+} binding and that, although Ca^{2+} binding to the activating sites is cooperative in both cases, there is no allosteric interaction between these different sites. As shown in Fig. IV.1., Rijk refers to the different states of the channel: i is equal to 1 or 0 depending on whether $InsP_3$ is bound or not to the channel, j represents the number of activating sites occupied by Ca^{2+} (j=0,

1 or 2), and k represents the number of desensitizing sites occupied by Ca^{2+} (k=0,1 or 2). It is assumed that the channel is in the open state only when Ca^{2+} is present on the $InsP_3$ binding site and on both activating sites while not present on any of the desensitizing sites, i.e. the open state is R120. The channel is closed in all other situations.

When the channel is open, the Ca^{2+} concentration in the vicinity of the channel is higher than that in the bulk cytosolic phase and, thus, the kinetics of Ca^{2+} association to the desensitizing sites depends on this local concentration at the mouth of the channel (Ca^{2+}_{mouth}). When the channel closes, excess Ca^{2+} disappears by diffusion. In order to simulate Ca^{2+} binding to activatory and desensitizing sites, this local Ca^{2+} concentration at the mouth of the channel must be computed at every instant.

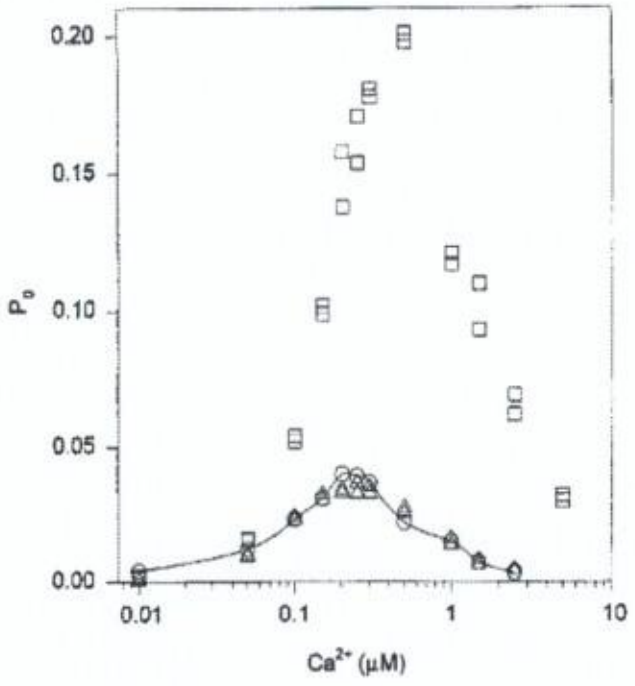

Fig. IV.2. Stochastic simulation of the model under bilayer conditions: relationship between the channel open probability and the Ca^{2+} concentration in the *cis* chamber (correponding to the cytosolic side). The stochastic simulation of the model proposed in Fig. IV.1 was based on the set of parameter values defined in Table IV.2, chosen to account for the experimental data illustrated here by circles joined by a solid line (Bezprozvanny *et al.*, 1991). The simulated open probabilities were obtained with an unitary current of either 1.1 pA (triangles) or 0.1 pA (squares).

IV.2.2. Stochastic simulation of the channel behaviour

Simulation of the activity of a single channel requires a stochastic approach, which takes random transitions between the different channel states into account. Assuming that the channel is in a certain state at time t, the numerical procedure has to calculate the probability of the different transitions and to determine into which state the channel will transform after a short time interval Δt. This stochastic procedure can be described by using the following example. Let us suppose that all binding sites of the channel are vacant at time t (the channel is in state R000). From this state, the three possible events are: $InsP_3$ binding, Ca^{2+} binding to an activating site, or Ca^{2+} binding to a desensitizing site (the corresponding states into which the channel may transform during a time interval Δt are R100, R010 and R001). If the interval Δt is sufficiently small to allow at most one transition, the probabilities for the channel to transform into the various possible states within this short time interval are given by:

$$P_{(000\rightarrow 100)} \equiv k_{i+}\left[InsP_3\right]\Delta t \qquad \text{(IV.1)}$$

$$P_{(000\rightarrow 010)} \cong k_{a1+}\left[Ca^{2+}_{mouth}\right]\Delta t \qquad \text{(IV.2)}$$

$$P_{(000\rightarrow 001)} \cong k_{d1+}\left[Ca^{2+}_{mouth}\right]\Delta t \qquad \text{(IV.3)}$$

with rate constants defined in Fig. IV.1. Note that the Ca^{2+} concentration referred to in these equations is the local Ca^{2+} at the mouth of the channel (computed as indicated below), not the bulk cytosolic Ca^{2+}. The probability for the channel to remain in its initial state (R000) is equal to:

$$P_{(000\rightarrow 000)} \cong 1-\left(k_{i+}\left[InsP_3\right]+k_{a1+}\left[Ca^{2+}_{mouth}\right]+k_{d1+}\left[Ca^{2+}_{mouth}\right]\right)\Delta t \qquad \text{(IV.4)}$$

Practically, we chose time intervals Δt short enough to ensure that the probability that the channel remains in the same state after Δt was always higher than 0.95. The interval [0,1] was divided into four sub-intervals, corresponding to the four possible states:

interval $\left[0, P_{(000\rightarrow 100)}\right]$ for R100

interval $\left[P_{(000\rightarrow 100)}, P_{(000\rightarrow 100)}+P_{(000\rightarrow 010)}\right]$ for R010

interval $\left[P_{(000\rightarrow 100)}+P_{(000\rightarrow 010)}, P_{(000\rightarrow 100)}+P_{(000\rightarrow 010)}+P_{(000\rightarrow 001)}\right]$ for R001

and interval $\left[P_{(000\rightarrow 100)}+P_{(000\rightarrow 010)}+P_{(000\rightarrow 001)}, 1\right]$ for R000.

The stochastic procedure randomly generated a number between 0 and 1; the sub-interval which contained this random number then defined the channel state at time $t+\Delta t$. The procedure was then reproduced over and over to generate a stochastic succession of channel states.

IV.2.3. Three dimensional Ca^{2+} diffusion from a point source

Diffusion in a cytosolic-like medium

Since the present study only considers the activity of a single channel placed in a homogeneous three dimensional space, Ca^{2+} diffusion was described in spherical coordinates: the time-dependent distribution of Ca^{2+} concentration was calculated along the radial direction. For the actual simulation of channel behaviour in a cytosolic environment (Figs. IV.4-IV.7), space discretization was defined as follows: the source was located in a central sphere characterized by a small radius Δr. This sphere was surrounded by N successive concentric shells, all with the same thickness equal to Δr. The Ca^{2+} concentration next to the outer shell was kept constant. For simulation of short range diffusion and evaluation of the local Ca^{2+} concentration at the mouth of the channel (Fig. IV.3), the space for diffusion consisted of hemispheres only.

In the absence of buffer, the Ca^{2+} distribution obeys the equation:

$$\frac{\partial C(r,t)}{\partial t} = D_C \nabla^2 C(r,t) + \sigma(r,t) \qquad \text{(IV.5)}$$

where ∇^2 is the Laplacian operator, here equal to :

$$\frac{2}{r}\frac{\partial}{\partial r}+\frac{\partial^2}{\partial r^2}$$

C(r,t) is the Ca^{2+} concentration at time t and at distance r from the center where the source is placed, D_C is the Ca^{2+} diffusion coefficient, and $\sigma(r,t)$ is the Ca^{2+} influx at the source, i.e. $\sigma(r,t)$ is different from zero only for r = 0.

For the kind of discretization described above, we approximated the Laplacian operator applied to a function F(r) by operator L, defined as follows:

$$L(F_i)=\frac{1}{\Delta r^2}\left[\left(1-\frac{1}{i+\frac{1}{2}}\right)F_{i-1}-2F_i+\left(1+\frac{1}{i+\frac{1}{2}}\right)F_{i+1}\right] \qquad \text{i=1,2...N} \qquad \text{(IV.6)}$$

where F_i approaches the function F in the ith shell. We checked that these approximations gave results in agreement with the analytical solution for a simple system consisting of a constant Ca^{2+} point source placed in an infinite space.

Buffer	Total concentration (μM)	Ca^{2+} dissociation constant (μM)	Diffusion coefficient ($\mu m^2 s^{-1}$)
Endogenous			
Stationary	300[a]	10[a]	0
Mobile	50[b]	10[b]	15[c]
Exogenous			
Calcium Green-1	50[a]	0.7[d]	31[e]

Table IV.1. Assumed characteristics for the Ca^{2+} buffers in the cytosol. a: Parker *et al.* (1996); b: Smith *et al.* (1996); c. Gabso *et al.* (1997); d: The K_d of Calcium-Green-1 is only known under *in vitro* conditions (about 250 nM (Eberhard and Erne, 1991)), and related dyes under such conditions have a dissociation constants which is several fold higher than in protein-free solution (Bassani *et al.*, 1995; Zhao *et al.*, 1996); we thus tentatively estimated that the dissociation constant for Calcium Green-1 to be used was around 700 nM. e: We assumed for Calcium Green-1 a diffusion coefficient similar to the one previously measured for the comparable dye Fura-2 (Blatter and Wier, 1990); note that the same authors measure a lower diffusion coefficient (15 $\mu m^2 s^{-1}$) for Indo-1. See also the even lower value (8 $\mu m^2 s^{-1}$) for Calcium Green-1 itself in muscle fibers (Zhao *et al.*, 1996).

In the presence of Ca^{2+} buffers in the diffusion space, mathematical analysis of Ca^{2+} diffusion is more difficult. Since our study was intended to be semi-quantitative only, we used the rapid buffering approximation proposed by Smith *et al.* (1996). These authors have shown that this approximation is acceptable to mimic physiological buffers, both in the absence and in the presence of moderate concentrations of Ca^{2+} indicator dyes like Calcium Green-1. The procedure calculates Ca^{2+} concentration at time t+Δt in the central sphere (C_0) and in the successive shells (C_i, i=1 to N) as functions of the Ca^{2+} concentrations obtained at time t:

$$C_i(t+\Delta t)=C_i(t)+\Delta t\beta_i(t)\left[L(F_i(t))+\sigma\delta_{i0}\right] \qquad \text{i=0,1,...N} \qquad \text{(IV.7)}$$

with

$$\delta_{00}=1,\ \delta_{0i}=0 \text{ for i>0} \qquad \text{(IV.8)}$$

$$\beta_i(t)=\left[1+\frac{K_S B_{S,tot}}{\left(K_S+C_i(t)\right)^2}+\frac{K_m B_{m,tot}}{\left(K_m+C_i(t)\right)^2}+\frac{K_e B_{e,tot}}{\left(K_e+C_i(t)\right)^2}\right]^{-1} \qquad \text{(IV.9)}$$

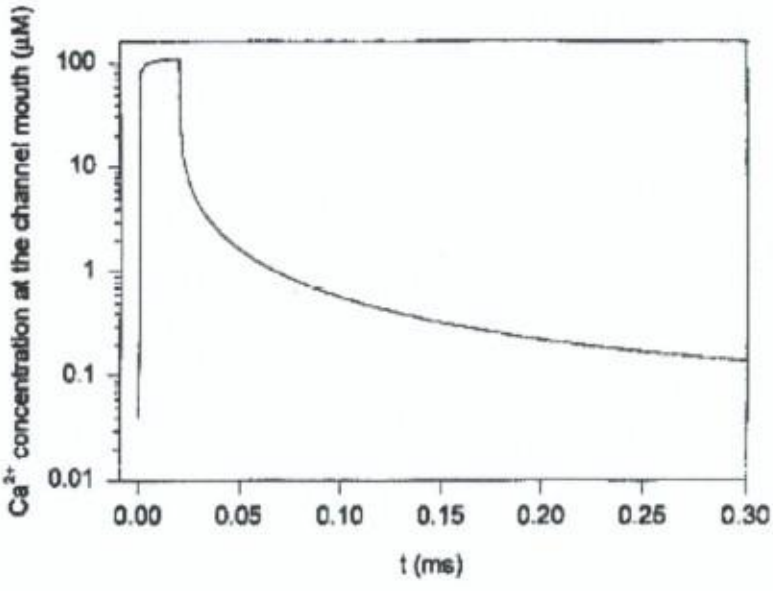

Fig. IV.3. Ca^{2+} concentration in the vicinity of a Ca^{2+} point source placed in a cytosolic-like medium. The simulation considered a Ca^{2+} point source generating, during 20 µs, a current of 0.1 pA into a cytosolic medium described by a hemispherical space made of 166 shells of 6 nm thickness each. The basal Ca^{2+} concentration was set to 40 nM, and only endogenous buffers were considered, whose characteristics are listed in Table IV.1. Ca^{2+} diffusion was simulated according to equ. (IV.7). The curve represents the Ca^{2+} concentration in the central hemisphere of 6 nm radius containing the point source. Fitting of the fast component decay curve (first 15 µs after source closure) by a bi-exponentional function gave:

$$Ca^{2+}_{mouth} = 91\mu M \exp\left(-\frac{t-t_{closure}}{0.17\mu s}\right) + 19\mu M \exp\left(-\frac{t-t_{closure}}{5.6\mu s}\right) + 0.04\,\mu M$$

$$F_i(t) = D_c C_i(t) + D_m \frac{B_{m,tot} C_i(t)}{K_m + C_i(t)} + D_e \frac{B_{e,tot} C_i(t)}{K_e + C_i(t)} \qquad \text{(IV.10)}$$

where indices s and m refer to stationary and mobile endogenous buffers, and index e refers to mobile exogenous buffer; the K_i, $B_{i,tot}$ and D_i are the equilibrium dissociation constants, total buffer concentrations and diffusions coefficients of the mobile buffers, respectively. D_c is the diffusion coefficient of free Ca^{2+} in the cytosol, which was chosen to be equal to 250 $\mu m^2/s$ (Allbritton *et al.*, 1992). Parameters chosen to describe the immobile and mobile endogenous buffers, as well as the mobile exogenous buffer (Ca^{2+} dyes, as mentioned below), are shown in Table IV.1.

Diffusion in a water-like medium

Under conditions corresponding to an electrophysiological bilayer experiment, where Ca^{2+} diffusion into a Ca^{2+}-buffered *cis* chamber, the stationary Ca^{2+} profile in a hemispherical space can be approached analytically (see (Smith *et al.*, 1996) for further justifications). At the mouth of the channel, one gets:

$$Ca^{2+}_{mouth} \approx \frac{\sigma}{2\pi D_c r} e^{-\frac{\lambda}{r}} \qquad \text{(IV.11)}$$

where r represents the distance between the Ca^{2+} desensitizing sites and the center of the pore, and λ is a characteristic length which depends on the kinetics of Ca^{2+} binding to the buffer (Neher, 1986). For

instance, taking the experimental conditions from the experiments reported by Bezprozvanny *et al.* (1994) into account (i = 1.1 pA, 1mM EGTA) and assuming that $D_c = 600\ \mu m^2 s^{-1}$ characterizes Ca^{2+} diffusion in water (Kushmerick and Podolsky, 1969), we find $\sigma = 5.73\ 10^{-18}$ mols^{-1} and $\lambda = 632$ nm. Since the cytoplasmic part of the $InsP_3$-sensitive Ca^{2+} channel appears to be roughly square-shaped with sides about 12 nm long (Katayama *et al.*, 1996), r should be a few nm, say r = 3 nm. Thus, in such experiments, the computed stationary $[Ca^{2+}_{mouth}]$ turns out to be about 500 μM. A different value can be computed if a different Ca^{2+} current is assumed (see following section).

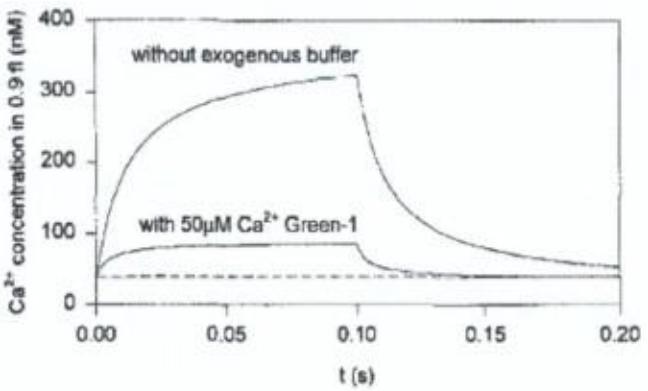

Fig. IV.4. Ca^{2+} concentration in a macroscopic (0.9 fl) cytosolic volume surrounding a Ca^{2+} point source. The simulation considered a Ca^{2+} point source generating, during 100 ms, a current of 0.1 pA into a cytosolic medium described here by a spherical space made of 20 shells of 100 nm thickness each. The basal Ca^{2+} concentration was set to 40 nM (dashed line). Ca^{2+} diffusion was simulated according to Equ. IV.7. The curves (solid lines) represent the average Ca^{2+} concentration in the six central shells (600 nm total radius), corresponding to a 0.9 fl total volume. The curves were obtained assuming an endogenous buffer composition as defined in Table IV.1, either in the absence of in the presence of 50 μM Calcium Green-1, as indicated.

IV.3. Simulation of the Ca^{2+} dynamics around one $InsP_3$-sensitive Ca^{2+} channel

IV.3.1. Stochastic simulation of a single channel under bilayer conditions and determination of parameter values for our model

Our first goal was to define a set of values for the parameters of the model (Fig. IV.1), allowing to account for the electrophysiological data (Bezprozvanny *et al.*, 1991; 1994) obtained with Ca^{2+} channels incorporated in a planar bilayer. In these experiments, the ionic current flowing through the $InsP_3$-sensitive channel was measured in the presence of a high $InsP_3$ concentration and in the presence of various Ca^{2+} concentrations on the *cis* and *trans* sides of the bilayer : the maximal open probability of a single channel was found to be rather low (around 0.04). With the optimally activating concentration of 200 nM Ca^{2+} in the *cis* chamber, the channel mean open time was found to be either 2.9 or 4.7 ms, depending on whether Ca^{2+} was present (44 mM) or not in the *trans* chamber (Sr^{2+} was added to complement the carrier concentration to 55 mM) (Bezprozvanny *et al.*, 1994).

	Binding rate constant	**Dissociation rate constant**
$InsP_3$ site	$k_{i+} = 5\ 10^6\ M^{-1}s^{-1}$	$k_{i-} = 5\ s^{-1}$
First activating Ca^{2+} site	$k_{a1+} = 8.3\ 10^7\ M^{-1}s^{-1}$	$k_{a1-} = 250\ s^{-1}$
Second activating Ca^{2+} site	$k_{a2+} = 4.7\ 10^9\ M^{-1}s^{-1}$	$k_{a2-} = 208\ s^{-1}$
First desensitizing Ca^{2+} site	$k_{d1+} = 2.6\ 10^5\ M^{-1}s^{-1}$	$k_{d1-} = 57\ s^{-1}$
Second desensitizing Ca^{2+} site	$k_{d2+} = 5.7\ 10^8\ M^{-1}s^{-1}$	$k_{d2-} = 19\ s^{-1}$

Table IV.2 Set of parameter values used to simulate the model defined in Fig. IV.1

According to our model (Fig. IV.1), the channel closes when any one out of the three following events occurs: (i) dissociation of $InsP_3$; (ii) dissociation of Ca^{2+} from one of the activating sites; or (iii) binding of Ca^{2+} to one of the desensitizing sites. Since the kinetics of these three events are characterized by k_{i-}, k_{a2-} and k_{d1+} $[Ca^{2+}_{mouth}]$, respectively, the two values of the mean open time mentioned above can be used to estimate two of these three kinetic parameters, on the basis of the equation:

$$\text{Mean open time} = \frac{1}{k_{i-} + k_{a2-} + k_{d1+}\left[Ca^{2+}_{mouth}\right]} \qquad \text{(IV.12)}$$

where $[Ca^{2+}_{mouth}]$ is the Ca^{2+} concentration in the vicinity of the Ca^{2+} desensitizing site of the open channel. In this equation, the rate of $InsP_3$ dissociation, k_{i-}, can be considered to be $5s^{-1}$ as previously measured (Hannaert-Merah *et al.*, 1995); in the absence of Ca^{2+} flux in the bilayer experiments, we assume here that $[Ca^{2+}_{mouth}]$ is identical to the bulk Ca^{2+} concentration in the *cis* chamber (200 nM), and in the presence of 1.1 pA Ca^{2+} flux (once the channel is open), we assume that $[Ca^{2+}_{mouth}]$ is stationary and, because of the size of the channel and the properties of Ca^{2+} diffusion in the *cis* compartment, equal to 500 µM (see section IV.2). From the two corresponding values cited above for the mean open time, we thus conclude that $k_{a2-} = 208\ s^{-1}$ and $k_{d1+} = 2.6\ 10^5\ M^{-1}s^{-1}$. Note that since the contributions of the three reactions to closing the channel are in the ratio $k_{i-}/k_{a2-}/k_{d1+}$, i.e. in the ratio 5/208/132, the rate of Ca^{2+} dissociation from the activating sites appears to play a dominant role, but the contribution of the Ca^{2+} induced desensitizing process is highly significant under these conditions of large luminal Ca^{2+} concentration (44 mM) and, therefore, of large Ca^{2+} flux (1.1 pA) and high Ca^{2+} concentration (500 µM).

The other kinetic parameters describing Ca^{2+} binding cannot be estimated by direct calculation: stochastic simulation of the model is required to define a set of parameter values compatible with the bell-shaped curve describing the channel open probability as a function of the Ca^{2+} concentration in the *cis* chamber (Bezprozvanny *et al.*, 1991). The values presented in Table IV.2 were found to fit reasonably well the experimental data (compare circles (experimental data) and triangles (simulated points) in Fig. IV.2; these results were obtained assuming a concentration for $InsP_3$ 10 times higher than the dissociation constant). We repeated twice the numerical simulation in order to show the small variations inherent to stochastic processes. At 200 nM Ca^{2+} in the cis chamber, the mean open times corresponding to the simulated experiments were equal to 2.8 and 3.1 ms, respectively, in these duplicate simulations.

It should be kept in mind that the experimental data simulated in Fig. IV.2 were obtained in the presence of 44 mM *trans* (luminal) Ca^{2+}, a concentration which resulted in a large Ca^{2+} flux through the channel. Bezprozvanny and Ehrlich have already pointed out that, under physiological conditions, since the luminal Ca^{2+} concentration was certainly lower, the resulting Ca^{2+} current would be lower; on the basis of an estimated luminal concentration of 2.5 mM, a Ca^{2+} current of about 0.5 pA was predicted (Bezprozvanny *et al.*, 1991). However, several recent studies have shown that in a variety of cell types, the luminal Ca^{2+} concentration is still lower, ranging from 40-700 µM (Chatton *et al.*, 1995; Combettes *et al.*, 1996; Hofer and Schulz, 1996; Tanimura and Turner, 1996; Miyawaki *et al.*, 1997; Montero *et al.*, 1997). On the basis of an intermediate value of 500 µM, and assuming a linear relationship between the current and the luminal Ca^{2+} concentration in this range of concentrations (Bezprozvanny *et al.*, 1991), an even smaller value of 0.1 pA can, therefore, be predicted for the physiological unitary Ca^{2+} current. In this case, the calculation of $[Ca^{2+}_{mouth}]$ (equ. IV.11) leads to a value of 46 µM, and stochastic simulation of the model based on this corrected value of luminal Ca^{2+} concentration leads to a second bell-shaped curve for the channel open probability, also shown in Fig. IV.2 (squares). This second curve exhibits a much higher P_o peak value, of about 0.2, and it is

slightly shifted to the right compared to the curve obtained with a larger current. This is because Ca^{2+}-induced desensitization is less effective for smaller currents, since the local Ca^{2+} concentration in the vicinity of the open channel is lower: k_{d1+} $[Ca^{2+}_{mouth}]$ is then only equal to $12s^{-1}$, compared to 132 s^{-1} in the previous case.

IV.3.2. Deterministic simulation of Ca^{2+} diffusion in the cytosol

Precise stochastic simulation of the channel behaviour under physiological conditions not only depends on an acceptable choice of the luminal concentration of Ca^{2+} (see squares in Fig. IV.2), but also depends on the time evolution of the Ca^{2+} concentration at the mouth of the channel. Thus, the actual Ca^{2+} profile in the cytosolic compartment when the channel opens and closes must be computed under physiological conditions. Since the gradient of Ca^{2+} concentration is very steep in the vicinity of the channel mouth, the computation of Ca^{2+} concentration is this region requires a very small spatial grid, in the range of a few nanometers. This high level of discretization increases the computing time enormously. Therefore, the strategy that has been used here was to simulate, once for all under appropriate conditions, the evolution of the Ca^{2+} concentration at the channel mouth, and on the basis of curve fitting, to express this Ca^{2+} concentration as an empirical function of time, for subsequent use in simulations based on a larger spatial grid. Short range diffusion of Ca^{2+} into the cytosol was simulated according to the method of Smith *et al.* (1996), using parameters for buffer characterization and composition given in Table IV.1. We defined the space for Ca^{2+} diffusion close to the channel mouth as an hemisphere made of 166 concentric shells, with a spatial discretization $\Delta r = 6$ nm (the choice of an hemispheric geometry is justified by the fact that, for such short-range diffusion, the membrane of the Ca^{2+} reservoir locally creates a quasi-planar barrier to the diffusion of cytosolic molecules).

The basal Ca^{2+} concentration was set equal to 40 nM. Fig. IV.3 shows the kinetics of Ca^{2+} accumulation in the central hemisphere after channel opening (the central hemisphere with its 12 nm diameter was considered to reflect the dimensions of the cytosolic domain of the channel), as well as its decay after channel closure. The Ca^{2+} point source was supposed to contribute a 0.1 pA current (see above). It can be seen that, once the channel opens, the Ca^{2+} concentration very rapidly reaches a rather high value, around 110 μM (characteristic time less than 1 μs). It is also apparent that after channel closure, the Ca^{2+} decay curve is multiphasic, with an initial fast decay over the first few microseconds (note the short time scale in Fig. IV.3: Ca^{2+} at the channel mouth drops to submicromolar values within much less than a millisecond). The Ca^{2+} concentration at the channel mouth (in the central sphere of 6 nm radius) is almost indistinguishable from the average Ca^{2+} concentration calculated in the central sphere of 100 nm radius after about 15 μs (not shown). Thus, within this short time period of 15 μs, the Ca^{2+} concentration was fitted to a biexponential function for subsequent stochastic simulations based on a larger spatial grid (the radius of the central sphere will be 100 nm). In those simulations, we will consider that the Ca^{2+} concentration close to to the channel mouth (whose estimation is required to compute the probability of Ca^{2+} binding to activating and desensitizing sites) obeys the following rule: once the channel opens, the Ca^{2+} concentration instantaneously reaches its plateau value; when the channel closes, the bi-exponentional function (defined in the legend to Fig. IV.3) describes the fast Ca^{2+} decay. The same simulation was repeated to determine the evolution of Ca^{2+} when 50 μM of an exogenous Ca^{2+} -sensitive dye, Calcium Green-1 (whose assumed properties are also summarized in Table IV.1) was added to the cytosolic medium, and a new set of parameter values for this bi-exponential function was obtained by curve fitting (result not shown).

Before turning to the actual stochastic simulation of an isolated channel in a cytosolic environment, we also evaluated, with the same deterministic approach as above, whether the channel activity was likely to be detectable under experimental conditions, i.e. when the average Ca^{2+} concentration is measured in a macroscopic volume, of the order of the femtoliter (see below). For this purpose, we evaluated long-range diffusion away from the channel mouth: the space for Ca^{2+} diffusion was now

defined as a complete sphere made of 20 concentric shells of 100 nm thickness each (the radius of the largest cell was thus 2 μm; this choice of complete spheres was made because their dimensions now largely exceed the thickness of the tubules of the endoplasmic reticulum). The diffusion space was again supposed to contain an initial basal Ca^{2+} concentration of 40 nM, as well as homogeneously distributed endogenous buffers, defined in Table IV.1; the same Ca^{2+} source was placed in the center. Since 'elementary' or even 'fundamental' events of $InsP_3$-dependent Ca^{2+} release are nowadays recorded from femtoliter volumes in the presence of Ca^{2+}-sensitive indicator dyes (Parker and Yao, 1996), we computed the kinetics of Ca^{2+} accumulation into the 6 central shells after channel opening, as well as its decay after channel closure: these 6 shells with a total radius of 600 nm, correspond to a volume of 0.9 fl. The channel was supposed to provide, during the first 100 ms, a constant Ca^{2+} source (σ) equal to 5.73 10^{-18} $mols^{-1}$ (which corresponds to the 0.1 pA unitary current of the $InsP_3$-sensitive Ca^{2+} channel). Fig. IV.4 shows the results obtained, both in the absence (upper curve) and in the presence (lower curve) of 50 μM Calcium-Green-1. In the absence of any exogenous dye, under conditions where the basal Ca^{2+} concentration was 40 nM, the mean Ca^{2+} concentration in the 0.9 fl volume rose to more than 300 nM upon channel opening, and the time required to attain the half maximal amplitude, $t_{1/2}$, was about 11 ms, both in the rising phase, when the current was turned on, and during its decay, current turned off. In the presence of 50 μM Calcium Green-1, which acted as a mobile Ca^{2+} buffer, the amplitude of the Ca^{2+} rise was reduced to about 50 nM above the basal value, and the kinetics of the Ca^{2+} concentration changes were accelerated, as indicated by a $t_{1/2}$ value of about 5 ms. This smaller amplitude of 50 nM is, nevertheless, compatible with the experimentally observed Ca^{2+} signals corresponding to the so-called 'blips' (Yao and Parker, 1996; Bootman *et al.*, 1997).

IV.3.3. Stochastic simulation of an isolated channel in the cytosol

The model developed above now allows us to simulate a single channel in a realistic physiological environment. The cytosol was again simulated by considering 20 concentric shells of 100 nm thickness each (the total radius was thus 2 μm), initially containing a basal Ca^{2+} concentration of 40 nM; the diffusing space was supposed to contain physiological concentrations of endogenous buffers, and the Ca^{2+} concentration surrounding the largest shell was maintained at 40 nM. A channel was placed in the center of the sphere, and $InsP_3$ was supposed to be present at half-saturating concentration. When the channel opened, it contributed a current of 0.1 pA. Fig. IV.5A shows a 10s run simulating the stochastic transitions between the various states of the channel. As expected from the relatively slow rate of $InsP_3$ dissociation ($k_- = 5\ s^{-1}$), the $InsP_3$ bound state (second line in Fig. IV.5A) was more stable than the Ca^{2+} bound states (third and fourth lines in Fig. IV.5A). Ca^{2+} binding to the desensitizing sites (fourth line in Fig. IV.5A) was a relatively rare event, which generally followed the opening of the channel (first line in Fig. IV.5A) because of the higher Ca^{2+} concentration at the channel mouth after its opening (in this case, the maximal rate of Ca^{2+} binding to these sites, $k_{d1+}\ Ca^{2+}_{mouth}$ was 29 s^{-1}).

An attractive finding was that the channel presented bursts of activity, resulting from repetitive openings of the channel (see first line in Fig. IV.5A, and the same results plotted on an expanded time-scale in IV.5B). This phenomenon can be interpreted as the consequence of the high Ca^{2+} concentration at the channel mouth just after channel closure, which makes rebinding of Ca^{2+} at the activating site a likely event. The mean duration of the closed state within one such burst of activity was found to be very short (mean closed time equal to 8 μs).

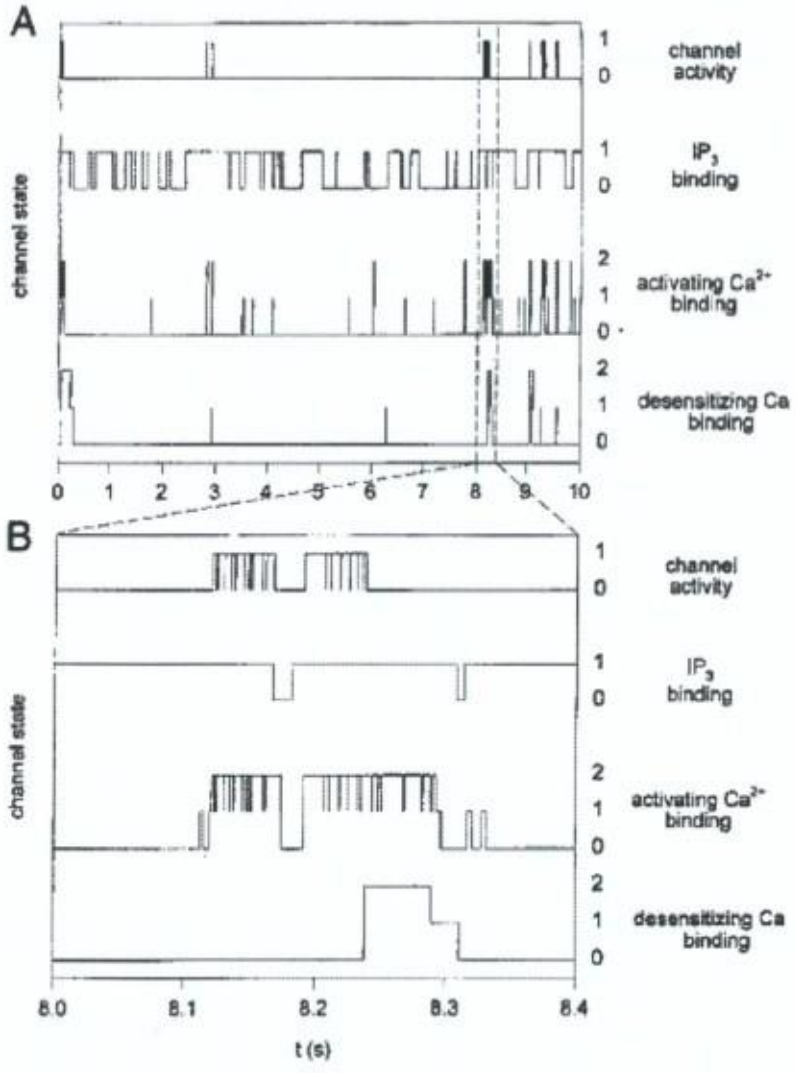

Fig. IV.5. Stochastic simulation of the model under physiological conditions: evolution of the channel states, with respect to $InsP_3$ and Ca^{2+} binding. The stochastic simulation considered the channel placed in a cytosolic medium described by a spherical space, again made of 20 shells of 100 nm thickness each. The basal Ca^{2+} concentration was set to 40 nM, and only endogenous buffers were considered (with the characteristics indicated in Table IV.1). The $InsP_3$ concentration was set to its K_d value (1 μM). (A) 10 s traces of (i) the activity state (1 and 0 refer to open and closed states, respectively) and of the occupancy of the channel sites by (ii) $InsP_3$, (iii) activating Ca^{2+} ions, and (iv) desensitizing Ca^{2+} ions. (B) Same traces as in (A), plotted on an expanded time scale.

Stochastic simulation of the time course of Ca^{2+} accumulation in the same spherical volume of 0.9 fl as above was then performed, now letting the channel flicker between its open and closed states. Three distinct traces, simulated in the absence of any indicator dye, are shown in Fig. IV.6A, with a time origin in each case corresponding to the beginning of the activity burst. We previously showed (Fig. IV.5) that repetitive opening of the Ca^{2+} channel could occur under physiological conditions. It appears in Fig. IV.6A that these repetitive openings lead to transient rises in Ca^{2+} concentration (as measured in our femtoliter spherical volume) which last much longer (up to several tens of milliseconds) than would be expected on the basis of the experimentally found mean open time of the channel (2.9 ms as measured in bilayer experiments, see above). These long durations in the simulated traces are reminiscent of those in the experimentally observed Ca^{2+} blips, corresponding to Ca^{2+} rises in femtoliter volumes of cytosol at low $InsP_3$ concentration (Parker and Yao, 1996) (note than in our

simulations of the behaviour of isolated channels, the same activity bursts show up both at high and low $InsP_3$ concentrations, but of course with different frequencies). Since an activity burst is produced by channel flickering between the open state R120 and the short-lived closed state R110, we defined the burst 'length' as the time interval between the first channel opening and the transition to a state different from R120 or R110. This burst length is a random variable which was characterized by the analysis of 300 events. The distributions of the number of channel openings per activity and of the burst length are shown in Fig. IV.6B, C respectively. On average, a burst comprised 6 channel openings, and lasted about 26 ms. For the long-lasting bursts, Ca^{2+} concentration attained a plateau value close to 300 nM, which is in agreement with the previous results obtained with the deterministic approach (Fig. IV.4). Only the shortest bursts of activity were characterized by lower Ca^{2+} amplitudes, because of the charateristic time of Ca^{2+} accumulation. For this reason, the amplitude of the rise in Ca^{2+} concentration during a burst presented a bell-shaped distribution, with a mean value for the peak Ca^{2+} concentration equal to 201 nM (Fig. IV.6D).

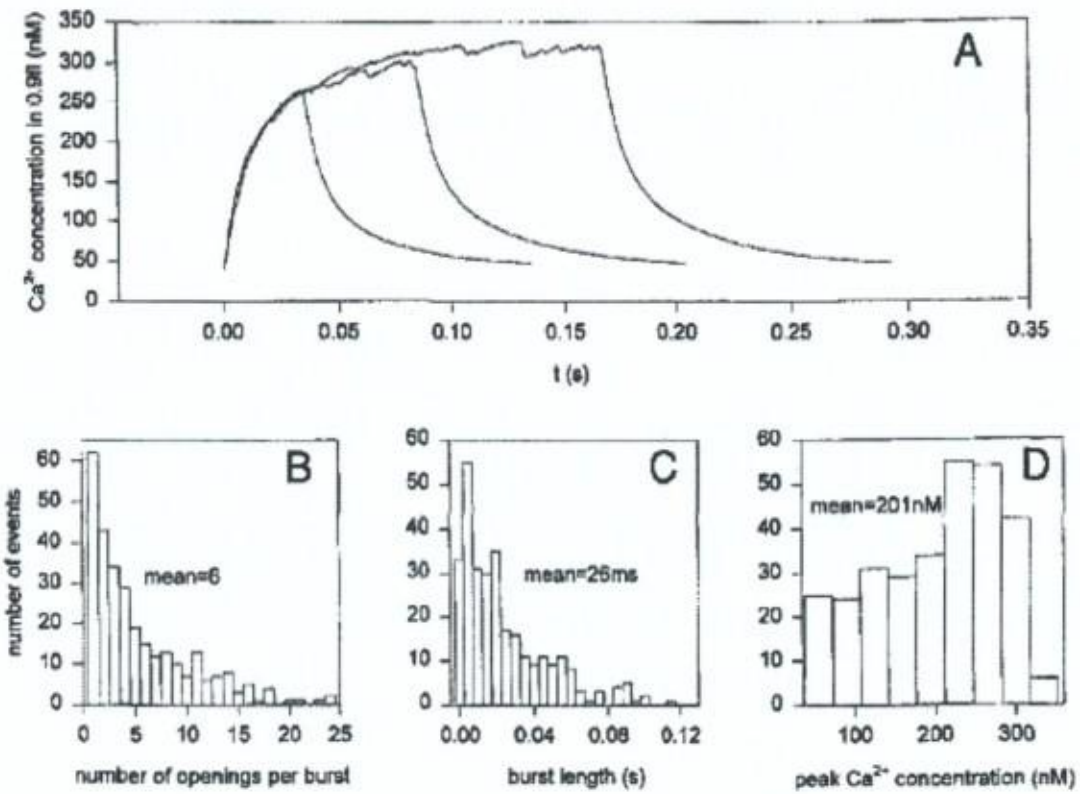

Fig. IV.6. Stochastic simulation of Ca^{2+} transients in a macroscopic (0.9 fl) cytosolic volume, in the absence of exogenous buffer. The stochastic simulation, performed under the same conditions as in Fig. IV.5, was repeated to generate 300 bursts of channel activity; during each of these bursts, the average Ca^{2+} concentration in a 0.9 fl volume (the 6 central shells) was calculated, and statistical analysis was performed. (A) Three activity bursts were selected in order to show the time courses of the corresponding rises in Ca^{2+} concentration, and shown with their time origin aligned. (B) Distribution of the number of channel openings during an activity burst. (C) Distribution of the burst length. (D) Distribution of the maximal or 'peak' Ca^{2+} concentration attained during the burst.

Since Ca^{2+} blips were experimentally observed after including Ca^{2+} fluorescent dyes in the cytosol, we repeated the stochastic simulation of the system under these conditions (Fig. IV.7). As expected from Fig. IV.4, the inclusion of these additional mobile buffers (50 μM Calcium Green-1) reduced the amplitude of this rise in Ca^{2+} concentration upon channel opening, as well as the average number of channel openings per burst (to about 3) and the length of the burst (to about 14 ms) (compare

Fig. IV.6B,C,D and Fig. IV.7B,C,D). However, channel repetitive opening was still present, again leading to bursts of activity of much longer duration than expected on the basis of the channel mean open time. Fig. IV.7A demonstrated that the set of parameters used may lead to blips lasting up to several tens of milliseconds and exhibiting an increment in Ca^{2+} concentration of about 40 nM. These simulated results satisfactorily reproduce experimental observations (Parker and Yao, 1996). We thus propose that the blips experimentally observed under physiological conditions in the presence of 50 mM Calcium Green-1 are explained by repetitive opening of a single Ca^{2+} channel.

IV.3.4. Interpretation of the results

These simulations were originally performed with the final aim of simulating the mutual influence of channels clustered in what has been called a 'puff site'. To do so, we first elaborated a minimal model for an isolated single channel, which led us to an unexpected result. Under realistic conditions for the buffering capacity of the cytosol, such a simulated isolated channel inside the cytosol was found to display bursts of activity, arising from repetitive openings. In our model, where Ca^{2+} binding to activating sites (or its dissociation) is responsible per se for channel opening (closing), these repetitive openings are due to the fact that Ca^{2+} ions diffusing away from the channel mouth after its closure in fact diffuse slowly enough to allow rebinding with a significant probability. These simulated results were obtained with a simple molecular model which might not be the exact description of the $InsP_3$-sensitive channel (for instance, $InsP_3$ binding might well be cooperative, and there might be some necessary order in the binding of $InsP_3$ and Ca^{2+} (Dawson, 1997)).

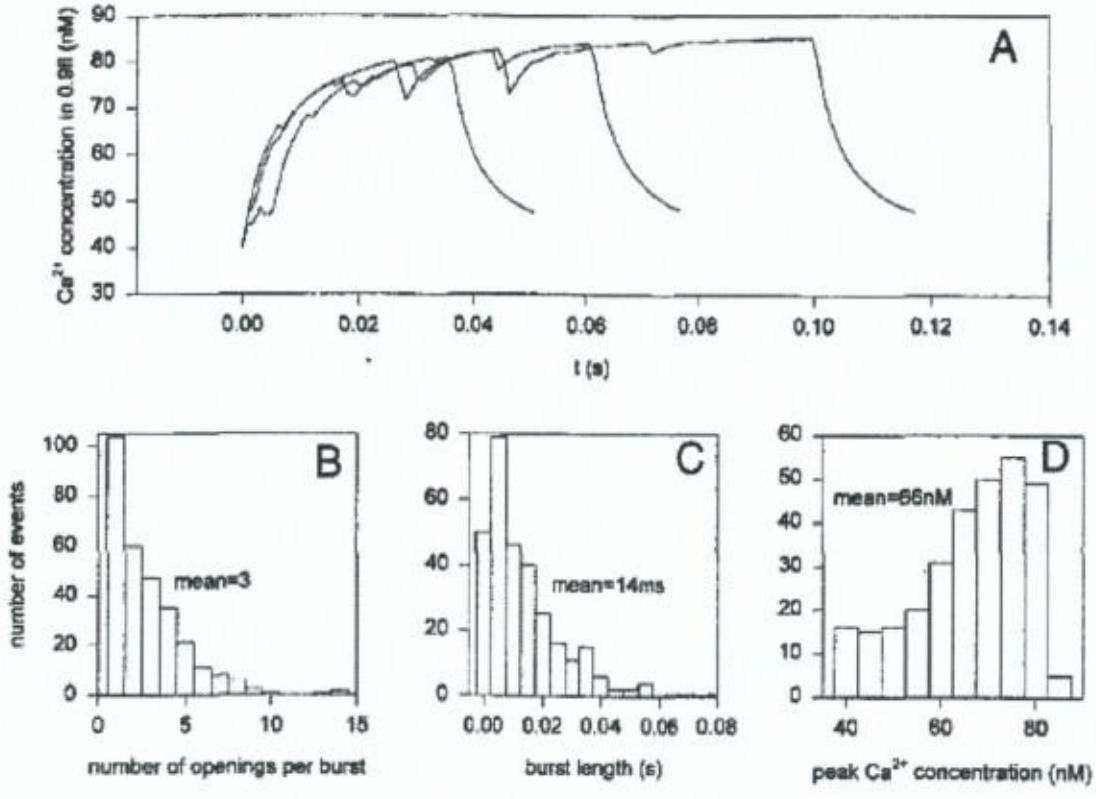

Fig. IV.7. Stochastic simulation of Ca^{2+} transients in a macroscopic (0.9 fl) cytosolic volume in the presence of 50 μM Calcium Green-1 added to the physiological buffer, with the characteristics shown in Table IV.1.

Nevertheless, these repetitive openings of the channel are the mere consequence of channel activation by Ca^{2+}, irrespective of the detailed mechanism for this activation. In fact, using a related but different

model, Stern *et al.* (1997) independently arrived at similar conclusion for the ryanodine-sensitive channel.

As stated above, we suggest that these repetitive openings could explain why previously observed blips, considered to correspond to the opening of single channels (Parker and Yao, 1996), have an apparent duration much longer than what would be expected on the basis of bilayer characterization of the $InsP_3$-sensitive channel. In fact, from our simulations in Figs. IV.6 and IV.7, it appears that under *in vivo* cytosolic-like conditions, i.e. in the absence of exogenous mobile buffers, bursts of channel activity might be even more prominent. These long bursts of activity appear to be simply due to the relatively slow Ca^{2+} diffusion in the cytosol, and do not require for explanation any regulatory difference in the state of the $InsP_3$ receptor under *in vitro* and *in vivo* conditions.

As shown in Fig. IV.7D, the distribution of the simulated maximal Ca^{2+} concentrations reached by the blips is bell-shaped. This distribution is reminiscent of the experimental results reported by Parker and Yao (1996). These authors proposed that the approximately Gaussian shape of the experimental distribution was due either to a roughly constant amount of Ca^{2+} released in each blip, or to the possibility that many undetectable blips had been ignored. In contrast, our simulation shows that such a distribution can be obtained simply as the consequence of the fast rising phase of Ca^{2+} accumulation: thus, although the blip duration and the total amount of Ca^{2+} released during the blip may vary widely, the Ca^{2+} plateau attained by these blip does not change to the same extent.

Situation	K_d (nM) assumed for Ca^{2+} Green-1	D ($\mu m^2 s^{-1}$) assumed for Ca^{2+} Green-1	Maximal amplitude (nM)	$t_{1/2}$ (ms)
a (Fig. IV.7)	700	31	45	4.5
b	270	31	23	4
c	270	8	81	10
d	270	0	291	34
e (Fig. IV.6)	-	-	299	11

Table IV.3. Effect of the assumed characteristics of Calcium Green-1 on the kinetics of simulated transient accumulation of Ca^{2+} into a 0.9 fl volume.

It must be noted that although all parameter values used here to mimic these blips were deduced from experimental measurements (Table IV.1), the reasonable agreement obseved between simulated behaviour and experimental facts critically depends on these values. In particular, as shown in Fig. IV.6 and IV.7, the amplitudes and rising times of the simulated blips are highly sensitive to the characteristics assumed for the Ca^{2+} indicator Calcium Green-1. Independently of stochastic simulations, this can also be easily recognized on the basis of simple deterministic simulations (like the one in Fig. IV.4) of the Ca^{2+} rise resulting from channel opening. Thus, Table IV.3 explores the effect of making various assumptions for different parameters. Situation (a) corresponds to the hypotheses in Fig. IV.7 (as also used for the lower curve in Fig. IV.4), in which the simulated blips were obtained assuming that the diffusion coefficient of Calcium Green-1 was equal to the diffusion coefficient experimentally measured for Fura-2 in a cytosolic medium, i.e. 31 $\mu m^2 s^{-1}$ (Blatter and Wier, 1990), and that the K_d value for Calcium Green-1 was 2-3 times higher (see, e.g. (Bassani *et al.*, 1995), (Zhao *et al.*, 1996)) than its value measured in water (Eberhard and Erne, 1991). Situation (b) corresponds to an assumed K_d value of 270 nM for Calcium Green-1 (as used in (Parker *et al.*, 1996)), corresponding to the value measured in water without corrections for binding to cytoplasmic components: in this case, the maximal blip amplitude predicted would drop to only 23 nM above the basal level (situation (b)), and such a low amplitude might be below the detection level. On the other hand, situation (c) corresponds to the situation where, since most of Calcium-Green-1 (94% in muscle fibers, according to (Blatter and Wier, 1990)) appears to be bound to cytoplasmic components and,

therefore, does not diffuse in the cytoplasm more rapidly that the components to which it is bound, its apparent diffusion coefficient was assumed to be lower than that in Table IV.1: for instance, if Calcium Green-1 were to move as slowly as actually measured in muscle fibers, its apparent diffusion coefficient would be reduced down to 8 $\mu m^2 s^{-1}$ (see Table 3 in (Zhao *et al.*, 1996)), and the maximal Ca^{2+} signal would then increase to 81 nM, while the kinetics of Ca^{2+} accumulation would appear to be slower. Finally, the amplitude of the Ca^{2+} signal would become even higher if the Ca^{2+} indicator were completely immobilized (situation (d)). This would correspond to a mere increase in the concentration of stationary buffers, and, as previously shown (Naraghi and Neher, 1997), such an increase would reduce both the effective current, in terms of free Ca^{2+}. The effective rate of Ca^{2+} diffusion, with the result that the kinetics of Ca^{2+} accumulation would be slowed down, but, the steady state would remain virtually unchanged (compare the characteristics of situation (d) with those obtained in the absence of Ca^{2+} indicator, i.e. situation (e)). Thus, as suggested in previous works (Stern, 1992; Smith *et al.*, 1996; Naraghi and Neher, 1997), the simulated effect of added Calcium Green-1 under the assumption of Table IV.1 (situation (a)) appears to be mainly due to the fact that it is a mobile buffer: it thus contributes to faster Ca^{2+} dissipation by diffusion, leading to lower values of Ca^{2+} steady state rises and shorter rise times.

Although the simulated burst lengths shown here are compatible with those of experimental blips, our simulated blips present, in agreement with other theoretical simulations (Smith *et al.*, 1996; Parker *et al.*, 1996), Ca^{2+} decay phases much faster than the ones experimentally observed. The characteristic time of a simulated Ca^{2+} decay is about 10 ms (Fig. IV.7A), whereas experimental decay curves exhibit a characteristic time of about 100 ms (Parker and Yao, 1996). Since the decay rate is only due to diffusion, this discrepancy might point to a misunderstanding of the characteristics of this diffusion. One appealing possibility might be that the cytosolic medium presents physical barriers to macroscopic diffusion. Such a possibility is substantiated by a previous numerical study of the Ca^{2+} dynamics around the plasma membrane Ca^{2+} channels in smooth muscle cells (Kargacin, 1992), in which the effect of imposing a barrier to free Ca^{2+} diffusion was investigated. This barrier, possibly corresponding to an intracellular organelle, was defined as a region in which the diffusion coefficient of Ca^{2+} was 10 times lower than in the rest of the cytoplasm, and was supposed to be located about 100 nm away from the plasma membrane. Under such conditions, it was shown that, due to the opening of a single plasma-membrane Ca^{2+} channel, high concentrations of Ca^{2+} developed in the restricted diffusion space between the plasma membrane and the intracellular organelle, and an elevated Ca^{2+} level persisted for 100-200 ms. This interesting possibility has not been included in our model, but would solve the apparent discrepancy mentioned above.

IV.4. Stochastic simulation of a cluster of $InsP_3$-sensitive Ca^{2+} channels

As a first step towards a quantitative analysis of the hierarchy of Ca^{2+} signalling events, we have studied in the previous section the behaviour of a single channel placed in its cytosolic environment by stochastic simulations. We now wish to go a step further (Swillens *et al.*, 1999) to understand how clusters of $InsP_3$-sensitive channels could generate blips and puffs, accepting as a basic concept that the fact that blips and puffs form a continuum of events of graded size and variable time course can be thought of within a simple framework: at relatively low $InsP_3$ concentration, most opening events in a given cluster of $InsP_3$-sensitive channels are likely to be blips because an active channel is generally not surrounded by other channels with $InsP_3$ bound to them, whereas higher $InsP_3$ concentrations are able to induce the concomitant opening of several $InsP_3$-bound channels nearby in the same cluster, and thus generate puffs. The stochastic nature of channel opening as well as simple geometrical proximity considerations should then result in a broad distribution of amplitudes and durations of calcium signalling events.

An additional important fact, however, is that at concentrations of $InsP_3$ appropriate for producing Ca^{2+} puffs, the relative occurrence of blips is rather scarce (Sun *et al.*, 1998; Thomas *et al.*, 1998), as

if, once a channel opened, it readily recruited several other channels in the cluster. Such an efficient channel synchronization requires that, during the burst of activity of the leader channel (i.e. the first one to open), the Ca^{2+} signal is able in most cases to propagate up to a neighbouring $InsP_3$-bound channel of the same cluster and activate it. Since synchronization efficiency obviously depends on the distance between activatable $InsP_3$-bound channels, this experimental observation implies relatively short inter-channel distances. Within a cluster, however, the current spatial definition of confocal microfluorimetry allows to visualize neither the number of channels nor the inter-channel distances.

To estimate these parameters which are not attainable through experiments, we have performed in this study computer stochastic simulations of $InsP_3$-induced activation of channels, grouped in a cluster and placed in a cytoplasmic-like environment. Following our previous study (section IV.3), the kinetic parameters for channel gating and Ca^{2+} diffusion in the cytoplasm were chosen to allow optimal fit to previously published experimental observations, and we searched for geometrical characteristics of the channel cluster allowing appropriate channel synchronisation within the cluster. From our simulations, we conclude that a Ca^{2+} releasing site probably consists of a few tens of very closely packed $InsP_3$-sensitive Ca^{2+} channels: a square-shaped lattice of 25 channels in close contact leads to theoretical distributions of Ca^{2+} signal amplitudes compatible with experimentally observed distributions.

IV.4.1. Simulation procedures

The numerical procedure used to generate Ca^{2+} signals is based on the stochastic simulation of the transitions between the various states of the $InsP_3$-sensitive Ca^{2+} channel (Fig. IV.1), and on deterministic calculation of Ca^{2+} diffusion in a buffered cytosolic-like medium. This procedure is the same as the one described in section IV.2., except for the order of the $InsP_3$ binding reaction (third order instead of second order). In contrast, simulation of the behavior of a channel cluster, consisting of multiple point sources distributed on a planar portion of the ER, required a 3-D cartesian discretization in small cubic boxes. The 25 channels of the square-shaped cluster (see below) were distributed in a 2-D array of 5x5 contiguous boxes placed in the center of the space. The diffusion space extended 1 μm away from the cluster in every direction, the boundary condition consisting of a constant Ca^{2+} concentration equal to 40 nM (basal level). The diffusion equation was solved by the finite difference method applied to this discretized space and according to the rapid buffering approximation (Smith *et al.*, 1996).

IV.4.2. Preliminary analysis of the average number of channels open during a standard puff event.

The amplitudes of $InsP_3$-induced Ca^{2+} signals produced during elementary events like blips and puffs were previously estimated in *Xenopus* oocytes (Parker and Yao, 1996) and Hela cells (Bootman *et al.*, 1997): mean Ca^{2+} amplitude of puffs was about 170 nM above the basal concentration, whereas amplitudes of blips reached about 5-fold lower values (30 nM above basal level). Moreover, Sun *et al.* (1998) reported that the rates of rise of "signal mass" (obtained by integrating the fluorescence signal throughout three dimensions) computed for averaged traces was about 6 times higher for puffs than for blips. Therefore, if a blip reflects the opening of a single channel, a puff is likely to involve the concerted opening of only a few channels, say of about 5 on average.

IV.4.3. Adaptation of model parameters to the kinetic experimental constraints.

Another preliminary step in the present work was to make use of newly available information about latencies before channel opening, to refine our previously proposed model of the gating mechanism of $InsP_3$-sensitive Ca^{2+} channels (see Fig. IV.1). In this model, the delay observed before opening of any channel is mainly due to rate-limiting association of Ca^{2+} with the first activating Ca^{2+}-binding site on

this channel (Sun *et al.*, 1998). On the other hand, opening of a channel in a cluster can initiate concerted activation of other channels, and hence a puff, only if the Ca^{2+} signal which reaches these neighbouring channels is sufficiently high to allow Ca^{2+} binding to them within the short duration of the transient Ca^{2+} signal. The value of the kinetic parameter describing the rate of Ca^{2+} binding to its first activation site on the channel, k_{a1+}, is therefore critical for channel synchronization. Experimental information about this kinetic parameter can be derived from recently published measurements of the lag between flash photolysis of caged $InsP_3$ and the first observed elementary event reflecting the onset of Ca^{2+} liberation by any channel of a *Xenopus* oocyte Ca^{2+} release site: this latency was found to decrease with increasing $InsP_3$ concentration, down to a limiting value of 80 ms (Callamaras *et al.*, 1998). Under saturating $InsP_3$ conditions, all channels in the cluster are expected to bind $InsP_3$ almost immediately, and the minimal 80 ms delay therefore corresponds to the average period of time elapsed before Ca^{2+} binds to an activating site on any one of the channels of the cluster, under conditions of basal Ca^{2+} concentration, i.e. $(k_{a1+}[Ca^{2+}]_{basal})^{-1}$ / N. Indeed, the transitions between channel states being considered as Poisson processes, the mean time to observe the first transition R_{i0k} to R_{i1k} in the population of N channels is N times lower than the mean time required by a single channel to undergo this transition, which is equal to $(k_{a1+}[Ca^{2+}]_{basal})^{-1}$.

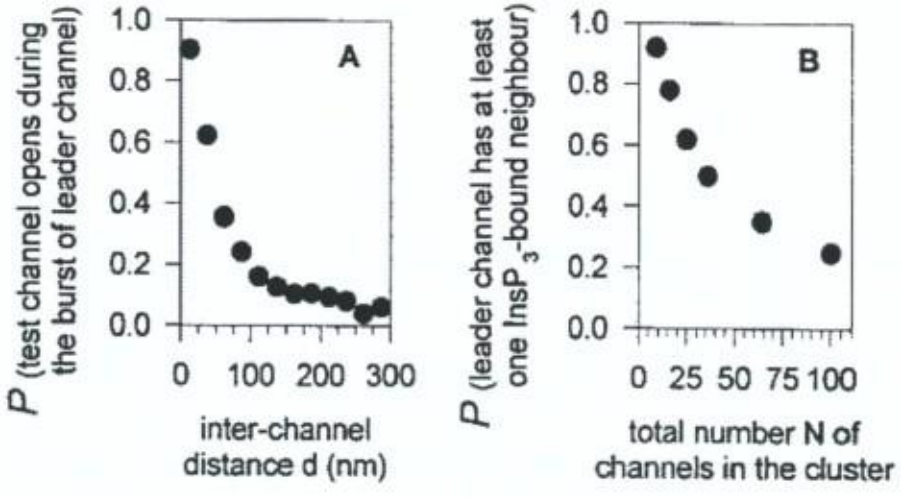

Fig. IV.8. Estimation of cluster characteristics leading to efficient inter-channel communication

(A) Probability that a test channel, placed at a distance d of the leader channel and sensing the fluctuations of Ca^{2+} concentration produced by the active leader channel, opens during the activity burst (blip) of the leader channel, as a function of the inter-channel distance. For large distances, the probability reaches a small value, reflecting the low probability that a channel opens during bursting of another non-communicating channel. (B) Probability that the leader channel in a cluster with N channels has at least one $InsP_3$-bound neighbour, as a function of N, assuming that each channel has a probability of 5/N to be $InsP_3$-bound. In this and all subsequent figures of this chapter, results have been obtained with the following parameter values: $k_{i+} = 5\ 10^{12}\ M^{-2}s^{-1}$; $k_{i-} = 5\ s^{-1}$; $k_{a1+} = 1.25\ 10^{7}\ M^{-1}s^{-1}$; $k_{a1-} = 64\ s^{-1}$; $k_{a2+} = 4.7\ 10^{9}\ M^{-1}s^{-1}$; $k_{a2-} = 208\ s^{-1}$; $k_{d1+} = 2.6\ 10^{5}\ M^{-1}s^{-1}$; $k_{d1-} = 380\ s^{-1}$; $k_{d2+} = 5.7\ 108\ M^{-1}s^{-1}$; $k_{d2-} = 1.9\ s^{-1}$. Note that since the binding of $InsP_3$ is assumed to be positively cooperative ($n_H = 2$), k_{i+} is a tri-molecular binding rate constant but the apparent K_d is still 1 μM, as in section IV.3.

Assuming that a Ca^{2+} releasing site consists of 25 channels (see below), the average latency before opening of an isolated single $InsP_3$-bound channel would thus be about 2 s (80 ms x 25), and for a basal Ca^{2+} concentration of 40 nM, $k_{a1+} = 1.25\ 10^{7}\ M^{-1}s^{-1}$. Note that the k_{a1+} value estimated from these latencies depends on the number of channels in the cluster in a reciprocal way. Therefore, if the cluster contains a larger number of channels, a smaller k_{a1+} value will be obtained, and hence less efficient channel synchronization (see below).

The k_{a1+} value estimated above is about 6.6 times smaller than the value we had previously used to simulate the behaviour of an isolated single channel (see section IV.3). In order to remain in agreement with the other experimental results originally selected as reference, we were led to alter some of the other Ca^{2+} binding parameters (k_{a1-}, k_{d1} and k_{d2} have been divided by 3.9, 0.15 and 10, respectively). In addition, because of the experimentally observed shape of the relationship between latency and $InsP_3$ concentration (Callamaras *et al.*, 1998), $InsP_3$ binding was now assumed to exhibit positive cooperativity ($n_H = 2$). The new set of parameter values (see legend to Fig. IV.8) satisfactorily fitted Bezprozvanny's (1991) data about the open probability of isolated channels under bilayer conditions, and was also able to generate blip events as resulting from the flickering of a single channel during a few tens of ms (data not shown).

IV.4.4. Estimation of the distance between $InsP_3$-sensitive Ca^{2+} channels within a cluster

In order to gain some understanding of synchronization between channels, we analyzed how far the Ca^{2+} signal generated by a leader channel could be expected to propagate in the cytosol and thus activate a neighbouring channel. We considered the leader channel as an isolated channel in a cytosolic-like environment, initially in the open R_{220} state and subsequently experiencing a classical activity burst of random duration. Ca^{2+} was considered to diffuse in an hemi-spherical 3-D space, representing the cytosolic volume adjacent to the ER membrane. A test channel was also placed in this space, at a certain distance (d) from the leader channel. Like the leader channel, this test channel was also assumed to be $InsP_3$-bound initially, but its Ca^{2+} binding sites were initially vacant (R_{200} state). Our simulation procedure (section IV.3) was applied, leading to a transient burst of activity of the leader channel. The numerical procedure monitored whether the test channel opened during this burst, and stopped the simulation at that moment. After repeating the simulation 300 times, we counted the number of runs for which the test channel had opened during the activity burst of the leader channel. This was an indication for synchronization, since otherwise the average delay before opening of an isolated channel would have been much longer, about 2 seconds, as indicated above. Fig. IV.8A shows that, under cytosolic-like conditions (with a mobile Ca^{2+}-sensitive dye present), activation of the test channel before closure of the leader channel was relatively frequent only when the two channels were rather close to each other: when the inter-channel distance was 12 nm, i.e. the minimal value corresponding to the lateral dimensions of the channel (Katayama *et al.*, 1996), synchronization between the two channels took place in about 90 % of the cases, but when the two channels were 50 nm apart, synchronization occurred in less than half of the cases. This very short effective range of Ca^{2+}-mediated communication between channels is in fact the consequence of the steep gradient of Ca^{2+} concentration created by a Ca^{2+} point source in a buffered medium (Llinas *et al.*, 1995; Klingauf and Neher, 1997). Our results were obtained using a k_{a1+} value corresponding to a hypothetical number of 25 channels per Ca^{2+} releasing site, but, synchronization efficiency would have been even worse if the cluster had been supposed to be bigger, because of the lower k_{a1+} value.

Since synchronization between channels appears to require closely packed channels, the functional Ca^{2+} releasing site must be restricted to a very small portion of the membrane of an ER tubule. Thus, for subsequent simulations, we considered that the channel cluster extends over a flat surface as a 2-D pattern, which for simplicity we assumed to be a square-shaped lattice.

IV.4.5. Estimation of the number of $InsP_3$-sensitive Ca^{2+} channels within a cluster.

Since the amplitude of a mean puff event requires the concerted activation of about 5 channels, the total number of $InsP_3$-bound channels in the cluster has also to be close to about 5. Indeed, if a cluster of moderate size were to contain many more $InsP_3$-bound channels, the puff amplitude would be too high, because the Ca^{2+} concentration around the cluster would presumably be sufficient to induce the opening of most $InsP_3$-bound channels (see below Fig. IV.11 for confirmation). Each channel has thus a probability of about 5/N to be $InsP_3$-bound, N being the total number of channels in the cluster. We then estimated the probability that in such a cluster at least one $InsP_3$-bound channel is adjacent to the leader active channel, as follows. In square-shaped clusters containing N channels, $InsP_3$-bound channels were first chosen at random, with a probability of 5/N. If at least two channels turned out to be $InsP_3$-bound, one of them was randomly chosen as the active leader channel initiating the Ca^{2+} signal. The procedure then checked whether the leader active channel was adjacent to any one of the other $InsP_3$-bound channels. Analysis of the results obtained by repeating this procedure allowed us to estimate the probability that at least one of the nearest neighbours of the active channel was $InsP_3$-bound. Fig. IV.8B shows that this probability rapidly decreases as the total number of channels in the cluster increases: a probability as low as 0.5 is already obtained with a cluster consisting of only 36 channels.

On the basis of this simple counting procedure, we predict that an upper limit for the cluster content should be 20 to 30 channels. Indeed, if the cluster were to contain more channels, the probability to generate a puff would vanish for two reasons, firstly, because the channel activation rate would be too slow (k_{al+} decreases as N increases), and, secondly, because the distance that the Ca^{2+} signal should cover to activate a second channel would be too large (the probability that a direct neighbour is $InsP_3$-bound being equal to 5/N). On the other hand, the experimental observation that increasing $InsP_3$ concentrations produce Ca^{2+} puffs with higher amplitudes (Fig. 6 in (Thomas *et al.*, 1998)) requires the recruitment of more than 5 channels per cluster under these circumstances, and suggests that 10 to 20 should be a lower limit for the number of channels in the cluster. At this point, we thus propose the tentative guess that a typical cluster contains 25 channels.

One may wonder whether a value of 25 channels per Ca^{2+} releasing site is realistic with respect to actual cells. In *Xenopus* oocytes, which are thought to contain 3 10^{14} tetrameric $InsP_3$ receptors per liter of cytoplasm (Parys and Bezprozvanny, 1995), $InsP_3$-sensitive Ca^{2+} release sites have been predominantly localized within a 6 μm thick sub-plasmalemmal band (Callamaras and Parker, 1999). If all the receptors are concentrated in this band, a simple calculation indicates that the mean spacing between adjacent clusters of 25 channels is equal to 1.44 μm. This figure should be a lower limit, since $InsP_3$ receptors were immunolocalized not only in this region (Callamaras and Parker, 1999), but also in the perinuclear region (Callamaras *et al.*, 1998). Values of 1.6 μm and 2.25 μm were recently reported for the mean spacing between adjacent Ca^{2+} releasing sites in the animal and vegetal hemispheres of *Xenopus* oocytes, respectively (Callamaras *et al.*, 1998). Thus, defining a cluster as an assembly of 25 densely packed channels is certainly not unreasonable.

IV.4.6. Stochastic simulation of a 25 (5x5) channel cluster in a cytosolic environment.

The previous simulations aimed at anticipating likely features of the spatial organization of Ca^{2+} releasing site. We have now to demonstrate that a theoretical cluster made of 25 closely packed channels may generate Ca^{2+} signals compatible with experimental observations. We already mentioned a recently reported, remarkable experimental observation (Sun *et al.*, 1998; Thomas *et al.*, 1998): despite the fact that a given $InsP_3$ stimulus always leads to a broad distribution of event amplitudes, when puffs involving the concerted activation of a few channels only were generated, pure blip events were rare. In this case indeed, the amplitude distribution was unimodal with amplitude values corresponding to puffs (Fig. 8 in (Sun *et al.*, 1998); Fig. 6 -0.1 μM histamine- in (Thomas *et al.*,

1998)). This reveals highly efficient communication between these few activatable $InsP_3$-bound channels, since weak inter-channel communication would rather favour the production of blips. The aim of our next simulation was therefore to determine under which conditions the simulated distribution of amplitude has a shape compatible with the experimental observations.

The simulation was performed for a 2-D square-shaped cluster of 25 channels surrounded by a 3-D cytosolic-like space containing a basal Ca^{2+} concentration of 40 nM, and in the presence of an $InsP_3$ concentration of 0.5 μM, leading to an average of 5 $InsP_3$-bound channels within the cluster. The channels with $InsP_3$ bound were chosen at random, according to the probability associated with the $InsP_3$ concentration used, and one of them, at random, was designated as being in the active state (R_{220}) at time zero. The stochastic procedure was then initiated to simulate both the state transitions for all channels and the diffusion of Ca^{2+} in the whole cytosolic space. The average Ca^{2+} concentration in a volume of 1 fl, centered on the cluster, was simultaneously calculated, up to the end of the Ca^{2+} release event. The procedure was repeated 100 times and, each time, the maximal Ca^{2+} concentration was recorded. To analyze the amplitude distribution, the sole events for which the Ca^{2+} concentration rose to more than 20 nM above the basal level were considered, to account for the existence of a detection threshold compatible with the fact that blips of 30 nM blip amplitude can be detected (Thomas *et al.*, 1998). Fig. IV.9 shows the amplitude distribution obtained with four different clusters in which adjacent channels were separated by a center to center distance (d) of 12, 20, 30 and 40 nm, respectively. A bell-shaped, unimodal distribution can be observed only in the case of the smallest distance, corresponding to the situation where neighbouring channels are in close contact. Blips, i.e. events characterized by a Ca^{2+} concentration increment ranging from 20 to 40 nM and corresponding thus to the opening of a single channel, represent only 3 % of all detectable events. When adjacent channels are separated by only a few nm (d = 20 nm), the production of puffs is still abundant but the occurrence of blips is already sufficient (17 %) to distort significantly the distribution shape.

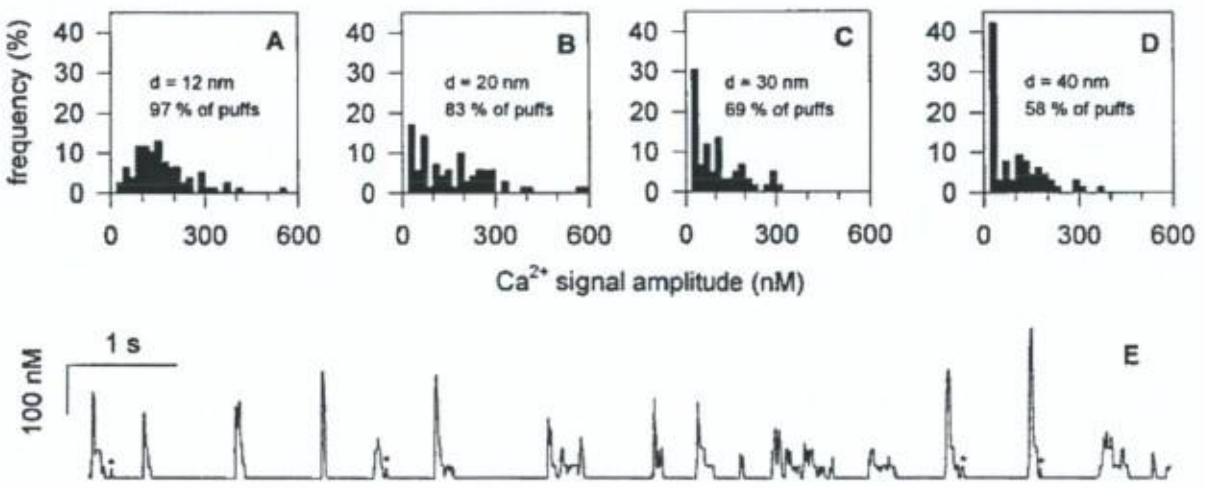

Fig. IV.9. Effect of the inter-channel distance in a 25 channel cluster on the distribution of Ca^{2+} signal amplitudes in the presence of 0.5 μM $InsP_3$. Ca^{2+} signals generated by a square-shaped 25 channel cluster placed in a cytosolic environment in the presence of 50 μM Ca^{2+} Green-1 were simulated. The $InsP_3$ concentration was set to 0.5 μM, and the center to center distance (d) between adjacent channels was 12, 20, 30 and 40 nm in panels (A), (B), (C) and (D), respectively. The Ca^{2+} concentration in a 1 fl volume centered on the cluster was followed up to the end of the release event. The amplitude of the Ca^{2+} signal characterizing one event was calculated as the peak Ca^{2+} increase above the basal value. Events with amplitudes between 20 and 40 nM, or higher than 40 nM were referred to as blips or puffs, respectively. Panel (E) shows the time dependence, over 10 s, of the Ca^{2+} concentration simulated under the conditions of panel (A) (closely packed channels), exhibiting a series of puffs and a few blips (marked by stars).

As anticipated, the situation is even worse for larger inter-channel distances. This demonstrates that, within the framework of the proposed model, a cluster of 25 channels must be as compact as possible to generate a Ca^{2+} amplitude distribution of appropriate shape. This distribution exhibits a median amplitude of 149 nM which is reasonably consistent with experimental observations. This realistic simulation result a posteriori justifies our initial choices concerning the size of the cluster and the number of $InsP_3$-bound channels required to generate standard puffs. The same stochastic simulation procedure was used to simulate, over a long period, successive Ca^{2+} signals generated by the same cluster of 25 closely packed channels stimulated by 0.5 μM $InsP_3$. The simulated trace of the Ca^{2+} concentration in a volume of 1 fl centered on the cluster exhibits puffs and a few blips, separated by time intervals of random length (Fig. IV.9E). The rising phase of puffs is quite short, because of fast recruitment of $InsP_3$-bound channels within the cluster, whereas the subsequent Ca^{2+} decline is generally slower, because this phase is governed by progressive Ca^{2+}-induced desensitization of the channels. Interestingly, previous theoretical simulations (section IV.3) suggested that the termination of a blip event could result from the dissociation and absence of rebinding of activating Ca^{2+}, because of the fast decrease of local Ca^{2+} concentration once the channel closed. On the contrary, our simulation shows that, at the end of a puff, most channels are desensitized, including the $InsP_3$-free ones which did not open during the puff. The reason is that the Ca^{2+} concentration in the vicinity of the cluster remains high as long as at least one channel is open. Note that, a priori, a subsequent Ca^{2+} release event might then start as soon as resensitization of an $InsP_3$-bound channel occurs. If this resensitization (i.e. Ca^{2+} dissociation from the desensitizing sites) were to be relatively slow, compared to channel activation (i.e. Ca^{2+} association to the activating sites), the first $InsP_3$-bound channel resensitized would be able to re-open before a second one is resensitized, and only blips would subsequently be observed. In contrast, as a consequence of a relatively fast resensitization, compared to activation, most channels resensitize before any one of them has an opportunity to re-open again, and simulation results in sequential puffs, as experimentally observed (Yao *et al.*, 1995).

When simulations were repeated for channels in close contact (d = 12 nm) but with increasing $InsP_3$ concentrations (up to 0.65 μM and 1 μM, corresponding to an average of 7.4 and 12.5 $InsP_3$-bound channels in the cluster, respectively), the amplitude distribution became broader and shifted to larger values for the Ca^{2+} signal (Fig. IV.10C and D), in agreement with the reported distributions of puff amplitudes obtained with stimuli of increasing strength (Fig. 6 in (Thomas *et al.*, 1998)). Among the 100 simulation runs with these two higher $InsP_3$ concentrations, no detectable blip event was obtained, confirming the high degree of synchronization between the channels. On the contrary, in the presence of a distinctly lower $InsP_3$ concentration, 0.35 μM (leading to an average of only 2.7 $InsP_3$-bound channels in the whole cluster), 36 % of the Ca^{2+} release events were pure blips, the population of which was now clearly detectable in the amplitude distribution (Fig. IV.10A).

The previous simulations show that puffs can be mimicked by simulating the concerted opening of about 5 $InsP_3$-bound channels in a cluster of 25 closely packed channels. Because of their close proximity, virtually all the $InsP_3$-bound channels in such a cluster participate to a single event. Despite this analysis, one might wonder whether puffs could not be obtained with clusters consisting of less tightly packed channels but with a number of $InsP_3$-bound channels larger than 5, to allow simultaneous recruitment, partly by chance, of 5 of them, as required for the production of puffs with an acceptable amplitude. In order to test this alternative hypothesis, we simulated the behaviour of a 25-channel cluster with a 40 nm center to center distance in the presence of a higher $InsP_3$ concentration (1 μM), leading thus to a higher number of $InsP_3$-bound channels in the cluster (12.5 in average). As expected, increasing the $InsP_3$ concentration (Fig. IV.11A and B) led to more frequent occurrence of puffs, but then, the average amplitude of the puffs was too high, and too many blip events were still observed. It thus appears that too distant and thus functionally independent channels cannot give rise to the appropriate distribution of amplitudes. This confirms our conclusion that a Ca^{2+} releasing site must consist of a quite limited number of efficiently communicating channels, in fact in close contact.

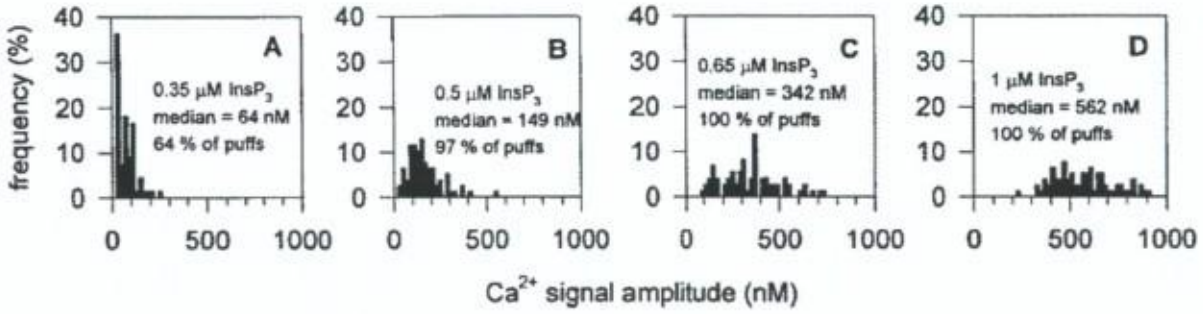

Fig. IV.10. Effect of $InsP_3$ concentration on the distribution of Ca^{2+} signal amplitudes with a 25 closely packed channel cluster. A stochastic simulation was performed under the same conditions as for Fig. IV.9A (d = 12 nm), but with $InsP_3$ concentrations equal to 0.35, 0.5, 0.65 and 1 μM in panels (A), (B), (C) and (D), respectively.

IV.5. Discussion

Discrete hot spots of $InsP_3$-sensitive Ca^{2+} release have been observed in the cytoplasm of different cell types (Sneyd *et al.*, 1995), but due to the limitations of microfluorimetric detection methods, neither their spatial dimensions (which are smaller than 1 μm^3) nor their actual contents could be estimated precisely. Hot spots presumably consist of clusters of $InsP_3$-sensitive Ca^{2+} channels, in which only a few channels open in a concerted way during a Ca^{2+} release event. The aim of the present study was to deduce from stochastic computer simulations the cluster characteristics required to permit efficient synchronization of the channels, and to solve the experimental paradox that, despite the small number of channels open during such release events, blip events –which involve the opening of a single channel– only rarely occur.

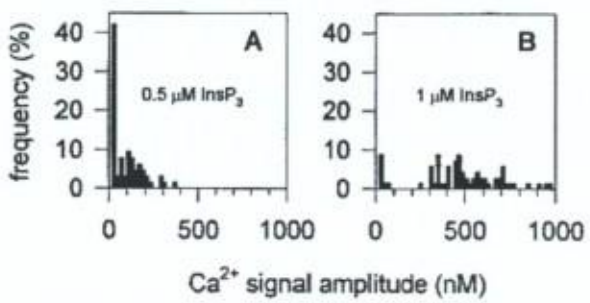

Fig. IV.11. Efficiency of puff production with a loosely packed channel cluster. A stochastic simulation was performed under the same conditions as for Fig. IV.9D (d = 40 nm), but with two different $InsP_3$ concentrations, 0.5 and 1 μM in panels (A) and (B), respectively.

The conceptual core of our analysis is that, if a puff is generated by the concerted activation of about 5 $InsP_3$-bound channels, these channels must be located in close proximity to permit inter-channel communication and thus, synchronization. We in fact demonstrate that, within the framework of our gating model, and taking into account experimental physiological constraints (diffusion coefficient for cytoplasmic Ca^{2+}, unitary channel current, channel activation kinetics and latencies before opening, etc.), efficient inter-channel communication only takes place if the $InsP_3$-bound channels are in close contact. This implies that channel clusters responsible for puffs might have a spatial arrangement similar to that observed for channels in Purkinje cell dendrites, i.e. a quasi–crystalline organization (Katayama *et al.*, 1996). We also demonstrate that the 5 $InsP_3$-bound

channels required to generate a Ca^{2+} puff of appropriate mean amplitude can be in close proximity only if the cluster does not contain more than two or three tens of channels, i.e. has lateral dimensions of the order of 60 nm. This cluster is therefore a very localized region, whose experimental characterization will presumably only be made possible by electron microscopy, as has been the case for the junctional region in sarcoplasmic reticulum. In the latter case, stochastic simulations have convincely established the competence of ryanodine receptor and dihydropyridine receptor organized clusters for generating characteristic patterns of calcium release events (Stern *et al.*, 1997).

The results shown here were obtained by a numerical procedure involving stochastic simulation within a 3-D cartesian space, each channel occupying a certain position inside the cluster on the ER membrane and being in contact with the Ca^{2+} concentration in the adjacent small cubic volume of 12x12x12 nm^3. Because of the high level of proximity between these channels, we wondered whether it was possible to reproduce the results by using a numerical procedure based on a more macroscopic view of the cluster, e.g. by considering all channels of this cluster as being homogeneously distributed in a single domain of larger volume and in which a homogenous Ca^{2+} concentration would prevail. We then resorted to a numerical method based on central symmetry (see Fig. IV.3), in which a central sphere represents the cluster domain. With a diameter of 40 nm, this central sphere has a volume roughly equal to the sum of the 25 small cubic volumes adjacent to the channels in the procedure described above. In these new simulations, we were able to obtain a distribution of Ca^{2+} signal amplitudes similar to that illustrated in Fig. IV.9A (data not shown). Thus, it appears that the kinetic behaviour of a cluster may be satisfactorily simulated by considering a virtual domain, a few tens of nm wide, in which all the channels of a cluster and the Ca^{2+} ions close to them are homogeneously distributed. This result may be viewed as a rational basis for the operational concept of intermediate domain (between the channel cluster and the bulk cytosolic medium), which was previously introduced to permit empirical simulation of the so-called incremental Ca^{2+} detection and of the long-period Ca^{2+} oscillations (Dupont and Swillens, 1996). In this context, such an intermediate domain would be associated with a cluster of closely packed channels. It is thus larger than the microdomains formed around the mouth of single open channels (Llinas *et al.*, 1995), but smaller than the submembrane domains containing distant channels, recently described (Klingauf and Neher, 1997).

Further simulations are in progress for defining the conditions under which synchronization of Ca^{2+} releasing sites may occur through long range Ca^{2+}-mediated communication, leading to Ca^{2+} waves and oscillations.

PART 3 : WAVES

CHAPTER V

Propagation of intercellular Ca^{2+} waves among connected hepatocytes

V.1. Introduction

In the liver, many important physiological processes such as bile secretion, bile flow, glycogen breakdown, and cell survival are regulated by an increase in the level of cytosolic Ca^{2+} (Nathanson and Schlosser, 1996). These Ca^{2+} signals can be elicited in isolated cells by a large array of stimuli and often occur as repetitive Ca^{2+} waves. The regenerative mechanism of these Ca^{2+} waves is beginning to be well understood (Berridge, 1997). In isolated multicellular systems, or in intact organs, Ca^{2+} waves are not restricted to the cytosol of one cell but propagate toward other cells as intercellular calcium waves (Sanderson *et al.*, 1994; Sanderson, 1996). Theoretically, intercellular Ca^{2+} signaling may occur through different pathways, namely paracrine or junctional routes. Numerous studies have reported that paracrine and/or junctional routes are involved in the propagation of intercellular calcium waves in a large spectrum of cell types including, for example, astrocytes (Charles *et al.*, 1992; Venance *et al.*, 1997), chondrocytes (D'Andrea and Vittur, 1997), hepatocytes (Schlosser *et al.*, 1996), pancreatic acinar cells (Loessberg-Stauffer *et al.*, 1993; Yule *et al.*, 1996), or tracheal epithelial cells (Hansen *et al.*, 1993; 1995). Most of these studies were performed under particular experimental conditions, i.e., after mechanical stimulation of a single cell from a cultured monolayer, which induces the propagation of Ca^{2+} waves in the connected cells. Such experimental studies on epithelial tracheal ciliated cells, glial cells, and endothelial cells allowed Sneyd *et al.* (1995b) to propose a theoretical model accounting for the propagation of intercellular Ca^{2+} waves in these cell types. This model is based on the passive diffusion of inositol 1,4,5-trisphosphate ($InsP_3$) between adjacent cells through gap junctions. $InsP_3$ is produced in the mechanically stimulated cell and provokes the release of Ca^{2+} from internal stores, in the form of an intracellular Ca^{2+} wave propagating via Ca^{2+}-induced Ca^{2+} release (Berridge, 1997). Because $InsP_3$ is supposed to move through gap junctions, similar Ca^{2+} waves are initiated in adjacent cells. This phenomenon reproduces itself as long as the amount of $InsP_3$ entering a cell is large enough to induce a Ca^{2+} wave. The model thus accounts for the propagation of a restricted intercellular Ca^{2+} wave after focal stimulation of one individual cell, as well as for asynchronous Ca^{2+} oscillations that occur after the passage of the wave, as often observed in glial cells (Sneyd *et al.*, 1998; Charles *et al.*, 1992).

In contrast to the studies that led to the model proposed by Sneyd *et al.* (1995b), some experiments have been performed in freshly isolated systems of connected cells that are globally stimulated by hormones, or intact organs perfused with agonists (Loessberg-Stauffer *et al.*, 1993; Nathanson and Burgstahler, 1992; Combettes *et al.*, 1994; Nathanson *et al.*, 1995; Robb-Gaspers and Thomas, 1995). Especially in the liver, a striking feature of the responses observed in the latter experimental conditions is the sequential pattern of Ca^{2+} increases in the different coupled cells, creating the appearance of intercellular Ca^{2+} waves. This occurs both in hepatocyte doublets and triplets and in liver cell plates from whole perfused organs. The same sequence of Ca^{2+} responses is observed for each spike for intermediate doses of agonists that cause Ca^{2+} oscillations (Combettes *et al.*, 1994). This sequence of cellular responses to a given agonist is maintained when stimulation is repeated and does not depend on agonist concentration. Thus, interhepatocyte Ca^{2+} waves, although elicited by global agonist stimulation, appear to be oriented in a specific direction in multiplets or in the perfused intact liver (Combettes *et al.*, 1994; Nathanson *et al.*, 1995; Robb-Gaspers and Thomas, 1995).

Experimental results obtained in multiplets of connected hepatocytes and in the perfused liver suggest that the mechanism for intercellular calcium wave propagation in hepatocytes considerably differs from that in tracheal epithelial cells or endothelial cells. First, in contrast with the latter cell types in which only one Ca^{2+} wave propagates concentrically after focal stimulation, repetitive Ca^{2+} waves propagate in multiplets of hepatocytes (Combettes *et al.*, 1994; Tordjmann *et al.*, 1997; 1998) or in the intact perfused liver (Nathanson *et al.*, 1995; Robb-Gaspers and Thomas, 1995). Second, each hepatocyte needs a stimulus (here in the form of an agonist such as vasopressin or

norepinephrine) to relay the intercellular Ca^{2+} wave (Tordjmann *et al.*, 1997). However, gap junction permeability is essential for coordinating Ca^{2+} oscillations in the coupled cells (Nathanson and Burgstahler, 1992; Tordjmann *et al.*, 1997). Coordinated intercellular Ca^{2+} signals in connected hepatocytes thus require both effective gap junctions and global hormonal stimulation. Third, a crucial aspect of interhepatocyte Ca^{2+} signals is the spatial orientation of the Ca^{2+} wave, which is unidirectional for a given agonist, as described above. We have suggested that this oriented pattern relies on the observed gradient in hepatocyte sensitivity to agonists along the liver cell plate (Tordjmann *et al.*, 1998). The appearance of intercellular Ca^{2+} waves could thus arise from the fact that each individual hepatocyte in the liver cell plate (or in multiplets) displays repetitive Ca^{2+} spikes with a slight phase-shift with respect to neighboring cells.

The aim of this study (Dupont *et al.*, 2000a) is to develop a theoretical model for the propagation of intercellular Ca^{2+} waves in connected hepatocytes, which could account for this dual control by gap junction permeability and hormonal stimulation. The model is based on the observation that the number of external receptors on the membrane of a hepatocyte depends on its location in the liver cell plate (Tordjmann *et al.*, 1998). Thus, we assume in the model that a multiplet of connected hepatocytes behaves as a set of individual Ca^{2+} oscillators characterized by slightly different periods, since the period of Ca^{2+} oscillations directly depends on the number of hormonal receptors that have been stimulated (via intracellular $InsP_3$). These oscillators are in turn coupled by an intercellular messenger, which may *a priori* be either Ca^{2+} or $InsP_3$ diffusing through gap junctions. Our results suggest that there is a better agreement between the model and the experimental data when $InsP_3$ is considered as the coordinating messenger. The model based on the hormonal sensitivity gradient and the diffusion of $InsP_3$ through gap junctions leads to theoretical predictions that are confirmed experimentally.

V.2. Material and Method

Materials

Fura 2/AM and Fura 2 were obtained from Molecular Probes, Inc. or Teflab, William's medium E was from Life Technologies, Inc., ionomycin was from Calbiochem, and collagenase was from Boehringer. All other chemicals were purchased from Sigma and were of the highest grade available commercially.

Preparation of hepatocytes

Single hepatocytes and multicellular systems were prepared from fed female Wistar rats by limited collagenase digestion of the liver, as described previously (Combettes *et al.*, 1994). After isolation, rat hepatocytes were maintained (2 10^6 cells/ml) at 4°C in William's medium E supplemented with 10% fetal calf serum, penicillin (200,000 units/ml), and streptomycin (100 mg/ ml). Cell viability, assessed by trypan blue exclusion, remained greater than 96% for 4–5 h.

Loading of hepatocytes with Fura 2

Hepatocytes were loaded with Fura 2 either by injection (see below) or by incubation with the dye, as described previously (Tordjmann *et al.*, 1997). Small aliquots of the suspended hepatocytes (5 10^5 cells) were diluted in 2 ml of William's medium E modified as described above. The cells were then plated onto dish glass coverslips coated with collagen I, and incubated for 60 min at 37°C under an atmosphere containing 5% CO_2. After cell plating, the medium was removed and replaced with a William's medium E containing 3 mM Fura 2/AM. The hepatocytes were then incubated for 30 min at 37°C under an atmosphere containing 5% CO_2. The coverslips were then washed twice with a saline solution (10 mM HEPES, 116 mM NaCl, 5.4 mM KCl, 1.8 mM $CaCl_2$, 0.8 mM $MgCl_2$, 0.96 mM NaH_2PO_4, 5 mM $NaHCO_3$, and 1 g/l glucose, pH 7.4). An Eppendorf microinjector (5242) was used to microinject Fura 2 as described previously (Tordjmann *et al.*,

1997). After microinjection, cells were allowed to recover for at least 10 min. The success of microinjection was assessed by monitoring the morphology of cells before and after manipulation and checking the ability of the cell to retain injected Fura 2 and low $[Ca^{2+}]i$. Freshly isolated doublets and triplets were distinguished from aggregates of non-connected cells in conventional light microscopy by screening for dilated bile canaliculi, which are indicators of maintained functional polarity (Gautam *et al.*, 1987).

Determination of $[Ca^{2+}]_i$ changes in hepatocytes

Dish coverslips were put onto a thermostated holder (34°C) on the stage of a Zeiss Axiovert 35 microscope set up for epifluorescence microscopy. The excitation light was supplied by a high-pressure xenon arc lamp (75 W), and the excitation wavelengths were selected by 340 and 380 nm filters (10-nm bandwidth) mounted in a processor-controlled rotating filter wheel (Sutter) between the ultraviolet lamp and the microscope. Ca^{2+} imaging was performed as described by Combettes *et al.* (1994). Briefly, fluorescence images were collected by a low-light-level ISIT camera (Lhesa, France), digitized, and integrated in real time by an image processor (Metafluor, Princeton, NJ).

Superfusion

Cells were continuously superfused with control or test solutions (at 34°C) by six inlet tubes converging on the coverslip chamber. The perfusion rate was 1.5 to 2 ml/min and the chamber volume was 0.2 ml. The medium was continuously renewed by aspiration. Agonists were rapidly removed during the Ca^{2+} response with this superfusion system, by increasing the perfusion rate to 4 ml/min to improve the washing efficiency.

Microperfusion

As described previously (Tordjmann *et al.*, 1997), agents were applied locally by positioning a micropipette (Femtotips, Eppendorf) close to the cell of interest and applying a constant pressure (120 hPa) via the Eppendorf injector. This allowed the delivery of picoliter quantities of agonist-containing solution. To monitor the extent of microperfusion, fluorescein (30 μM) was included in the micropipette and the fluorescein image was monitored at 510 nm using an excitation wavelength of 480 nm.

V.3. Description of the model

In this study, the intracellular Ca^{2+} dynamics of each hepatocyte are described by a model based on sequential activation-deactivation of the $InsP_3$ receptor/Ca^{2+} channel ($InsP_3R$) already described in Table I.3. This model accounts for intracellular Ca^{2+} oscillations resembling those observed experimentally. By incorporating diffusion of cytosolic Ca^{2+} in equ. (I.6), the model also accounts for the propagation of intracellular Ca^{2+} waves. Here, we focus on multiplets of connected hepatocytes (doublets or triplets), which allow us to look at our system in one dimension.

It should be pointed out, however, that our results describing a possible mechanism for intercellular Ca^{2+} wave propagation do not depend on the precise model used to describe the intracellular Ca^{2+} dynamics. We have verified that the outcome remains qualitatively unchanged when the intracellular Ca^{2+} dynamics are described by the model developed by Atri *et al.* (1993). Other models for intracellular Ca^{2+} oscillations and waves, also involving the stimulation of the $InsP_3R$ activity by Ca^{2+}, could also have been used (De Young and Keizer, 1992; Goldbeter, 1996; Tang *et al.*, 1996). Moreover, we neglect any possible spatial inhomogeneity in the intracellular distribution of $InsP_3$ receptor because the main rate-limiting processes are related to $InsP_3$ synthesis, degradation, and passage through gap junctions; the characteristic time for $InsP_3$ diffusion through a hepatocyte is indeed on the order of 100 ms, whereas the characteristic times for the other processes are at least of the order of a few seconds.

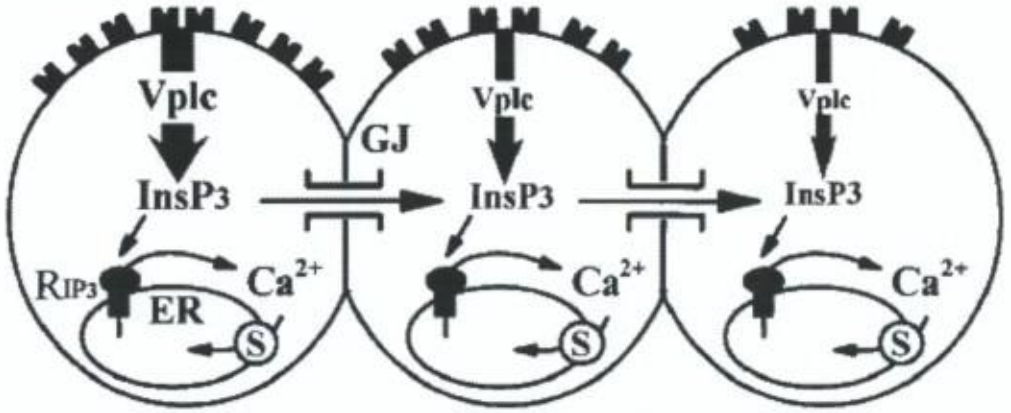

Fig. V.1. Schematic diagram of the receptor-oriented and coordinated intercellular Ca^{2+} waves in rat hepatocytes. ER: endoplasmic reticulum. S: SERCA. Vplc: velocity of $InsP_3$ synthesis by PLC. GJ: gap junction. RIP_3: IP_3 receptor/Ca^{2+} channel.

In view of the fact that in the model $InsP_3$ can diffuse through gap junctions (Fig. V.1), its progression over time needs to be considered in the description of the Ca^{2+} dynamics in each individual cell. To this end, we have incorporated in the model a general equation describing synthesis of $InsP_3$ by phospholipase C (PLC) and $InsP_3$ metabolism by $InsP_3$ 3-kinase and 5-phosphatase (see Chapter II and Dupont and Erneux, 1997). The change in $InsP_3$ over time is therefore determined by:

$$\frac{dIP}{dt} = V_{PLC} - V_K \frac{Ip}{K_k + Ip} \frac{C_{cyto}^{n_d}}{K_d^{n_d} + C_{cyto}^{n_d}} - V_{PH} \frac{Ip}{K_{PH} + Ip} \qquad \text{(V.1)}$$

where V_{PLC} is the velocity of $InsP_3$ synthesis by PLC, which depends on the level of stimulation. V_K and V_{PH} are the maximal velocities of $InsP_3$ metabolism by 3-kinase and 5-phosphatase, respectively, and K_K and K_{PH} are the Michaelis constants characterizing the latter enzymes. In Equ. (V.1), the rate of $InsP_3$ synthesis is assumed to be independent of the level of cytosolic Ca^{2+} (Renard *et al.*, 1987). Stimulation of $InsP_3$ 3-kinase activity by Ca^{2+} (in reality through Ca^{2+}/calmodulin) is reflected in Equ. (V.1) by K_d, which is the threshold constant for activation, and n_d, the Hill coefficient characterizing the latter process. In fact, as emphasized in a previous study (Chapter II; Dupont and Erneux, 1997), $InsP_3$ metabolism is dominated by $InsP_3$ 5-phosphatase. In the model, oscillations of $InsP_3$ due to the stimulation of 3-kinase activity by Ca^{2+} are negligible. In contrast to the studies specifically devoted to the effect of the incorporation of $InsP_3$ metabolism, the product of $InsP_3$ phosphorylation by the 3-kinase ($InsP_4$) is not considered here.

As previously reported (Thomas *et al.*, 1996), in the simulations of the model defined by Eqs. (I.5)-(I.8) and (V.1), the latency (that is, the time interval between the onset of stimulation and the peak of the first Ca^{2+} spike) directly depends on the rate of $InsP_3$ synthesis, V_{PLC}. The first Ca^{2+} spike indeed occurs when the concentration of $InsP_3$ reaches a threshold value. Thus, to approximately match the theoretical latencies with experimental observations, we have chosen parameter values characterizing $InsP_3$ synthesis and metabolism such as to get a half-time for an increase in $InsP_3$ of about 45 s at low levels of stimulation which, in the model, leads to a latency of about 70 s.

Incorporation of gap junctions

In the liver or in freshly isolated multicellular systems of rat hepatocytes, cells are tightly coupled by gap junctions (Spray *et al.*, 1994). The latter's allow the diffusion of diverse small-sized molecules between adjacent cells. We have attempted to incorporate $InsP_3$ diffusion through gap junctions in our model. If Ca^{2+} was the messenger, the same equation would hold after changing *I*p into *C*cyto (see below). Thus, in the model we assume that at each cell boundary the flux is dependent on both the concentration difference across the membrane and on the permeability of the gap junction to $InsP_3$. We have therefore used the same mathematical formulation as Sneyd *et al.* (1998). At each boundary between two cells:

$$D_{IP}\frac{\partial IP^{-}}{\partial x} = D_{IP}\frac{\partial IP^{+}}{\partial x} = F_{IP}\left(IP^{+} - IP^{-}\right) \qquad \text{(V.2)}$$

where the superscripts + and - indicate the $InsP_3$ concentration at the right and left limits of the border, respectively. The spatial coordinate is indicated by x. The intracellular diffusion coefficient for $InsP_3$ is represented by D_{IP}. The junctional permeability to $InsP_3$, F_{IP} , is an unknown parameter whose value was chosen such as to best mimic experimental observations. If $F_{IP} = 0$, no $InsP_3$ can diffuse between adjacent cells, and Equ. (V.2) reduces to no flux boundary conditions.

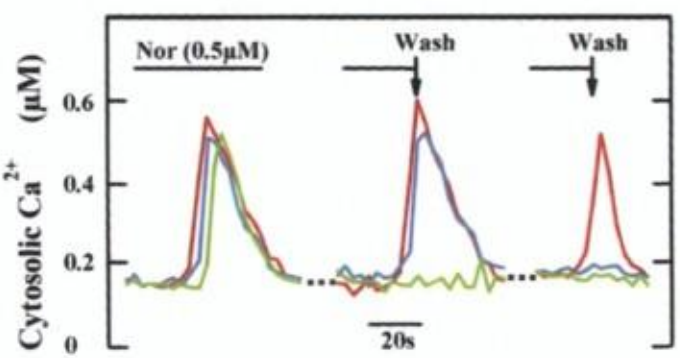

Fig V.2. Sensitivity gradient to Noradrenaline. Hepatocytes injected with fura2 were challenged with noradrenaline (Nor, 0.5μM) for the time shown by the horizontal bar. The solution was rapidly washed out as indicated by the arrow. Following noradrenaline addition to the bath, intercellular Ca^{2+} waves initiated in cell 1 (red) propagate to cells 2 (blue) and 3 (green). Following washout of noradrenaline at the peak of the $[Ca^{2+}]_i$ increase in cell 2 (middle) or cell 1 (right), there was no further propagation to associated cells (respectively cell 3 or 3 and 2). These results are representative of those obtained using 4 triplets in 3 independent experiments.

The model equations (I.5)-(I.8) and (V.1)-(V.2) were solved by the finite difference method on an array of two or three cells, each containing 20 grid points. Each cell was assumed to be 20 µm long. Integration was performed numerically using a fourth-order, variable time-step Runge-Kutta method. Parameter values are listed in Table V.1, except for the rate of $InsP_3$ synthesis (V_{PLC}) and the junctional permeability to $InsP_3$ (F_{IP}), whose values are discussed below.

Gradient of hormonal sensitivity among connected hepatocytes

It is well known that hepatocytes contribute differently to a large number of biological processes depending on their location in the portocentrilobular axis of the liver acinus (Jungermann and Kietzmann, 1996). In the same manner, there is morphological evidence for a gradient of vasopressin receptors along the liver cell plate (Nathanson *et al.*, 1995). This increasing density of hormonal receptors from the periportal to the perivenous zones of the liver cell plate may account for a gradient of sensitivity to vasopressin that we have observed recently (Tordjmann *et al.*,

1998). Indirect evidence suggesting the existence of a similar gradient for α-adrenoceptors has been reported previously (Tordjmann *et al.*, 1998). In this experiment, global perfusion of norepinephrine elicited a sequential Ca^{2+} response in a hepatocyte triplet (Fig. V.2, left). When the agonist was quickly removed from the medium, immediately after Ca^{2+} levels increased in the second cell, the third cell did not respond (Fig. V.2, middle). Similarly, when the agonist was removed by rapidly washing the medium immediately after Ca^{2+} levels increased in the first cell, the second and the third cells did not respond (Fig. V.2, right). Thus, in conditions where cells are uniformly perfused with norepinephrine, the time of contact between the agonist and the cell necessary to induce a Ca^{2+} response is largest in the last and shortest in the first responding hepatocyte. This experiment thus argues for a gradual change in hepatocyte sensitivity to norepinephrine in multiplets.

Parameter	Value
n_i	4
n_a	3
k_+	$25\ s^{-1}\mu M^{-4}$
k_-	$2.5\ 10^{-3}\ s^{-1}$
K_{act}	$0.34\ \mu M$
k_1	$42\ \mu M^{-1}s^{-1}$
b	10^{-4}
V_{MP}	$8\ \mu Ms^{-1}$
K_P	$0.4\ \mu M$
n_P	2
α	0.1
Ca_{tot}	$60\ \mu M$
K_{IP}	$1\ \mu M$
V_K	$7.5\ 10^{-3}\ \mu Ms^{-1}$
V_{PH}	$7.5\ 10^{-2}\ \mu Ms^{-1}$
K_K	$1\ \mu M$
K_{PH}	$10\ \mu M$
K_d	$0.5\ \mu M$
n_d	2
D_{IP}	$210\ \mu m^2s^{-1}$
D_{Ca}	$30\ \mu m^2s^{-1}$

Table V.1. List of parameter values used in the model for intercellular Ca^{2+} wave propagation in hepatocytes defined by eqs. (I.5)-(I-8) and (V.1)-(V.2)

Such sensitivity gradients are taken into account in the model (illustrated in Fig. V.1) by assuming that each cell has a different velocity of $InsP_3$ synthesis by phospholipase C (V_{PLC}). It has been estimated that the mean number of V1a vasopressin binding sites in the perivenous zone of the cell plate exceeds by 40% the mean number of the same binding sites in the periportal zone (Tordjmann *et al.*, 1998). Thus, assuming that the average number of cells in a cell plate is 20, then the model presumes that V_{PLC} differs by 5% between two neighboring hepatocytes. In the model, for the parameter values listed in Table V.1, a 5% difference in V_{PLC} leads to variations of about 20% in the period of Ca^{2+} oscillations.

Cellular heterogeneity is clearly dominated by these variations in the rate of $InsP_3$ synthesis; indeed, when caged $InsP_3$ is microinjected into one cell of Fluo3-loaded doublets and triplets of

hepatocytes, the Ca^{2+} increases observed after flash photolysis appear to be nearly identical and simultaneous in the connected cells (Tordjmann *et al.*, 1998). This strongly suggests that the behavior of distinct hepatocytes, which were originally closely located in the cell plate, is nearly identical when the steps responsible for $InsP_3$ synthesis are bypassed.

V.4. Theoretical estimation of the permeability of gap junctions in rat hepatocytes

Several studies have suggested that the propagation of an intercellular hepatic Ca^{2+} wave requires junctional connectivity (Nathanson *et al.*, 1995; Robb-Gaspers and Thomas, 1995), mainly because the microinjection of large amounts of Ca^{2+} or $InsP_3$ in one cell of a doublet increases Ca^{2+} in the connected cell (Saez *et al.*, 1989). It has also been reported that gap junctional permeability is essential for coordination of Ca^{2+} signaling in coupled hepatocytes (Nathanson and Burgstahler, 1992; Tordjmann *et al.*, 1997). However, little is known about the extent of $InsP_3$ intercellular diffusion during agonist stimulation. We have shown recently that when one cell within a doublet is stimulated by submaximal doses of norepinephrine, the amount of messenger diffusing to induce a Ca^{2+} response in the adjacent cell (Tordjmann *et al.*, 1997). Similarly, as shown in Fig. V.3A, focal vasopressin stimulation of a single cell in a doublet induces Ca^{2+} oscillations that are limited to the stimulated hepatocyte and do not show up in the connected cell. At the end of the experiment, when the doublet is globally superfused with vasopressin (0.1 nM), both cells exhibit Ca^{2+} oscillations that are sequential and well coordinated (Fig. V.3B).

We have used this experiment to evaluate the permeability coefficient (F_{IP}), to be incorporated in the model. To this end, we considered a theoretical doublet, consisting of two Ca^{2+} oscillators whose values for V_{PLC}, the parameter reflecting the rate of $InsP_3$ synthesis, differ by 5%. We then performed successive trials to determine a value for F_{IP} that allows for both coordination of Ca^{2+} spiking when the whole doublet is stimulated (lower limit for F_{IP}), and for the absence of Ca^{2+} variations in an unstimulated cell connected to an oscillating one (upper limit for F_{IP}). In Fig. V.3C, D, each color represents the change in Ca^{2+} concentration in a given cell. For a value of the permeability coefficient (F_{IP}) equal to 0.88 μm/s, Ca^{2+} oscillations were restricted to the stimulated cell (in blue), as shown in Fig. V.3C; on global stimulation both cells oscillated, with a slight phase-shift (Fig. V.3D). A similar result was obtained for other F_{IP} values differing by about 10%. This value for the permeability coefficient F_{IP}, which is close to the one predicted in previous theoretical studies (Sneyd *et al.*, 1995; 1998; Wilkins and Sneyd, 1998), was thus used for the remaining simulations.

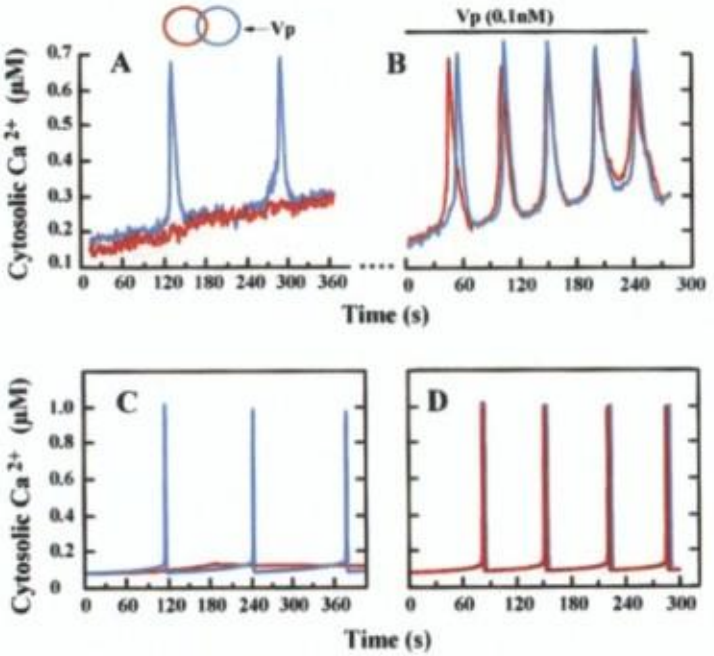

Fig V.3 : Focal stimulation of connected rat hepatocytes.

Panels A and B. Hepatocytes were loaded or injected with fura2. The figures show successive measures of $[Ca^{2+}]_i$ in the same hepatocyte doublet. One cell within the doublet was focally microperfused with vasopressin (Vp; 10μM in the micropipette), as described in the Materials and Methods section. Only the stimulated cell (indicated by arrow) within the doublet responded (panel A). The micropipette was then removed and the cell preparation was washed. After 5 min, the doublet was globally superfused with vasopressin (0.1 nM) for the time shown by the horizontal bars. Both cells of the doublet exhibited tightly coordinated $[Ca^{2+}]_i$ oscillations (panel B). Tracings were interrupted during the washing process (the gap represents 4 min).

Panels C and D. Numerical simulations of the experiments shown above. A value of 0.88 μms^{-1} for the $InsP_3$ permeability coefficient (F_{Ip}) allows the model to reproduce the experimental results shown above. If only one cell is assumed to be stimulated (panel C), it fails to induce Ca^{2+} spikes in the connected, unstimulated cell. In contrast, when both cells are stimulated, coordinated Ca^{2+} spiking is observed (panel D). Results were obtained by numerical integration of the model defined by eqns. (I.5)-(I.8) with parameter values listed in Table V.1, with $V_{PLC} = 6.5 \times 10^{-4}$ μMs^{-1} (red line) and 2.77×10^{-3} μMs^{-1}(blue line) for panel C, and $V_{PLC} = 2.205 \times 10^{-3}$ μMs^{-1} (red line) and 2.1×10^{-3} μMs^{-1} (blue line) for panel D. Initial conditions are resting states corresponding to $V_{PLC} = 6.5 \times 10^{-4}$ μMs^{-1}.

V. 5. Phase waves of Ca^{2+} increases among connected hepatocytes

We have simulated the behavior of three hepatocytes whose values for V_{PLC} differ by 5%. These cells were assumed to be connected by gap junctions allowing the diffusion of $InsP_3$, by considering the boundary conditions given in Eq. 4 and the permeability coefficient estimated above. As shown in Fig. V.4A, the Ca^{2+} oscillations generated by the model were tightly coordinated among the three cells. The change in cytosolic Ca^{2+} in the most sensitive cell, i.e., the one with the largest value for V_{PLC}, is shown in red; less-sensitive cells are shown in blue and green, respectively. As previously observed experimentally (Combettes *et al.*, 1994; Tordjmann *et al.*, 1998), peaks of cytosolic Ca^{2+} appeared sequentially in cells 1 (red), 2 (blue), and 3 (green), giving the appearance of an intercellular Ca^{2+} wave. Because we assumed in the model that no Ca^{2+} is transported from one cell to another, this wave is in fact a "phase wave" (Murray, 1989). This means that the appearance of a wave propagation phenomenon comes from the slight phase-shift between the individual oscillators. This phase-shift originates because the three cells of the triplet

do not simultaneously enter into the oscillatory domain because of their different values for V_{PLC}.

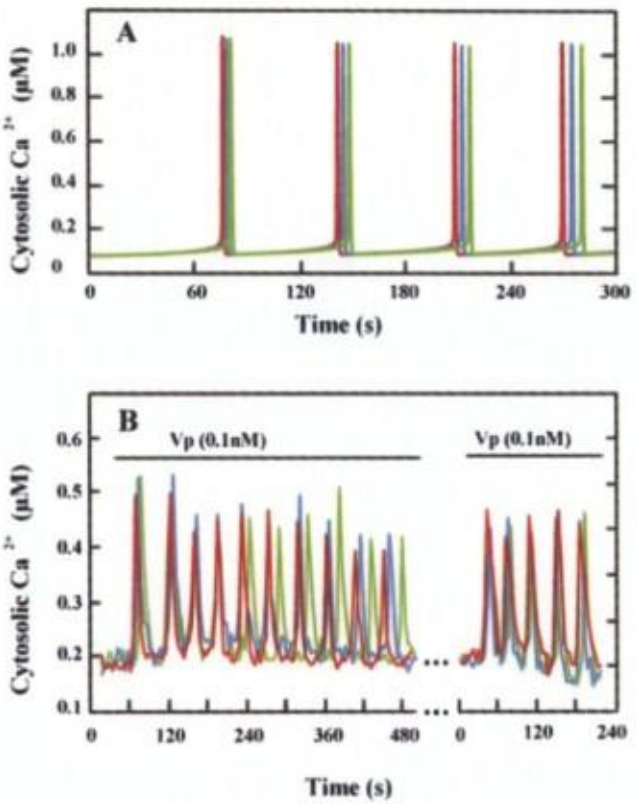

Fig V.4 : Ca^{2+} oscillations and intercellular Ca^{2+} waves induced by vasopressin in a triplet of hepatocytes.

Panel A. Numerical simulation of the Ca^{2+} response in three cells differing in their sensitivity to the agonist, i.e. in their values for parameter V_{PLC}. Spikes appear in a sequential manner, giving the appearance of intercellular Ca^{2+} waves. However, coordination is progressively lost because the three cells have different stationary levels of $InsP_3$. Results were obtained by numerical integration of the model defined by eqns. (I.5)-(I.8)and (V.1)-(V.2) with parameter values listed in Table V.1, with $V_{PLC} = 2.3x10^{-3}$ μMs^{-1} (red line), $2.2x10^{-3}$ μMs-1 (blue line), and $2.1x10^{-3}$ μMs^{-1} (green line). Initial conditions are resting states corresponding to $V_{PLC} = 6.5x10^{-4}$ μMs^{-1}. The permeability coefficient for $InsP_3$ (F_{ip}) is 0.88 μms^{-1}.

Panel B. Hepatocytes loaded with fura2 were stimulated with vasopressin (Vp, 0.1nM) for the time shown by the horizontal bars. Addition of Vp to the bath induced coordinated $[Ca^{2+}]i$ oscillations in the three cells, which progressively desynchronized (panel B, left). Vp was then removed and cells were extensively washed (5 min). The same concentration of Vp was then re-applied and the three cells rapidly recovered synchronized $[Ca^{2+}]i$ oscillations (panel B, right). These results are representative of those obtained using 8 triplets in 4 independent experiments. Recording of the traces was interrupted during the washing process (5 min).

V.6. Theoretical predictions of the model

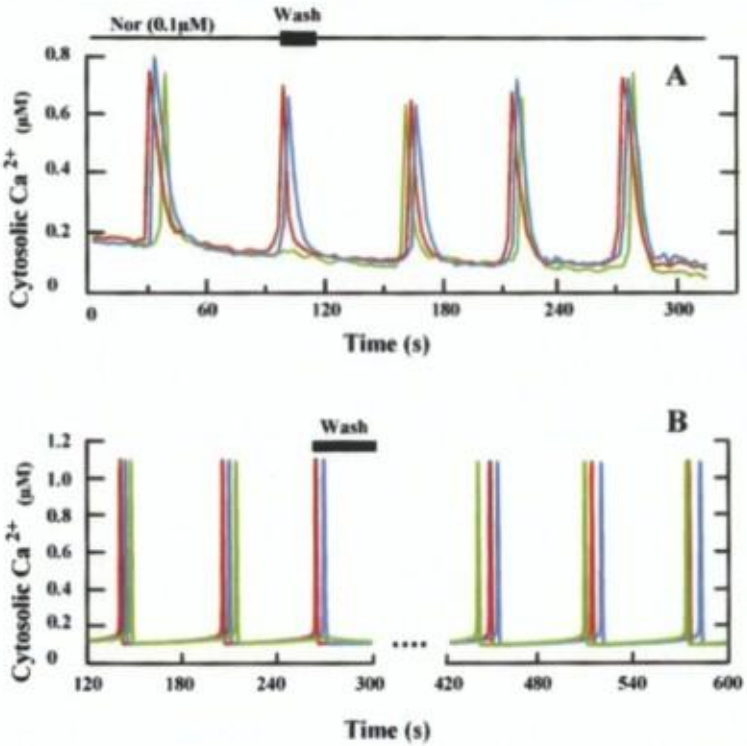

Fig. V.5. Effect of agonist removal during synchronized Ca^{2+} oscillations

Panel A. Results were obtained as in Fig. V.2. Hepatocytes loaded with fura2 were stimulated with noradrenaline (Nor, 0.1μM) for the time shown by the horizontal bar. The solution was rapidly washed out, as indicated by the black area. These results are representative of those obtained using 5 triplets in 4 independent experiments.

Panels B. Simulations of the experiment shown in A. Washing is simulated by an instantaneous return of V_{PLC} to its basal level just after the appearance of a Ca^{2+} spike in the intermediate cell. When the washing time is short, the cell which had failed to respond spikes first after the readdition of the agonist (panel B, green line). Results have been obtained as in Fig. V.3A, except that V_{PLC} is set at the resting value (6.5×10^{-4} μMs^{-1}) between t = 275 s and t = 375 s (panel B), as indicated by the horizontal bars.

A peculiar feature of intercellular Ca^{2+} waves in hepatocytes, as compared to other cell types, is that they require the continuous presence of an agonist (Tordjmann *et al.*, 1997). Thus, we compared the results of the model with that of the real cells when the agonist is removed. In Fig. V.5A, noradrenaline was used to stimulate a triplet and then, during oscillations, the agonist was rapidly washed out. Spiking did not occur in cell 3 after washing, probably because the level of $InsP_3$ in this cell was too low due to the absence of the agonist. Simulation of this experiment, with the same parameter values as in Figs. V.3 and V.4, is shown in Fig. V.5B. A sudden decrease of V_{PLC} to its basal value in the three connected cells (at t=275 s) prevented Ca^{2+} spiking in cell 3. When V_{PLC} was returned to its stimulated value in all three cells, coordinated Ca^{2+} spiking recovered, similar to that observed in the experiments (Fig. V.5B). However, in contrast to the situation "before washing", cell 3 (green line) spiked first after the agonist was reapplied. This was due to the fact that the fraction of 'activatable' $InsP_3$ receptors was slightly higher in this cell because the levels of $InsP_3$ and Ca^{2+} were already raised before washing (see Fig. V.5B).

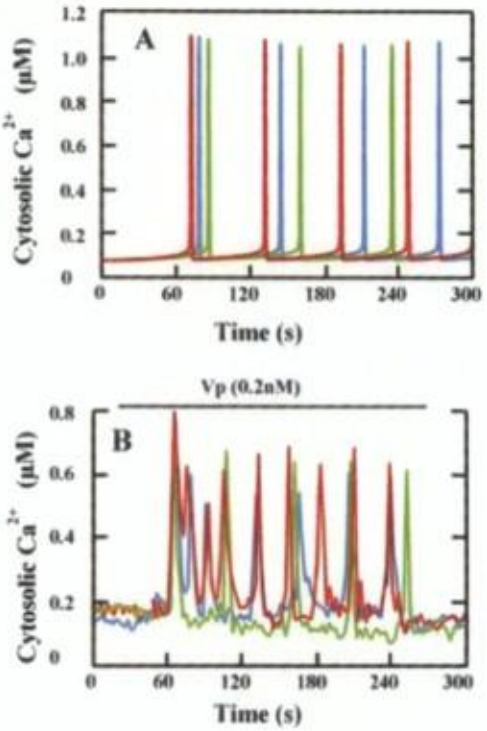

Fig. V.6. Ca^{2+} oscillations in AGA-treated hepatocytes in response to stimulation by vasopressin.

Panel A. Simulation of the Ca^{2+} increase in three uncoupled cell ($F_{IP} = 0$) differing by their V_{PLC} values. The first Ca^{2+} spike appears in a more or less coordinated manner, although subsequent spikes occur independently in the different cells. Results have been obtained as in Fig. V.4A, except that F_{IP} is equal to 0.

Panel B. Hepatocytes loaded with fura2 were incubated with AGA (20μM) for 20 min. Then, vasopressin (Vp, 0.2nM) was added for the time shown by the horizontal bar in presence of AGA. These results are representative of those obtained using 4 triplets (and 7 doublets) in 3 independent experiments.

Experimentally, such an inversion in the sequence of responses was also observed. Fig. V.5A shows that when the washing time was short (see below), the initial sequence (cell 1, 2 then 3) was modified (cell 3, 1 then 2). In the model, the initial sequence (cell 1 to 3) recovered after 5 coordinated spikes, while in the experiments, recovery generally occured sooner (see Fig. V.5A). A straightforward prediction of the model is that when the time interval during which no $InsP_3$ synthesis occurs (i.e. the washing time) becomes very large, the sequence of Ca^{2+} spikes occuring in response to the second addition of the hormone will be imposed by the hormonal sensitivity, as it is for the first addition of agonist (data not shown). This prediction is in good qualitative agreement with the experimental results, although the time scales do not match the experimental observations (i.e. the washing time needs to be longer in the model than in reality). Analysis of 12 multiplets of connected hepatocytes (7 doublets and 5 triplets) showed that when the washing time was greater than 50 seconds, no inversion was observed. In contrast, the cell which had been prevented to respond was the first responding cell after washing when the washing time was below 30 seconds.

Experimental observations have clearly shown that effective gap junctions are necessary to coordinate Ca^{2+} spiking in connected hepatocytes. In the model, gap junctions reduced the differences in the levels of $InsP_3$ because of the imposed gradient in the rates of $InsP_3$ synthesis (V_{PLC}). Because the gradient in hormonal sensitivity is tenuous (a value of 5% between 2 adjacent cells is used in the simulations), it is expected that some level of coordination in Ca^{2+} spiking should be observed in neighboring cells, even if the cells are not connected through gap junctions.

This point is illustrated by the results shown in Fig. V.6A; this simulation was performed under the same conditions as Fig. V.4A, except that the permeability of the gap junctions to $InsP_3$ (F_{IP}) was set to zero. It is clearly visible that the first Ca^{2+} spike is coordinated in the 3 cells. This is due to the fact that, after the rise in $InsP_3$ resulting from the increase in V_{PLC}, the 3 cells enter the oscillatory domain at about the same time. However, because the stationary values of $InsP_3$ concentrations are significantly different, each cell oscillates afterwards at its own frequency and spiking occurs independently in the different cells.

This property of the model is corroborated by the experiment shown in Fig. V.6B. The first Ca^{2+} spike after stimulation of a triplet of hepatocytes pre-treated with AGA, a gap junction inhibitor, occured nearly at the same time in all three cells, although thereafter there was no coordination of Ca^{2+} spiking among the three cells.

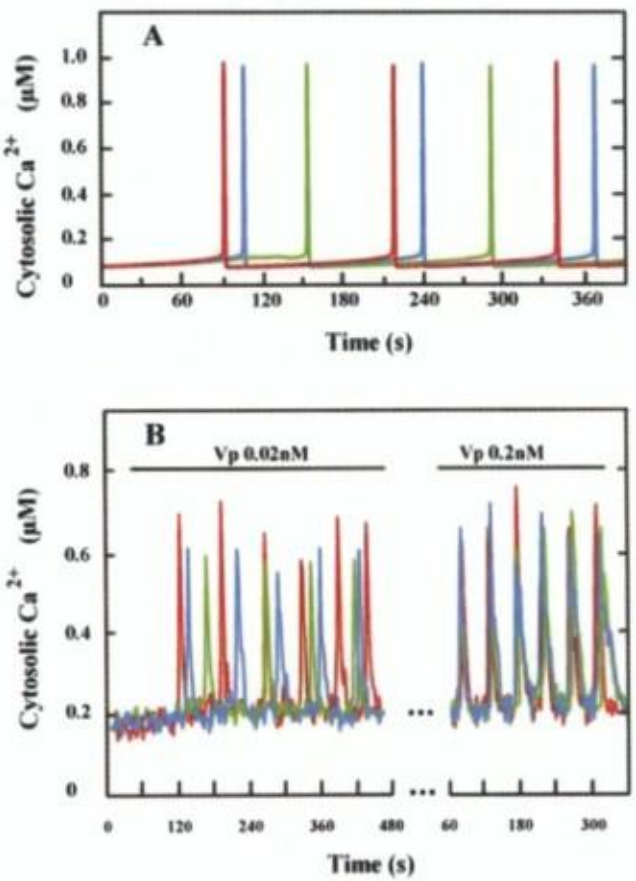

Fig. V.7. Absence of coordination among the Ca^{2+} spikes in connected hepatocytes at low stimulation levels. Panel A. Simulation of Ca^{2+} spikes in a triplet of connected hepatocytes in response to a low level of stimulation, i.e. $V_{PLC} = 1.9 \times 10^{-3}\ \mu Ms^{-1}$ (red), $V_{PLC} = 1.8 \times 10^{-3}\ \mu Ms^{-1}$ (blue) and $V_{PLC} = 1.7 \times 10^{-3}\ \mu Ms^{-1}$ (green). The cells responded in an asynchronous manner because the relative differences in the levels of $InsP_3$ are important. Except for the values of V_{PLC}, results have been obtained as in Fig. V.4A. Panel B. Left and right parts of the figure show successive measurement of $[Ca^{2+}]_i$ in the same hepatocyte triplet loaded with fura2. In the left part, vasopressin (Vp, 0.02nM) addition to the bath was followed by oscillations in the three cells which were not coordinated. However, after washing (5 min) addition of vasopressin (Vp, 0.2nM) induced well coordinated oscillations among the three connected hepatocytes (right part). These results are representative of those obtained using 8 triplets in 5 independent experiments.

The last prediction presented here pertains to the behavior of connected hepatocytes stimulated by very low doses of agonist. In the model indeed, coordination of Ca^{2+} spikes relied on close levels of $InsP_3$. If the intensity of stimulation is low, the relative differences between the

concentrations of $InsP_3$ among the connected cells are more important, although the gradient in the number of receptors remains the same. As shown in Fig. V.7A, in the model, very low levels of stimulation led to non-coordinated spiking among a triplet of connected cells. Similar results were also found experimentally (Fig. V.7B); the same triplet exhibited no coordination at low agonist levels (0.02nM vasopressin) and good coordination at higher agonist doses (0.2 nM vasopressin).

V.7. Further investigation of the respective roles of Ca^{2+} and $InsP_3$ diffusion in coordination of Ca^{2+} signals between hepatocytes

An alternative model to that proposed here above (section V.3) for the propagation of Ca^{2+} signals among connected hepatocytes, developped simultaneously, suggests that the gap-junctional diffusion of Ca^{2+}, and not of $InsP_3$, is required to reproduce the experimental observations (Höfer, 1999). Both models are however based on the same description of the intracellular Ca^{2+} dynamics. In Höfer's model (1999), oscillations are in fact more than 'coordinated'; instead of phase waves, there is an active entrainment through the coupling of oscillators leading to the synchronization (1:1 entrainment) of Ca^{2+} oscillations for appropriate values of the gap-junctional permeability. In order to try to discriminate between both mechanisms of the apparent propagation of intercellular Ca^{2+} waves in multiplets of hepatocytes, we have designed and performed further experiments (Clair *et al.*, 2001).

V.7.1. Is it possible to detect a Ca^{2+} increase induced by gap-junctional diffusion?

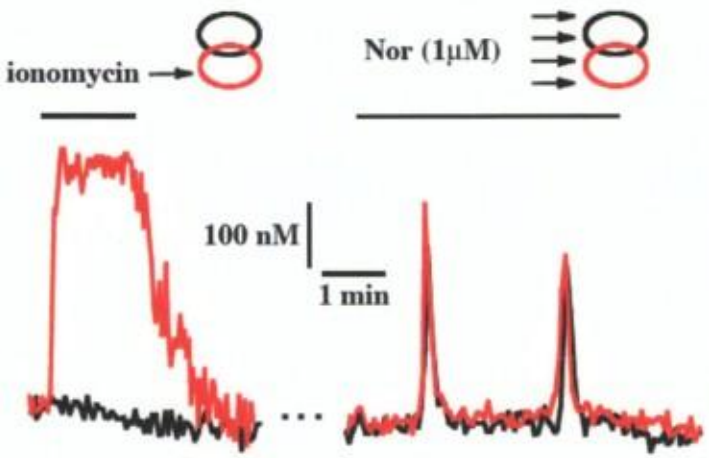

Fig. V.8. Focal application of ionomycin to connected rat hepatocytes. Hepatocytes were injected with fura2. The two parts of the figure show successive measures of $[Ca^{2+}]_i$ in the same hepatocyte doublet and are representative of those obtained using 4 doublets in 3 experiments. The first part of the figure shows the Ca^{2+} response when one cell within the doublet was focally microperfused with ionomycin (500 nM in the micropipette) for the time shown by the upper horizontal bars. In these conditions, only the stimulated cell (arrow) within the doublet was focally microperfused with ionomycin (500 nM in the micropipette) for the time shown by the upper horizontal bars. In these conditions, only the stimulated cell within the doublet responded. Following ionomycin wash out, global superfusion of the doublet with noradrenaline (1 µM) induced coordinated $[Ca^{2+}]_i$ oscillations in both cells. For convenience, tracings were interrupted (gap of 3 minutes).

Previous reports using microinjected Ca^{2+} suggest that this messenger diffuses through gap junctions in hepatocyte doublets (Saez *et al.*, 1989). However little information is available on the ability of Ca^{2+} to pass through gap junctions under less invasive techniques and/or more physiological stimulation. In a previous study, we have shown that focal stimulation of one hepatocyte of a doublet with a low agonist concentration induced Ca^{2+} oscillations that were

restricted to the stimulated cell (Tordjmann *et al.*, 1997). The latter results suggest either that Ca^{2+} was not able to diffuse through gap junctions under these conditions or that the change in Ca^{2+} associated fluorescence was too low to be detected. In the present study, we first aimed to further investigate if Ca^{2+} can flow through hepatic gap junctions under physiological conditions. For this purpose, single-cell stimulation was performed either by a focal application from a glass micropipette filled with ionomycin (500 nM) or by a global perfusion of maximal agonists concentrations. In both types of experiments, fura2 loading was performed by microinjection of the dye in one cell, fura2 diffusion via gap junctions ensuring that the two cells were efficiently coupled.

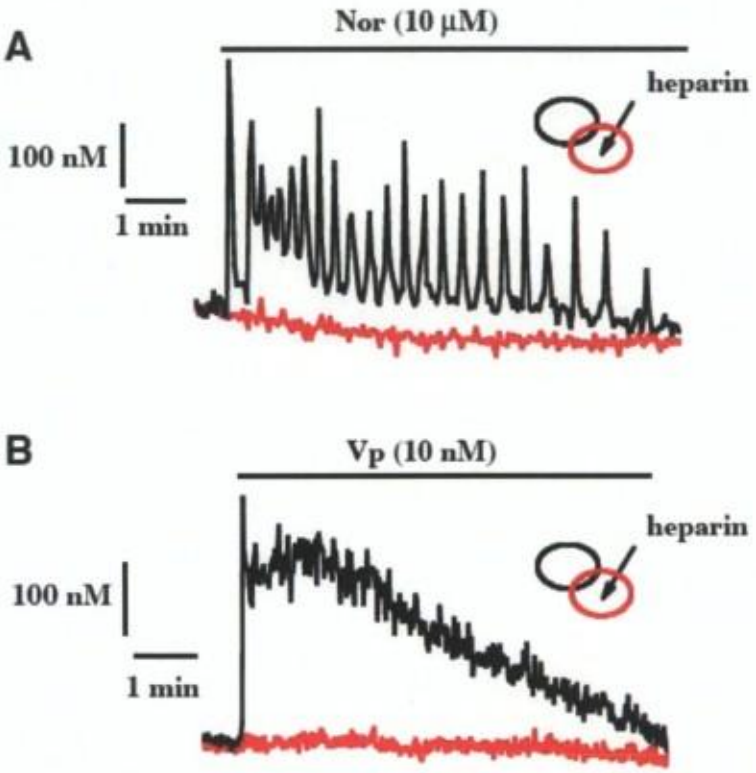

Fig. V.9. Absence of apparent Ca^{2+} diffusion between connected rat hepatocytes. Hepatocyte doublets were injected with fura2 and heparin (10 mg/ml in the pipette) as described in methods section. After injection, perfusion (for the time shown by the horizontal bars) of high concentration of noradrenaline (Nor; 10 µM, A) or vasopressin (Vp; 10 nM, B), induced a rapid and strong increase in $[Ca^{2+}]_i$ in the noninjected cell only. Although this $[Ca^{2+}]_i$ increase was maintained for more than 3 minutes in the responding cell, no diffusion of Ca^{2+} was observed in the connected cell injected with heparin. These results are representative of those obtained using 10 doublets in four independent experiments.

Focal application of a Ca^{2+} ionophore

Focal application of the Ca^{2+} ionophore ionomycin was achieved by positioning a glass micropipette close to the cell of interest and applying a constant pressure via the Eppendorf injector, delivering picoliter quantities of ionomycin-containing solution (500 nM). As shown in Fig. V.8 (left panel), the ionomycin microperfused cell exhibited a rapid and high $[Ca^{2+}]_i$ rise; by contrast, $[Ca^{2+}]_i$ remained at a basal low level in the nonmicroperfused cell. However, after ionomycin was washed away, global perfusion of noradrenaline (1 µM) induced well coordinated $[Ca^{2+}]_i$ oscillations within the two cells (right panel).

Global application of supra-maximal agonists concentrations.

In these experiments, one of two connected hepatocytes was injected with fura2 and heparin. Heparin inhibits both $InsP_3$ binding and the resulting $InsP_3$-induced Ca^{2+} release (Worley *et al.*, 1987; Cullen *et al.*, 1988). As shown in Fig. V.9, which is representative of 10 doublets, perfusion of maximal concentrations of vasopressin (10 nM) or noradrenaline (10 μM) elicited an immediate Ca^{2+} rise in the non-injected cells, which was maintained at a high level for at least 3 minutes, especially in the presence of vasopressin (Fig. V.9B), whereas no change of fluorescence was observed in the heparin-injected cell. By contrast, addition of thapsigargin or ionomycin induced a $[Ca^{2+}]_i$ increase in the two connected cells (data not shown).

V.7.1. Possible role of $InsP_3$ as a coordinating messenger for Ca^{2+} spiking among connected hepatocytes

Ca^{2+} signals in response to increasing agonist concentrations

The other likely candidate that could be responsible for the coordination of Ca^{2+} spiking among connected hepatocytes is $InsP_3$. If junctional $InsP_3$ diffusion is involved, it can be expected that the degree of coupling increases with the level of $InsP_3$, and thus also with the concentration of the agonist. To test this hypothesis, hepatocyte multiplets were perfused with increasing concentrations of $InsP_3$-dependent agonists (Fig. V.10). Note that the proportion of responsive cells in these conditions was low (30-50%). Nevertheless, application of very low concentrations of noradrenaline (0.02 μM), to doublet or triplet of hepatocytes sometimes induced Ca^{2+} oscillations (Fig. V.10 and data not shown).

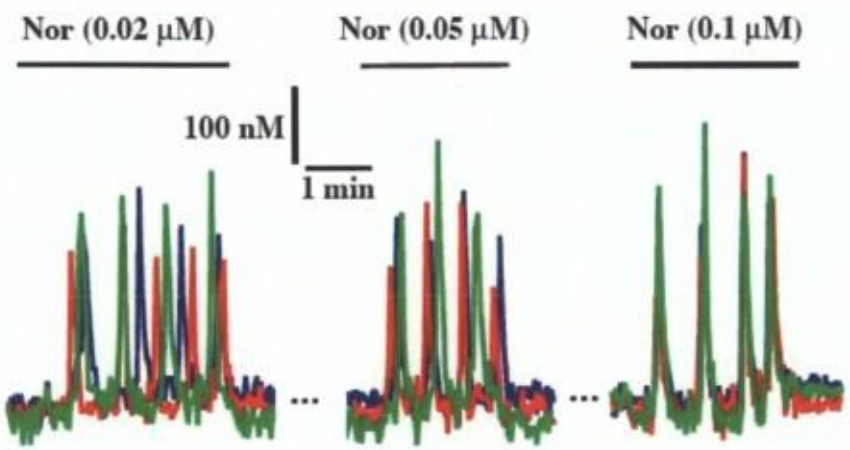

Fig. V.10. Coordination of Ca^{2+} oscillations increases with the increase of agonist concentration in connected hepatocytes. Hepatocytes were loaded or injected with fura2. The figures show successive measures of $[Ca^{2+}]_i$ in the same hepatocyte triplet. Cells were sequentially stimulated with increasing concentrations of noradrenaline (0.02, 0.05 and 0.1 μM) for the time shown by the horizontal bars. Addition of the lowest dose of noradrenaline to the bath was followed by oscillations in the three cells that were not coordinated (left). After washing, addition of a higher concentration of noradrenaline (0.05 μM) induced coordinated Ca^{2+} oscillations (middle part). Finally, very well coordinated oscillations were observed in the presence of 0.1 μM noradrenaline (right). The same results were obtained in hepatocyte doublets and are representative of those obtained using 12 triplets and 21 doublets in five independent experiments. Recording of the traces was interrupted during the washing process (5 minutes).

However, these oscillations were not coordinated, as if the cells were not functionally coupled by gap junctions (each cell having its own oscillation frequency) even though gap junctions efficiently connected these cells as they were loaded by cell to cell diffusion of microinjected fura2. Raising the concentration of noradrenaline (0.05 μM) not only increased the frequency of

the Ca^{2+} oscillations as expected (see blue and green traces in Fig. V.10 for example), but also led to coordinated oscillations (Fig. V.10, middle panel). Finally, perfusion of a higher concentration of noradrenaline (0.1 μM) induced a good coordination of the Ca^{2+} oscillations among the connected hepatocytes. Because, in contrast with the amplitude of Ca^{2+} oscillations, the $InsP_3$ level increases with increasing concentrations of agonists (Thomas *et al.*, 1996), these results suggest that $InsP_3$, rather than Ca^{2+}, is responsible for the coordination of Ca^{2+} oscillations between connected hepatocytes. At low stimulation, production of $InsP_3$ is indeed too small to allow for an efficient junctional $InsP_3$ diffusion, and the cells thus oscillate at their own intrinsic frequencies; raising the level of $InsP_3$, via the increase of agonist concentrations, allows the diffusion of significant amounts of $InsP_3$ through gap junctions, a phenomenon that can account for the observed coordination in Ca^{2+} oscillations.

Effect of the increase of $InsP_3$ 5-phosphatase activity in hepatocytes

Finally, we have studied the role of a putative $InsP_3$ intercellular diffusion in synchronization of Ca^{2+} oscillations by microinjection of type I $InsP_3$ 5-phosphatase in the intermediate cell of a triplet. Type I $InsP_3$ 5-phosphatase is the most widespread $InsP_3$ 5-phosphatase and efficiently metabolizes $InsP_3$ to produce inositol 1,4-bisphosphate, which does not mobilize Ca^{2+} (Putney *et al.*, 1989; Erneux *et al.*, 1989; Verjans *et al.*, 1994a). It has been shown recently that overexpression of this enzyme in CHO cells deeply affected the pattern of Ca^{2+} oscillations; in some cases it even abolished the stimulus-induced Ca^{2+} signal (De Smedt *et al.*, 1997). In the present study, we thus used microinjected $InsP_3$ 5-phosphatase to specifically decrease the level of $InsP_3$ in a particular hepatocyte. Triplets were first loaded with fura2 and treated with noradrenaline (0.1 μM), which elicited trains of coordinated Ca^{2+} oscillations in the three connected cells (Fig. V.11, left panel). After washing out noradrenaline, the intermediate cells of the triplets were microinjected with $InsP_3$ 5-phosphatase. In the vast majority of injected multiplets (9/13), the renewed superfusion of noradrenaline (0.1 μM) elicited Ca^{2+} oscillations in the non-injected cells only, whereas Ca^{2+} remained at a low basal level in the $InsP_3$ 5-phosphatase injected cell. In the remaining injected cells (4 out of 13), the frequency of oscillations was strongly reduced (data not shown). In all cases, Ca^{2+} oscillations in the two remaining responding cells appear uncoordinated (n=13 triplets). It is worth noting that $InsP_3$ 5-phosphatase did not inhibit gap junction permeability because, when fura2 was co-injected with 5-phosphatase into the intermediate cells of the triplets, the dye diffused into the two adjacent connected cells and again, no coordination was observed in the two remaining responding cells (n=3, data not shown).

Thus, it can be concluded that, if the level of $InsP_3$ is too low in the intermediate cell, coordination cannot be achieved between the two end cells of the triplet. It could be argued that such an absence of coordination is simply due to the fact that the Ca^{2+} increases cannot propagate through the intermediate cell in the absence of an effective $InsP_3$-sensitive Ca^{2+}-induced Ca^{2+} release; in other words, as diffusion of Ca^{2+} is very slow, the increase of Ca^{2+} occurring in the first cell of the triplet could not be detected by the last one in the absence of any regenerative process. That this is not the case is clearly visible in the last panel of Fig. V.11, which shows Ca^{2+} oscillations in the three cells of the same triplet at 1 μM noradrenaline. There, owing to the high level of stimulation, the concentration of $InsP_3$ is clearly sufficient to activate the $InsP_3Rs$ even in the 5-phosphatase-injected cell (Fig. V.11, right panel). However, even in this case, the Ca^{2+} oscillations remained uncoordinated among the three cells of the triplet. Thus, the absence of coordination in the Ca^{2+} oscillations in the $InsP_3$ 5-phosphatase-injected cells can be explained only by a difference in the levels of $InsP_3$ between the connected cells, which cannot be erased by the low permeability of the gap junctions. Moreover, the latter experiment indicates that the intermediate cell had not been damaged during the 5-phosphatase microinjection process. It also gives an idea of the efficiency of the $InsP_3$ 5-phosphatase to metabolize $InsP_3$. Indeed, Ca^{2+} oscillations such as those seen in the intermediate cell are usually observed at 10 time lower

because Ca^{2+} is known to be the principal regulator of its own release through an increase in the effect of $InsP_3$ on its receptor (reviewed by Taylor, 1998), it has been suggested in other cell types, such as aortic endothelial cells, pancreatic acinar cells or articular chondrocytes, that the diffusion of small amounts of Ca^{2+} between adjacent cells could serve to sensitize $InsP_3R$ in the neighboring cells and thus allow for the intercellular propagation of the signal (Yule *et al.*, 1996; D'Andrea and Vittur, 1997; reviewed by Tordjmann *et al.*, 2000). Our results in hepatocytes cannot exclude any role for Ca^{2+} in the coordination of Ca^{2+} spiking in this cell type. It remains plausible that diffusion of Ca^{2+} might play a role when the Ca^{2+} sequestration mechanism is partly impaired (i.e. at high levels of $InsP_3$). In this case, intercellular diffusion of Ca^{2+} could smooth out the differences in Ca^{2+} signals among connected cells caused by possible heterogeneities in cell shape or in the diverse $InsP_3$-independent fluxes (Höfer, 1999). Our results show however, that even if such Ca^{2+}-activated Ca^{2+} release through $InsP_3R$ takes place in hepatocytes (Taylor, 1998), it is not crucial for the coordination of Ca^{2+} oscillations induced by $InsP_3$-dependent agonists among connected cells. By contrast, coordination of Ca^{2+} oscillations among connected hepatocytes is fully dependent on the level of $InsP_3$ diffusing from cell to cell.

CHAPTER VI

Simulations of calcium waves in ascidian eggs. Insights into the origin of the pacemaker sites and into the possible nature of the sperm factor.

VI.1. Introduction

In all eggs, fertilization induces a dramatic increase in cytosolic Ca^{2+}. This rise in Ca^{2+} occurs as a wave propagating through the whole egg from the site of sperm-egg fusion and drives egg activation (Stricker, 1999). In many species, among which ascidians and mammals, this fertilization wave is followed by repetitive Ca^{2+} waves of shorter duration and smaller amplitude (McDougall and Sardet, 1995; Stricker, 1999) similar to those observed in a variety of somatic cells stimulated by hormones, growth factors or neurotransmitters (Berridge *et al.*, 2000). Ascidian eggs moreover have the unique property of displaying 2 stereotypic series of Ca^{2+} waves (McDougall and Sardet 1995, Dumollard *et al.*, 2002). Series I Ca^{2+} waves consists of the large amplitude fertilization wave, followed by a few smaller spikes. Series I lasts for about 8 min and drives meiosis I up to the extrusion of the first polar body. Ca^{2+} oscillations then stop for about 5 min. A second series of Ca^{2+} waves then resumes with a progressively increasing, and then decreasing amplitude. This series II lasts for 15-20 min., drives meiosis II and stops just before the extrusion of the second polar body (McDougall and Sardet, 1995). It is known that in most cell types the signal-induced Ca^{2+} increases rely on the production of inositol 1,4,5-trisphosphate ($InsP_3$), a diffusible second messenger that activates Ca^{2+} release from the endoplasmic reticulum (ER). As the activity of the $InsP_3$ receptor ($InsP_3R$) is also stimulated by cytosolic Ca^{2+}, an initially localized Ca^{2+} increase triggers the regenerative propagation of the Ca^{2+} wave throughout the egg while sustained activation of the $InsP_3Rs$ gives rise to Ca^{2+} oscillations and waves (Berridge *et al.*, 2000).

A universal trigger for the initial Ca^{2+} release at fertilization has not yet been identified. Sperm-egg fusion can however be replaced by the injection of a soluble sperm extract (Swann and Parrington 1999, Runft *et al.*, 2002). In mammals, it has been proposed that the active component of this sperm extract, known as sperm factor (SF), is a new isoform of phospholipase C (PLC, the enzyme responsible for $InsP_3$ synthesis; see Chapter II) known as PLCζ (Saunders *et al.*, 2002; Cox *et al.*, 2002; for a review, see Kurokawa *et al.*, 2004). In ascidians, the key factor is a still-unidentified protein with a size comprised between 30 and 100 kDa (Kyozuka *et al.*, 1998). It could be either a soluble PLC or an as yet unknown activator of PLC (Runft and Jaffe, 2000; Runft *et al.*, 2002).

Given the pivotal role played by the Ca^{2+} dynamics in the activation of the egg and its development into an embryo (Dupont, 1998; Ozil, 1998; see also section VII.4), a detailed understanding of the biochemical events responsible for the temporal and spatial organization of cytoplasmic Ca^{2+} signals at fertilization is required. To this aim, simulations provide a useful complementary approach to the numerous experimental studies (Dupont and Dumollard, 2004).

The basic mechanism of Ca^{2+} oscillations in eggs does not differ much from that of Ca^{2+} oscillations in somatic cells. Most models ascribe the oscillations to the autocatalytic regulation exerted by cytoplasmic Ca^{2+} on its own release from the ER (Goldbeter *et al.*, 1990; Sneyd *et al.*, 1995; Fig. VI.1). Some studies however stress the possible role of the activation of PLC by Ca^{2+}, a regulation that also leads to a regenerative increase in cytosolic Ca^{2+} (Meyer and Stryer, 1988; Hirose *et al.*, 1999). Despite numerous theoretical approaches (for review, see Schuster *et al.*, 2002), no model until now has focussed on the rather typical shape of the repetitive Ca^{2+} waves which are triggered at fertilization.

Theoretically, Ca^{2+} wave propagation can be ascribed to the same regulatory processes as oscillations (Sneyd *et al.*, 1995; Goldbeter, 1996). It is clear however that the detailed characteristics of the waves much depend on the cell type. In eggs, these waves can take the form of sharp fronts, spirals or tides (Lechleiter *et al.*, 1991; McDougall and Sardet, 1995; Fontanilla and Nuccitelli, 1998). The detailed shape of the front can also vary: both convex and concave fronts have been observed (Stricker, 1999). Moreover, the large size of the eggs allows a clearer manifestation of the effects related with the spatial inhomogeneity of the cytoplasm. Distinct subcellular regions that repetitively initiate Ca^{2+} waves have been identified in the ascidian egg (McDougall and Sardet, 1995; Dumollard

and Sardet, 2001; Dumollard *et al.*, 2002). Three such regions, called "calcium wave pacemakers (PM)", have been reported: (1) PM1 is defined as the initiation sites of the first series of Ca^{2+} oscillations (series I). PM1 is a moving Ca^{2+} wave pacemaker: the fertilization wave indeed initiates at the site of sperm entry, while the initiation sites of the subsequent waves progressively migrate with the sperm aster towards the vegetal contraction pole. (2) Pacemaker PM2 is stably localized in the vegetal contraction pole, a cortical constriction of 15-20 μm in diameter. It is a region of dense ER and mitochondria accumulation. (3) An artificial pacemaker called PM3 is located in the animal hemisphere, and is defined as the cellular region most sensitive to an artificial stimulation by $InsP_3$. It probably corresponds to a region rich in ER clusters, present around the meiotic spindle in the mature unfertilized egg (Dumollard and Sardet, 2001).

Some theoretical models have already investigated the spatial characteristics of the Ca^{2+} increase occuring at fertilization (Wagner *et al.*, 1998; Bugrim *et al.*, 2003; Hunding and Ipsen, 2003). It was shown that the correct shape of the fertilization wave in *Xenopus* oocyte can be reproduced by assuming that $InsP_3$ is locally generated at the fertilization site (Bugrim *et al.*, 2003). Moreover, these studies emphasize the role of the spatial inhomogeneities in the ER distribution (Bugrim *et al.*, 2003; Hunding and Ipsen, 2003), in the $InsP_3Rs$ distribution (Bugrim *et al.*, 2003) or in $InsP_3$ production (Wagner *et al.*, 1998) to reproduce the experimentally observed spatial profiles. None of these studies however deals with repetitive Ca^{2+} waves, as those observed at fertilization of many species, among which ascidians and mammals. In the case of the *Xenopus* oocytes, the fertilization Ca^{2+} wave is indeed seen as a switch in a bistable system. Recovery, i.e. return to the basal Ca^{2+} level, is seen to occur on a much longer time scale than the increase in Ca^{2+}.

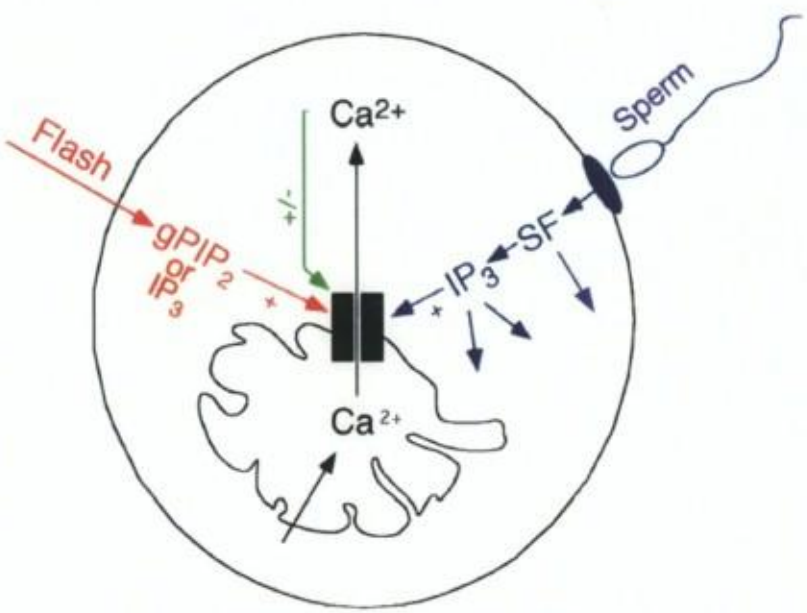

Fig. VI.1. Schematic representation of the model developed to account for Ca^{2+} oscillations and waves in ascidian eggs. The red pathway schematizes experiments of $gPIP_2$ flash photolysis, while the blue pathway shows the events supposed to occur at fertilization. The model is adapted from Dupont and Swillens (1996), and from Dupont and Erneux (1997).

In the present study, we simulate repetitive Ca^{2+} waves with a spatio-temporal pattern analogous to that of series I oscillations in ascidian eggs. We focus on the Ca^{2+} waves induced by $InsP_3$ or its poorly metabolizable analog $gPIP_2$ and on series I Ca^{2+} oscillations. We first simulate an existing model for Ca^{2+} and $InsP_3$ dynamics and show that it can reproduce the experimentally observed Ca^{2+} waves triggered by flash photolysis of $InsP_3$ or $gPIP_2$ when considering an appropriate inhomogeneous

distribution of ER. We then show the results of simulations of the model predicting the effect of a localized injection of a large amount of $gPIP_2$. This prediction is confirmed experimentally. In a second part, we use our model to simulate the fertilization wave and the series I Ca^{2+} oscillations. We find that the best agreement with the experimental data is obtained if it is assumed that the SF in ascidian eggs is a Ca^{2+}-sensitive, highly diffusible PLC, and that PIP_2, the substrate for PLC, is homogeneously distributed in the whole egg.

VI.2. Model for the spatio-temporal Ca^{2+} dynamics in ascidian eggs

VI.2.1. Evolution equations

In ascidian eggs, Ca^{2+} oscillations can be generated by a single and long-lasting increase of the poorly-metabolizable analog of $InsP_3$, $gPIP_2$ (Dumollard and Sardet, 2001; and see below); in such conditions, Ca^{2+} oscillations can be ascribed to the well-known biphasic regulation of the type 1 $InsP_3R$ by Ca^{2+} (Bezprozvanny *et al.*, 1991; Finch *et al.*, 1991; Miyakawa *et al.*, 1999). Moreover, only the type 1 $InsP_3R$ can be found in the ascidian genome (http://genome.jgi-psf.org/cgi-bin/searchGM2.cgi?db=ciona4). The model used in the present study to describe the evolution of the levels of Ca^{2+}, InsP3 and active receptors is a modified version of a prototypic model describing the sequential activation-inhibition of the receptor as the level of cytosolic Ca^{2+} increases (Fig. IV.1; Table I.3; Dupont and Swillens, 1996).
The evolution of the fraction of receptor in an inactive (desensitized) state, R_{des}, is given by :

$$\frac{dR_{des}}{dt} = k_+\left(1 - R_{des}\right)\frac{C_{cyto}^{n_i}}{1+\left(\frac{C_{cyto}}{K_{act}}\right)^{n_a}} - k_-R_{des} \qquad \text{(VI.1)}$$

where k_+ is the rate of inhibition of the $InsP_3R$ by cytosolic Ca^{2+} and k_- the rate of relief from this inhibition. Activation of the receptor by Ca^{2+} is assumed to be instantaneous and characterized by a threshold constant K_{act}. The level of cytosolic Ca^{2+} (C_{cyto}) varies through Ca^{2+} release via the $InsP_3Rs$ and Ca^{2+} pumping by Ca^{2+} ATPases located in the membrane of the ER. We do not consider Ca^{2+} exchanges with the extracellular medium, as it is known that Ca^{2+} oscillations in ascidian eggs can occur in the absence of extracellular Ca^{2+} (Speksnijder *et al.*, 1989; Carroll *et al.*, 2003). Taking diffusion into account, the evolution equation for the concentration of cytosolic Ca^{2+} can be written:

$$\frac{\partial C_{cyto}}{\partial t} = \lambda(r)\left[\alpha(r)k_1\left(b + IR_a\right)\left(C_{lum} - C_{cyto}\right) - V_{MP}\frac{C_{cyto}^2}{K_p^2 + C_{cyto}^2}\right] + D_{cyto}\frac{\partial^2 C_{cyto}}{\partial r^2} \qquad \text{(VI.2)}$$

In this equation, IR_a represents the fraction of $InsP_3Rs$ in an active state, and is given by :

$$IR_a = \frac{IR_{able}}{1 + \left(\frac{K_{act}}{C_{cyto}}\right)^{n_a}} \qquad \text{where}$$

$$IR_{able} = (1 - R_{des}) \left(\frac{IP}{K\left(1 + \frac{gPIP_2}{K_{gPIP_2}}\right) + IP} + \frac{gPIP_2}{K_{gPIP_2}\left(1 + \frac{IP}{K}\right) + gPIP_2} \right) \qquad \text{(VI. 3)}$$

where IP and $gPIP_2$ represent the $InsP_3$ and the $gPIP_2$ concentrations, respectively. $gPIP_2$ is explicitely considered in the model, since we simulate experiments of flash-photolysis of this poorly metabolizable analog of $InsP_3$. Parameter k_1 fixes the rate of Ca^{2+} release through the $InsP_3R$ and k_1b is a leak term. The second term of equ. (VI.2) represents the pumping of Ca^{2+} into the ER by the ATPases. The last term is a classical Fick term for diffusion.

The distribution of ER is taken into account through 2 parameters: λ and α, which are both functions of space (r) to allow heterogeneity. Two parameters are necessary because the amount of ER affects both the number of $InsP_3Rs$ and Ca^{2+} pumps (located in the ER membrane), and the local volumes of the ER and cytosol, respectively. Thus, the first parameter (λ) scales the number of channels ($InsP_3Rs$ and Ca^{2+} pumps) and similarly affects all flux terms across the ER membrane. The other parameter (α) is defined as the local ratio between the volumes of the endoplasmic reticulum and the cytosol. It accounts for example for the fact that the release of a given number of *moles* of Ca^{2+} from the ER will induce a lower increase of the Ca^{2+} *concentration* in the cytosol than the associated decrease of Ca^{2+} *concentration* in the ER, due to the different volumes of these compartments. In this study, we always assume that the distribution of ER follows the same distribution than that of Ca^{2+} channels (Fink *et al.*, 2000). Thus, there is a fixed relationship between $\lambda(r)$ and $\alpha(r)$: assuming a spherical shape for the ER, any change in a of a factor x will be accompanied by a change in λ of a factor $x^{2/3}$, given the surface/volume ratio of a sphere. In the following, we will discuss changes in ER distribution in terms of α.

In contrast to other models, we do not assume that the Ca^{2+} concentration inside the ER remains constant, as the fertilization Ca^{2+} wave implies a massive release of Ca^{2+} from the ER. In our model, the evolution of the concentration of Ca^{2+} inside the ER lumen (C_{lum}) is given by :

$$\frac{\partial C_{lum}}{\partial t} = \lambda(r)\left[\frac{V_{MP}}{\alpha(r)}\frac{C_{cyto}^2}{K_p^2 + C_{cyto}^2} - k_1\left(b + IR_a\right)\left(C_{lum} - C_{cyto}\right)\right] + D_{ER}\frac{\partial^2 C_{lum}}{\partial r^2} \qquad \text{(VI.4)}$$

Implicit in the latter equation is the fact that the ER behaves as a continuous compartment invading the whole egg. In Eqs. (VI.2) and (VI.4), all fluxes must be seen as effective ones, as Ca^{2+} buffers are not explicitly incorporated in the model.

Finally, $InsP_3$ is assumed to be synthesized from PIP_2 by PLC and degraded by both a phosphatase and a kinase. Thus, the evolution of the concentration of $InsP_3$ (IP) follows :

$$\frac{\partial IP}{\partial t} = I_{IP_3} + V_{PLC} - V_{5P}\frac{IP}{K_{5P} + IP} - V_{3K}\frac{IP}{K_{3K} + IP}\frac{C_{cyto}}{K_{A3K} + C_{cyto}} + D_{IP_3}\frac{\partial^2 IP}{\partial r^2} \qquad \text{(VI.5)}$$

I_{IP3} allows us to simulate the experiments of $InsP_3$ flash-photolysis (in this case, this parameter takes a non-zero value during the simulated flash). V_{PLC} represents the basal rate of $InsP_3$ synthesis in a non-fertilized egg. In equ. (VI.5), this rate is assumed to be Ca^{2+}-insensitive, in the absence of further indication as to the PLC isoform present in the ascidian egg. However, given that V_{PLC} is a small

term –because it must lead to a basal low level of $InsP_3$– the behaviour of the model remains unchanged if V_{PLC} is made Ca^{2+}-sensitive. V_{5P} and V_{3K} stand for the maximal rates of $InsP_3$ 5-phosphatase and 3-kinase, respectively, while K_{5P} and K_{3K} are the Michaelis constants of the same enzymes. Stimulation of $InsP_3$ 3-kinase activity by Ca^{2+} is taken into account; the constant for half-maximal activation is represented by K_{A3K}. As discussed in section VI.4, the concentration of PIP_2 (the substrate for PLC) is assumed to be homogeneous throughout the whole egg and to remain constant or at least not limiting (Xu *et al.*, 2003).

VI.2.2. Inhomogeneities in the endoplasmic reticulum distribution

The ascidian egg is a large cell, the diameter of which is comprised between 100 and 150 μm. As in many other eggs, the cytoplasm is highly structured in specific domains that host different concentrations of intracellular organelles (mitochondria, yolk platelets and endoplasmic reticulum). It is also known that a spectacular reorganization of these egg structures occurs at fertilization (Roegiers *et al.*, 1999). In particular, a wave of cortical contraction leads to the formation of the contraction pole in the vegetal hemisphere, a region containing an accumulation of cortical ER (Roegiers *et al.*, 1999; Dumollard and Sardet, 2001). Since we focus here on the Ca^{2+} changes induced by the injection of $InsP_3$ or $InsP_3$ analogs, or occurring just after fertilization, we do not consider these rearrangements in the present study.

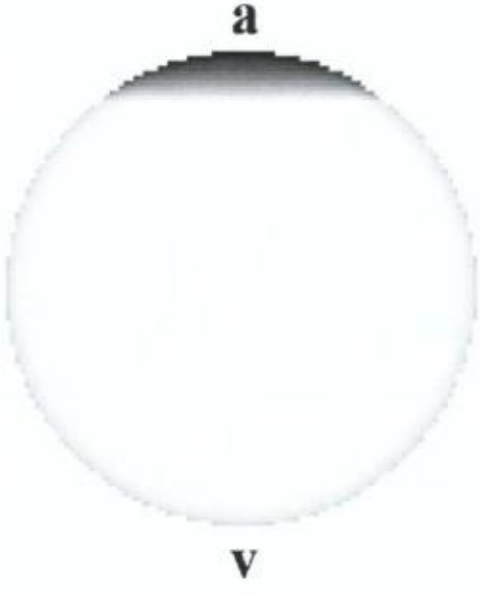

Fig. VI.2. Gray-scale representation of the density of the endoplasmic reticulum (parameter α) used in the simulations of Ca^{2+} oscillations and waves in ascidian eggs. The ER is assumed to be more concentrated in the cortex of the egg, with a maximal value in the animal cortex. Parameter α measures the local ratio between the ER and the cytosolic volumes. Scale: black: $\alpha = 0.12$, white: $\alpha = 0.07$. This ER density is given by eqs. (VI.6) and (VI.7) with the following parameter values: $\alpha_B = 0.07$, $\alpha_C = 0.10$, $w = 0.04$, $r_C = 75$ µm, $h = 0.04$ and $d = 15$ µm. a : animal pole; v : vegetal pole.

To simplify the simulations, we have chosen a 2D geometry. This assumption amounts to looking at a slice through the egg, but introduces a bias on the value of the fluxes. However, as most parameter values are not known for the ascidian eggs, we think that this assumption –which much reduces the computing time– is worthwhile.

The ER is modelled as a continuous network of varying density throughout the cytosol. Thus parameter α, defined as the ratio between the volumes occupied by the endoplasmic reticulum and by the cytosol, is a function of space (r). As suggested by direct observations on mature eggs (Dumollard

and Sardet., 2001; Sardet *et al.*, 2002), we assume that the density of the reticulum is higher in the cortex than in the cytosol. The thickness of this higher density region is of a few microns. In the model, it is assumed that there is a gradient of reticular density from the periphery to the center, given by :

$$\alpha'(r) = \alpha_B\left(1 + \alpha_C e^{\frac{r - r_c}{wr_c}}\right) \qquad \text{(VI.6)}$$

where α_B is the basal density of ER, α_C reflects the amplitude of the gradient, r_c is the radius of the egg and w reflects the steepness of the gradient. The spatial coordinate r is calculated in a system centered on the center of the egg.

Moreover, we consider another type of inhomogeneity strongly suggested by recent experimental observations ; it has been shown that the artificial pacemaker located in a broad cortical region of the animal hemisphere (PM3) serves as the initiation site of the Ca^{2+} waves induced by exogenous injections of $InsP_3$ or $gPIP_2$ (Dumollard and Sardet, 2001). We thus use numerical simulations to investigate the hypothesis that a higher density of ER suffices to explain all the observations performed with respect to this new pacemaker. To account for the possible existence of such a region, we assume that α is maximal at the cortex of the animal pole and linearly decreases towards the center of the egg (vertical variation only). Thus, in the region called pacemaker 3 (PM3),

$$\alpha(r) = \alpha'(r) - \frac{h}{d}y + h \qquad \text{if } y \le d \qquad \text{(VI.7)}$$

where y stands for the vertical distance from the upper point of the egg, h for the maximal increment of ER density and d for the characteristic length of the pacemaker region. The ER distribution defined by eqs (VI.6)-(VI.7) is assumed to remain unchanged in the course of the simulations.

The resulting distribution of the ER for our particular set of parameter values is shown in Fig. VI.2. The average density of the ER equals 8%, which is of the order of experimental measurements performed in other cell types (Depierre and Dallner, 1975; Fink *et al.*, 2000). The resting cytosolic and luminal [Ca^{2+}] result from an equilibrium between Ca^{2+} fluxes across the ER membranes; in consequence, the steady-state level of Ca^{2+} in the absence of stimulation depends on ER density and this level of Ca^{2+} is inhomogeneous both in the cytosol and in the lumen. Although in the ER this inhomogeneity is not significant, cytosolic Ca^{2+} varies from 0.106 µM to 0.167 µM depending on the ER density (the higher the density, the higher the concentration). This effect is due to the locally lower cytosolic volume in the regions of high ER density (parameter α). In contrast, variations in λ affect both release and pumping and do thus not affect the steady-state levels of Ca^{2+}.

VI.2.3. Sperm factor

In the last part of our study, we investigate the sperm factor hypothesis. We start from the basic assumption that SF is a soluble PLC (Swann, 1996; Saunders *et al.*, 2002; Cox *et al.* 2002; Howell *et al.*, 2003). Thus, we simulate fertilization by assuming that a large amount of PLC is locally introduced in the egg. This additional PLC is superimposed on the basal PLC activity of the egg. SF is assumed to diffuse and to be degraded. The value of the diffusion coefficient will be discussed later. The time scale of SF degradation is chosen to fit the observed duration of series I Ca^{2+} oscillations in ascidian eggs. We also made the assumption that the activity of the injected PLC is stimulated by cytosolic Ca^{2+} (see below for the justification of this hypothesis).

Thus, when modelling fertilization, a new equation describing the evolution of the level of sperm factor activity is introduced:

$$\frac{\partial SF}{\partial t} = -k_{SF} SF + D_{SF} \frac{\partial^2 SF}{\partial r^2} \qquad \text{(VI.8)}$$

where k_{SF} stands for the rate constant of SF degradation and D_{SF} for the diffusion coefficient. Introduction of SF occurs through appropriate initial conditions. Moreover, equ. (VI.5) is modified to take into account the PLC activity of the SF:

$$\frac{\partial IP}{\partial t} = V_{PLC} + V_{SF}[SF]\frac{C_{cyto}^2}{K_{ASF}^2 + C_{cyto}^2} - V_{5P}\frac{IP}{K_{5P} + IP} - V_{3K}\frac{IP}{K_{3K} + IP}\frac{C_{cyto}}{K_{A3K} + C_{cyto}} + D_{IP_3}\frac{\partial IP^2}{\partial r^2} \qquad \text{(VI.5')}$$

K_{ASF} is the threshold constant characterizing the stimulation of the PLC activity of the SF by Ca^{2+}. The values of V_{PLC} and V_{SF} are taken as constant in the whole egg, based on the assumption that PIP_2 is homogeneously distributed (see section VI.4).

VI.2.4. Simulation method

Numerical simulations have been performed using a variable time-step Gear method. To simulate diffusion, the Laplacian is discretized using the finite difference method. The egg is divided into mesh points, using a cartesian grid with no flux boundary conditions. The circular shape of the egg is reproduced by applying the appropriate no-flux boundary conditions at all grid points located at a given distance from the center (corresponding to the egg radius). The egg radius equals 75 μm and the mesh size equals 1.5 μm.

VI.3. Injections of $InsP_3$ and $InsP_3$ analogs in ascidian eggs: simulations and experiments

VI.3.1. An artificial pacemaker site (PM3) is revealed by flash-photolysis of $InsP_3$ or $gPIP_2$

Experimentally, caged $InsP_3$ was photo-released either locally (i.e. the flash was restricted to a small region of the egg) or globally (Dumollard and Sardet, 2001). The amount of $InsP_3$ released is set by the duration of the UV flash and always remains rather small (less than 0.1 μM). Flash-photolysis of increasing amounts of $InsP_3$ initiated a Ca^{2+} wave that spreads further from the site of the UV-flash. This observation is reproduced by the model (Fig. VI.3). The Ca^{2+} wave remains limited to a portion of the egg for $InsP_3$ flashes of short duration because, in these cases, passive diffusion of $InsP_3$ remains localized. Only when the amount of released $InsP_3$ is large enough (Fig. VI.3, third row) does the level of $InsP_3$ reach the threshold required to trigger a Ca^{2+} wave which traverses the whole egg. $InsP_3$ can thus induce spatially restricted Ca^{2+} signals and $InsP_3$ does not act as a global messenger in a large cell such as the ascidian egg. For the parameter values used in the simulations, the characteristic time for $InsP_3$ diffusion (80s) is larger than that of $InsP_3$ degradation (about 12s).

Also in agreement with a relatively fast degradation of $InsP_3$, activation of the eggs by a single injection of $InsP_3$ cannot induce repetitive Ca^{2+} waves, neither in the model, nor in the experiments. As modelled above (Fig. VI.3) and observed in the experiments (Dumollard and Sardet, 2001), when the $InsP_3$ flashes are localized, the Ca^{2+} wave originates from the site of $InsP_3$ release. More surprisingly, when $InsP_3$ or its poorly metabolizable analog $gPIP_2$ is homogeneously increased in the whole egg, the Ca^{2+} wave is always seen to originate from the cortex, in a broad area near the animal pole of the eggs (Dumollard and Sardet, 2001). As proposed in the experimental study, the existence of this pacemaker revealed by an artificial type of stimulation (called PM3) can be ascribed to a denser distribution of ER near the cortex of the animal pole. We have tested this hypothesis in the model. In Fig. VI.4, $gPIP_2$ is assumed to be homogeneously released in the whole egg. However, the Ca^{2+} wave clearly initiates in the region with the highest density of ER (see Fig. VI.2 for the distribution of the ER). The shape of

this region of higher density (see section VI.2.2) has been fitted in the simulations to get the best agreement with the experimentally observed forms of the Ca^{2+} wave. The best results are thus obtained when the gradient in a (ER density) is only vertical (along the animal-vegetal axis). Equally important

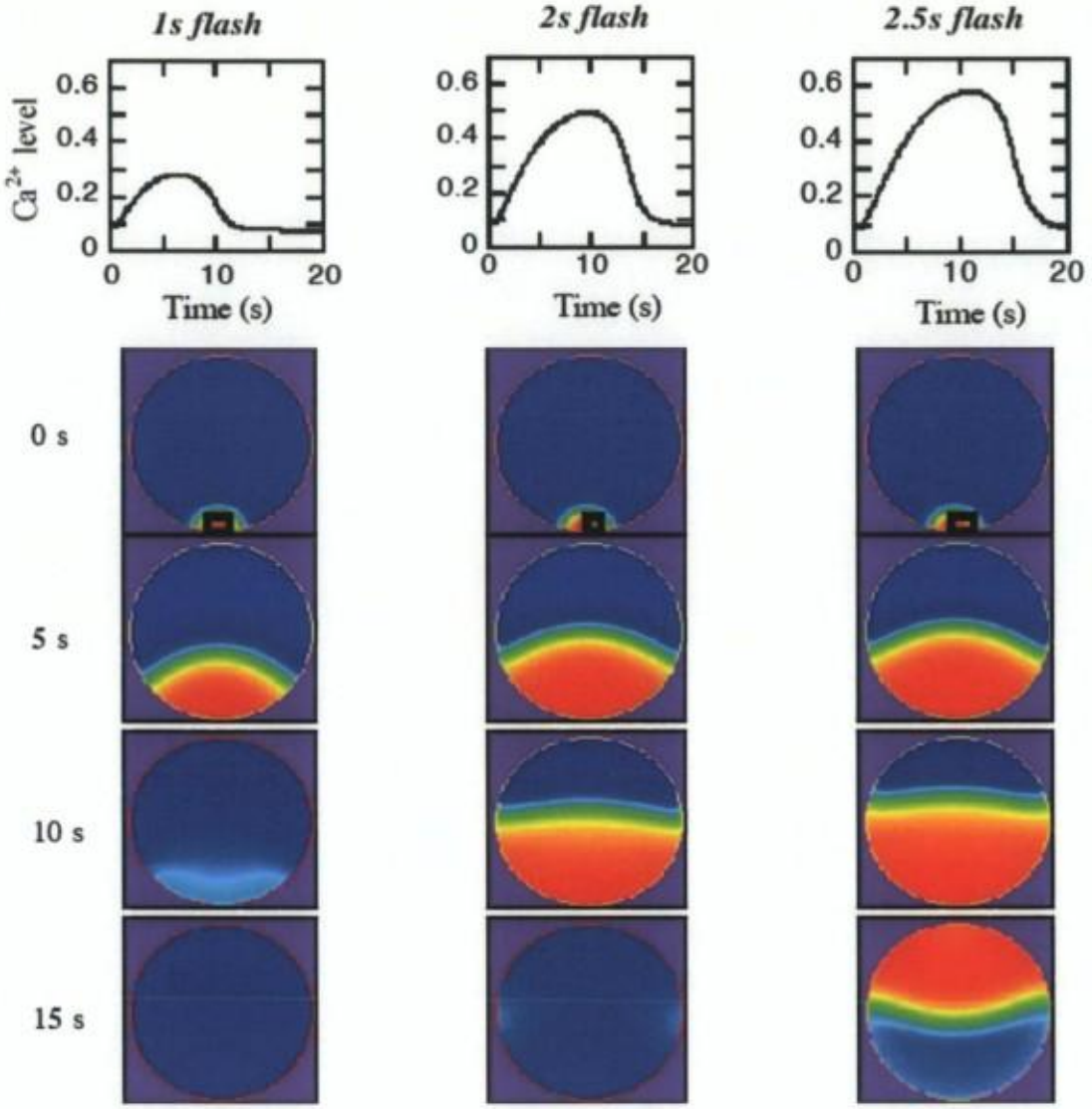

Fig. VI.3. Simulations of the effect of localized $InsP_3$ injections. Results have been obtained by integration of eqs. (VI.1) to (VI.5) with the ER density represented in Fig. (VI.2) and the following parameter values: $D_{cyto} = 40\ \mu m^2 s^{-1}$, $D_{ER} = 4\ \mu m^2 s^{-1}$, $D_{IP3} = 280\ \mu m^2 s^{-1}$, $K_{act} = 0.54\ \mu M$, $K_{inh}\ (= (k_-/k_+)^{1/ni}) = 0.28\ \mu M$, $k_- = 4\ 10^{-3}\ s^{-1}$, $k_1 = 1.285\ s^{-1}$, $b = 2.5\ 10^{-4}$, $K = 1\ \mu M$, $v_{MP} = 1.2\ \mu M s^{-1}$, $K_P = 0.35\ \mu M$, $V_{PLC} = 0.015\ \mu M s^{-1}$, $V_{5P} = 0.67\ \mu M s^{-1}$, $K_{5P} = 8\ \mu M$, $V_{3K} = 3.35\ 10^{-2}\ \mu M s^{-1}$, $K_{3K} = 0.5\ \mu M$, $K_{A3K} = 0.3\ \mu M$, $n_a = 2$, $n_i = 3$. Most of these values come from previous modelling studies, where they were either taken from the litterature or fitted to get agreement with the observations (Dupont and Erneux, 1997; Dupont *et al.*, 2000a). In the 3 simulations, during the flash time $I_{IP3} = 7\ \mu M s^{-1}$ in the mesh points (46 to 54) along the X axis, and (89 to 97) along the Y axis (this region is indicated as a black square in the first panel). The resulting $InsP_3$ increase averaged on the whole egg ranges between 0.05 and 2.5 μM depending on the flash duration. Initial conditions are $C_{cyto} = 0.1\ \mu M$, $C_{lum} = 875\ \mu M$ and the corresponding steady-states values of the other variables . To perform the simulations, mesh points are labelled from 1 to 100 from left to right, and from top to bottom. To account for the circular shape of the egg (in 2 dimensions), the appropriate mesh points are excluded from the system. In this and all subsequent figures, the level of cytosolic Ca^{2+} is represented by the amount of Ca^{2+} bound to an indicator whose $K_{1/2}$ for Ca^{2+} is 0.7 μM. When representing the Ca^{2+} waves, the scale is different for each image, with red and blue representing respectively the highest and the lowest instantaneous levels of cytosolic Ca^{2+}.

for the appropriate shape of the Ca^{2+} wave is the slightly more elevated quantity of ER in the cortex. Because of this inhomogeneity, the wave propagates faster in the periphery, allowing for the transformation of a convex front at the onset of the propagation into a slightly concave one as the wave spreads through the egg (Fig. VI.4), as seen in the experiments.

From a theoretical point of view, α (ER density) is a bifurcation parameter. In other words, increasing the value of α qualitatively changes the behaviour of the system, from resting, to excitable and finally to oscillatory. Thus, at a given fixed level of stimulation ($InsP_3$ or $gPIP_2$), the cytoplasm is excitable for eliciting a Ca^{2+} wave only when α is above a critical level. The values of α and of the stimulation intensity used in Fig. VI.4 are such that PM3 is the only part of the egg initially able to generate a Ca^{2+} spike. In the rest of the cytoplasm and in the cortex, the synergy between this low level of stimulus and the Ca^{2+} increase coming through diffusion from an adjacent region of the cell is required to generate a Ca^{2+} spike.

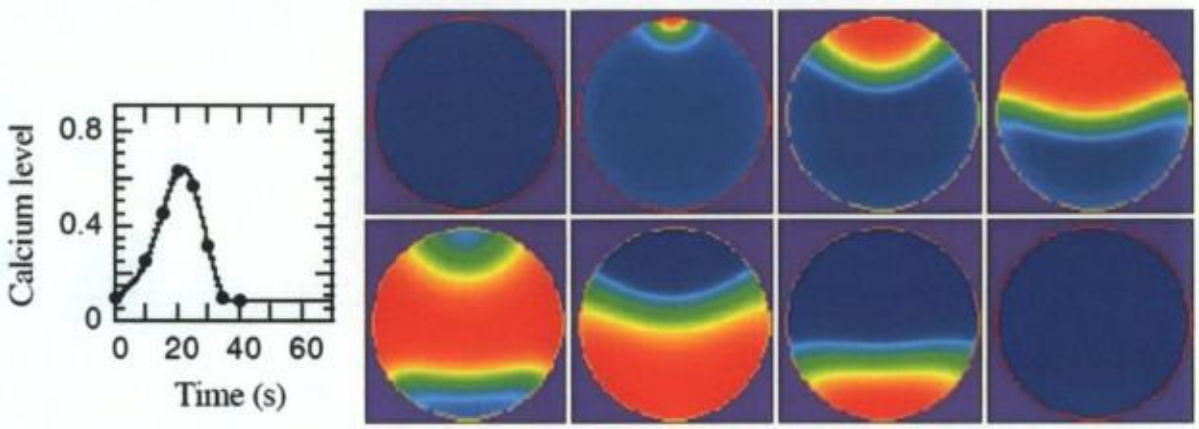

Fig. VI.4. Simulation of the effect of a global increase in [$gPIP_2$]. Results have been obtained by integration of eqs. (VI.1) to (VI.5) with the ER density represented in Fig. (VI.2) and the same parameter values as in Fig. VI.3, except for the fact that $gPIP_2$ has been used instead of $InsP_3$. Thus the rates of degradation (V_{5P} and V_{3K}) have been divided by 10. To simulate the activation of the $InsP_3R$ by both $gPIP_2$ and the basal $InsP_3$ level, we consider that $InsP_3$ and $gPIP_2$ bind to the same site of the receptor, and that $gPIP_2$ has less affinity for the receptor ($K_gPIP_2 = 8\ \mu M$). A basal level of $InsP_3$ equal to 18 nM (corresponding to the stationary state in $InsP_3$ with the basal PLC activity) is always present. During the flash time (2s), $I_{gPIP2} = 0.045\ \mu Ms^{-1}$ in the whole system. The successive panels show the spatial distribution of Ca^{2+} at the times indicated by the points on the curve on the left.

The level of stimulation (simulated here in the form of the amplitude of the $gPIP_2$ influx) can also be viewed as a bifurcation parameter. The model accounts for the experimental observation (Dumollard and Sardet, 2001) that the global amplitude and the propagation velocity of the Ca^{2+} wave both increase with the amount of $gPIP_2$ released into the egg (Fig. VI.5). These increases in Ca^{2+} wave amplitude are associated with a widening of the Ca^{2+} front but the local maximal amplitudes do not change when varying the level of stimulation (not shown). The wave-like behaviour exemplified in Fig. VI.4 is restricted to a limited range of stimulation levels. Both in the model and in the experiments, if the magnitude of the global $gPIP_2$ increase is too low (below $0.03\mu Ms^{-1}$), it only generates a spatially-limited Ca^{2+} increase confined to the animal pole region. In contrast, for the largest influx terms (above $0.05\ \mu Ms^{-1}$), the Ca^{2+} increase occurs simultaneously in the entire egg. For all situations represented in Fig. VI.5, the local variations of ER Ca^{2+} associated with the wave of cytosolic Ca^{2+} are very small given the high level of Ca^{2+} in this compartment. We have taken an initial value of 875 μM for the Ca^{2+} concentration in the ER (Montero *et al.*, 1995; Hofer and Schulz, 1996).

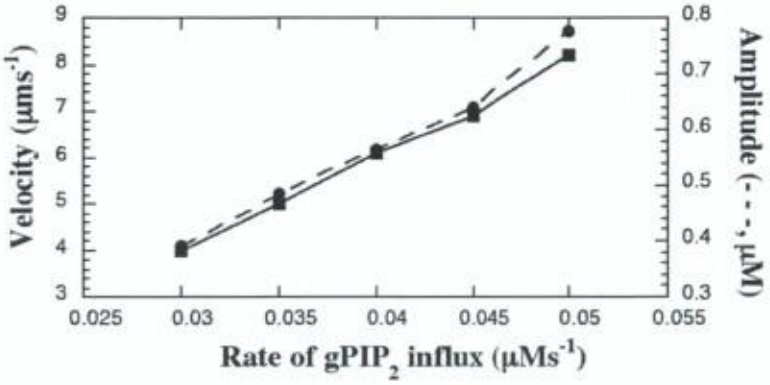

Fig. VI.5. Relationship between the mean velocity and global amplitude of the artificially induced Ca^{2+} waves and the intensity of the stimulus. Points have been obtained as in Fig. VI.4 with the same parameter values, except for the rate of $gPIP_2$ influx. For influx rates lower than 0.03 μMs^{-1}, the Ca^{2+} waves do not propagate throughout the whole egg (abortive waves). On the other hand, for influx rates higher than 0.05 μMs^{-1}, the Ca^{2+} increases occur nearly homogeneously over the whole egg.

In contrast to $InsP_3$, $gPIP_2$ is very slowly metabolized and its level remains elevated for a long time. As a consequence, several Ca^{2+} spikes can be generated by a single flash. The model can reproduce this behaviour if the rate of degradation of $gPIP_2$ is assumed to be 10 times smaller than that of $InsP_3$ degradation as it was found experimentally (Bird *et al.*, 1992). Fig. VI.6A indeed shows that in response to a localized $gPIP_2$ increase of high amplitude, two Ca^{2+} waves are generated; the first one originates from the region of stimulation (here chosen to be in the vegetal pole), while the second one starts in the region of higher ER density in the animal pole region (PM3). A close look at the evolution of the variables of the model indicates that at that time (125 s), $gPIP_2$ is homogeneously distributed in the egg; the second wave thus originates from the region which is the most sensitive to a homogeneous level of $gPIP_2$. This prediction is corroborated by the experimental results shown in Fig. VI.6B.

VI.3.2. Injections of large amounts of $gPIP_2$ mimic the temporal pattern of Ca^{2+} seen at fertilization.

Large amounts of $gPIP_2$ globally released in the egg induce a complex series of Ca^{2+} increases that strikingly resemble the first phase of Ca^{2+} waves observed at fertilization of ascidian eggs (Dumollard and Sardet, 2001). Fig. VI.7 shows the simulation of the injection of a large amount of $gPIP_2$ (red trace). At time 0, the concentration of the latter compound is increased up to a high value; it then decreases to zero according to equ. (VI.5), in which the maximal velocities have been adapted for $gPIP_2$ (instead of $InsP_3$; see legend to Fig. VI.4). The high level of $gPIP_2$ causes a long-lasting Ca^{2+} increase, followed by 2 shorter spikes (black trace). Also visible are the changes of Ca^{2+} concentration within the ER (blue trace); note that Ca^{2+} depletion of the ER (up to ~ 40%) is significant only for the first Ca^{2+} increase. As far as the spatial aspects are concerned, the first massive Ca^{2+} increase propagates so rapidly that it seems to occur quasi-instantaneously in the whole egg. The second (and other subsequent) peaks clearly originate from the cortical area of the animal hemisphere, which possesses the highest ER density. These theoretical results are in full agreement with the experimental results (Dumollard and Sardet, 2001).

VI.4. Simulation of the series I Ca^{2+} oscillations induced by fertilization

Given the observed agreement between our simulations and the experimental observations, we have used the model to make some theoretical predictions about the possible nature of the sperm factor (SF). We simulate fertilization as a localized rise in SF concentration from zero up to an arbitrary

value. If we assume that the SF is a Ca^{2+} sensitive PLC that can diffuse in the cytosol (eqs. (VI.5') and (VI.8)), the model reproduces the temporal pattern of cytosolic Ca^{2+} changes observed at fertilization of ascidian eggs (Fig. VI.8). Also visible are the predicted changes in the Ca^{2+} level in the ER, which mirror the variations in cytosolic Ca^{2+}. The level of PLC activity rises instantaneously (corresponding to the injection of SF) and then decays exponentially, due to the first-order degradation term. As to $InsP_3$, it massively rises with the step-wise increase in PLC; it then globally decays due to its catabolism by the $InsP_3$ 3-kinase and 5-phosphatase and to the decrease in PLC. However, because of the stimulation of PLC activity by Ca^{2+}, the concentration of $InsP_3$ oscillates in synchrony with Ca^{2+} oscillations (Meyer and Stryer, 1988).

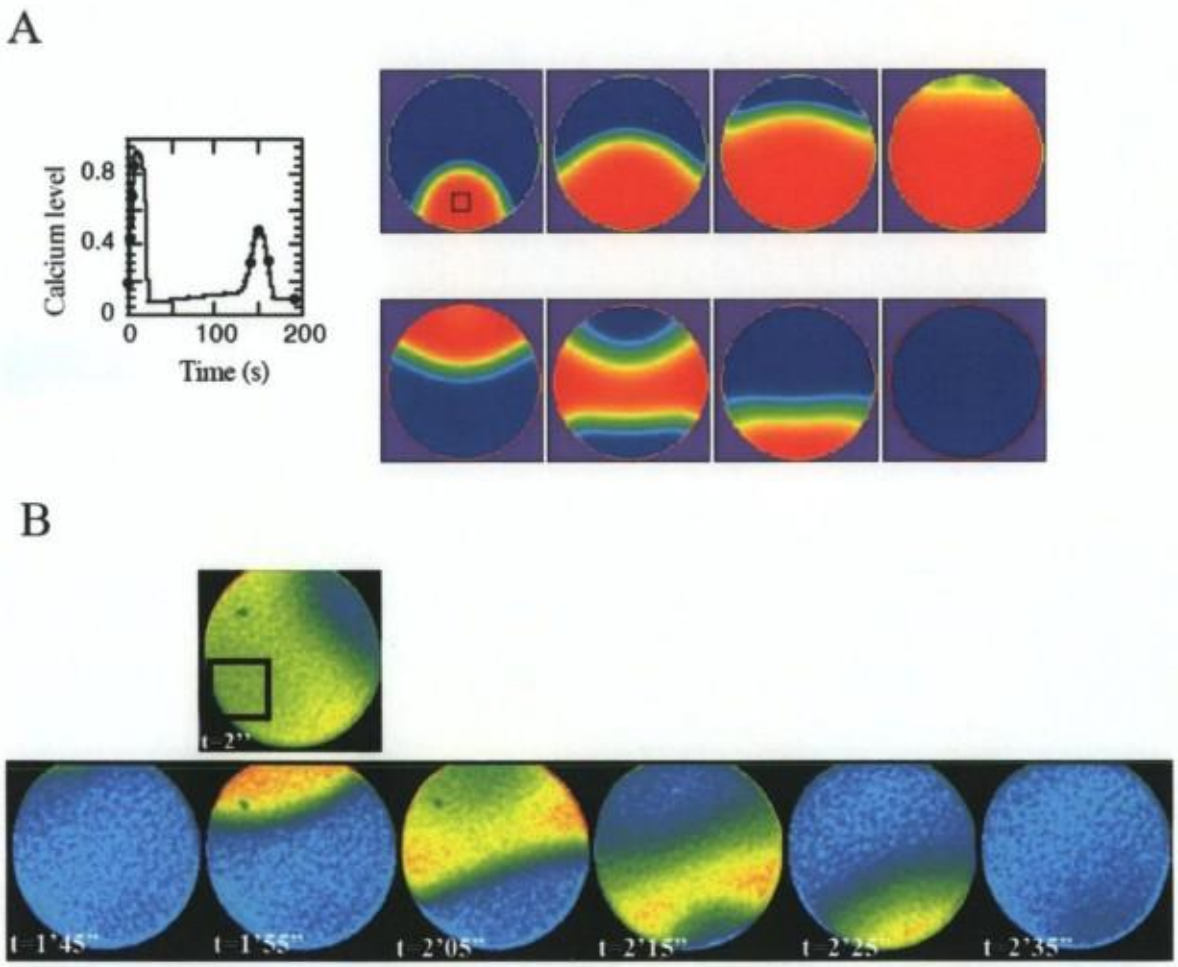

Fig. VI.6. A. Theoretical prediction of the effect of a $gPIP_2$ increase in the vegetal hemisphere of the ascidian egg. A high amplitude increase in $gPIP_2$ initiated in the vegetal hemisphere of the egg (indicated by a black square) evokes 2 successive Ca^{2+} waves, the first one emanating from the locus of stimulation and the second one emanating from the region of higher ER density in the animal pole region (PM3). Simulations have been performed as in Fig. VI.4 with a $gPIP_2$ increase $IgPIP_2 = 12$ μMs^{-1} for 4 s, at the mesh points (45 to 55) along the X axis and (80 to 90) along the Y axis, as indicated by the black box in the first panel. The successive panels show the spatial distribution of Ca^{2+} at the times indicated by the points on the curve on the left.

B. Effect of local photorelease of $gPIP_2$ in an unfertilized ascidian egg. First row : confocal image of $[Ca^{2+}]_c$ taken 2 sec after local UV uncaging, the area of UV uncaging is indicated by a black square. Second row: At t=1'45" a Ca^{2+} wave is initiated in the animal pole and traverses the whole egg.

The spatial properties of the Ca^{2+} oscillations shown in Fig. VI.8 have not yet been investigated in the model. Simulations of the moving pacemaker observed in series I Ca^{2+} oscillations (PM1) of the ascidian egg indeed require both additional hypotheses and new simulation techniques. It may be that the source of $InsP_3$ is moving along the cortex as a consequence of the cortical contraction-induced movement of the sperm aster towards the vegetal hemisphere (Dumollard and Sardet, 2001; Dumollard *et al.*, 2002; Carroll *et al.*, 2003).

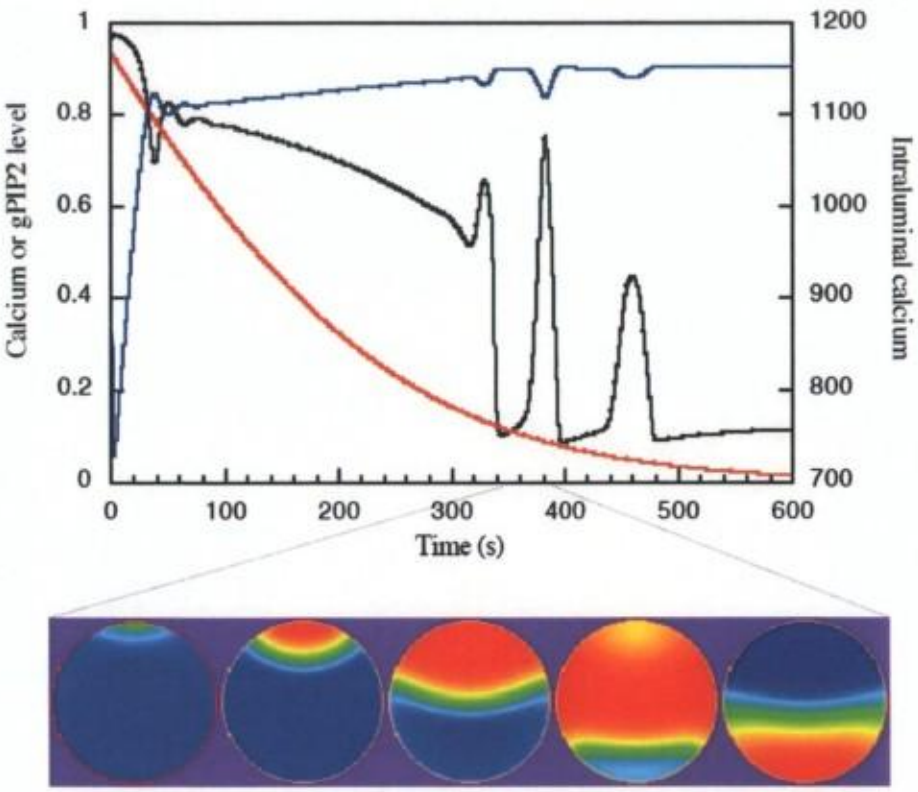

Fig. VI.7. Simulation of the effect of a massive, global increase of $gPIP_2$ in the ascidian egg. The temporal pattern of the Ca^{2+} spike much resembles that observed at fertilization. Simulation has been performed as in Fig. VI.4 with $IgPIP_2 = 25\ \mu Ms^{-1}$ in the whole system during the flash time (0.3 s). The black, red and blue trace represent the average level of cytosolic Ca^{2+}, $gPIP_2$ and luminal Ca^{2+} respectively.

We have assumed that the Ca^{2+}-sensitive PLC supposed to represent the SF has a relatively high diffusion coefficient ($150\ \mu m^2 s^{-1}$). If this is not the case, partial Ca^{2+} waves propagating only in the region of the egg opposite to the site of SF increase are observed, while the $[Ca^{2+}]_C$ remains constantly elevated in the region closer to the injection site (not shown). This is due to the fact that far away from the site of SF increase, the level of $InsP_3$ is still in the oscillatory regime, because the level of PLC in this region is relatively low as significant diffusion has not yet occurred.

Finally, we have investigated in the model the effect of changing the amount of SF injected into the egg. As shown in Fig. VI.9, our preliminary model predicts that the amount of SF influences the shape of the first large fertilization spike. As expected intuitively, the duration of the fertilization spike increases with the dose of SF introduced into the egg. Interestingly, the shape of the spike also depends on the dose of SF. The number of small-amplitude spikes superimposed on the plateau increase of Ca^{2+} rises if the dose of SF decreases. For lower doses of SF (Fig.VI. 9A), the level of $InsP_3$ is close to that able to induce oscillations. In contrast, if [SF] is large (Fig. VI.9B), the $InsP_3$ concentration is so high that Ca^{2+} remains at a high steady-state level set by the actual $InsP_3$ concentration.

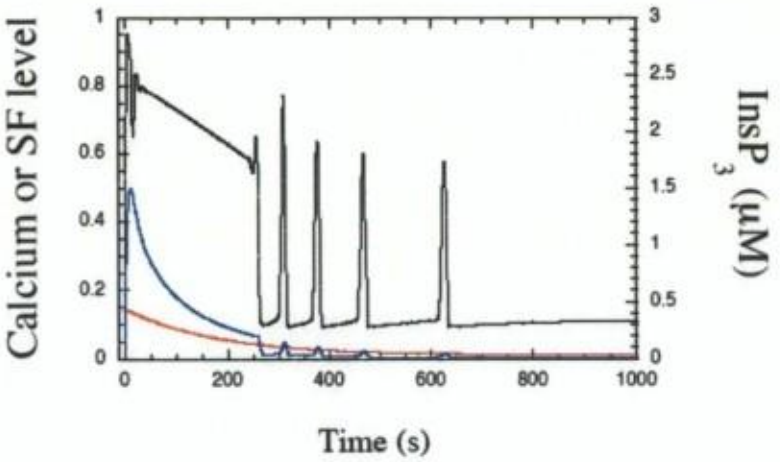

Fig. 8. Simulation of the series I Ca^{2+} oscillations induced by fertilization. Shown are the evolutions of the average concentrations in Ca^{2+} (black), $InsP_3$ (blue) and SF (red). Results have been obtained by numerical simulations of eqs. (VI.1)-(VI.4), (VI.5') and (VI.7) with the same parameter values as in Fig. VI.3. Moreover $K_{ASF} = 0.15$ µM, $k_{SF} = 5.56\ 10^{-3}\ s^{-1}$ and $D_{SF} = 150\ \mu m^2 s^{-1}$. Initial conditions are the same as in Fig. VI.3, except that [SF] = 50 µM in the mesh points (16 to 20) along the X and Y axes.

VI.5. Discussion

To our knowledge, we have presented here the first theoretical study devoted to the specific characteristics of the oscillatory Ca^{2+} signal occurring at fertilization. Our approach relies on the experimental observations performed by Dumollard and Sardet (2001). The modelisation of the experiments of flash photolysis of caged $InsP_3$ and its analog first allowed us to focus on the events downstream from $InsP_3$ generation; we were able to 'fit' our equations and parameter values to adequately describe the Ca^{2+} dynamics observed experimentally. Moreover, to account for the observed spatial characteristics of these artificial waves, we were led to make some reasonable assumptions about the ER distribution in the cortex and cytoplasm. About this first part of the study, we would like to insist on the following results:

(1) If the ER density is modelled by taking into account the respective volumes accessible to both compartments (the ER and the cytosol), it represents a bifurcation parameter that can determine the excitability of a given part of the cell, unlike in other existing models (Wagner *et al.*, 1998; Fink *et al.*, 2000, Bugrim *et al.*, 2003; Hunding *et al.*, 2003). Under these conditions, the regions with higher ER density naturally play the role of pacemaker sites. This assumption also allowed us to make an experimental prediction about the initiation site of the successive waves induced by the local release of high doses of $gPIP_2$ (Fig.VI. 6A); this prediction is corroborated by the experiments (Fig. VI.6B).

(2) We propose for the first time that the spatial distribution of the pacemaker site is in fact a key factor in determining the shape of the wave front. In particular, to reproduce the rather flat shape of the Ca^{2+} wave front observed in ascidian eggs, it is most appropriate to assume that the ER density varies only along the animal-vegetal axis. In the model, we have also assumed a higher ER density just below the plasma membrane to support the higher speed of propagation of the Ca^{2+} waves in the ascidian egg cortex. Such assumption was also found to be necessary to reproduce the correct shape of the fertilization Ca^{2+} wave in frog eggs (Bugrim *et al.*, 2003).

(3) Simulations highlight the fact that $InsP_3$ is not a global messenger in a cell as large as an ascidian egg and that it can have a local action. In fact, this was already manifest from the experimental results showing that abortive Ca^{2+} waves are generally induced by localized flash photolysis of

$InsP_3$ (Dumollard and Sardet, 2001). In immature *Xenopus* oocytes, such abortive Ca^{2+} waves in response to localized $InsP_3$ flashes have also been recorded (Marchant *et al.*, 1999).

(4) Significant variations in the Ca^{2+} content of the ER are predicted in the model only in the case of high amplitude and long-lasting cytosolic Ca^{2+} increases such as those induced by a massive and global $gPIP_2$ increase. Moreover, the initial level of Ca^{2+} in the ER much influences the shape and duration of these long lasting cytosolic Ca^{2+} increases, as it directly modulates the $InsP_3$-sensitive Ca^{2+} rise in the cytosol.

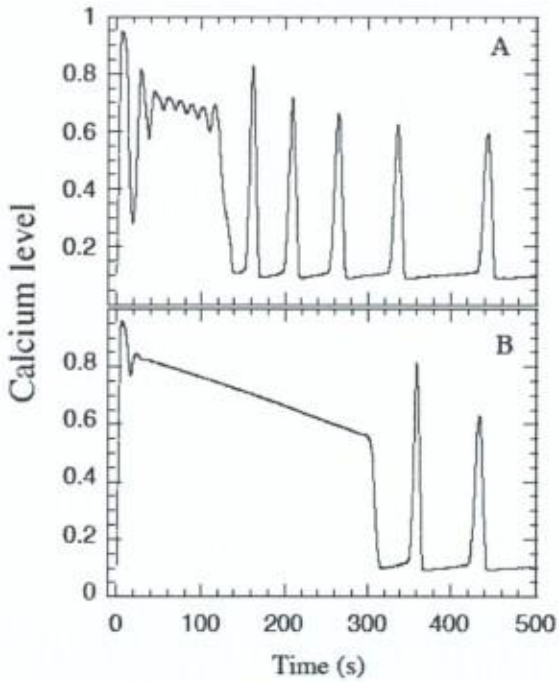

Fig. VI.9. Effect of varying the dose of SF injected into the egg. Simulations are the same as in Fig. VI.8, except for the initial localized rise in [SF], which equals 35 μM for panel A and 60 μM for panel B.

In a second part of our study, we have used our model to investigate in a theoretical manner what could be the events upstream from $InsP_3$ formation at fertilization. On the basis of the available data, we have made the assumption that the SF is a soluble factor like PLC (Swann *et al.*, 2001). While the best candidate for the sperm factor in mammals is a new form of PLC (PLCζ, Saunders *et al.*, 2002; Cox *et al.*, 2002), the activity of the sperm factor of ascidians can be blocked by the injection of SH2 domains of PLCγ supposed to inhibit any PLCγ activity (Runft and Jaffe, 2000; Runft *et al.*, 2002). It thus seems that the sperm factor of ascidians is a PLC or an activator of it.

Besides the experimental evidences in favour of the fact that the SF would be a PLC-like factor or its activator, we have ruled out the possibility that the SF in ascidians could be a molecule similar to $InsP_3$. We have indeed seen above (section VI.3.1) that $InsP_3$ appears to be a local messenger which cannot, through a single increase, induce repetitive Ca^{2+} rises. In contrast, a theoretical study of the fertilization Ca^{2+} wave in *Xenopus* oocyte (Bugrim *et al.*, 2003) concludes that an elevated concentration of $InsP_3$ near the site of fertilization appears as the most probable mechanism to reproduce the experimental observations. The contradiction between the latter theoretical results and ours can be explained by the fact that the study for *Xenopus* oocytes simulates the unique fertilization wave as a switch between a stable state with low cytosolic Ca^{2+} and another stable state with a high cytosolic Ca^{2+}. The passage from one state to the other can, in this case, be induced by a sufficient perturbation, i.e. the initial localized rise in $InsP_3$. This hypothesis cannot hold for fertilization in ascidians or in mammals, where wave propagation must obviously be associated with an oscillatory (and not a bistable) dynamics.

The main conclusions which can be drawn from the above can be summarized as follows:

(1) If the SF is a PLC, it must be Ca^{2+} sensitive. Otherwise, only spatially-restricted Ca^{2+} waves would propagate when the level of SF becomes too low. The assumption of a Ca^{2+}-sensitive PLC appears crucial in the model to avoid the progressive decrease of the amplitude of the secondary Ca^{2+} spikes. In the case of a Ca^{2+}-insensitive PLC (not shown), the extent of the Ca^{2+} wave propagation decreases together with the level of $InsP_3$, which itself follows that of PLC activity. Thus, the amplitude of the Ca^{2+} spikes decreases with the level of PLC. This effect is also observed for $gPIP_2$ injections (Fig. VI.7) and is the same as that observed and simulated with different doses of $InsP_3$ (Fig. VI.3). In contrast, when PLC is stimulated by Ca^{2+}, a Ca^{2+} wave always invades the entire egg as the Ca^{2+} front itself generates the $InsP_3$ required to propagate further. A recent study, published after we finished our simulations, reports that PLCζ is indeed Ca^{2+}-sensitive (Kouchi *et al.*, 2004). Surprisingly, the characteristics of this Ca^{2+} activation quantitatively match our predictions; Kouchi *et al.* (2004) indeed report that the activation constant of PLCζ by Ca^{2+} lies around 10^{-7} M (K_{ASF} = 0.15 μM in our model) and that this activation occurs cooperatively with a Hill coefficient of 1.7 (a value of 2 was put in equ. (VI.5')). On the other hand, our results would also agree with the other hypothesis that the SF in the ascidian could act via a PLCγ (Runft and Jaffe, 2000; Runft *et al.*, 2002), another Ca^{2+}-sensitive isoform of the PLC.

(2) The diffusibility of the SF must be rather high. In the model, we have assumed a diffusion coefficient of 150 $\mu m^2 s^{-1}$, which is higher that the value that would be predicted on the basis of the molecular mass of the PLCζ (about 70 kDa (Cox *et al.*, 2002), which would correspond to a diffusion coeffecient of about 50 $\mu m^2 s^{-1}$). However, our results have been obtained on the basis of an egg diameter of 150 μm (corresponding to an ascidian egg), which is larger than that of a mouse egg (about 70 μm), where the PLCζ has been identified. In the ascidian egg, the molecular weight of the still-unknown sperm factor was estimated to lie in a range from 30 to 100 kDa (Kyozuka *et al.*, 1998). This discordance might suggest that in ascidian eggs, the sperm factor could be an activator of a Ca^{2+}-sensitive PLC, with a lower molecular weight than PLC itself.

(3) Further hypotheses have to be put forward to account for the observed relocalization of PM1. We have not yet simulated the possible movement of a source of SF. Simpler hypotheses such as the existence of a region more sensitive to $InsP_3$ in the vegetal pole, or a preferential localization of the SF in this same region have been tested in our model but did not lead to a good agreement with experimental results. We think however that the modelling of the movement of PM1 (and thereby the appearance of PM2) would be premature. Indeed, although the temporal Ca^{2+} patterns seen at fertilization or in response to massive $gPIP_2$ release are very similar, the spatial characteristics of both Ca^{2+} responses are different: in the case of $gPIP_2$ release, the second and successive Ca^{2+} waves emanate from PM3 in the animal pole, whereas in the case of fertilization, the initiation sites of the successive Ca^{2+} waves progressively relocate towards the vegetal pole. There is thus obviously a fertilization-related event –probably not mediated by Ca^{2+}– that dictates the spatial characteristics of the late fertilization Ca^{2+} spikes triggered by PM1 and that needs to be better understood.

(4) The simulations shown here above all assume that the source of $InsP_3$, i.e. PIP_2, is present in the entire egg. This assumption was found to be necessary to allow a correct propagation of the Ca^{2+} wave in the entire egg. If PIP_2 is assumed to be located only in the plasma membrane, the Ca^{2+} wave does not reach the center of the egg and does not show the correct wave front. Again, this can be explained by the fact that $InsP_3$ is not a global messenger in a cell as large as an egg. From a physiological point of view, a plausible hypothesis would be that PIP_2 is in fact associated with intracellular organelles (Rice *et al.*, 2000).

(5) Based on the results of our simulations, we propose that the temporal shape of the first large Ca^{2+} wave depends on the quantity of SF introduced into the egg. Thus, both the duration and the appearance of smaller amplitude Ca^{2+} spikes on the plateau phase can be modulated by the

amount of SF supposed to be introduced into the egg (Fig. VI.9). Although such smaller-amplitude spikes on the plateau are not observed at the fertilization of *Phallusia mammillata* (Dumollard and Sardet, 2001; Dumollard *et al.*, 2002), they are clearly visible in other species such as *Ascidiella aspersa* (McDougall *et al.*, 2000) or even in mammals (Swann *et al.*, 2001). However, even though these additional spikes have been observed during the fertilization Ca^{2+} wave after natural fertilization, sperm extract or sperm factor RNA injections in *Ascidiella* or mouse eggs, no correlation between the amount of sperm extract or sperm factor injection and the appearance of these spikes has yet been established.

In conclusion, our study demonstrates that when $InsP_3$ is produced throughout the whole ascidian egg, spatial inhomogeneities in the ER distribution are responsible for the appearance of the artificial Ca^{2+} wave pacemaker PM3 in the animal pole of the egg and dictates the spatio-temporal characteristics of the Ca^{2+} waves triggered by this pacemaker. This model also predicts that the activity of the natural pacemaker PM1 induced by fertilization is regulated by a soluble Ca^{2+}-activated PLC which is injected into the egg. This PLC should hydrolyse PIP_2 in the whole egg and its activity would oscillate leading to oscillatory changes in $InsP_3$ mediating PM1 function. This latter prediction could only be tested by monitoring the spatio-temporal variations in $InsP_3$ levels in a single egg undergoing fertilization. In the future, the model could be extended to investigate the origins of the detailed characteristics of the Ca^{2+} waves in the eggs of different species as, for example, the periods of the waves, the existence of pacemaker zones other than those obseved in ascidian eggs or the shapes of the Ca^{2+} spikes.

PART 4 : FREQUENCY CODING

CHAPTER VII

Theoretical insights into the physiological implications of Ca^{2+} oscillations

VII.1. Introduction

It is well known that Ca^{2+} is one of the most important intracellular messenger. A rise in the concentration of this ion mediates fundamental physiological processes such as fertilization, secretion, contraction, synaptic plasticity, gene expression, cell proliferation or apoptosis (Berridge *et al.*, 1998). To be able to transmit such diverse types of information, Ca^{2+} signals are highly versatile, both in time and space. As Ca^{2+} rises in response to external stimulation most often take the form of oscillations, much information can be encoded in the temporal characteristics of these spikes. It was also found experimentally that an oscillatory Ca^{2+} signal can optimize the response of the cell ; this has been shown for gene expression in B-lymphocytes (Dolmetsch *et al.*, 1998 ; Llopis *et al.*, 1998), fertilization in mammals (Ozil, 1998), tumor necrosis factor-induced degranulation in neutrophils (Richter *et al.*, 1990) and exocytotic secretion from rat chromaffin cells (Malgaroli and Meldolesi, 1991). In pancreatic acinar cells, intermediate levels of acetylcholine (Ach)-producing Ca^{2+} oscillations induce more secretion than higher concentrations of ACh inducing a high steady-state level of Ca^{2+} (Kasai and Augustine, 1990). In the liver, the mitochondrial metabolic Ca^{2+} output has also shown to be optimized by an oscillatory level of Ca^{2+}. Cytosolic Ca^{2+} increases are indeed rapidly transported into the mitochondrial matrix. This increase in mitochondrial Ca^{2+} in turn stimulates various mitochondrial dehydrogenases. As the uptake mode of the mitochondria is short-lived, a sustain Ca^{2+} increase in the cytosol only induces a transient increase in oxidative metabolism. In contrast, in the presence of cytoplasmic Ca^{2+} oscillations, the resulting mitochondrial Ca^{2+} oscillations are integrated and produce a sustained increase in NADH (Hajnoczky *et al.*, 1995 ; Robb-Gaspers *et al.*, 1998)

Besides the optimization of the physiological response by the oscillatory pattern of the Ca^{2+} rise, within the oscillatory domain, both the level of cellular response and the frequency of oscillations increase with the intensity of the external stimulation. Examples of such a *frequency encoding* phenomenon are numerous. In blowfly salivary gland (Rapp and Berridge, 1981) or in pituitary cells (Holl *et al.*, 1988), the secretion rate clearly increases with the frequency of the repetitive Ca^{2+} spikes. In the brain, several aspects of neuronal differentiation are encoded in the frequency of Ca^{2+} oscillations (Gu and Spitzer, 1995). Moreover, diverse neuronal processes such as synaptic plasticity and neurotransmitter release exhibit frequency-dependent modulation (Malenka and Nicoll, 1999). At the molecular level, it has been shown that the autonomous activity of the widespread Ca^{2+}/calmodulin-sensitive kinase II (CaMKII) is sensitive to the frequency of Ca^{2+} oscillations (De Koninck and Schulman, 1998).

The question however arises as how the cellular response can be sensitive to the frequency of Ca^{2+} oscillations. Diverse theoretical mechanisms have early been proposed. In particular, a model based on a reversible phosphorylation cycle in which the kinase is activated by Ca^{2+} can induce a highly nonlinear relationship between the frequency of Ca^{2+} oscillations and the level or phosphorylated substrate, assumed to correspond to the level of a hypothetical cellular activity (Dupont and Goldbeter, 1992b). The existence of efficient frequency coding depends on the kinetic properties of the kinase and phosphatase involved in the phosphorylation cycle ; in particular, low Michaelis-Menten constants corresponding to the saturation of the kinase and the phosphatase –conditions that give rise to the phenomenon of 'zero-order ultrasensitivity'(Goldbeter and Koshland, 1981)–favor the existence of a sharp threshold in the frequency-activity relationship. An alternative mechanism called 'solitary spike detector' leads to the conclusion that the cell is sensitive to the number of spikes, rather than to its frequency (Meyer and Stryer, 1991). It assumes the existence of kinases possessing multiple phosphorylation sites. As these sites differ by their sensitivity to Ca^{2+}, such kinases would be sensitive to the temporal pattern of Ca^{2+} changes.

In this chapter, we focus on three specific physiological systems in which the frequency coding phenomenon can be studied at the molecular level. In the first section, we theoretically investigate the effect of Ca^{2+} oscillations on the phosphorylation-dephosphorylation cycle controlling the activation

of glycogen phosphorylase in hepatocytes (section VII.2 ; Gall *et al.*, 2000). Although the molecular pathway leading to glycogen degradation is well-known to be activated by Ca^{2+}, the effect of an oscillatory Ca^{2+} signal is experimentally unknown, due to the lack of techniques allowing such an investigation. In the second section, we develop a simple model for the widespread CaMKII which however quantitatively accounts for the experimental results obtained by De Koninck and Schulman (1998) in *in vitro* experiments (section VII.3 ; Dupont *et al.*, 2003). One of the main advantage of this model is that it provides a 'toolkit' that can be incorporated in more elaborated models aimed at understanding the effect of Ca^{2+} oscillations in complex signallling cascades. Finally, we present in the last section a more predictive model that investigates the link between the Ca^{2+} oscillations seen at fertilization in mammals and the resumption of the cell cycle (section VII.4 ; Dupont, 1998).

VII.2. Activation of the liver glycogen phosphorylase by Ca^{2+} oscillations : a theoretical study

VII.2.1. Introduction

In this section (Gall *et al.*, 2000), we theoretically explore the possible role of Ca^{2+} oscillations in the regulation of a phosphorylation-dephosphorylation cycle involved in glycogen degradation by glycogen phosphorylase in hepatocytes (for review see Bollen *et al.*, 1998). This process plays a vital role in the regulation of glycaemia, providing glucose for the organism between feeding. Hormones control hepatic glycogen metabolism through transmembrane signalling pathways dependent on cAMP and/or Ca^{2+}. In particular, glycogenolysis can be promoted by hormones, like vasopressin, acting primarily through the phosphoinositide signalling pathway (Kraus-Friedmann and Feng, 1996) and leading to intracellular Ca^{2+} mobilization. The corresponding rise in the level of cytosolic Ca^{2+} affects the dynamics of phosphorylase kinase, activating glycogen phosphorylase which controls glycogen degradation (see Fig. VII.1). On the other hand, it has been shown that repetitive Ca^{2+} spikes occur in hepatocytes in the presence of vasopressin (Woods *et al.*, 1986). Therefore, the control of glycogen phosphorylase by Ca^{2+} provides a prototypic system to study the impact of Ca^{2+} oscillations on cellular regulation.

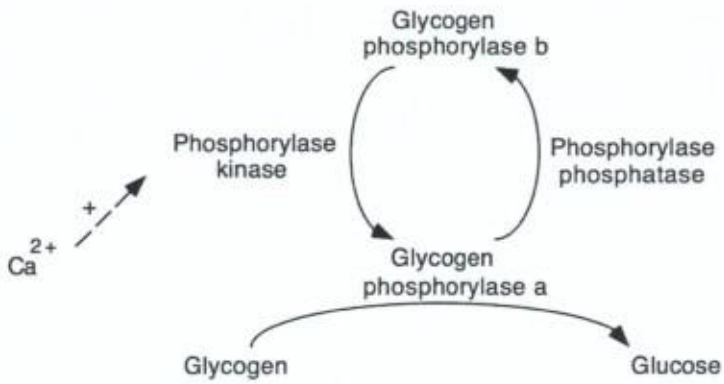

Fig. VII.1. Scheme of the phosphorylation-dephosphorylation cycle considered for the control of glycogen degradation. The system involves glycogen phosphorylase and its converter enzymes. The activation of phosphorylase kinase by Ca^{2+} is taken into account.

VII.2.2. Model for Ca^{2+} control of glycogen phosphorylase

The function of glycogen phosphorylase is to govern glycogen degradation. The enzyme acts as a sensor of blood glucose level, liberating glucose from stored glycogen as needed. The dynamics of the Ca^{2+}-associated phosphorylation-dephosphorylation cycle involving glycogen phosphorylase is illustrated in Fig. VII.1. Glycogen phosphorylase is converted from the inactive *b* form into the active

a-form by phosphorylase kinase, and inactivated by a phosphatase. Phosphorylase kinase is a hexadecamer composed of four different subunits ($\alpha_4\beta_4\gamma_4\delta_4$). The δ subunit is identical to calmodulin and mediates the Ca^{2+}-sensitivity of phosphorylase kinase (Cohen *et al.*,1978).

The minimal model we use for the phosphorylation-dephosphorylation cycle is based on the bicyclic cascade model proposed by Cardenas and Goldbeter (1996) for the control of glycogen phosphorylase and glycogen synthase by glucose. This model has proven to be consistent with experimental findings concerning the sequential changes in the activity of glycogen phosphorylase and glycogen synthase observed following the addition of suprathreshold amounts of glucose. From the original model, we have only retained the equation pertaining to the dynamics of the phosphorylation-dephosphorylation cycle controlling the activation of glycogen phosphorylase. We have extended the model to take into account the activation of glycogen phosphorylase by cytosolic Ca^{2+} (Z). The balance equation governing the time evolution of the fraction of active glycogen phosphorylase (*Pha*) is given by :

$$\frac{dPha}{dt} = V_1(Z)\frac{1-Pha}{K_1(Z)+1-Pha} - V_{M2}\frac{1+\alpha\dfrac{Glc}{K_{a1}+Glc}Pha}{\dfrac{K_2}{1+\dfrac{Glc}{K_{a2}}}+Pha} \qquad \text{(VII.1)}$$

where *Glc* represents the intracellular concentration of glucose. All maximum rates and Michaelis constants for the converter enzymes are normalized by division by the total concentration of glycogen phosphorylase. The glucose dependency in equ. (VII.1) arises from the fact that the binding of glucose to the active site of the enzyme makes it more susceptible to inactivation by dephosphorylation (Stalmans *et al.*, 1987). Thus, glucose is assumed to act on both the maximal velocity and the Michaelis constant of the phosphatase. The sensitivity of phosphorylase phosphatase to glucose allows the glycogen phosphorylase to act as a glucose sensor. We focus here on the activation of glycogen phosphorylase by Ca^{2+} (Z). We assume a constant cAMP level, so that the rates of phosphorylation of glycogen phosphorylase kinase by the cAMP-dependent kinases are taken as constant parameters. Moreover, we consider here a situation where the glucose level is constant and low (10 mM), promoting the activation of the glycogen phosphorylase. Concerning the Ca^{2+} dependency of the phosphorylase kinase, it has been shown experimentally (Doorneweerd *et al.*, 1982) that Ca^{2+} stimulates phosphorylase kinase activity by increasing its maximum rate and lowering its Michaelis constant for phosphorylase b. In this model, we assume that Ca^{2+} activates the phosphorylase kinase (of maximum rate V_{M1} and normalized Michaelis constant K_1) by decreasing the K_m of the enzyme, with an activation constant K_{a6}, and further activates the enzyme by enhancing its maximum rate by a multiplicative factor γ, with an activation constant K_{a5}. In addition, there is a Ca^{2+}-independent term in the expression for V_1 because some basal activity of the liver phosphorylase kinase is still observed in the absence of Ca^{2+}:

$$V_1 = V_{M1}\left(1+\gamma\frac{Z^4}{K_{a5}^4+Z^4}\right), \qquad K_1 = \frac{K_1^1}{1+\dfrac{Z^4}{K_{a6}^4}} \qquad \text{(VII.2.)}$$

As calmodulin is involved, we assume that the activation of phosphorylase kinase by Ca^{2+} is a cooperative process (Klee and Vanaman, 1982). The activation constants (K_{a5} and K_{a6}) were chosen to be 0.5 μM in agreement with the values observed in crude rat liver fractions (Khoo and Steinberg, 1975; Vandenheede *et al.*, 1977). In view of the regulatory role exerted by Ca^{2+} in physiological conditions, such values seem plausible, even if lower values have been reported for the purified

enzyme (Chrisman and Jordan, 1982).

VII.2.3. Effect of Ca^{2+} oscillations on glycogen phosphorylase activity

Our initial approach is to compare the activation of glycogen phosphorylase by Ca^{2+} oscillations relative to the activation obtained by a stimulation with a constant level of cytosolic Ca^{2+} (Z) of the same average value. To this end, we first have to determine the response of the model to a stimulation by a sustained Ca^{2+} level. This corresponds to the stable steady-state values for *Pha* as a function of Z. The solution can be obtained analytically and is defined by $dPha/dt = 0$ with $0 \leq Pha \leq 1$ [eqns (VII.1) and (VII.2)]. The result is shown in Fig. VII.2(a). It can be seen that the relation between the fraction of active phosphorylase and the cytosolic Ca^{2+} concentration has a steep sigmoidal nature. This result is a direct consequence of the saturation of the converter enzymes by their substrates, leading to a phenomenon known as 'zero-order ultrasensitivity' (Goldbeter and Koshland, 1981), and of the cooperativity in the kinase activation by Ca^{2+} (Dupont and Goldbeter, 1992b). Interestingly, in the case of muscle glycogen phosphorylase (Meinke *et al.*, 1986), 'zero-order ultrasensitivity' has indeed been demonstrated experimentally. To study the effects of Ca^{2+} oscillations on the dynamics of the phosphorylation-dephosphorylation loop, we investigate the effects of sinusoidal Ca^{2+} oscillations on the phosphorylase a levels. Thus, we describe the level of cytosolic Ca^{2+} as a function of time t as:

$$Z = A + B\sin(2\pi\nu t) \qquad \text{(VII.3)}$$

where ν stands for the frequency of the sinusoidal variation of Z and the parameters A and B are chosen to match the observed amplitudes of Ca^{2+} oscillations in hepatocytes ($A = 0.3$ μM, $B = 0.25$ μM).

Although sinusoidal-shaped oscillations do not resemble the oscillations observed experimentally, their temporal characteristics are easily controlled through the different parameters. This allows a clearer analysis of the impact of the pattern of Ca^{2+} oscillations on the dynamics of the phosphorylation-dephosphorylation cycle. It has been shown experimentally (Woods *et al.*, 1986) that the frequency of the oscillations increases with the level of stimulation while their amplitude remains approximately constant. To test whether the activation of glycogen phosphorylase could be sensitive to the frequency of Ca^{2+} oscillations, ν, we have compared the phosphorylase a levels averaged over one period of the sinusoidal oscillation, $\langle Pha \rangle$ for different values of ν with the steady-state value of *Pha* corresponding to the mean value $Z = A$. The $\langle Pha \rangle$ levels are obtained by numerical integration of eqn (VII.1) with Z given by eqn (VII.3). The time series obtained for increasing values of the Ca^{2+} oscillations frequency, ν and the corresponding $\langle Pha \rangle$ are shown in Fig. VII.2(a) and (b), respectively.

At low frequency [dotted curve in Fig. VII.2(a)], the phosphorylation-dephosphorylation dynamics is faster than the kinetics of Ca^{2+} oscillations, thus the kinase and the phosphatase can proceed so rapidly that the system stays close to its steady state. Even in this situation, the average phosphorylase a levels are higher than those obtained with a stimulation by an equivalent sustained Ca^{2+} level of 0.3 μM [compare solid and dotted curves in Fig. VII.2(b)]. This effect is a direct consequence of the steep sigmoidal nature of the relation between the fraction of active phosphorylase and the cytosolic Ca^{2+} concentration. Indeed, the latter relation allows the increase in Ca^{2+} concentration occurring during the half-period when Z is above its mean value ($A = 0.3$ μM) to switch the system from a situation in which most of the phosphorylase is unphosphorylated into a situation in which this enzyme is largely phosphorylated.

As the frequency of Ca^{2+} oscillations increases, the kinetics of the phosphorylation-dephosphorylation cycle starts to play a substantial role. The change in Ca^{2+} concentration becomes faster than the change in phosphorylation. The instantaneous fraction of phosphorylated protein is not able to reach its steady-state value. This is illustrated in Fig. VII. 3(b)-(d) where the time series have

been plotted in the (*Pha*, $[Ca^{2+}]_i$) plane for different values of v. Moreover, the kinetics of the converter enzymes allows on its own a further increase of the <*Pha*> levels. This increase is induced by the fact that the maximum rate of the phosphorylase activation by the kinase is higher than the maximum rate of inactivation by the phosphatase. Therefore, significant dephosphorylation of glycogen phosphorylase is only possible when the time interval between two successive Ca^{2+} spikes is large enough. At higher frequency, dephosphorylation between successive Ca^{2+} spikes is not complete and higher <*Pha*> levels can be maintained. This dependence of <*Pha*> levels on the frequency of Ca^{2+} oscillations could allow a dependence of the physiological response of the cell on the sole frequency of Ca^{2+} oscillations, a phenomenon that we refer to as 'pure frequency encoding'.

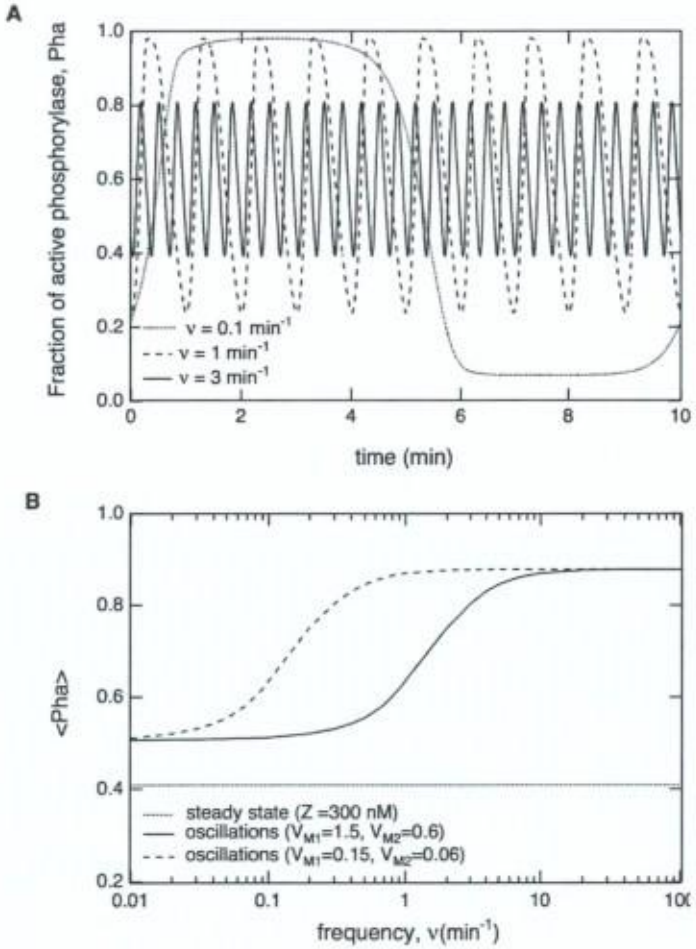

Fig. VII.2. Effect of a stimulation by a sustained elevation of cytosolic Ca^{2+} concentration and by sinusoidal Ca^{2+} oscillations on phosphorylase a levels, *Pha*. Panel (a) shows the phosphorlyase a levels time series for increasing values of the Ca^{2+} oscillations frequency, v, obtained by numerical integration of eqn. (VII.1) with Z given by eqn. (VII.3) with A = 300 nM and B = 250 nM. The values of the parameters are Glc = 10 mM, $K_1 = 0.1$, $K_2 = 0.2$, $K_{a1} = K_{a2} = 10$ mM, $K_{a5} = K_{a6} = 0.5$ µM, $\alpha = \gamma = 0.9$, $V_{M1} = 1.5$ min^{-1}, $V_{M2} = 0.6$ min^{-1}. Using the same parameters as in (a) : (...) v = 0.1 min^{-1}, (- - -) v = 1 min^{-1}, (–) v = 3 min^{-1}. (b) Shows the frequency sensitivity of the phosphorylation-dephosphorylation cycle, obtained by evaluating the phosphorylase a levels averaged over the period of oscillation, <*Pha*> as a function of (——). The Pha levels obtained with a stimulation by an equivalent sustained Ca^{2+} level (Z = 350 nM) are shown for comparison (...). The - - - shows the effect of a ten-fold decrease in the maximum rates V_{M1} and V_{M2} on the frequency response of the system : steady state (Z = 300 nM), . . . ; oscillations ($V_{M1} = 1.5$ min^{-1}, $V_{M2} = 0.6$ min^{-1}), —— ; oscillations ($V_{M1} = 0.15$ min^{-1}, $V_{M2} = 0.06$ min^{-1}), - - -.

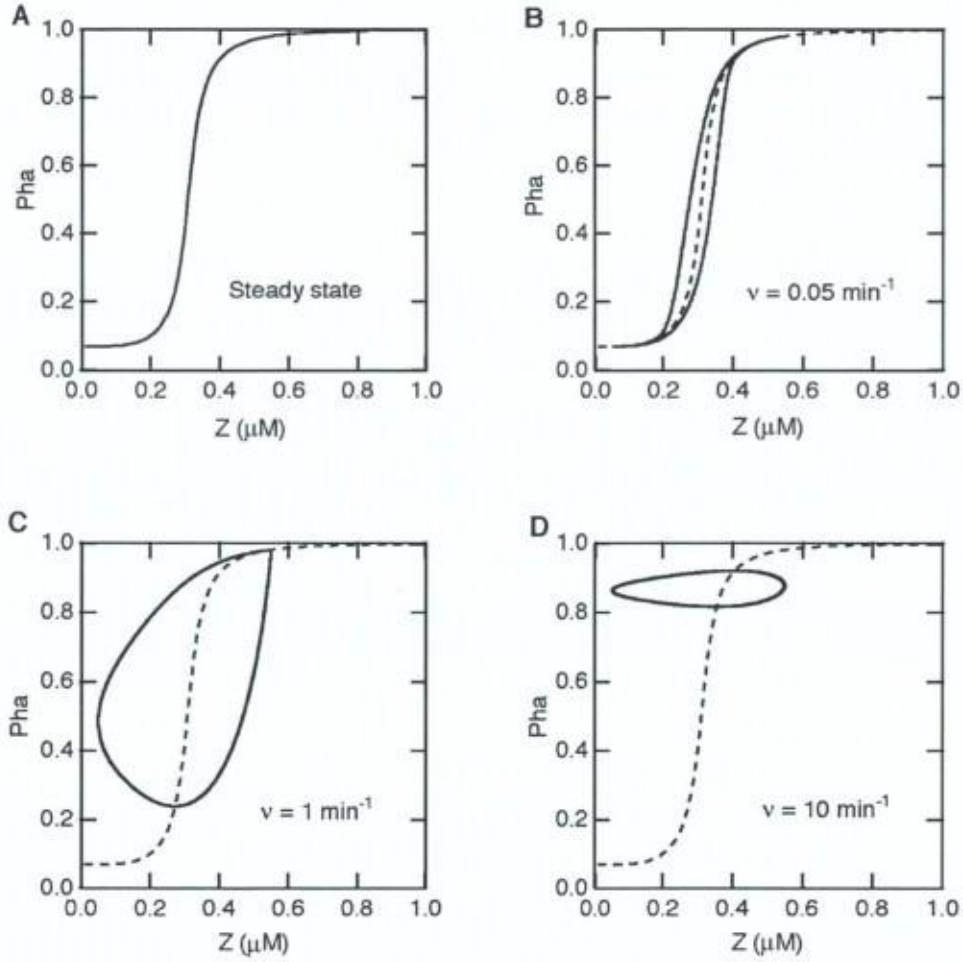

Fig. VII. 3. Dynamics of the phosphorylation-dephosphorylation cycle in response to stimulation by a sustained elevation of cytosolic Ca^{2+} concentration or by sinusoidal Ca^{2+} oscillations. The —— shown in (a) gives the stable steady-state values for *Pha* as a function of *Z*. The values of the parameters are *Glc* = 10 mM, $K_1 = 0.1$, $K_2 = 0.2$, $K_{a1} = K_{a2} = 10$ mM, $K_{a5} = K_{a6} = 0.5$ μM, $\alpha = \gamma = 0.9$, $V_{M1} = 1.5$ min^{-1}, $V_{M2} = 0.6$ min^{-1}. The closed curves in (b)-(d) are projections, for increasing values of the Ca^{2+} oscillations frequency ν, of the time series obtained by numerical integration of eqn VII.1 with *Z* given by eqn (VII.3) (same parameter values as in Fig. VII.2). For increasing ν the system moves away from its steady-state values (shown in - - - -) and the progressive accumulation of phosphorylase a can be observed.

We have also investigated the effect of the maximum rates of the phosphorylase kinase and phosphatase on the relation between <*Pha*> and the frequency of Ca^{2+} oscillations. We have thus varied the parameters V_{M1} and V_{M2} while keeping their ratio constant, so that the steady-state values for *Pha* as a function of *Z* are unchanged. The corresponding result is illustrated in Fig. VII.2(b) where the dashed curve shows the effect of a tenfold decrease of the maximum rates V_{M1} and V_{M2} on the frequency response of the system. As expected intuitively, at low frequencies of Ca^{2+} oscillations, the difference between the response of the system to a constant Ca^{2+} increase and the response to an oscillating Ca^{2+} is larger when the kinase and phosphatase are slower. Again, this slow enzymatic kinetics implies that *Pha* does not adjust to its steady-state value. Because the kinase is faster than the phosphatase, *Pha* remains phosphorylated most of the time and, in consequence, the <*Pha*> levels start to increase at lower frequencies in Fig. VII.2(b). This suggests that processes characterized by different intrinsic time-scales are sensitive to different ranges of frequencies of Ca^{2+} oscillations.

VII.2.4. Potentiation of hormonal stimulation of glycogenolysis by Ca^{2+} oscillations

As mentioned above, Ca^{2+} oscillations that occur in physiological conditions in hepatocytes are not sinusoidally shaped. Furthermore, it is interesting to study the impact of Ca^{2+} oscillations in the physiological context of hormone-induced glycogenolysis. Indeed, the level of hormonal stimulation affects both the frequency of Ca^{2+} oscillations and the mean level of Ca^{2+}. Here, we use a theoretical approach to investigate if realistic Ca^{2+} oscillations confer a signalling advantage in the hormonal stimulation of glycogenolysis. In hepatocytes, repetitive Ca^{2+} spikes can be obtained by the application of Ca^{2+}-mobilizing agonists, acting through the phosphoinositide signalling pathway (Woods *et al.*, 1986). Each transient rises within 3 s from basal Ca^{2+} (about 100 nM) levels to a peak of at least 600 nM and has a duration of approximately 7 s. The oscillation period varies, from 0.3 to 4 min, depending on the agonist concentration. In these conditions, a rise both in the frequency of Ca^{2+} oscillations and in the average Ca^{2+} concentration is observed. Several models have been proposed to explain the underlying mechanism of these simple periodic oscillations (for review, see Sneyd *et al.*, 1995; Dupont, 1999). In this study, we have chosen to use the minimal model originally proposed by Goldbeter *et al.* (1990) which assumes that the oscillations are caused by the interplay between two releasable pools of Ca^{2+}, one sensitive to the $Ins(1,4,5)P_3$ and the other activated by Ca^{2+} (see Table I.2). Even if this model does not represent accurately the exact physiological mechanism underlying Ca^{2+} oscillations in hepatocytes (Thomas *et al.*, 1996), it provides a realistic Ca^{2+} spike generator. In addition, we have checked that the results presented here below remain qualitatively unchanged when using another model for Ca^{2+} oscillations. This is intuitively obvious as there is no feedback of phosphorylase kinase activity on Ca^{2+} oscillations.

The model for control of phosphorylase activity by hormone induced Ca^{2+} oscillations is constituted by combining eqns (I.1)-(I.4) with eqn (VII.1). Figure VII.4 shows the time courses of cytosolic Ca^{2+}, Z, and of the fraction of active phosphorylase, Pha, at a given level of stimulation $\beta = 0.3$, obtained by numerical integration of the equations of the model. In the presence of incremental concentrations of Ca^{2+}-mobilizing agonist, the increase in $Ins(1,4,5)P_3$ leads to a rise in the stimulation parameter β and, subsequently, to a higher frequency of Ca^{2+} oscillations and an increased mean Ca^{2+} level $\langle Z \rangle$.

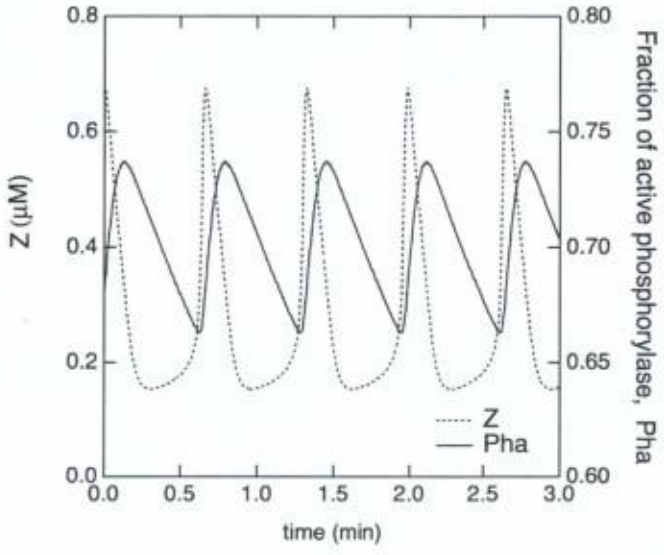

Fig. VII.4. Cytosolic Ca^{2+} concentration, Z (- - -) and phosphorylase a levels, Pha (——) time courses at a given level of stimulation corresponding to $\beta = 0.3$. The curves are obtained by numerical integration of eqns (I.1)-(I.4) and (VII.1). The values of the parameters are Glc = 10 mM, $K_I^I = 0.1$, $K_2 = 0.2$, $K_{aI} = K_{a2} = 10$ mM, $K_{a5} = K_{a6} = 0.5$ μM, $\alpha = \gamma = 0.9$, $V_{MI} = 1.5$ min^{-1}, $V_{M2} = 0.6$ min^{-1}, $n = m = 2$, $p = 4$, $v_0 = 1$ μMmin^{-1}, $v_1 = 5.7$ μMmin^{-1}, $V_{M2} = 30$ μMmin^{-1}, $V_{M3} = 325$ μMmin^{-1}, $K_2 = 0.5$ μM, $K_R = 1.7$ μM, $K_A = 0.46$ μM.

We have examined if this frequency encoding is more efficient than the encoding based on varying the amplitude of a steady level of cytosolic Ca^{2+}. For this purpose, we have numerically evaluated the phosphorylase a levels averaged over one period of the Ca^{2+} oscillation, $\langle Pha \rangle$, for increasing values of β. The result is illustrated in Fig. VII.5(a) where the response of the model to a stimulation by a sustained cytosolic Ca^{2+} concentration is also shown for comparison. It is clear that in the range of β values producing oscillations ($0.1 < \beta < 0.46$) the average fraction of phosphorylated phosphorylase is larger than in the corresponding steady state situation. Figure VII.5(b) which is based on the same results as Fig. VII.5(a), provides a comparison between the $\langle Pha \rangle$ induced by a constant (dashed line) and that by an oscillating level of Ca^{2+} (solid line) as a function of the average Ca^{2+}. It should be noted that as periodic Ca^{2+} spikes can only be obtained in a limited range of β values, $\langle Pha \rangle$ values are only computed in the corresponding $\langle Z \rangle$ range. Outside this domain, $\langle Pha \rangle$ corresponds to steady-state values of Pha. For all values of $\langle Z \rangle$ where periodic Ca^{2+} oscillations exist, the $\langle Pha \rangle$ levels are higher than those obtained with an equivalent stimulation by a steady cytosolic Ca^{2+} concentration. This clearly demonstrates that frequency coding based on Ca^{2+} oscillations potentiates the cell response to a hormonal stimulation.

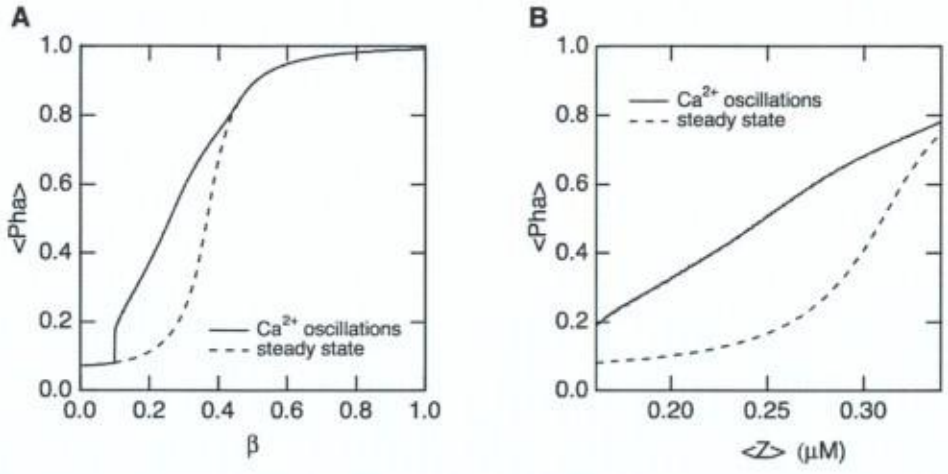

Fig. VII. 5. Potentiation of a hormonal stimulation by Ca^{2+} oscillations. In the presence of incremental concentrations of hormone, the increase in $Ins(1,4,5)P_3$ leads to a rise in the stimulation parameter β and, subsequently, to a higher frequency of Ca^{2+} oscillations and an increased mean Ca^{2+} level $\langle Z \rangle$. We compare this frequency encoding to the encoding based on varying the amplitude of a steady level of cytosolic Ca^{2+}. Panel (a) shows the phosphorylase a levels averaged over one period of the Ca^{2+} oscillations, $\langle Pha \rangle$, for increasing values of the stimulation parameter β (——) and the $\langle Pha \rangle$ levels obtained with a stimulation by an equivalent sustained cytosolic Ca^{2+} concentration (corresponding to the steady-state values of eqns (I.1)-(I.4), given by $(v0+v1\beta)/k$) (- - - -). Periodic Ca^{2+} spikes can only be obtained in a bounded range of β values. For all values of β where periodic Ca^{2+} oscillations occur, the $\langle Pha \rangle$ levels are higher than those obtained with an equivalent stimulation by a steady cytosolic Ca^{2+} concentration. Panel (b) shows the $\langle Pha \rangle$ values in the limited $\langle Z \rangle$ range where periodic Ca^{2+} spikes are obtained. Except for β, the values of the parameters are the same as in Fig. VII.2: ——, Ca^{2+} oscillations; - - - , steady state.

VII.2.5. Discussion

Our minimal model for the control of glycogen phosphorylase activity by Ca^{2+} suggests that Ca^{2+} oscillations could play an important role in the regulation of glycogenolysis in hepatocytes. Indeed, we have first shown by simulating sinusoidal variations of the level of cytosolic Ca^{2+}, Z, that a given level of active phosphorylase can be induced by lower average Ca^{2+} levels when Ca^{2+} oscillates. In other words, oscillations decrease the effective Ca^{2+} threshold for the activation of glycogen phosphorylase. In that respect, we recover the experimental results obtained by Dolmetsch *et al.* (1998) as to the

expression of transcription factors in lymphocytes. It would thus be highly interesting to investigate if similar experimental techniques could be used to measure the effect of Ca^{2+} oscillations on glycogenolysis.

In addition to this effect, a further modulation of the <*Pha*> levels can be induced when the frequency of the oscillations reaches a similar time-scale as the maximum rate of the converter enzymes involved in the phosphorylation-dephosphorylation cycle. This dependence of <*Pha*> levels on the oscillations frequency could allow 'pure frequency encoding" (i.e. coding by an increase in Ca^{2+} spiking frequency without modification of the mean Ca^{2+} level). This kinetic effect leads to substantial regulation of <*Pha*> levels for a large (ten-fold) variation in the oscillation frequency [see Fig. VII.2(b)]. In physiological conditions, the $[Ca^{2+}]_i$ oscillation frequency does vary in such a range in hepatocytes (Woods *et al.*, 1986), between 0.3 and 4 min^{-1}. Nevertheless, as shown in Fig. VII.2(b), substantial regulation by 'pure frequency encoding" occurs in a definite frequency interval requiring a fine tuning of the kinetic parameters of the phosphorylation-dephosphorylation cycle. In this context, it is remarkable that our results, based on an already tested model (Cardenas and Golbeter, 1996), show that the interval of frequencies of Ca^{2+} oscillations providing a sizable modulation of the activation of glycogen phosphorylase lies precisely in the physiological range. Therefore, 'pure frequency encoding' is likely to play a substantial role in the regulation of glycogenolysis.

Another interesting feature of the present model concerns the fact that the level of activity of the phosphorylase kinase oscillates in phase with Ca^{2+} oscillations. That the latter assumption is realistic from the point of view of the intrinsic time-scales of phosphorylase kinase activation is corroborated by experimental observations on pancreatic acinar cells (Craske *et al.*, 1999). In this cell type indeed, it has been shown that calmodulin translocation into the nucleoplasm by a Ca^{2+}-CaM-dependent pathway allows the calmodulin concentration to oscillate in synchrony with Ca^{2+} spikes in the apical region. As the δ subunit of phosphorylase kinase is identical to calmodulin and mediates the Ca^{2+} sensitivity of the enzyme, the variations in the level of activity of the phosphorylase kinase could indeed follow the hormone-induced Ca^{2+} spikes. Furthermore, using a model for realistic Ca^{2+} oscillations based on the mechanism of Ca^{2+} -induced Ca^{2+} release (CICR), we have explored the impact of Ca^{2+} oscillations on the cell response to hormonal stimulation. An increase in the stimulation parameter (β) induces a higher frequency of Ca^{2+} spiking and also a larger mean value for the Ca^{2+} concentration. In these conditions, it appears that both effects are involved in the increase in the average fraction of phosphorylated phosphorylase occurring after a rise in stimulation in hepatocytes. Thus, in addition to avoiding potential damage to the cell and increasing the robustness in signal detection at low levels of stimulation (Rapp *et al.*, 1981; Rapp, 1987), Ca^{2+} oscillations seem to optimize the effect of hormonal stimulation. In conclusion, this theoretical study suggests that Ca^{2+} oscillations could play a functional role in the regulation of glycogenolysis at the single-cell level. Interestingly, recent experimental findings plead in favour of this hypothesis, also at the multicellular level. The intracellular Ca^{2+} waves recently observed in intact livers perfused with vasopressin have indeed been shown to allow the coordination of the glycogenolytic response at the level of the whole organ (Eugenin *et al.*, 1998).

VII.3. Sensitivity of CaM kinase II to the frequency of Ca^{2+} oscillations: a simple model

VII.3.1. Introduction

In neurons, muscle and many non-excitable cells, stimulation by a neurotransmitter or a hormone leads to the onset of repetitive Ca^{2+} spikes, sparks, puffs, and waves (Meyer and Stryer, 1991; Berridge and Dupont, 1995; Berridge *et al.*, 2000; Bootman *et al.*, 2001; Schuster *et al.*, 2002). These oscillatory intracellular Ca^{2+} signals in turn mediate various cellular processes such as gene expression, secretion, contraction, cell proliferation, fertilization, synaptic plasticity or neurotransmitter release (Berridge *et al.*, 2000; Thomas *et al.*, 1996). Many of these phenomena have been shown to be influenced by the

frequency of Ca^{2+} oscillations, as well as their subcellular location (Holl *et al.*, 1998; Gu and Spitzer, 1995; Hajnoczky *et al.*, 1995; Dolmetsch *et al.*, 1998; Llopis *et al.*, 1988; Eshete and Fields, 2001; Petersen, 2002). A key candidate as molecular link between these cellular responses and the oscillatory Ca^{2+} signal is the ubiquitous multifunctional Ca^{2+}-calmodulin kinase II (CaMKII). This multisubunit protein has indeed long been proposed to be a decoder of the frequency of Ca^{2+} spikes, as a result of numerous detailed molecular and biochemical analyses of the rules that govern its activation and autophosphorylation (Braun and Schulman, 1995; Hudmon and Schulman, 1992a). More recently, this proposal was tested experimentally, leading to the demonstration that CaMKII is indeed able to decode the number and frequency of Ca^{2+} oscillations (De Koninck and Schulman, 1998). Such feature of CaMKII may be involved in the frequency-dependent forms of synaptic plasticity, learning and memory that the kinase controls [for reviews, see Malenka and Nicoll, 1999 and Lisman *et al.*, 2002].

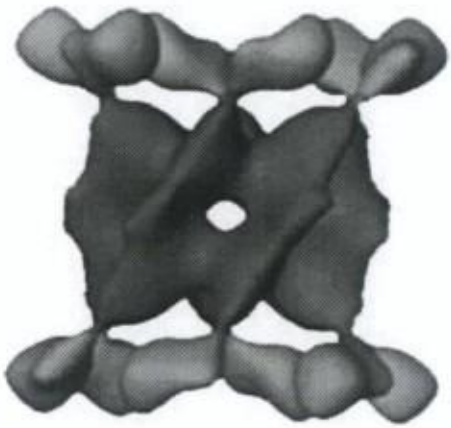

Fig. VII.7. Schematic representation of the structure of CaMKII dodecameric holoenzyme, based on the structural model of (Kolodziej *et al.*, 2000). Radiating catalytic subunits are attached to a central core of association domains. Given spatial constraints, inter-subunit phosphorylation is expected to occur only between immediate neighbors, which both bind Ca^{2+}-CaM simultaneously.

CaMKII (Fig. VII.7) is composed of ~12 subunits, made of closely related isoforms that are arranged in a unique "hub and spoke" structure, with the catalytic and regulatory sites on the outside (spokes) and the supramolecular association domain (hub) inside (Kanaseki *et al.*, 1991; Kolodziej *et al.*, 2000; Morris *et al.*, 2001). Activation of CaMKII corresponds to the suppression of an auto-inhibitory mechanism. In low Ca^{2+}, the catalytic site is thought to be covered by an inhibitory segment. When Ca^{2+} rises, binding of the Ca^{2+}-CaM complex induces a conformational change, relieving the auto-inhibition mechanism. The Ca^{2+}-CaM-bound subunit then becomes fully active (Braun and Schulman, 1995; Schulman *et al.*, 1992; Hanson *et al.*, 1994; Soderling *et al.*, 2001). Such a subunit can then phosphorylate various substrates as well as Ca^{2+}-CaM-bound neighboring subunits of the same holoenzyme (Hanson *et al.*, 1994; Mukherji and Soderling, 1994; Rich and Schulman, 1998). This inter-subunit reaction occurs at Thr^{286} or Thr^{287}, for α- and β-isoforms respectively, and disrupts the interaction between the autoinhibitory domain and the catalytic site; in consequence, an autophosphorylated subunit keeps some level of activity (20-80% depending on the substrate) even after dissociation of Ca^{2+}-CaM. Interestingly, autophosphorylation also modifies the rate of dissociation of CaM by an increased factor of 1000 to 10000. CaM is thus said to be 'trapped' by the multimeric complex (Meyer and Stryer, 1991; Singla *et al.*, 2001). CaM trapping was believed to be a key element in the ability of CaMKII to decode the frequencies of Ca^{2+} (Meyer and Stryer, 1991; Hanson *et al.*, 1994; Holmes, 2000; Coomber, 1998).

The complex regulation of this molecule and the attractive hypothesis that it may act as a molecular decoder of Ca^{2+} oscillations have prompted several groups to develop theoretical models to gain further understanding in its dynamical behavior. In most models however, the frequency-dependent autonomous activity of CaMKII must be ascribed to the simultaneous presence of phosphatases (Hanson *et al.*, 1994; Holmes, 2000; Coomber, 1998; Prank *et al.*, 1998; Michelson and Schulman, 1994; Dosemeci and Albers, 1996; Okamoto and Ichikawa, 2000; Lisman and Zhabotinsky, 2001). Yet, the experimental results of De Koninck and Schulman (1998) revealed that the isolated kinase itself exhibits frequency-dependent autonomy. Indeed, when CaMKII was immobilized inside PVC tubing and subjected to pulses of Ca^{2+}-CaM of variable amplitude, duration and frequency, the kinase's response was highly sensitive to the frequency, duration and amplitude of Ca^{2+}-CaM spikes, even in the absence of phosphatases. A recent model developed by Kubota and Bower (2001) accounts for the latter results. Here, we concentrate on building a minimal model for the regulation of CaMKII by Ca^{2+}-CaM, which quantitatively reproduces experimental results (Dupont *et al.*, 2003a). Indeed, tightly limiting the parameters of the model to experimental conditions has first been important to properly test its validity. The model then investigates the role of several characterized features of the kinase –as well as some that are not easily attainable by experiments– in its frequency-dependent responses. We find that CaM trapping accounts for only a small effect in the sensitivity of the kinase to the frequency of Ca^{2+} oscillations. Our simulations lead to a novel prediction on the behavior of the kinase when it is exposed to brief forms of Ca^{2+} spikes, such as those observed at cellular microdomains (e.g. neuronal synapses, Ca^{2+} store membranes). Our simple model provides a useful tool to dissect the regulatory features of CaMKII and should be helpful in the design of more comprehensive cellular models of Ca^{2+} signaling.

VII.3.2. Model description

In our model for CaMKII activation by Ca^{2+}-CaM, we focus on the time-evolution of the amounts of subunits in the different states, regardless of their association to a specific holoenzyme. Each concentration is scaled by the total amount of subunits. In the absence of CaM and prior to stimulation, all the subunits are in the inactive form W_I; after binding of the Ca^{2+}-CaM complex, the subunit is called W_B. An autophosphorylated subunit is represented by the W_P symbol. When Ca^{2+} dissociates from CaM bound to the phosphorylated form, the form becomes W_T (i.e. with 'trapped' CaM). Finally, the phosphorylated state of the subunits from which CaM has dissociated (which is said to be autonomous) is represented by W_A (see Table VII.1). Each possible state of the subunits is moreover characterized by an 'activity coefficient' (c_i) that measures its phosphorylation activity compared to the maximum Ca^{2+}-CaM-stimulated CaMKII activity, which occurs for the subunits in the phosphorylated state (W_P). As in the case of the experimental demonstration (De Koninck and Schulman, 1998), we are limiting our model to the activation of CaMKII by the Ca^{2+}-CaM complex (Ca^{2+}-saturated CaM), without introducing different binding modes and kinetics of Ca^{2+} to CaM.

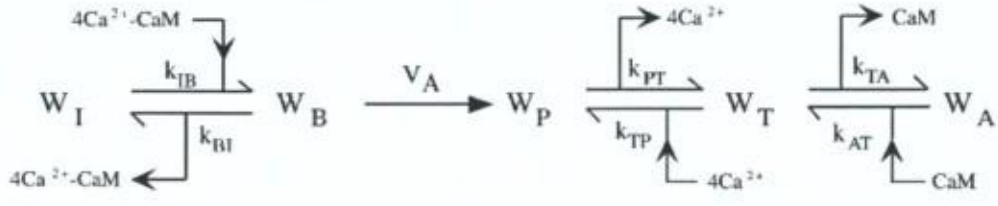

Fig. VII.8. Schematic representation of the simple model for the activation of CaMKII by the Ca^{2+}-CaM complex. The model describes the evolution of the fractions of subunits in each possible state. These states are listed in Table VII.I. Thus, the model does not explicitly consider the location of the subunits in the spatially organized holoenzyme. All transitions are assumed to be reversible, except for the autophosphorylation step (V_A) due to the absence of phosphatases.

	Symbol	Ligand	Phosphorylation at Thr^{286}	Coefficient of kinase activity
Inactive	W_I	-	no	0%
Bound	W_B	$4Ca^{2+}$-CaM	no	75%
Phosphorylated	W_P	$4Ca^{2+}$-CaM	yes	100%
Trapped	W_T	CaM	yes	80%
Autonomous	W_A	-	yes	80%

Table VII.1: List of the possible states of the subunits of CaMKII that are considered in the model. The experimental values for the activity coefficients are difficult to obtain with certainty (Hanson and Schulman, 1992; Colbran, 1993). The values indicated here above are those used in the model; the effect of changing these coefficients is discussed in section VII.3.4.

The transitions between the various possible states of the kinase subunits are schematized in Fig. VII.8. In order to make the model simple and realistic, we describe the transitions between the various states shown in Fig. VII.8 by classical kinetic expressions.

Binding and dissociation of Ca^{2+}-CaM to and from the unphosphorylated form W_I are assumed to be Ca^{2+}-independent reaction steps characterized by the kinetic constants k_{IB} (association) and k_{BI} (dissociation):

$$\frac{dW_I}{dt} = k_{BI}W_B - k_{IB}\left[Ca_4^{2+}/CaM\right]W_I \qquad \text{(VII.4)}$$

where $\left[Ca_4^{2+}/CaM\right]$ represents the concentration of CaM in its most active form, i.e. bound to 4 Ca^{2+} ions. The Ca^{2+}-CaM-bound form W_B can both release its ligand or be phosphorylated. The latter reaction occurs between a subunit in the W_B form and another Ca^{2+}-CaM-bound subunit (W_B), or any other phosphorylated subunit (W_P, W_T or W_A). Thus the rate of phosphorylation of W_B into W_P depends on the amounts of subunits in the different states and can be phenomenologically written as:

$$V_A = K_A\left((c_B W_B)^2 + (c_B W_B)(c_P W_P) + (c_B W_B)(c_T W_T) + (c_B W_B)(c_A W_A)\right) \qquad \text{(VII.5)}$$

However, as such, equ. (VII.5) does not consider the fact that subunits probably have to be neighbors within a holoenzyme (Braun and Schulman, 1995; Hudmon and Schulman, 2002a; 2002b) for phosphorylation to occur. To incorporate this requirement in Equ. (VII.5), we make K_A dependent on the total fraction of active subunits ($T=W_B+W_P+W_A+W_T$): if the fraction T is low, the probability of an arbitrarily selected bound subunit to be adjacent to an active subunit is very low (and thus K_A must be very small). The probability increases with T in a non-linear manner as the subunits progressively fill the "hub and spoke" structure. Among other possibilities, such conditions are qualitatively satisfied by a cubic function of T such as:

$$K_A = K'_A\left\{aT + bT^2 + cT^3\right\} \qquad \text{(VII.6)}$$

The latter empirical function allows us to keep the model as simple as possible without considering explicitly the location of each simulated subunit. Simpler expressions for the autophosphorylation rate V_A depending only on W_B did not allow us to reproduce the experimental results. Parameters a, b and c are fitted to get good agreement with experimental data [Fig. 3A of (De Koninck and Schulman, 1998)], with the other parameter values taken from the litterature (see below and Table VII.2).
The evolution equation for W_B thus reads:

$$\frac{dW_B}{dt} = k_{IB}\left[Ca_4^{2+}/CaM\right]W_I - k_{BI}W_B - V_A \qquad \text{(VII.7)}$$

Once phosphorylated, we reason that trapped CaM on the kinase may release Ca^{2+} when local Ca^{2+} is low. Thus,

$$\frac{dW_P}{dt} = V_A - k_{PT}W_P + k_{TP}\left[Ca^{2+}\right]^4 W_T \qquad \text{(VII.8)}$$

If autophosphorylation is assumed to be bi-directional (as it is the case in most simulations), the $K_A(c_B W_B)^2$ term in Equ. VII.5 is multiplied by 2. Other terms are left unchanged as when a Ca^{2+}-CaM bound subunit is adjacent to a phosphorylated (W_P), trapped (W_T) or autonomous (W_A) one, only one phosphorylation reaction can occur (on W_B) because the other subunit is already phosphorylated. However, the values of the phenomenological parameters appearing in the expression of K_A (Equ. VII.6) have to be changed also as compared to the unidirectional case, as a bound subunit can now be phosphorylated by an active neighbor on its right or on its left. Trapping is taken into account by assuming that the kinetic constant for CaM dissociation from a phosphorylated subunit (k_{TA}) is 1000 times lower than the same reaction from a non-phosphorylated subunit (k_{BI}). Binding and dissociation of Ca^{2+} to and from the kinase/CaM complex are assumed to be fast reactions (see Table VII.2). The last 2 equations of the model describing the reaction scheme illustrated in Fig. VII.8 thus read:

$$\frac{dW_T}{dt} = k_{PT}W_P - k_{TP}\left[Ca^{2+}\right]^4 W_T - k_{TA}W_T + k_{AT}\left[CaM\right]W_A \qquad \text{(VII.9)}$$

$$\frac{dW_A}{dt} = k_{TA}W_T - k_{AT}\left[CaM\right]W_A \qquad \text{(VII.10)}$$

The latter equation must in fact not be integrated explicitly, as the sum of all subunit fractions must remain constant and equal to 1. The value of the k_{AT} constant, which represents the rate of binding of naked CaM to an autonomous subunit of CaMKII, is not known but can be assumed to be very small. However, as we will see below, this binding does not occur in the simulations of the experimental protocol of De Koninck and Schulman (1998) as the autonomous form (W_A) only accumulates once the stimulatory protocol has stopped (see Fig. VII.10), in which case there is no CaM anymore.

A possible dephosphorylation of the subunits by phosphatases is not considered as these were not included in the experimental protocol of De Koninck and Schulman (1998). The effect of $Thr^{305/306}$ phosphorylation, which generally follows 1) Th^{286} phosphorylation and 2) a drop in Ca^{2+} (Patton *et al.*, 1990; Hanson and Schulman, 1992) has not been incorporated in our model. These 2 threonines lie in the CaM binding site, and thus their phosphorylation blocks further CaM binding. While this phosphorylation reaction has been incorporated in previous models (Coomber, 1998; Dosemeci and Albers, 1996; Kubota and Bower, 2001), De Koninck and Schulman (1998) did not observe a significant role for this reaction in the sensitivity of the kinase to Ca^{2+} oscillation frequencies (unpublished) in their experimental setting. Nevertheless, we address in the discussion a possible consequence of this reaction –known as "capping"– in our model.

Thus, the latter set of equations provides a 4-variable system of differential equations, which can be easily integrated. Binding and dissociation of Ca^{2+} to and from CaM is considered to be always at equilibrium as these reactions occur in the pressurized chamber before being in contact with the immobilized CaMKII (De Koninck and Schulman, 1998). The Hill coefficient equals 4 and the K_D, 1 μM. Thus, at each time step, the concentration of bound CaM is given by:

$$\left[Ca_4^{2+}/CaM\right] = \left[CaM\right]_{TOT} \frac{\left[Ca^{2+}\right]^4}{\left[Ca^{2+}\right]^4 + K_D^4} \qquad \text{(VII.11)}$$

Consumption of free CaM, and of the Ca^{2+}-CaM complex through binding to the kinase is not considered, as in the experimental conditions where a rapid change of solution every second was performed. In the following, results have been obtained by integrating the model equations with a variable time step, fourth order Runge-Kutta algorithm.

Symbol	Physiological meaning	Value	Ref.
k_{IB}	Rate of association of CaM to a non-phosphorylated subunit	0.01 $nM^{-1}s^{-1}$	1,2,3,4
k_{BI}	Rate of dissociation of CaM from a non-phosphorylated subunit	0.8 s^{-1}	1,2,3,4
k_{PT}	Rate of dissociation of Ca^{2+} from CaM bound to a phosphorylated subunit	$1s^{-1}$	2,4
k_{TP}	Rate of association of Ca^{2+} to CaM bound to a phosphorylated subunit	1 $\mu M^{-4}s^{-1}$	2,4
k_{TA}	Rate of dissociation of CaM from a phosphorylated subunit	$k_{BI}/1000$	2,3
k_{AT}	Rate of association of CaM to a phosphorylated subunit	k_{IB}	2,3
K_D	Half maximal concentration characterizing Ca^{2+} binding to CaM	1μM	2,4,5
K'_A	Phenomenological rate constant for autophosphorylation	$0.29s^{-1}$	1,6,7

Table VII.2: List of the values for the kinetic parameters used in the simulations. These values have been taken from biochemical analyses of the enzyme. In the column 'References', 1: De Koninck and Schulman, 1998; 2: Schulman *et al.*, 1992; 3: Ishida *et al.*, 1996; 4: Miller and Kennedy, 1986; 5: Meyer *et al.*, 1992; 6: Bradshaw *et al.*, 2002; 7: Kubota and Bower, 2001.

VII.3.3. Comparison of the behavior of the model with experimental results

We first test if the simple model presented in the previous section can reproduce the experimental results about the autonomous activity of CaMKII after various stimulation protocols (De Koninck and Schulman, 1998). Thus in our simulations, we mimic the number, amplitudes and frequencies of Ca^{2+}-CaM pulses, as produced in the *in vitro* study; the read-out of the kinase autophosphorylation, namely the autonomy, was evaluated as the Ca^{2+}-independent activity and expressed as a percentage of the maximal Ca^{2+}-stimulated activity. Only the experiments related to the α isoforms of CaMKII were tested with the model.

We then simulate the exposure of CaMKII to various concentrations of Ca^{2+}-saturated CaM and its subsequent steady-state phosphorylation activity on a synthetic peptide, autocamtide-3 (AC-3). This exogenous substrate competitively prevents CaMKII autophosphorylation. In the experiments, the AC-3 phosphorylation activity of CaMKII at each concentration of Ca^{2+}-saturated CaM was compared to the activity obtained in the presence of a supra-maximal concentration of Ca^{2+}-saturated CaM, and this

ratio was plotted as a function of the concentration of Ca^{2+}-saturated CaM. Thus, the equivalent quantity of the model is the ratio between $c_B W_B$ and c_B, thus W_B. This amounts to the analytical solution of Equ. VII.4 at steady state, thus:

$$W_B = \frac{X}{\frac{k_{BI}}{k_{IB}} + X}$$

in agreement with the Hill coefficient equal to 1 obtained experimentally (De Koninck and Schulman, 1998). Values of the kinetic constants of CaM binding and dissociation have been chosen such that their ratio k_{BI}/k_{IB} equals 80 nM, which is the concentration of Ca^{2+}-saturated CaM producing half-maximal activation of CaMKII in the experimental study (De Koninck and Schulman, 1998).

Next, we evaluate the autonomy of CaMKII after 6s exposure to various concentrations of Ca^{2+}-saturated CaM. In such case, autophosphorylation induces a cooperative dependence of the activity of the enzyme on CaM concentration. This behavior is reproduced by the model, as shown in Fig. VII.9B. Agreement between experiments and simulations is very good, although at very high levels of CaM, the simulated curve does not quite reach the same maximal autonomy (0.65 versus 0.77 ± 0.4 in the experiment, with the autonomous activity being normalized by the maximal Ca^{2+}-CaM-stimulated activity). A detailed examination of the evolution of the variables of the model reveals that at high CaM levels, the rate of autophosphorylation saturates with time as the amount of available inactive subunits (W_I) progressively diminishes. Thus, if the time of exposure to Ca^{2+}-saturated CaM is increased, the level of maximal autonomy also increases. In the same manner, the $K_{1/2}$ of this dose-response curve (Fig. VII.9B here or Fig. 3A in the experiment of (De Koninck and Schulman, 1998)) also highly depends on the exposure time to CaM, such that longer stimulation leads to a shift toward lower $K_{1/2}$.

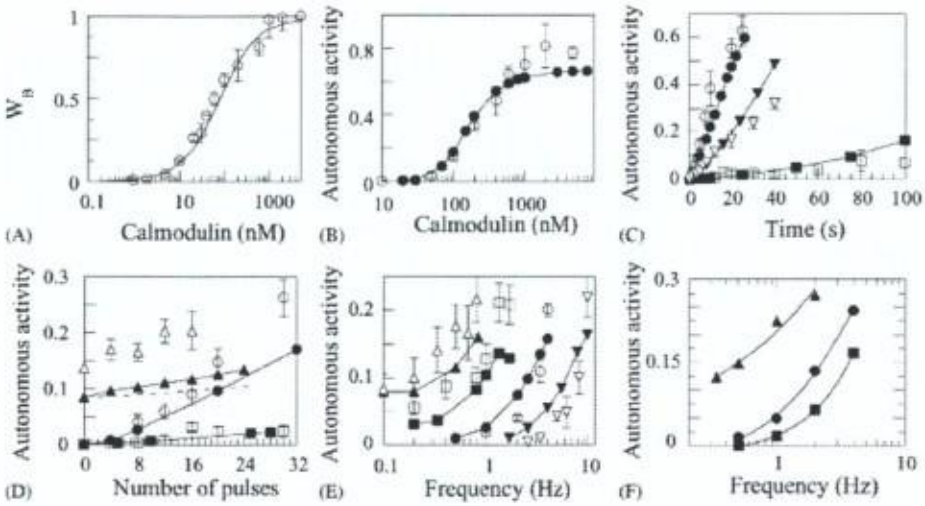

Fig. VII.9. Comparison of the behavior of the model with the experimental results obtained by De Koninck and Schulman (1998). The successive panels show the exact simulation of the experimental protocols developed by De Koninck and Schulman (1998), except for panel F (see below). In all panels, curves and filled symbols have been obtained by numerical simulations of the model, while open symbols represent the experimental results reproduced from De Koninck and Schulman (1998). All results shown here (theoretical and experimental) have been obtained for the α isoform of the kinase. Panel A shows the steady-state level of phosphorylation of an exogenous substrate (autocamtide-3) which competitively inhibits autophosphorylation (thus, $V_A = 0$ in the model). Panel B shows the level of autonomous activity obtained after a 6s exposure to a constant level of Ca^{2+}-CaM. The Hill coefficient (1.6) and the CaM_{50} (220nM) matches with the experimental values. Panel C shows the level of autonomy of CaMKII after repetitive pulses of Ca^{2+} (500 μM) and CaM (100nM), whose duration equals 200ms and frequencies equal 1 (squares), 2.5 (triangles) and 4 Hz (circles). Panel D reproduces the same data as panel C, for a 1 Hz (squares) and a 4 Hz (circles) stimulation protocol. For the triangles, CaMKII has been exposed to a strong, 300ms pre-pulse of Ca^{2+} (500 μM) and CaM (1 μM) which "pre-sets" the autonomy level to ~10%. When such

partially autonomous CaMKII is then submitted to a 1 Hz stimulation protocol, the increase in autonomy is faster than for the naïve form (compare with the dotted line which is the plain curve (squares) reported on the same origin). Panel E shows the effect of changing the duration of the Ca^{2+}-CaM pulses (triangles: 1000 ms, squares: 500 ms, circles: 200 ms; inverted triangles: 80 ms). In each case, the total exposure time of the kinase to the activators equals 6s (500 μM Ca^{2+}, 100nM CaM). Panel F corresponds to Fig. 4B of (De Koninck and Schulman, 1998), i.e. shows the effect of changing the amplitude of the pulses. Here, the agreement between model and experiments is qualitative only (see text); the amplitude and the number of pulses in the simulations are different from those in the experiments: 10 pulses of 400 nM (triangles), 40 pulses of 110 nM (circles) and 60 pulses of 70 nM (squares). In all cases, the pulse duration equals 200 ms. As the protocol is different from that used in the experimental study, experimental results are not shown in this panel.

All curves have been obtained by numerical integration of equ. (VII.4)-(VII.11) with the parameter values indicated in Table II and a = -0.220, b = 1.826, c = -0.800 . As the sum of the fractions of active subunits (T) is such that $0 \leq T \leq 1$, K_A(defined by equ. VII.6) is always positive.

We next examine the behavior of the model when submitted to 200ms pulses of Ca^{2+}-saturated CaM (100 nM) at various frequencies. The behavior of the model (Fig. VII.9C) is in very good quantitative agreement with the experimental results (De Koninck and Schulman, 1998). As shown in Fig. VII.10., at each Ca^{2+}-CaM spike of this duration and amplitude, a significant portion of subunits become activated (decrease in W_I, increase in W_B). At high frequency of stimulation (4Hz, lower panel), dissociation of CaM is very limited between 2 spikes. In consequence, W_B accumulates and after a few seconds, autophosphorylation can be initiated because the number of Ca^{2+}-CaM bound subunits in close proximity becomes significant. The rate of autophosphorylation then keeps on increasing because 1) the probability that 2 active subunits are neighbors increases in a non-linear manner with their number, and 2) because once phosphorylated, a subunit remains active even between spikes. In consequence, the fraction of phosphorylated subunits increases in an autocatalytic manner. In contrast, at low frequency (1Hz, upper panel of Fig. VII.10), Ca^{2+}-CaM nearly totally dissociates from CaMKII between 2 spikes: the amount of bound subunits W_B thus always remains below the threshold for autophosphorylation. The fractions of trapped (W_T) and autonomous (W_A) subunits are not shown on Fig. VII.10 because they are close to zero in this time interval. In fact, these states of the kinase become predominant once the stimulation protocol has stopped, as all the bound subunits (W_B) progressively lose their Ca^{2+} and CaM and transform into the autonomous forms.

As the autophosphorylation rate shows a non-linear dependence on W_B, it is expected that a given stimulation pattern will be more effective if some of the CaMKII subunits have already been pre-phosphorylated. This was shown experimentally [(De Koninck and Schulman, 1998; inset to Fig. 3B] by pre-exposing CaMKII to a 300ms pulse of Ca^{2+}-saturated CaM (1 μM), followed by a 400ms wash and a 1s delay. This protocol was reproduced in our simulations and led to ~10% autonomy, in good agreement with the experiments. As shown in Fig. VII.9D, a 1Hz-stimulation of this prephosphorylated CaMKII (dashed line with open squares) leads to a faster increase in autonomy as compared to the non-pretreated situation (dashed line, which corresponds to the full line with squares reported on the same origin for comparison).

The shape of the frequency-autonomy response has been shown to largely depend on the spike amplitude and duration (De Koninck and Schulman, 1998). For example, it is expected that this response becomes less steep if the length of the spike is increased (see Fig. VII.9E, to be compared with Fig. 4A of (De Koninck and Schulman, 1998)). In such case indeed (1000ms, triangles, for example), one spike provides enough Ca^{2+}-CaM to generate some autophosphorylation. In contrast, when the spikes are very brief (200 or 80 ms), shorter intervals are required to allow for accumulation of bound subunits sufficient for autophosphorylation. Therefore, the probability of coincident binding of CaM to neighboring subunits determines the threshold frequency required for significant autophosphorylation: the lower the probability, the higher the threshold.

In the case of spike amplitude, the experiment tested this intuitive prediction by increasing the effective amplitude of Ca^{2+} spikes, through raising the CaM concentration in the pulse system [(De

Koninck and Schulman, 1998), Fig 4B]. The results showed that the kinase responded to a broader range of Ca^{2+} oscillation frequency, when CaM concentration was increased. This is consistent with the inverse relationship between probability of inter-subunit phosphorylation during single spikes and threshold frequency of significant CaMKII autophosphorylation. Our simulation of this experiment qualitatively led to the same conclusion. We exposed the kinase to increasing amounts of CaM and observed a decreasing threshold of autonomy (Fig. VII.9F). The quantitative differences between the experiments and the results of the model mainly lies in the fact that at 30 nM CaM, 200 ms pulses did not generate autonomy in the model, even at high frequencies. This insensitivity of the kinase to such a low-amplitude stimulatory pattern (30 spikes of 200 ms duration and 30 nM amplitude) is directly related to the fact that the parameters for the rate of autophosphorylation (in Equ. VII.6) have been chosen such as to get very little autonomy after 6s of continuous stimulation (which can be viewed as 30 x 200 ms) at low levels of Ca^{2+}-saturated CaM (see Fig. VII.9B).

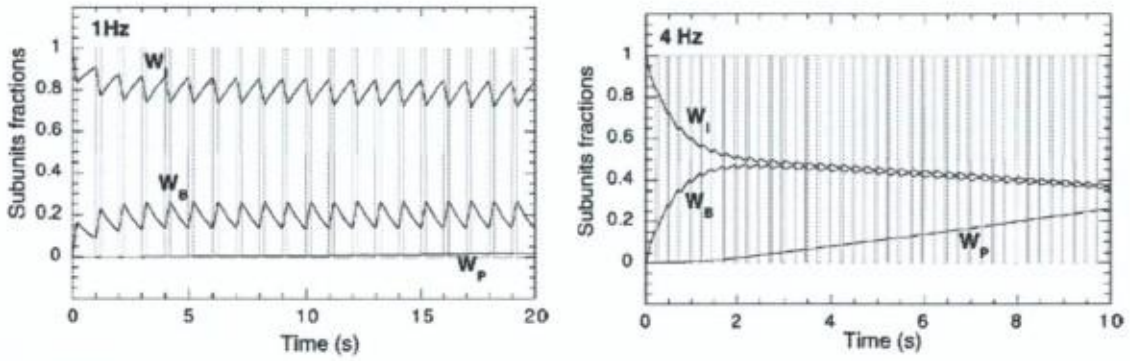

Fig. VII.10. Temporal evolution of W_I, W_B and W_P for a high and for a low frequency stimulation protocol. The Ca^{2+}-CaM spikes, normalized with respect to their maximal value (100 nM), are indicated in grey. Results have been obtained by numerical integration of equ. (VII.4)-(VII.11) with the same parameter values as in Fig. VII.9B.

We conclude from these results that our proposed simple biophysical model of CaMKII activation and autophosphorylation can closely simulate the behavior of the kinase measured experimentally. Therefore, such model should be useful to dissect further the mechanistic features of this molecular decoder of Ca^{2+} oscillations as well as predict how CaMKII will behave under Ca^{2+} oscillatory conditions that are difficult to reproduce experimentally, *in vitro*.

VII.3.4. Behavioral and mechanistic predictions from the model

Role of the activity coefficients

The various states of the active CaMKII subunits (W_B, W_P, W_A and W_T) are likely to have different activity coefficients (c_B, c_P, c_A and c_T). While these coefficients may play a role in the dynamical behavior of CaMKII, experimental data about their values are difficult to obtain with certainty. We have used our model to gain understanding on how the coefficient values might affect the Ca^{2+} oscillation frequency sensitivity of the holoenzyme. Fig. VII.11A shows the effect of changing the activity coefficient of the non-phosphorylated, Ca^{2+}-CaM bound form of the enzyme subunits (W_B) on the autonomy after 6s exposure to various concentrations of CaM. As expected intuitively, higher levels of autonomous activity at limited reaction times are favored by higher activity coefficients.

The more interesting effect of this parameter c_B is that it also plays an important role in determining the frequency sensitivity of the enzyme (see Fig. VII.11B). The higher the coefficient c_B, the steeper the frequency/autonomy relationship becomes. These results can be explained by the fact that increasing the kinase activity of W_B favors autophosphorylation (which is non-linear) to the

detriment of Ca^{2+}-CaM dissociation (which is linear). As the activity of the non-phosphorylated subunits bound to CaM (W_B) is essential in determining the potentiality of the subunits to autophosphorylate, the frequency sensitivity of the enzyme will increase with the activity coefficient of this form (c_B).

Following autophosphorylation, we asked whether changing the coefficients of trapped and autonomous forms of the kinase affects the frequency-autonomy relationship. Increasing or decreasing c_T and c_A leads to higher or lower absolute levels of autonomy respectively at every frequency tested, but the steepness of the response-curves were unchanged (data not shown). One could intuitively expect that CaM-trapped kinase has an increased coefficient of activity compared to a CaM-free autonomous kinase; while the sensitivity of the kinase to Ca^{2+} stimulation would be increased by trapping, its dependence on oscillation frequency would remain unchanged. This result can be explained by the first order dependence of the phosphorylation velocity on the activity coefficients of the trapped and autonomous forms (see Equ. VII.5).

Unidirectional versus bidirectional autophosphorylation

From an experimental point of view, it is still unclear whether autophosphorylation is a reciprocal reaction between adjacent subunits, or if there is some sterical hampering to this reaction in one of the rotation direction of the hub-and-spoke structure [(Kolodziej *et al.*, 2000) and see Fig. VII.7]. Up to now, we have considered that autophosphorylation is bidirectional. If we modify this assumption (see section VII.3.2 for an explanation of the changes in the equations), the level of autonomy after 6s exposure at various levels of CaM is altered (plain curve with triangles of Fig. VII.11C). As expected intuitively, less autonomy is obtained for the same level of stimulation if autophosphorylation is unidirectional (compare with the dotted curve of Fig. VII.11C). However, by changing the empirical parameters appearing in equ. VII.6 (K'_A, a, b and c), one can re-obtain the same autonomy response curve as in the case of bidirectional autophosphorylation (plain curve with filled circles of Fig. VII.11C). Applying then all the protocols of Fig. VII.9 to this unidirectional version of the model only shows negligible differences with respect to the previous case (see Fig. VII.11D for the frequency sensitivity). That phosphorylation in a clockwise direction or in both a clockwise and a counterclockwise direction amounts to a slight change in the parameter values was also found in another model for CaMKII (Kubota and Bower, 2001).

Range of frequencies for CaMKII sensitivity

Following the experimental data (De Koninck and Schulman, 1998), Fig. VII.9C indicates that CaMKII can act as a decoder in a range of frequencies of 1 to 5 Hz. However, this frequency response is highly sensitive to the amplitude of the spikes (Ca^{2+} and/or CaM levels), as shown experimentally and in Fig VII.9F. Furthermore, such frequency range is artificially set by the width of the spikes, which were, in Fig VII.9C, 200 ms. Changing them to 80 or 500 ms shifts the frequency-responses in either directions (Fig. VII.9E). Another way to present this data, independently of the spike width, is to express it in terms of duty cycle, defined as the ratio between the duration of the spikes and the period of stimulation. Fig. VII.12A shows the same data as Fig. VII.9 (together with the experimental points) but plotted against the duty cycles. It isolates the effect of the spike length on the slope of the response curves, independent of the frequency shift that the spike length imposes (Fig VII.9E). Hence, no frequency dependence would be observed with very long Ca^{2+} spikes, whereas very brief spikes should be sensed by the kinase only near maximal duty cycle, under limiting Ca^{2+}-CaM. This figure illustrates well the similarities between the effects that the spike length duration has on the experimental data versus the simulations.

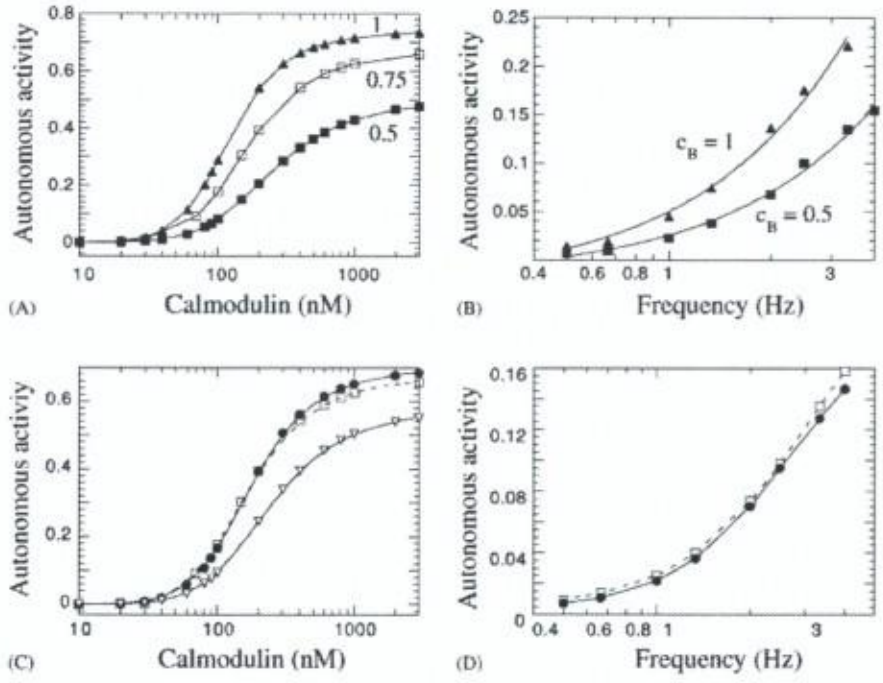

Fig. VII.11. Impact of CaMKII regulatory properties on frequency decoding of Ca^{2+} oscillations. A. Effect of changing the activity coefficient of W_B, the bound and unphosphorylated form of the kinase subunits. The curves have been obtained under the same conditions and with the same parameter values (except for c_B) as in Fig. VII.9B. B. Effect of changing the activity coefficient of W_B on the frequency sensitivity of CaMKII. A better sensitivity, i.e. a larger difference in the responses to distinct frequencies, is obtained for the largest value of this coefficient ($c_B = 1$). Points have been obtained by numerical integration of equ. (VII.4)-(VII.11) with the same parameter values as in Fig. VII.9C; the total number of spikes is equal to 30 for curve $c_B = 1$ and 60 for curve $c_B = 0.5$, to get an autonomy at 4 Hz of at least ~15%. If fitted by an $y = a \exp(bx)$ function, $b = 0.86$ for a c_B of 0.5 and $b = 0.98$ for a c_B of 1. C. Uni- versus bidirectional autophosphorylation. The dashed curve is identical to Fig. VII.9B (bidirectional autophosphorylation) while the plain curves show results obtained by assuming that autophosphorylation occurs only in a unidirectional manner; the curve with triangles has been obtained with the same parameter values as the plain curve, while the curve with squares has been obtained by changing the parameters of the empirical function describing autophosphorylation (equ. VII.6). Thus, for the plain curve with filled circles: $K'_A = 0.45\ s^{-1}$ and $a = 0.00366$, $b = 2.013$, $c = -1.0156$. D. Whether autophosphorylation occurs in a uni- or bidirectional manner in the holoenzyme does not affect its frequency-sensitivity. The dashed curve is obtained when assuming bidirectional autophosphorylation (and is thus identical to the 200ms curve of Fig. VII.9E); the plain curve is obtained when assuming unidirectional autophosphorylation, for the same parameter values as the plain curve with filled circles of panel C.

What both these experimental and modeling data show is that CaMKII has the ability to decode the frequencies of Ca^{2+} under a wide range of conditions. The model should then be used to predict how the kinase would behave under oscillatory Ca^{2+} conditions observed in cells. In nerve cells, where CaMKII is known to play a major role in frequency-dependent forms of synaptic plasticity [reviewed in Malenka and Nicoll, 1999; Lisman *et al.*, 2002; Rongo, 2002], several forms of Ca^{2+} spikes are very brief, such as those following action potentials (few ms), yet can locally reach very high amplitude, such as in dendritic spines [reviewed in Sabatini *et al.*, 2001]. Furthermore, CaMKII interacts with Ca^{2+} ion channels and intracellular Ca^{2+} stores [reviewed in Bayer and Schulman, 2001], which puts the enzyme very close to Ca^{2+} sources, reinforcing that the kinase regularly sees brief and large Ca^{2+} spikes. Moreover, if we take into account the time needed for Ca^{2+} to bind freely accessible CaM, which is thought to be the very limiting in cells (Persechini and Stemmer, 2002), CaMKII may conceivably be exposed to Ca^{2+}-saturated CaM for a only few ms upon Ca^{2+} spikes that last several tens of ms.

Fig. VII.12B and VII.12C show the simulated frequency sensitivity of CaMKII to 100 spikes of Ca^{2+}-CaM that ranged from 1 to 10 ms (constant amplitude of 2.5 μM) in duration and from 1 to 5 μM CaM (constant duration of 2 ms) in amplitude (estimates for CaM concentrations in cells fall in such range (Persechini and Stemmer, 2002). These simulations indicate that significantly high frequencies (>10 Hz) are required to induce autophosphorylation when the spikes are very brief, unless very high local concentrations of Ca^{2+}-CaM are present. The model thus shows that the frequency sensitivity of CaMKII also operates at much higher frequencies than those investigated in the experimental study (De Koninck and Schulman, 1998). Our simulations thereby suggest that CaMKII may be using its Ca^{2+} spike frequency sensitivity to selectively respond to high-frequency brief stimuli, such as Ca^{2+} fluxes at the mouth of ion channels.

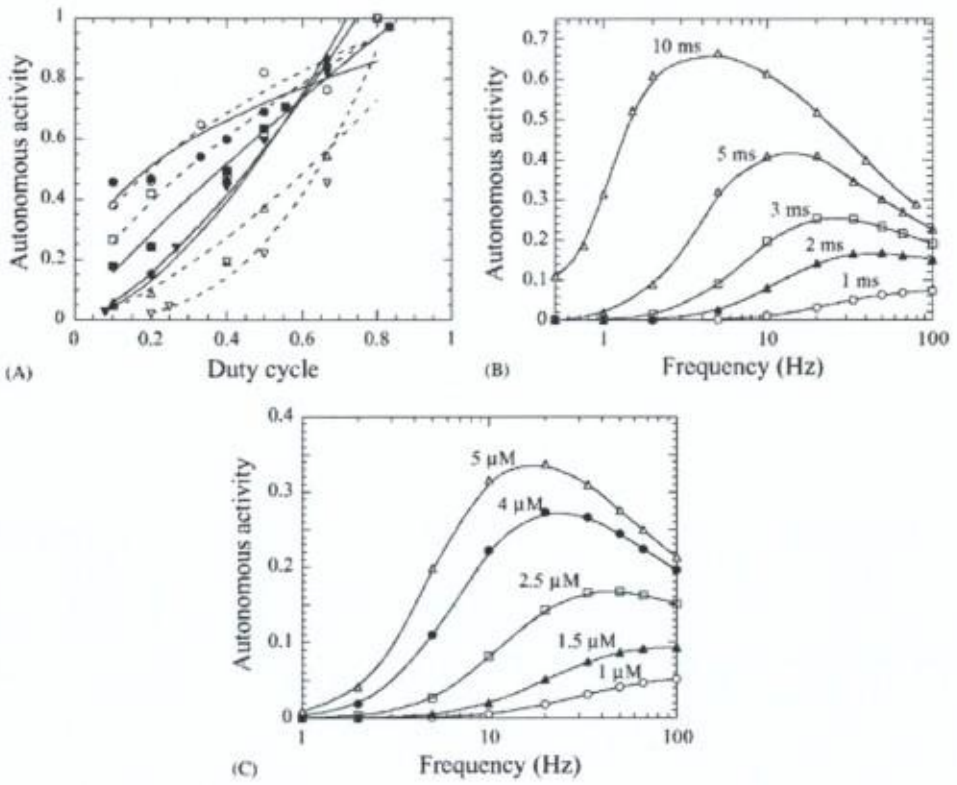

Fig. VII.12 Setting the frequency range of CaMKII response by the spike properties. A. Autonomy-response curve with different pulse lengths (∇ = 80ms, Δ = 200ms, □ = 500ms, o = 1000ms) as a function of the duty cycle, which represents the ratio between the duration of the spikes and the period of stimulation. Filled symbols = modeled values from Fig. VII.9E; open symbols = experimental values (De Koninck and Schulman, 1998). Maximal autonomy at 0.8 duty cycle was normalized to 1. B. Frequency sensitivity in response to 100 spikes of Ca^{2+}-CaM of high amplitude (2.5 μM) and various lengths. All other parameters are the same as in Fig. VII.9. C. Frequency sensitivity in response to 100 very brief (2ms) Ca^{2+}-CaM spikes of various amplitudes. All other parameters are the same as in Fig. VII.9E.

Tuning response

The simulations shown in Fig. VII.12B and VII.12C also predict that the CaMKII frequency-dependence may be tuned to optimal frequencies. As shown in Fig. VII.13A, tuning is not restricted to Ca^{2+}-CaM spikes of high amplitudes or short duration. It appears however that the longer the spikes, the less pronounced is the response tuned to an optimal frequency. To understand this decrease in autonomy at high frequencies, one must first recall that the total duration of the stimulatory protocol always decreases with frequency, because the number of spikes is kept constant. However, some autophosphorylation should occur during spike intervals, before Ca^{2+}-CaM fully dissociates from the

enzyme. The tuned response of the kinase to a fixed number of spikes will therefore be observed when the following 2 conditions are met: 1) when the spike intervals are becoming short (high frequencies). As the characteristic time for dissociation is 1.25 s in the model ($1/k_{BI}$), it is expected that tuning will not significantly occur for frequencies lower than 5-10 Hz. 2) for significant autophosphorylation to proceed during spike intervals, a certain level of autonomy is required. In consequence, the range of frequencies at which the autonomy starts to drop is expected to depend on the actual value of the autonomy. Fig. VII.13B (gathering results from Fig. VII.12B, VII.12C and VII.13A) illustrates this prediction of the model: the optimal frequency decreases with the level of autonomy at this optimal frequency.

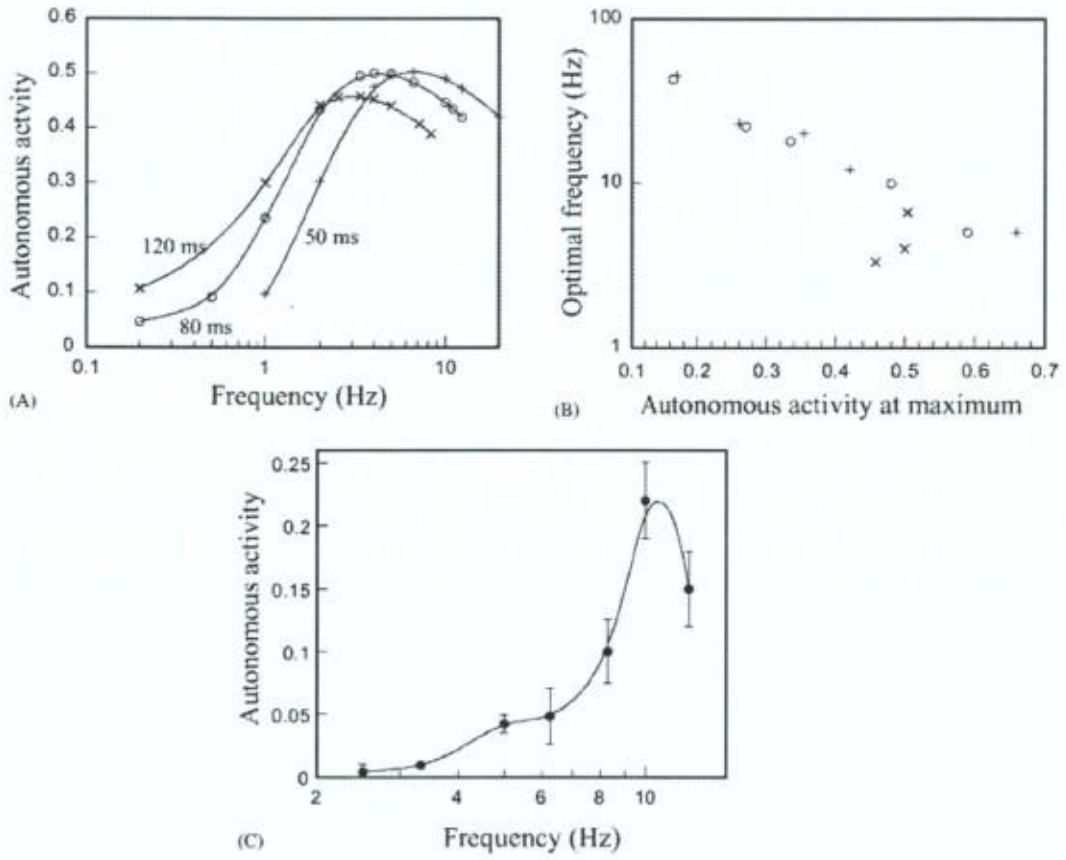

Fig. VII.13. Tuned response of CaMKII to Ca^{2+}/CaM oscillations. A. Frequency sensitivity in response to 30 spikes of Ca^{2+}-CaM of 400 nM amplitude and 120 ms duration (x); 50 spikes of Ca^{2+}-CaM of 400 nM amplitude and 80 ms duration (o); 80 spikes of Ca^{2+}-CaM of 400 nM amplitude and 50 ms duration (+). In all cases, the highest frequency corresponds effectively to continuous stimulation (defined as the inverse of the spike duration). This arbitrary point was plotted for comparison with the experimental result in Fig VII.13C. All other parameters are the same as in Fig. VII.9E. B. Optimal frequency of stimulation shown as a function of the value of autonomy corresponding to this maximum. This figure gathers the results shown in Fig. VII.12B, VII.12C and VII.13A. C. Experimental demonstration of the tuning effect. Shown is the frequency sensitivity to 80 ms spikes (30), under the same conditions as those defined in the legend to Fig. VII.9E. The maximal frequency tested (12.5 Hz) is effectively continuous stimulation (Ca^{2+}/CaM solution refreshed every second in the PVC tubing (De Koninck and Schulman, 1998). We used this protocol, since the pulse device could not produce spike intervals shorter than 20 ms.

To compare this novel prediction with experimental data, we combined data from De Koninck and Schulman (1998) that 1) compared the frequency response to 30 pulses of 100 nM Ca^{2+}-CaM with 80ms duration (total= 6 s) and 2) examined the response to continuous 6 s (which is effectively

equivalent to 12.5 Hz under this stimulus protocol). Fig VII.13C shows that indeed, experimentally, the response of the kinase is optimally tuned to 10 Hz.

VII.3.5. Discussion

After the experimental observations of Ca^{2+} oscillations in electrically non-excitable cells, it was rapidly suggested that in many cell types the nature and strength of stimulation could be encoded in the frequency of Ca^{2+} oscillations (Meyer and Stryer, 1991 ; Goldbeter *et al.*, 1990). In excitable cells such as neurons, stimulus frequency-dependent changes in synaptic transmission are well known [reviewed in (Malenka and Nicoll, 1999)]. These notions imply that the cell is in turn able to decode the frequency of Ca^{2+} oscillations. If true, such frequency coding would show many advantages over amplitude-coded signals (Meyer and Stryer, 1991 ; Goldbeter *et al.*, 1990). For example, frequency encoded signals provide an increased robustness with respect to external noise (Rapp and Berridge, 1981). Also, prolonged elevated Ca^{2+} plateaus during sustained stimulation are known to have deleterious effects on the health of cells (Berridge *et al.*, 2000 ; Bootman *et al.*, 2001).

Several possible mechanisms for the frequency decoding of Ca^{2+} oscillations have already been proposed (Dupont and Goldbeter, 1992 ; Dupont and Goldbeter, 1998 ; Tang and Othmer, 1995). All these systems differ from CaMKII by the fact that here, a single enzyme can act as a frequency decoder. On the other hand, this frequency decoder can be precisely tuned by the virtually unlimited diversity of CaMKII dodecameric holoenzymes that cells can produce via the co-assembly of 4 gene products with more than 20 splice variants (De Koninck and Schulman, 1998 ; Bayer *et al.*, 2001 ; 2002). Following the experimental demonstration of the Ca^{2+} oscillation frequency-decoding capability of CaMKII (De Koninck and Schulman, 1998), the present theoretical study confirms that a rather simple mode of regulation by Ca^{2+} can account for a finely tuned frequency sensitivity. The model emphasizes on the fact that the arrangement of the subunits in a hub-and-spoke structure plays a crucial role in this respect. Indeed, a good agreement between the model and the experiments is obtained when the rate constant of autophosphorylation depends in a non-linear manner on the number of active subunits (Equ. VII.6), a property which derives from the hub-and-spoke shape of the enzyme and the requirement of coincident CaM binding to 2 neighbouring subunits for autophosphorylation (Mukherji and Soderling, 1994 ; Rich and Schulman, 1998 ; Bradshaw *et al.*, 2002). A comparable description of the autophosphorylation rate has been used in a model for CaMKII/PS protein phosphatase 1 switch (Lisman and Zhabotinsky, 2001). In that model indeed, the per-site rate of autophosphorylation is defined as a step function with 2 different values: one for phosphorylation of the first subunit (initiation) and another one for phosphorylation of the subsequent subunits of the kinase (propagation).

The phenomenological description of the autophosphorylation step allows our model for the dynamical behavior of CaMKII to be mathematically very simple (4 ordinary differential equations instead of a few tens in models taking into account the location of the subunits within the holoenzyme), while providing a good quantitative agreement with the experiments. The present model could thus be easily re-used as a 'plug-in element' in larger models aimed at describing physiological situations in which CaMKII plays a role, as for example, regulation of carbohydrate, amino acid and lipid metabolism or neurotransmitter synthesis and release [see (Bayer and Schulman, 2001) for review]. However, in some cases, the model might require some changes in order to incorporate additional "restrictions", such as in the case of NMDA receptor-bound CaMKII at synapses, which contains a few autonomous subunits (independent of their phosphorylated state) (Bayer *et al.*, 2001). Our phenomenological description of the autophosphorylation step is moreover justified by the fact that carefully determined values for autophosphorylation rate have been lacking. Bradshaw *et al.* (2002) recently reported an autophosphorylation rate value of $12s^{-1}$ under conditions significantly different than those in the pulse protocol (De Koninck and Schulman, 1998). Our value for the rate

constant K_A cannot be directly compared to this value as it is not defined in the same manner (see Equ. 2 of (Bradshaw *et al.*, 2002)). Yet, in fact, our value of 0.29 s^{-1} for K_A allows us to reproduce the kinetics of increase in autonomy after constant exposure to Ca^{2+}-CaM (Bradshaw *et al.*, 2002). Using this value, we indeed got a theoretical curve for autophosphorylation lying between the experimental curves obtained at 100 and 500 μM ATP (see Fig. 3 of (Bradshaw *et al.*, 2002)). This is in agreement with the fact that our parameter values were chosen such as to simulate experiments performed at 250 μM ATP (De Koninck and Schulman, 1998).

Possible secondary autophosphorylation at $Thr^{305/306}$, known as capping (Hanson and Schulman, 1992), was not considered in our model, in part because the experiment [(De Koninck and Schulman, 1998) and unpublished] did not suggest it would play a significant role in the conditions tested (see model description). Indeed, in the time course tested (Colbran, 1993) capping likely occurs only on the autonomous form (W_A); as W_A only accumulates once the stimulation protocol has stopped (due to the long characteristic time for CaM dissociation from the trapped form), capping could only occur afterwards. Finally, our modeling of the role of the coefficients of activity of the various states (section VII.3.4) would argue that a change in the coefficient of activity of a capped autonomous subunit is unlikely to affect significantly the behavior of the kinase in response to Ca^{2+} oscillations. This phosphorylation could instead play a role in CaM-dependent targeting of the kinase (Bayer and Schulman, 2001). Also, our simulations suggest that the remarkable ability of CaMKII to trap calmodulin upon autophosphorylation, which has been proposed to be crucial in the frequency-dependence of CaMKII autophosphorylation (Hanson and Schulman, 1992), only plays a small part in short-term frequency-dependent stimuli.

As shown theoretically (Lisman and Zhabotinsky, 2001 ; Kubota and Bower, 2001), phosphatases are expected to play an important role in determining the long-term (asymptotic) sensitivity of a CaMKII/phosphatase system and certainly have to be taken into account to gain a full understanding of the effect of Ca^{2+} spikes in the post-synaptic density. However, the property of a single enzyme to act as a frequency decoder is most probably a unique feature, which requires a deep and thorough understanding. The frequency-sensitivity of CaMKII, independent of other decoders, may be of particular significance in the short-term (transient) response to brief Ca^{2+} spikes. Appropriate pulsatile activation of CaMKII may indeed extend its activity significantly beyond the period of Ca^{2+} elevation. We performed a simulation that would mimic very brief Ca^{2+}-CaM spikes (1-10 ms) of high amplitude (1-5 μM CaM). We reasoned that CaMKII is likely to sense such brief elevations of Ca^{2+}-CaM. Indeed, the kinase is thought to target immediately next to Ca^{2+} sources [see (Bayer and Schulman, 2001) for review]. Furthermore, because 1) Ca^{2+} is rapidly dispersed and buffered inside cells and 2) accessible free CaM is limiting (Persechini and Stemmer, 2002), it is expected that the effective Ca^{2+} spike (e.g. above threshold for Ca^{2+}-CaM activation) that the kinase actually sees, when bound, for instance, to ion channels, can be as short as a few milliseconds. We found that high CaM concentrations (few μM, in the physiological range, (Persechini and Stemmer, 2002)) were necessary for CaMKII autophosphorylation upon stimulation with as much as 100 spikes of 1-10 ms (Figs VII.12B and VII.12C). Interestingly, the simulation showed that considerably high frequencies (>10Hz) were required to cause significant CaMKII autophosphorylation under several conditions of spike amplitude and duration.

CaMKII –and its autophosphorylation– have been shown to play an important role in frequency-dependent changes in synaptic plasticity [see (Lisman *et al.*, 2002) and (Rongo, 2002) for review]. The frequency sensitivity of the kinase under such brief spiking conditions theoretically predicted in Figs VII.12B and VII.12C suggests that this behaviour might be involved in specifically decoding synaptic stimuli. Whether CaMKII is actually exposed to such brief and repetitive Ca^{2+} spikes at synapses or at other cellular compartments, such as at the membranes of Ca^{2+} stores (Bayer and Schulman, 2001), is unknown. That is because we still know little about the precise nature of Ca^{2+} signals in neurones, in terms of kinetics, frequencies and amplitude at the submicron scale (Sabatini *et al.*, 2001, Klee and Vanaman, 1982 ; Verkhratsky, 2002). There are, however, growing examples of Ca^{2+} signaling

mechanisms in cells that operate via Ca^{2+} microdomains, for example near NMDA receptors, allowing specific messages to be transduced all the way down to the nucleus to regulate specific gene expression (Hardingham and Bading, 2003). It is safe to predict that the effective Ca^{2+}-CaM that can activate CaMKII at any given spike should be very limiting (Persechini and Stemmer, 2002). Hence, subtle changes in CaM availability at any given subcellular compartment would have a significant effect on the local CaMKII frequency-response.

An intriguing prediction from our model is that CaMKII frequency-dependence may be tuned to optimal frequencies (Figs VII.12B and VII.12C). In fact, closer look at experimental data (De Koninck and Schulman, 1998) revealed that this behavior has been observed experimentally (Fig VII.13C). As discussed above, this property of the enzyme is likely due to an effective prolongation of the Ca^{2+}/CaM stimulation protocol at optimal frequencies. Such feature would endow a means to maximally activate CaMKII without reaching very high spiking frequencies or a sustained Ca^{2+} elevation. This feature would provide 2 advantages: 1) it ensures preferential activation of CaMKII over other Ca^{2+} effectors that require sustained Ca^{2+} or higher frequency Ca^{2+} spikes for activation, thus ensuring some specificity in Ca^{2+} -dependent cascades; 2) it avoids any potential harmful effects of excessive Ca^{2+} stimulation.

In conclusion our model may prove to be useful in understanding the autoregulation of CaMKII and its functions in cells by providing testable predictions, especially in view of the fact that the agreement with the experimental results is quantitative for nearly all cases tested (in fact all but Fig. VII.9F). The tuned response of CaMKII to a fixed number of spikes, described above, is a good example; a deeper look at the experimental data indeed confirmed the theoretical prediction. Furthermore, the model may be useful to study other signaling cascades that utilize similar regulatory features. One example could be the phosphorylation of CaM kinase IV by CaM kinase kinase, which requires coincident binding of CaM on both enzymes (Soderling *et al.*, 2001). However, the autoregulation of CaMKII involves several other factors that should be eventually included in more elaborate models, such as ATP binding, the detailed description of the CaM dynamics (Klee and Vanaman, 1982 ; Verkhratsky, 2002 ; Craske *et al.*, 1999) or the sub-cellular spatial organization of Ca^{2+} signals (Schuster *et al.*, 2002 ; Petersen, 2002). The simplicity of our model, to simulate the behavior of this molecular decoder in isolation, should indeed allow its incorporation into more elaborate ones to progressively build up comprehensive cell signaling models.

VII.4. Link between fertilization-induced Ca^{2+} oscillations and relief from metaphase II arrest in mammalian eggs : a model based on calmodulin-dependent kinase II activation.

VII.4.1. Introduction

In mammals, oscillations in the level of cytosolic Ca^{2+} are the primary signal responsible for the early development of the egg after fertilization (Jaffe, 1983 ; Kline and Kline, 1992 ; Swann and Ozil, 1994 ; McDougall and Sardet, 1995). Two hypotheses have been put forward to explain how these Ca^{2+} spikes are triggered by the spermatozoon. First, oscillations could be brought about by a soluble protein, called 'oscillin' or 'sperm factor', introduced by the sperm in the mature oocyte (Parrington *et al.*, 1996 ; Saunders *et al.*, 2002). Alternatively, the primary trigger could be the activation of an external receptor on the oocyte, which in turn stimulates G protein (Miyazaki, 1988 ; Dupont *et al.*, 1996 ; Snow *et al.*, 1996) or tyrosine kinase activity (Foltz *et al.*, 1993) to generate inositol 1,4,5-trisphosphate ($InsP_3$), a universal messenger for Ca^{2+} release from internal stores. As well as the pathway by which fertilization triggers repetitive Ca^{2+} spikes, the signal transduction mechanism between Ca^{2+} increases on one hand, and egg activation and entry into mitosis on the other hand is much investigated; the latter mechanism is the focus of the present study.

Mammalian eggs are ovulated in metaphase II (MII) of meiosis, ready to be fertilized. In this state, the eggs are characterized by high levels of cyclin B and maturation promoting factors (MPF). The

latter heterodimer, made of p34cdc2 kinase (or cyclin dependent kinase 1) and of a B-type cyclin, is a key component of the cell cycle oscillatory mechanism: the level of MPF indeed peaks at each cellular division. MPF itself possesses a histone H1 kinase activity leading to chromosome condensation, nuclear envelope breakdown and spindle assembly. From a practical point of view, it is interesting to remember that the capacity of the oocytes to phosphorylate histone H1 can be used to estimate their level of MPF. Exit from metaphase and entry into anaphase results from MPF inactivation, which generally occurs through cyclin proteolysis (Murray and Hunt, 1993). Cyclin degradation occurs through the formation of an ubiquitin-cyclin complex (Glotzer *et al.*, 1991). The ensuing return to a basal level of MPF activity allows the fertilized egg to enter in interphase, as marked by the formation of pronuclei.

MII arrest is mediated by an activity referred to as cytostatic factor (CSF), a c-mos protooncogene product that prevents ubiquitin-dependent degradation of cyclins, and thus inactivation of MPF. CSF activity was first discovered in *Xenopus* eggs (Sagata *et al.*, 1989 ; Watanabe *et al.*, 1991) and was later shown to be responsible for MII arrest in mammalian eggs as well (Verlhac *et al.*, 1994). Translation of c-mos is induced by progesterone; the level of c-mos protein increases during maturation, reaching a maximum at MII. Then, CSF activity remains at a high stable level that prevents cyclin degradation. Just how CSF restrains the activation of the ubiquitin-dependent proteasome pathway responsible for cyclin degradation remains unclear, but this process probably involves the control of the dynamics of the microtubule network (Kubiak *et al.*, 1993 ; Moses and Kline, 1995 ; Winston *et al.*, 1995). It is known moreover that CSF arrest is mediated by enzymes of the mitogen-activated protein (MAP) kinase family (Verlhac *et al.*, 1996). In consequence, the level of CSF activity can be estimated by assaying the oocytes for their capacity to phosphorylate myelin basic protein (MBP), a well-known substrate for MAP kinases.

Although CSF prevents the degradation of cyclin, the inactivation of CSF itself is not required for the proteolysis of the cyclin subunit of MPF and for the resulting exit from meiotic metaphase. In cytosolic extracts from MII arrested eggs of both amphibians and mammals, MPF is inactivated before CSF (Watanabe *et al.*, 1991 ; Verlhac *et al.*, 1994). However, the time scale appears to be very different in both types of organisms; the lag time between MPF and CSF inactivation is of the order of 10 min in *Xenopus* oocytes (Watanabe *et al.*, 1991) but of 3 h in mouse oocytes (Verlhac *et al* ., 1994).

Both MPF and CSF can be inactivated by the Ca^{2+}/calmodulin-dependent protein kinase II (CaMKII) upon fertilization. A truncated, constitutively active form of CaMKII indeed suffices to induce cyclin degradation and p34cdc2 kinase inactivation in cytosolic extracts from MII-arrested *Xenopus* eggs (Lorca *et al.*, 1993 ; Morin *et al.*, 1994). In the same manner, activation of mouse eggs is significantly delayed in the presence of the calmodulin antagonist W-7 (Xu *et al.*, 1996).

There is little doubt that the Ca^{2+} rise brought about by fertilization is the primary event responsible for early egg activation. In non-mammalian species, for which *Xenopus* eggs are a good prototype, a large, but unique increase in cytosolic Ca^{2+} is observed at fertilization and suffices to activate the egg. The question thus remains as to the possible function of Ca^{2+} oscillations in CaMKII-mediated activation of mammalian eggs. In a more general context, it has been suggested that the repetitive rises in cytosolic Ca^{2+} observed in a large variety of cell types are a means by which information carried by the extracellular signal is conveyed into the cell interior in a frequency-encoded manner (Rapp and Berridge, 1981 ; Meyer and Stryer, 1991 ; Dupont and Goldbeter, 1992). These studies, which do not focus on any specific signalling system, remain rather speculative. In the case of mammalian fertilization, the role of Ca^{2+} oscillations has been experimentally approached in great detail, allowing for the development of a specific theoretical model.

Sophisticated methods of cell membrane electroporation by electrical field stimulation allow one to study the effect of submitting mature, unfertilized mammalian eggs to repetitive Ca^{2+} spikes of various periods and amplitudes (Ozil, 1990 ; Vitullo and Ozil, 1992 ; Ozil and Swann, 1995). All these studies report that eggs are most successfully activated by repetitive Ca^{2+} spikes. In mouse eggs, the rate of pronucleus formation, which marks the entry of the fertilized egg into interphase before the first

mitotic division, increases with the frequency of the artificially induced Ca^{2+} spikes (Ozil and Swann, 1995). However, oscillations of Ca^{2+} are not a prerequisite for egg activation. In mice, parthenogenetic activation by high levels of ionophore can also be achieved (Vincent *et al.*, 1992); it is interesting to mention that activation by such a monotonous Ca^{2+} increase can only be carried out on 'old' eggs, in which the level of active MPF has started to decrease spontaneously. Equally interesting is the fact that after intracytoplasmic sperm injection of human eggs (ICSI), a non-oscillatory Ca^{2+} response is sometimes produced, and is compatible with the development of two pronuclei. No data however exist to assess the developmental potential of such zygotes (Tesarik, 1994). In summary, it appears that in mammals early parthenogenetic development of eggs is favoured by an oscillatory pattern of Ca^{2+} increases, although such repetitive spikes are not absolutely required.

A recent study performed on rabbit oocytes provides some biochemical clue to the understanding of the role of oscillatory Ca^{2+} dynamics at fertilization in mammals. It is shown indeed that the H1 kinase activity, which directly reflects the level of active MPF, rapidly decreases after the first, artificially induced Ca^{2+} spike. However, this inactivation is only transient. Repetitive Ca^{2+} increases are necessary to keep MPF inactivated on an extended period of time (Collas *et al.*, 1995).

In the present study (Dupont, 1998), we propose a theoretical model that could account for the fact that egg activation is optimized by an oscillatory Ca^{2+} signal. We assume that Ca^{2+} oscillations are generated independently from the cell cycle oscillator, but that Ca^{2+} affects the behaviour of the cell cycle at various levels. The model is based on the activation of CaMKII by cytosolic Ca^{2+}. The latter activated protein in turn possesses a dual role: on one hand, it triggers a decrease in CSF activity at each Ca^{2+} spike and on the other hand, active CaMKII indirectly induces MPF inactivation through a CSF-independent pathway. As the molecular mechanisms by which CaMKII governs MPF and CSF inactivation still remains to be elucidated, we assume in the present study that the different processes occurring in response to Ca^{2+} elevations are brought about by a cascade of post-translational modifications. The dual effect of Ca^{2+} on MPF activity (direct or mediated by CSF) is at the basis of the temporal pattern of MPF inactivation reproduced by the model; although a few Ca^{2+} spikes suffice to decrease transiently MPF activity, MPF can be kept inactivated for an extended period of time only if the total number of Ca^{2+} spikes is sufficient to bring CSF below a threshold level. The model also accounts for egg activation after ionophore application in appropriate conditions, as well as for arrest in metaphase III (MIII). The latter MIII arrest can be experimentally observed when an insufficient number of Ca^{2+} spikes is applied to the system or if a low dose of ionophore is given to a freshly ovulated egg (Vincent *et al.*, 1992). Finally, the present analysis predicts that no cellular division can occur as long as the egg is subjected to stimulation by repetitive Ca^{2+} spikes, a property of the model which could be easily tested experimentally.

In the following, we use a model previously developed for the embryonic cell cycle in *Xenopus* oocytes (Goldbeter, 1991). Our results however remain qualitatively independent from the detailed mechanism supposed to underlie periodic variations in MPF (Tyson, 1991). On the other hand, in the numerical simulations, the Ca^{2+} spikes are generated at regular time intervals by a mathematical function, to get, in a simple way, spikes of appropriate characteristics. Any biochemical model for Ca^{2+} oscillations (see (Sneyd *et al.*, 1995) ; (Tang *et al.*, 1996) and (Schuster *et al.*, 2002) for reviews) could also be used without altering the following results, as we do not assume any feedback of the species governing the cell cycle machinery on the mechanism generating the Ca^{2+} spikes. The important assumptions of the model concern the relationship between Ca^{2+} and MPF inactivation.

VII.4.2. Model

Overview of the minimal model previously proposed for the cell cycle

Unfertilized mammalian eggs are arrested in the metaphase of the second meiosis, in a state characterized by a high level of cyclin, and thus also a high level of the dimeric complex made of $p34^{cdc2}$ kinase and cyclin, called MPF. Here, it is assumed that except for the role of Ca^{2+}, the

termination of the second meiosis is governed by the same essential biochemical processes as the metaphase-anaphase transition in the mitotic cell cycle.

The periodicity of the cell cycle relies on a biochemical oscillator in which MPF plays a central role, each division being driven by a peak in MPF activity. The grey-shaded region of Fig. VII.14 provides a schematical representation of the minimal model for MPF oscillations proposed previously (Goldbeter, 1991), and used in the present study. The model considers three variables, namely the concentration of cyclin B (C), the fraction of active cdc2 kinase (M) and the fraction of active proteolytic complex (X). Cyclin B (C) is synthesized at a constant rate. It activates a phosphatase, called cdc25, which brings the inactive cdc2 (M+) in an active, dephosphorylated state (M). In reality, the active species is made of a complex between cyclin B and cdc2, but the inclusion of a step accounting for the formation of such a heterodimer does not qualitatively affect the behaviour of the model (Romond *et al.*, 1994). Phosphorylation (deactivation) of cdc2 is mediated by the wee1 kinase. Unphosphorylated cdc2 (M) triggers the activation of a proteolytic complex (X) known as APC (anaphase promoting complex), which labels cyclins for degradation through the ubiquitin pathway. Inactivation of APC occurs through dephosphorylation by a phosphatase. The negative feedback exerted by X on the level of cyclin is at the core of the oscillatory mechanism. Autocatalytic activation of cdc2 kinase, reported by some experimental studies (Cyert and Kirschner, 1988 ; Strausfeld *et al.*, 1991) and considered in other models (Tyson, 1991), can also be incorporated in the present model but appears unnecessary for the occurrence of oscillations (Goldbeter, 1993).

The temporal evolution of the three variables of the minimal model is thus given by the following ordinary differential equations (see Refs. (Goldbeter, 1991 ;1993) for a detailed presentation of the model) :

$$\frac{dC}{dt} = v_i - v_d X \frac{C}{K_d + C} - k_d C \qquad \text{(VII.12)}$$

$$\frac{dM}{dt} = V_{M1} \frac{C}{K_c + C} \frac{1 - M}{K_1 + 1 - M} - V_2 \frac{M}{K_2 + M} \qquad \text{(VII.13)}$$

$$\frac{dX}{dt} = V_{M3} M \frac{1 - X}{K_3 + 1 - X} - V_4 \frac{X}{K_4 + X} \qquad \text{(VII.14)}$$

In the above equations, C represents the concentration of cyclin B and is thus expressed in μM. In contrast, M and X both represent fractions of active protein, i.e. the concentration of the active form divided by the total concentration of the protein considered. In consequence, these quantities are dimensionless and (1 - M) and (1 - X) represent the fraction of inactive cdc2 kinase and of inactive APC, respectively. As to the parameters, v_i represents the constant rate of cyclin B synthesis, while v_d is its maximal degradation rate by X. K_d denotes the Michaelis constant for cyclin degradation. A non-specific degradation of cyclin B, characterized by a first order rate constant k_d, is also considered. Activation (dephosphorylation) of cdc2 kinase occurs at a maximal velocity noted V_{M1}, and is activated by cyclin through a michaelian process characterized by a constant K_c. V_2 stands for the maximal velocity of cdc2 deactivation (phosphorylation). Both V_{M1} and V_2 have been scaled by the total concentration of kinase. V_{M3} and V_4 are the scaled maximal velocities of the kinase and phosphatase supposed to activate and deactivate APC (X), respectively. The K_i (i = 1–4) represent the Michaelis constants characterizing the activation and deactivation processes, divided by the total amount of kinase (for K_1 and K_2) or of APC complex (for K_3 and K_4).

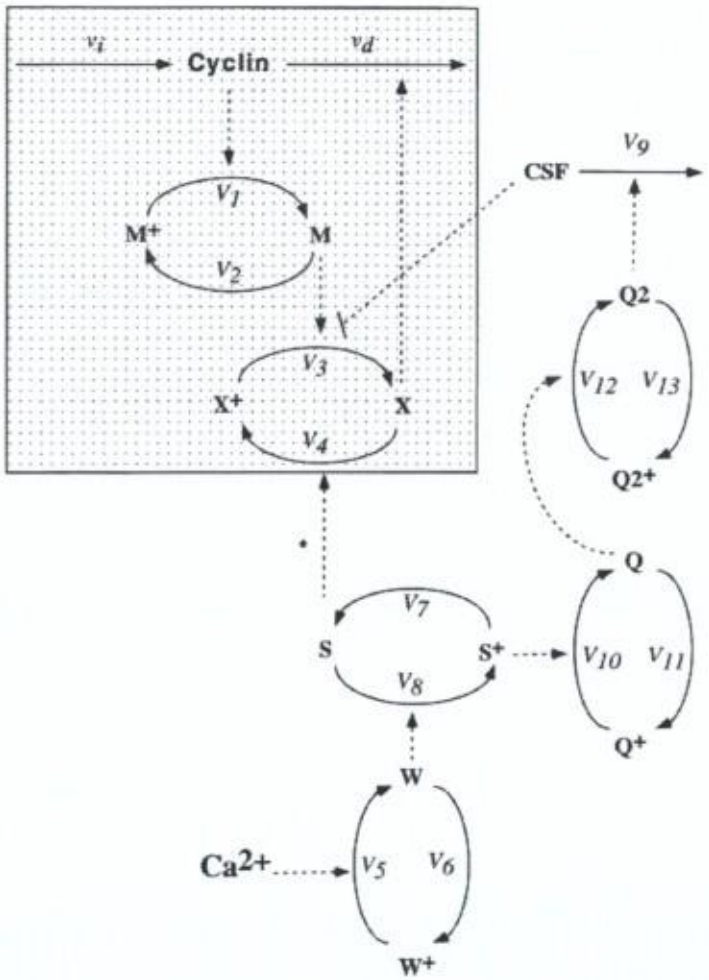

Fig. VII.14. Schematic representation of the mathematical model proposed to account for the effect of Ca^{2+} oscillations on MII arrested mammalian eggs. The grey-shaded region represents the model proposed previously for the early embryonic cell cycle (Goldbeter, 1991). Eggs are arrested in MII due to a high level of CSF, which inhibits the activation of the APC complex which initiates the degradation of cyclin. Ca^{2+} is supposed to activate CaMKII (*W*). The active form of this enzyme phosphorylates a hypothetical mediator protein (*S* into *S**). *S* deactivates the anaphase promoting complex *X*, while *S** indirectly leads to CSF inactivation. The different loops represent reversible phosphorylation pathways. Dashed arrows indicate activations, while the dashed line terminated by a hyphen stands for an inhibition. *C* stands for cyclin, *M* for MPF, *X* for the ubiquitin-dependent APC and *W* for CaMKII. Other letters represent unknown, hypothetical protein substrates. The * indicates the inactive form of the protein in all cases, except for the mediator *S* for which both forms are assumed to be active in different pathways. See text for details.

Sustained oscillations occur in the model provided that thresholds exist in the dependence of *M* on *C*, and of *X* on *M*; these sharp dependences are fulfilled as long as all the K_i's are considerably smaller than 1. Oscillations in the level of cyclin B, MPF and APC complex as obtained with the model defined by Eqs. (VII.12-14) are shown in Fig. VII.15A. These oscillations can be suppressed by appropriate changes in the maximal velocities characterizing the diverse activation and deactivation processes. Unfertilized mature eggs are arrested in a state of high cyclin and MPF because CSF prevents the degradation of cyclin. Of particular interest for modelling the MII arrest in the system defined by Eqs. (VII.12-14) is the fact that decreasing the maximal velocity of activation of the APC complex (V_{M3}) in the model described above, allows the system to quit the oscillatory domain; a steady state characterized by high levels of both cyclin and MPF is then established (Fig. VII.15.B; see also Strausfeld *et al.*, 1991). As to the mammalian MII arrest, we assume that CSF inhibits the transformation of the APC complex into an active form. This inhibition could be indirect, i.e. CSF

could have an effect at various stages of the ubiquitin pathway, but, for sake of simplicity, we consider that CSF directly inhibits the transformation of X^* into X (see Fig. VII.14). In the following, the situation shown in Fig. VII.15B will be considered as an initial condition for studying the effect of an oscillatory Ca^{2+} signal on MII arrested eggs.

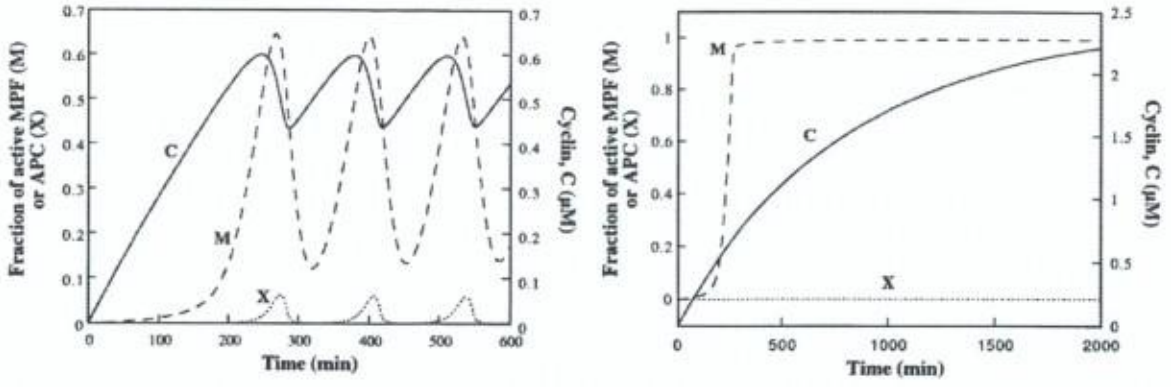

Fig. VII.15. (A) Sustained oscillations of cyclin, active MPF and active APC in the minimal model for the cell cycle (Goldbeter , 1991). Results have been obtained by numerical integration of Eqs. (VII.12-14) with the following parameter values: $v_i = 0.003$ μM min^{-1}, $v_d = 0.18$ Mμmin^{-1}, $K_d = 0.05$ μM, $k_d = 0.0012$ min^{-1}, $V_{M1} = 0.36$ min^{-1}, $K_c = 0.5$ μM, $V_2 = 0.186$ min^{-1}, $V_{M3} = 0.072$ min^{-1}, $V_4 = 0.048$ min^{-1}, $K_1 = K_2 = K_3 = K_4 = 0.005$. The total concentrations of MPF and APC are both supposed to be equal to 4 μM. (B) Arrest of the cell cycle in a state characterized by high levels of cyclin and active MPF, and by a low level of APC complex X, which corresponds to the situation observed in MII arrest. Cyclin concentration also evolves to a stable steady state ($C = 2.4$ μM). Results have been obtained by numerical integration of Eqs. (VII.12-14) with the same parameter values as in (A), except for $V_{M3} = 0.0045$ min^{-1}.

Full model for the resumption of the cell cycle in MII arrested eggs : rationale.

The model proposed to account for the Ca^{2+}-induced relief of mammalian eggs from MII arrest is schematized in Fig. VII.14. As mentioned above, the grey shaded region represents the minimal mechanism previously proposed to account for periodic MPF activity (Goldbeter, 1991); the remaining part indicates how Ca^{2+} and CSF are supposed to affect this oscillatory activity. It is assumed that Ca^{2+} and CSF both interfere with the cell cycle machinery by affecting the cyclin degradation pathway, i.e. the characteristics of the reversible phosphorylation loop of the APC complex noted X.

The first assumption is that CSF inhibits the transformation of X into the active state. To consider that CSF activity has reached its maximum in the mature egg ready to be fertilized, we assume in the model that CSF is initially at a high arbitrarily chosen value, and that this level can only decrease in response to Ca^{2+}. There is no renewal of CSF once fertilization has occurred. The latter level of CSF inhibits cyclin degradation.

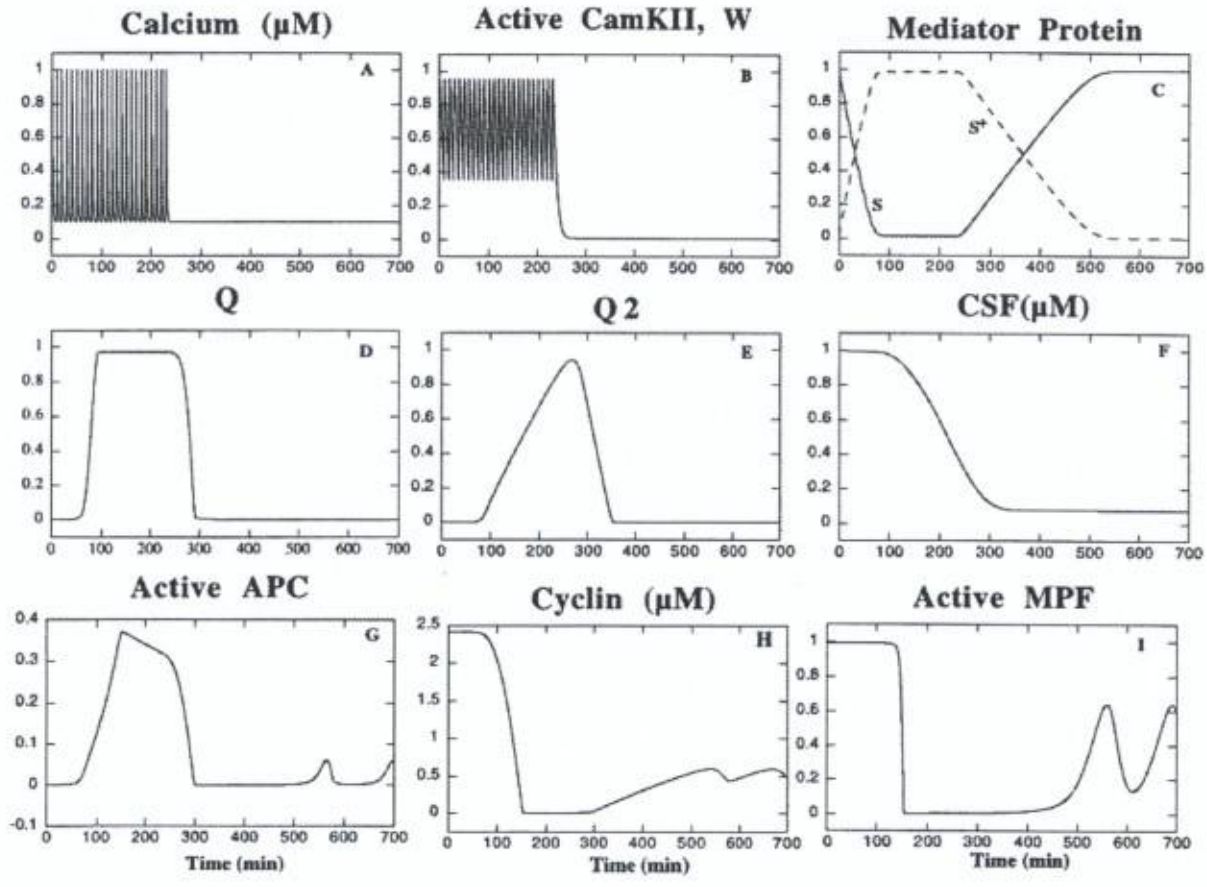

Fig. VII.17. Numerical simulation of the full model for the resumption of the cell cycle schematized in Fig. VII.14. Results have been obtained by numerical integration of the system defined by Eqs. (VII.12-13), (VII.15-20) using a simplified mathematical representation of the Ca^{2+} dynamics (see text for details). Parameters values are the same as in Fig. VII.15A with $V'_{M3} = 0.072$ min^{-1}, $V'_{M4} = 0.048$ min^{-1}, $K_1 = 0.5$ mM, $V_5 = 8.0$ min^{-1}, $V_6 = 0.2$min^{-1}, $K_5 = K_6 = 1$, $K_A = 0.7$ μM, $W_T = 10$ μM, $V_7 = 0.0045$ min^{-1}, $V_{M8} = 0.03$ min^{-1}, $K_7 = K_8 = 0.05$, $V_{M9} = 0.015$ μM min^{-1}, $K_9 = 0.5$, $k_9 = 0.0001$ min^{-1}, $V_{M10} = 0.2$ min^{-1}, $V_{M11} = 0.14$ min^{-1}, $V_{M12} = 0.02$ min^{-1}, $V_{M13} = 0.014$ min^{-1}, $K_{10} = K_{11} = K_{12} = K_{13} = 0.01$, $S_T = Q_T = Q_{2T} = 1$ μM. The Ca^{2+} dynamics is characterized by a period equal to 10 min, a basal level and a maximal amplitude equal to 0.1 and 1 μM, respectively, a half-width for exponential decay equal to 1.5 min and a total number of spikes equal to 24. The Ca^{2+}-independent decrease in CSF (term $-k_9\ CSF$ in Eq. VII.19) begins at time 0, i.e. simultaneously with the onset of the first Ca^{2+} spike.

An increase in cytosolic Ca^{2+} then deactivates CSF: according to experimental results (see section VII.3), it is assumed that Ca^{2+} activates CaMKII (W), which itself triggers the activation of a hypothetical protein substrate, called S. The latter species must be viewed as a still unidentified 'mediator' between CaMKII and the activity of the APC complex. The phosphorylated form of this substrate, denoted S+, triggers the degradation of CSF through two reversible phosphorylation loops. These loops introduce time-delays in the model, a phenomenon that will allow us to account for the observation that CSF isinactivated well after MPF (see below).

In principle, the latter model (i.e. Fig. VII.14 in which the dashed line marked * is ignored) could account on its own for the fact that a sufficient increase in cytosolic Ca^{2+} can resume the cell cycle. After an appropriate Ca^{2+} increase indeed, the inhibition of APC activation would be relieved and the cell cycle machinery could resume. It can be intuitively foreseen, however, that this mechanism in which CSF is the only brake to cell cycle resumption is not able to account for at least three main experimental observations. First, such a model would predict that the decrease in MPF activity always

follows that in CSF, while the opposite sequence is experimentally observed (Watanabe *et al.*, 1991 ; Verlhac *et al.*, 1994). Second, such a scheme cannot explain why, in rabbit oocytes, the Ca^{2+}-induced decrease in the level of active MPF is only transient if the number of Ca^{2+} spikes applied to the egg is too low (Collas *et al.*, 1995). Finally, this system cannot account for the so-called MIII arrest, a pathological state resulting from an incomplete activation of the egg (Vincent *et al.*, 1992 : Kubiak, 1989). In this case indeed, extrusion of the second polar body is observed, a phenomenon which reflects a decrease in the level of MPF activity, but, afterwards, a new metaphase spindle is formed, suggesting that MPF activity has risen again; this arrested egg can be reactivated. The second assumption of the model is that there is some CSF-independent pathway for egg activation by Ca^{2+}. The central idea of the full model is to assume that CaMKII has a dual role, and affects the level of active APC both indirectly through CSF inactivation and directly through activation of the APC complex (see Fig. VII.14). We thus consider that the mediator S, whose phosphorylation finally results in CSF inactivation, also possesses some intrinsic activity when it is unphosphorylated: the transformation of the APC from its active (X) to its inactive (X^*) form is assumed to be activated by the unphosphorylated form of the mediator. As S is high in the absence of Ca^{2+} and decreases in response to Ca^{2+} spikes, increasing cytosolic Ca^{2+} triggers a decrease in the rate of inactivation of X. The resulting higher level of active APC in turn triggers cyclin degradation. This mechanism provides a rapid and CSF-independent control of the level of active MPF by cytosolic Ca^{2+}.

Mathematical equations of the full model

In addition to the three variables of the basic cell cycle model, five other variables need to be considered in the full model. As the detailed kinetics of the events occurring at cell cycle resumption is far from being identified, the model is phenomenological. The dynamics of activation–deactivation of CaMKII (W) is described by a reversible phosphorylation loop, the interconversion between both forms being catalyzed by a kinase and a phosphatase acting with Michaelis–Menten kinetics (Dupont and Goldbeter, 1992b ; Goldbeter and Koshland, 1981). Thus, the evolution of the fraction of active CaMKII is given by the following differential equation:

$$\frac{dW}{dt} = V_5 \frac{1-W}{K_5+1-W} - V_6 \frac{W}{K_6+W} \qquad \text{(VII.15)}$$

in which : $V_5 = V_{M5} \dfrac{Z^4}{K_A^4 + Z^4}$

In these equations, W is defined as the concentration of CaMKII in the active form, with W_T being the total amount of protein substrate. The fraction of inactive CaMKII is thus given by (1-W). Moreover, V_{M5} and V_6 denote the effective maximal rates of the kinase and the phosphatase, divided by W_T; K_5 and K_6 are the normalized Michaelis constants of the two latter enzymes. K_A denotes the threshold constant of activation of the kinase by cytosolic Ca^{2+}. The Hill coefficient taken as equal to 4 allows for the observed high level of cooperativity in the activation of CaMKII by Ca^{2+} (Schulman, 1988). Active CaMKII (W) triggers the phosphorylation of S into S^*. Thus:

$$\frac{dS}{dt} = V_7 \frac{1-S}{K_7+1-S} - V_8 \frac{S}{K_8+S} \qquad \text{(VII.16)}$$

in which $V_8 = V_{M8}$ and where S represents the fraction of unphosphorylated mediator protein. V_7 and V_{M8} denote, respectively, the maximal rates of phosphorylation and dephosphorylation, divided by the total amount of substrate (S_T). K_7 and K_8 are the normalized Michaelis constants associated with these processes. The phosphorylated form of S (S^*) allows another protein to become active. If Q_T is the total

concentration of this substrate, Q and Q^* (=1-Q) represent the fraction of protein into the active and inactive state, respectively. The evolution of the fraction of substrate in the active form is given by:

$$\frac{dQ}{dt} = V_{10}\frac{1-Q}{K_{10}+1-Q} - V_{11}\frac{Q}{K_{11}+Q} \qquad \text{(VII.17)}$$

in which $V_{10} = V_{M10}(1-S)^4$

V_{M10} and V_{11} indicate, respectively, the maximal rates of activation and inactivation, divided by Q_T. K_{10} and K_{11} are the normalized Michaelis constants associated with these processes. Activation of Q by the phosphorylated form of the mediator S is assumed to be highly cooperative. In the same manner,

$$\frac{dQ_2}{dt} = V_{12}\frac{1-Q_2}{K_{12}+1-Q_2} - V_{13}\frac{Q_2}{K_{13}+Q_2} \qquad \text{(VII.18)}$$

in which $V_{12} = V_{M12}Q$.

Parameters related to Eq. VII.18 have been defined in the same manner as in Eq. VII.17.

The ultimate effect of the pathway defined by Eqs. VII.15-18 is to trigger CSF inactivation. This phenomenon is supposed to obey the following kinetics:

$$\frac{dCSF}{dt} = V_{M9}Q_2\frac{CSF}{K_9+CSF} - k_9 CSF \qquad \text{(VII.19)}$$

where V_{M9} stands for the maximal velocity of *CSF* inactivation and K_9 is the half-saturation constant of this process. We also assume that *CSF* can be inactivated in a Ca^{2+}-independent manner with first-order kinetics (k_9). This term, which is much smaller than the Ca^{2+}-activated degradation of *CSF*, reflects that, as time goes on, less Ca^{2+} is needed to activate the egg; following Eq. VII.19 indeed, the level of *CSF* will spontaneously decrease, thus allowing the APC complex to slowly reactivate. For simplicity, the level of *CSF* activity is represented by the concentration of the still unknown species assumed to play that role.

Finally, we have to transform Eq. VII.14, which gives the evolution of the fraction of active APC complex, to incorporate the regulations of its activation–deactivation loop by *CSF* and by the unphosphorylated mediator *S*. Eq. VII.14 becomes:

$$\frac{dX}{dt} = V_3\frac{1-X}{K_3+1-X} - V_4\frac{X}{K_4+X} \qquad \text{(VII.20)}$$

in which $V_3 = V'_{M3}M\dfrac{K_i^4}{K_i^4+CSF^4}$ and $V_4 = V'_{M4}S$.

K_i stands for the constant characterizing the inhibition by *CSF* of APC activation. Eqs. VII.12-13, VII.15-20 represent a system of eight ordinary differential equations which can be numerically integrated. In the simulations, fertilization is assumed to correspond to the time at which Ca^{2+} is increased in a stepwise manner up to a fixed, maximal amplitude. Ca^{2+} is then decreased following an exponential law back to its basal level. This artificial procedure to generate a Ca^{2+} spike is repeated periodically. The Ca^{2+} dynamics is thus characterized by a resting level $[Ca^{2+}]_0$, a maximal amplitude A, a period T and a half-time for exponential decay from A to $[Ca^{2+}]_0$, τ.

VII.4.3. Simulations of Ca^{2+}-induced relief from metaphase II arrest in mammalian eggs

After fertilization, mouse oocytes display Ca^{2+} oscillations with a period typically equal to 10 min, although a high variability can be observed among different individuals of the same species (Vitullo and Ozil, 1992). These oscillations can last for up to 4 h. Fig. VII.16A shows the temporal pattern of repetitive Ca^{2+} spikes which has been chosen to mirror the physiological situation (24 Ca^{2+} spikes of 1 μM amplitude, with a periodicity of 10 min and a half-time for exponential decay equal to 1.5 min). According to Eq. VII.15, these repetitive Ca^{2+} increases lead to successive spikes in the level of activated CaMKII (Fig. VII.16B). The high level of cooperativity in CaMKII activation by Ca^{2+} allows the fraction of active CaMKII to follow the same temporal pattern as the level of Ca^{2+}. It is important to note that CaMKII does not return to basal activity between two successive Ca^{2+} spikes; this is due to the fact that V_6 has been taken smaller than V_5 (i.e. the rate of dephosphorylation of CaMKII is low, as compared to the rate of phosphorylation). Such a partial deactivation of CaMKII is important in the behaviour of the full model, as we will see below. These peaks in CaMKII activity in turn induce the progressive transformation of S into S^* (see Eq. VII.16 and Fig. VII.16C); the maximal velocity of the latter transformation is such that only a small fraction of this mediator protein can be converted in response to a Ca^{2+} peak (low value of V_{M8} as compared to the Ca^{2+} dynamics). Moreover, it is assumed that the system has no time to reverse between two spikes, a phenomenon which allows the CSF degradation pathway to integrate the total number of Ca^{2+} spikes. The absence of transformation of S^* into S between two Ca^{2+} spikes is due both to the assumption that V_7 is smaller than V_{M8} and to the fact that the fraction of CaMKII in the active form remains relatively high (about 0.4) between two Ca^{2+} spikes.

Crucial to the behaviour of the model is the fact that the CaMKII-induced changes in the balance between the S and S^* form of the mediator has two effects. First, the decrease in the fraction of substrate in the S form directly affects the activity of the APC complex (X), responsible for cyclin degradation (Fig. VII.16G). As S decreases, the balance between the active (X) and inactive (X^*) forms of the APC complex switches towards the active form. As a direct result, the level of cyclin drops (Fig. VII.16H), and consequently, the level of MPF (Fig. VII.16I). This stage corresponds to the entry of the fertilized egg in interphase. On the other hand, the increase in the amount of mediator in the S+ form leads to a progressive decrease in CSF activity (Fig. VII.16F). Owing to the existence of two reversible phosphorylation loops between S^* and the decline in CSF activity (see Fig. VII.16D for Q and Fig. VII.16E for Q_2), CSF inactivation is delayed with respect to the primary Ca^{2+} increases. Finally, when both CSF activity and Ca^{2+} have come down to their basal levels, MPF can rise again and induce the first mitosis of the embryo.

The complex dynamics of this eight-variable system can be better understood when resorting to the analysis shown in Fig. VII.17. There, the region of oscillations in the minimal, three-variable cell cycle model (defined by Eq. VII12-14) is shown as a function of V_{M3} and V_4 (see also (Goldbeter and Guilmot, 1996)). The other variables of the full model interfere with the minimal model through these two maximal velocities characterizing the reversible phosphorylation loop of the APC complex (X). Thus, different typical situations of the full model can be visualized in this V_{M3}/V_4 stability diagram, thus allowing for a qualitative understanding of the dynamics of the eight-variable system. In fact, to visualize a given state of the full model in the stability diagram of the three-variable model, one has to consider that V_{M3} is given by

$$V_{M3}^{'}\frac{K_i^4}{K_i^4+CSF^4} \text{ and } V_4 \text{ is given by } V_{M4}^{'}S.$$

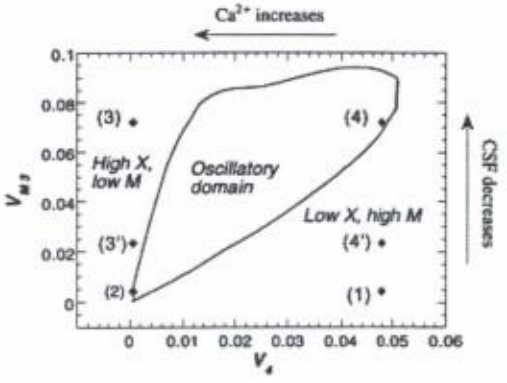

Fig. VII.17. Stability diagram of the minimal model for the cell cycle defined by Eq. VII.12-15, in the (V_4, V_{M3}) parameter space. These maximal velocities characterize, respectively, deactivation and activation of the APC complex. The evolution of the full, eight variable model in the same conditions as in Fig. VII.16 is successively represented by four points referred to as (1) to (4). (1) is the initial state of the system in MII arrest, characterized by a high level of CSF and a basal level of Ca^{2+}. (2) represents the situation after eight Ca^{2+} spikes. APC has been activated, allowing the active MPF to decrease and the egg to enter in interphase. CSF is still active. (3) represents the situation after 20 Ca^{2+} spikes; CSF is inactivated. (4) represents the state of the system once Ca^{2+} oscillations have stopped. This state is oscillatory, corresponding to the resumption of the cell cycle. The points indicated (3') and (4') stand for the situation simulated in Fig. VII.18, in which the number of Ca^{2+} spikes is not sufficient to restart the cell cycle. The values of the variables at the various points have been obtained by numerical integration of the full model.

The values of *CSF* and *S* are numerically evaluated at various characteristic stages. The initial state of the system simulated in Fig. VII.16 corresponds to a MII arrested egg characterized by a high level of *CSF* (1 μM) and a basal level of Ca^{2+} (0.1 μM). In such a state, *S* is high. The location of this point in the stability diagram (point (1) in Fig. VII.17) corroborates the fact that this state is stable and characterized by a low value of the fraction of active APC complex (*X*) and a high value of active MPF (*M*). Fertilization is simulated by applying to the system a series of Ca^{2+} spikes which repetitively activate CaMKII. Their first effect is to decrease *S* (and thus V_4). After this rapid decline, the state of the system corresponds to the point marked (2) in the stability diagram. This point is just on the opposite side of the oscillatory domain and corresponds to a stable state with a high fraction of active APC complex (*X*) and a low level of active MPF. This situation is reminiscent of what is observed during interphase. The second and slower effect of the Ca^{2+} spikes is to gradually decrease *CSF* activity. Thus, the value of V_{M3} progressively increases up to the point marked (3) in the stability diagram. The corresponding levels of cyclin, APC complex (*X*) and MPF are not significantly altered by the latter change. In contrast, when the Ca^{2+} spikes finally stop, V_4 rapidly increases again up to the point (4) which is in the oscillatory domain and thus corresponds to the resumption of the cell cycle.

The results shown in Fig. VII.16 have been obtained when assuming that most loops in the model (*M*, *X*, *S*, *Q* and Q_2) exhibit a threshold-like behaviour. In Fig. VII.16, these thresholds originate from the fact that the various kinases and phosphatases act in their region of zero-order kinetics (Goldbeter and Koshland, 1981), meaning that the enzymes are saturated by their substrates. Other assumptions as high levels of cooperativity or the inclusion of intermediate loops could however much relax these constraints on the parameter values, at the expense of an increased complexity of the model.

VII.4.4. Effect of the number, frequency and amplitude of Ca^{2+} spikes

Reducing the number of spikes at a given frequency

The theoretical model presented above can be used to investigate how the number of Ca^{2+} spikes affects the evolution of MPF. In Fig. VII.18, the number of Ca^{2+} spikes has been reduced as compared

to the situation shown in Fig. VII.16 (14 spikes in Fig. VII.18 as against 24 in Fig. VII.16); the period of Ca^{2+} oscillations remains unchanged. In the case of a low number of Ca^{2+} spikes, although MPF drops after eight Ca^{2+} spikes, this decline is only transient. The fraction of active MPF progressively rises back to a stable, elevated level when Ca^{2+} returns to its steady-state value. The dashed line in Fig. VII.18 indicates that CSF has only decreased by ~40% in response to 14 Ca^{2+} spikes, which explains the high stable level of active MPF. This situation is reminiscent of both the transient decrease in active MPF observed, *in vitro*, in rabbit eggs (Collas *et al.*, 1995) and of the MIII arrest reported in vivo for mouse eggs (Vincent *et al.*, 1992). From a theoretical point of view, one can understand this behaviour by resorting to the stability diagram shown in Fig. VII.17. In this figure, the points representative of the simulation shown in Fig. VII.18 are indicated by (1), (2), (3') and (4'). Because of an insufficient CSF inactivation (i.e. a too low increase in V_{M3} from (2) to (3')), the system does not end up in an oscillatory state when Ca^{2+} returns to its basal level.

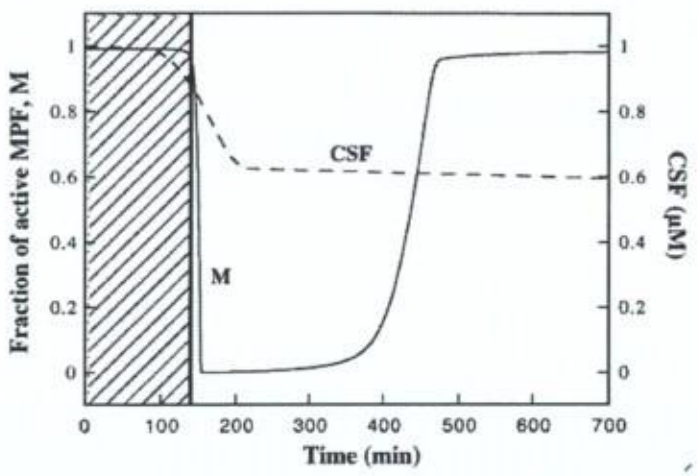

Fig. VII.18. Simulation of MIII arrest in an egg which has been stimulated by an insufficient number of Ca^{2+} spikes. The dashed region shows the time during which the system has been stimulated by repetitive Ca^{2+} increases with a periodicity of 10 min. MPF activity (plain line) decreases in response to Ca^{2+} spikes, but, as the number of Ca^{2+} spikes is too low, CSF activity (dashed line) does not decline to the basal level. Thus, MPF activity rises again when Ca^{2+} oscillations stop. Results have been obtained as in Fig. VII.16, except for the fact that the total number of Ca^{2+} spikes characterizing the Ca^{2+} dynamics is here taken as equal to 14.

Experiments performed with Ca^{2+} ionophores indicate that mature eggs can sometimes be activated in response to one Ca^{2+} spike. Such a situation can in principle be accounted for by the model, as shown in Fig. VII.19. In this figure, the half-time for exponential decay of the level of cytosolic Ca^{2+} is 70 min. A detailed numerical investigation of the behaviour of the model shows that, to decrease CSF back to the basal level and thus to allow for irreversible cell cycle resumption, Ca^{2+} has to remain elevated above a threshold value of 0.5 μM for 70 min (either continuously, or repetitively with a period which is short as compared to the intrinsic evolution of the APC complex (X), as we will see below). From a biological point of view, such a sustained Ca^{2+} increase would be lethal for the cell. In the model, a Ca^{2+} spike of much shorter duration can however activate the egg if it is assumed that the initial level of CSF activity is lower than in Fig. VII.16 (not shown). The latter situation could correspond to an 'older egg', in which the level of CSF has spontaneously declined, due to some endogenous protease activity. In that respect, it is interesting to mention that, in some cases, old eggs can even spontaneously activate. In summary, the present simulations suggest that egg activation by a non-oscillatory Ca^{2+} increase can be obtained either with a long-lasting stimulation by Ca^{2+}, or by assuming that CSF activity at time of activation is low, as it could be the case in old eggs.

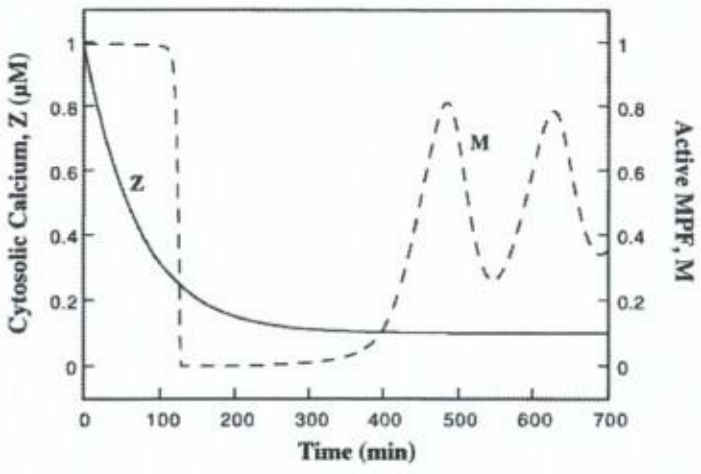

Fig. VII.19. Simulation of cell cycle resumption by a unique, long-lasting Ca^{2+} spike. The evolution of cytosolic Ca^{2+} is shown by the plain line, while the dashed line indicates the corresponding evolution of the level of active MPF. Results have been obtained as in Fig. VII.16, except for the fact that the number of Ca^{2+} spikes characterizing the Ca^{2+} dynamics is here equal to 1 and that the half-time for the exponential decay of this spike is taken as equal to 70 min.

Varying the frequency or the amplitude of the repetitive Ca^{2+} spikes

The effect of changing the frequency or the amplitude of Ca^{2+} oscillations is shown in Fig. VII.20. Two aspects must be considered. First, one can compute the time necessary to decrease MPF, which would correspond to the entry in interphase. In Fig. VII.20A, Ca^{2+} spikes of various frequencies are applied to the system. There is no restriction in the number of spikes, i.e. the latter are applied as long as necessary to inactivate MPF. In this case, the time to decrease MPF increases in a roughly exponential manner with the period of Ca^{2+} oscillations. The latter relation reflects the balance between activation and deactivation in the various loops involved in the transduction pathway between Ca^{2+} and cyclin degradation. As long as during a spike Ca^{2+} remains above the threshold value for CaMKII activation, the results are barely affected by the amplitude of oscillations. These results can be compared with the experiments performed by Ozil and Swann (1995) in which they varied the period of artificially induced Ca^{2+} spikes in mouse oocytes; in that system, the time for the pronucleus to become visible, a phenomenon which marks the entry in interphase, and thus the decline in the level of MPF, clearly increases in parallel with the period of the Ca^{2+} spikes. No attempt was made in the latter experiments to vary the amplitude of these artificially induced Ca^{2+} oscillations.

Second, one can compute the time between the first Ca^{2+} spike and the first peak in MPF, which would correspond to the first mitosis, as a function of the period of Ca^{2+} oscillations. In Fig. VII.20B, it is considered that the system is stimulated during 4 h by Ca^{2+} spikes of various frequencies. In consequence, the total number of spikes also varies from one numerical simulation to the other. The reason why such a 'protocol' has been adopted (and not the same as in Fig. VII.20A) is that, in our simulations, there is no cell cycle resumption as long as Ca^{2+} is spiking, as it will be discussed in the following section. Fig. VII.20B clearly shows that the time laps between the onset of stimulation and the first peak in MPF is little affected (~4%) by the frequency of the Ca^{2+} spikes. This time interval is merely imposed by the time taken by the cyclin to increase after the return of Ca^{2+} to its basal level, i.e. after the 4 h of stimulation. The time taken by cyclin to increase is itself dictated by the choice of parameter values characterizing the kinetics of the cell cycle but is practically independent of the parameters characterizing the preceding Ca^{2+} dynamics. In fact, the time for the first peak in MPF slightly decreases when the period of Ca^{2+} oscillations increases because the final level of CSF activity

increases in parallel with the period, due to the fact that the total number of Ca^{2+} spikes received by the system during 4 h becomes lower. The final rate of APC activation (V_3) is thus lower when the period of Ca^{2+} oscillations is larger. The latter change somewhat accelerates the increase in cyclin.

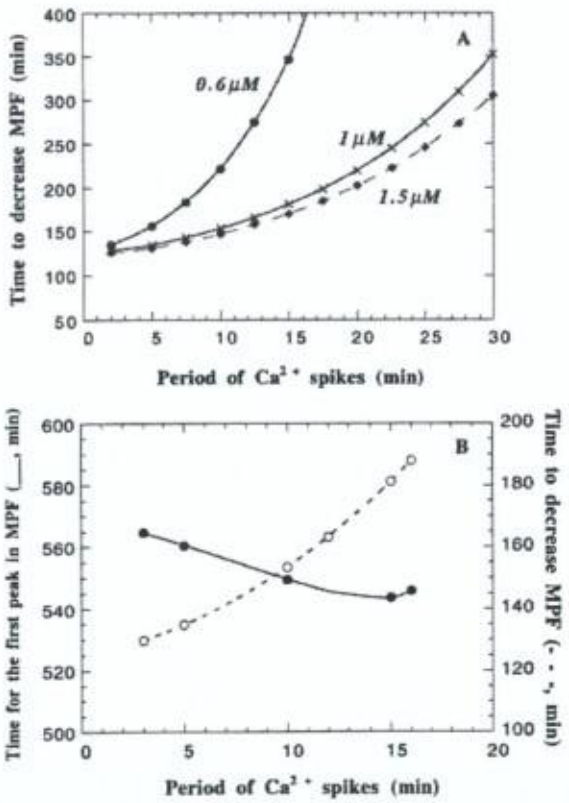

Fig. VII.20. Theoretical investigation of the influence of the Ca^{2+} dynamics on the kinetics of cell cycle resumption after fertilization. (A) shows the influence of the period of Ca^{2+} spiking on the time at which the level of active MPF drops. This stage corresponds to the entry of the activated egg in interphase. The various curves have been obtained for different amplitudes of Ca^{2+} spiking, as indicated. Ca^{2+} spikes are applied for 600 min. (B) shows the influence of the period of Ca^{2+} spiking on the time at which MPF reaches its first maximum, after the initial drop. This stage would correspond to the first mitosis. Ca^{2+} spikes are only applied during 4 h, which implies that the total number of Ca^{2+} spikes varies with the period. For comparison, the time taken for the first drop in MPF in these conditions (slightly different from (A)) is also indicated (dashed line). Results have been obtained as in Fig. VII.16.

For comparison, the time needed for the initial decrease in the level of active MPF in response to activation by Ca^{2+} is also shown in Fig. VII.20B. This relationship is not exactly the same as in Fig. VII.20A because in Fig. VII.20B, Ca^{2+} spikes are only applied during 4 h. The model thus predicts that the time taken by the egg to enter in interphase or to undergo the first division are differently affected by the Ca^{2+} dynamics. Pronucleus formation is accelerated when the frequency of the Ca^{2+} spikes is increased. In contrast, the time for the first division remains roughly independent from this frequency.

Increasing the number of Ca^{2+} spikes at a given frequency

An interesting property of the present model is that it suggests that the level of MPF cannot increase in the presence of a high level of Ca^{2+}, even in the absence of CSF activity as Ca^{2+} indirectly increases the activity of the APC complex (see Fig. VII.14). Furthermore, oscillations in the level of cyclin and active MPF can only occur when the Ca^{2+} level is low. This property can be understood by looking at the stability diagram shown in Fig. VII.17. There, it can be seen that oscillations cannot occur for low values of V_4, which correspond to minimal values of the mediator protein in the S form, and thus to

maximal Ca^{2+} concentrations. Thus, numerical simulations of the model schematized in Fig. VII.14 predict that the time required for resumption of the cell cycle will increase if the total stimulation time by Ca^{2+} is extended. The latter prediction is illustrated in Fig. VII.21. In comparison to Fig. VII.16, the number of Ca^{2+} spikes has been doubled (with the same frequency): simulations show a delay of nearly 4 h in the appearance of the first peak in MPF, as compared to Fig. VII.16. Such a prediction could be tested experimentally by activating the eggs by a very large number of artificial Ca^{2+} spikes.

Two experimental observations indirectly corroborate the latter theoretical prediction. First, it has been reported that after fertilization of mouse oocytes, Ca^{2+} oscillations cease during entry in interphase, at the time when pronuclei are forming (Jones *et al.*, 1995 ; Jellerette *et al.*, 2004). The second relevant observation comes from ascidian eggs, although the activation process is somewhat different in this species. In a recent study, the intracellular Ca^{2+} level has been measured simultaneously with histone H1 activity (Russo *et al.*, 1996); it appears that, at the second meiosis, MPF activity increases after the arrest of the Ca^{2+} spikes.

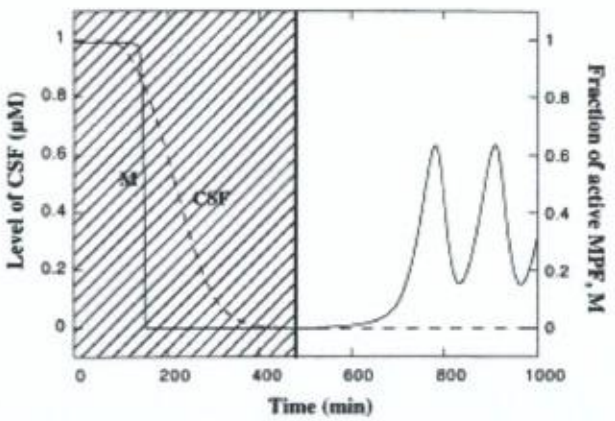

Fig. VII.21. Theoretical prediction of the model for cell cycle resumption schematized in Fig. VII.14: the time for the first mitosis is delayed when the egg receives a number of Ca^{2+} spikes that largely exceeds the number that is necessary for activation. Here, the egg is assumed to be activated during 8 h (with Ca^{2+} spikes of 10 min periods); as compared with the similar situation in which the number of Ca^{2+} spikes is equal to 24 (Fig. VII.16), the time for the first mitosis is delayed of about 4 h. Results have been obtained as in Fig. VII.16, except for the number of Ca^{2+} spikes which here equals 48.

VII.4.5. Discussion

In the present study, a model which qualitatively accounts for the Ca^{2+}-induced relief from MII arrest at fertilization of mammalian eggs has been developed. The central idea of the model is that the elevated Ca^{2+} level first overcomes inhibition of cyclin degradation by CSF, and later induces CSF inactivation. Activation of both pathways is mediated by CaMKII. Thus, the model assumes that the oscillatory level of CaMKII that follows the Ca^{2+} spikes has two effects, characterized by different time-scales. The first pathway simply counteracts the CSF-mediated arrest by directly activating the APC complex which initiates cyclin degradation, an effect that disappears when Ca^{2+} returns to its basal level. The second, irreversible and slow process activated by CaMKII is the inactivation of CSF. Thus, upon combination of these two effects, Ca^{2+} oscillations first decrease the level of active MPF, which allows the egg to enter in interphase, and later inactivate CSF. When CSF is sufficiently low and when Ca^{2+} oscillations stop, the egg can undergo the first mitosis.

Noteworthy is the fact that the model presented here remains qualitative. No attempt has been made to closely match the time scales of the events occurring in the simulations in response to Ca^{2+} spikes, with the experimentally determined time laps in the early development of the eggs from any mammalian species. Also the concentrations of the various chemical species appearing in the model

have been chosen rather arbitrarily. A quantitative approach would indeed be premature both because some parts of the model are speculative and because the kinetics of the events occurring between CaMKII activation by Ca^{2+} and the decrease in MPF is largely unknown. The aim of the study is both to provide a mechanism that can qualitatively account for many experimental observations and to emphasize the fact that the temporal pattern of early activation by Ca^{2+} clearly affects the developmental potentiality of the egg (Ozil, 1998).

The understanding of the role of the Ca^{2+} changes at fertilization is of great interest, particularly in the view that it might provide some insights into the causes of unsuccessful *in vitro* fertilization procedures in humans (Homa *et al.*, 1993). Although the present model is the first one to specifically investigate the link between Ca^{2+} oscillations and resumption of the cell cycle at fertilization, the relations between Ca^{2+} and the mitotic cell cycle have already been approached in a theoretical manner. As in the present model, these theoretical studies assume that CaMKII activates the degradation of cyclin. The first model relates the dynamics of cytosolic Ca^{2+} to progression through mitosis, G_1 and G_2 phase of the cell cycle, on the basis of the assumption that high levels of MPF trigger the release of $InsP_3$ (Baran, 1994 ; 1996). In that study, the Ca^{2+} dynamics is tightly coupled to the cell cycle oscillator, with a one to one peak correlation between Ca^{2+} and MPF. Such a situation cannot account for the coexistence between a basal level of Ca^{2+} and a high level of active MPF, as seen in MII arrested eggs, nor for the fact that numerous Ca^{2+} spikes are necessary for the egg to enter in interphase after fertilization.

Another theoretical investigation of the role of Ca^{2+} in the early embryonic cell cycle suggests that Ca^{2+} oscillations drive MPF activation cycles (Swanson *et al.*, 1997). Interestingly, the authors suggest that the Ca^{2+} dynamics could be autonomously oscillatory, while the MPF system would be excitatory or bistable. In that scheme, Ca^{2+} is assumed to activate both cyclin degradation and phosphorylation of cdc25, the phosphatase responsible for MPF activation. In the absence of additional assumptions, this model cannot account for the relief from MII arrest in response to a Ca^{2+} increase, as Ca^{2+} cannot induce an initial decrease in MPF activity in the presence of a high level of inhibition of cyclin degradation by CSF. However, it must be stressed that various relations between the Ca^{2+} dynamics and the MPF oscillator most probably prevail in different situations; in particular, it is reasonable to assume that mitosis is not regulated in the same manner as resumption of meiosis at fertilization.

Given the lack of experimental data, some of the regulatory pathways introduced in the model have been chosen rather arbitrarily. Other regulations could indeed lead to a behaviour similar to the one presented in Fig. VII.16. For example, the APC inactivation by the unphosphorylated form S of the mediator (V_4 on Fig. VII.14) could be substituted by the assumption that the Ca^{2+}-activated CaMKII in fact inhibits MPF activation (V_1 on Fig. VII.14). This possibility has been discarded because an opposite effect, namely the activation of cdc25 by Ca^{2+}, has been reported by an *in vitro* experimental study (Whitaker and Patel, 1990). In the same manner, the rather complex sequence of loops leading to a slow inactivation of CSF can be transformed into a CaMKII-activated, slow degradation of CSF which is inhibited by M. The reason why we have favoured the first possibility (sequence of activation–deactivation loops) is that MIII arrest is very difficult to simulate with the second pathway. Finally, that CaMKII can autophosphorylate and thus act as a biochemical switch (Meyer *et al.*, 1992) is another possibility that could explain the transition from a stable to an oscillatory MPF system. Again, we have not favoured this possibility on the basis that the variations in the level of MPF activity have to be reversible quite rapidly (MIII arrest or mitotic cell cycle).

In contrast, some assumptions of the model cannot be removed without affecting drastically the qualitative behaviour of the model. In particular, the results shown in Fig. VII.16 imperatively depend on the assumption that CaMKII has two different effects on the cell cycle. Moreover, the effect of Ca^{2+} on CSF activity has to be slow and irreversible, while the pathway that can overcome CSF-mediated arrest must be faster and reversible. Until now, there is no experimental evidence in favour of the existence of two different pathways targeted by CaMKII at egg activation.

In a first approximation, we have neglected any possible feedback of the cell cycle on the Ca^{2+} dynamics. Although such an effect most probably occurs (McDougall and Sardet, 1995 ; Kubiak *et al.*, 1993 ; Winston *et al.*, 1995), its inclusion in a theoretical model would be quite complex as it appears from the experimental data that it is mainly the reorganization of the microtubular network associated with the early development of the egg that interferes with the Ca^{2+} dynamics. Moreover, the interplay between the cell cycle machinery and the mechanism for Ca^{2+} release is bidirectional. Of particular interest in that respect is the observation that CaMKII might be associated with the spindle and could, in consequence be activated only as long as the latter microtubular organization remains intact (Winston *et al.*, 1995).

The present model provides an example of a system in which an oscillatory pattern of stimulation optimizes the cellular response in the absence of any frequency coding. This optimization in fact stems from the natural constraints of the system: to respond properly, the system indeed needs the long-lasting presence of the stimulus to fully deactivate CSF. Given the regulatory properties of the Ca^{2+} dynamics inside the cell, such a sustained increase in the level of Ca^{2+} is most successfully approached by oscillations. Although rapid Ca^{2+} spiking accelerates the activation process, there appears to be a large range of frequencies able to activate the egg. In that respect, the model recovers the experimental observation that egg activation is a very robust phenomenon which appears to be unaffected by large variations in the oscillatory pattern of Ca^{2+} increases.

CHAPTER VIII

Conclusions and perspectives

Oscillations and waves of cytosolic Ca^{2+} have been observed in various cell types, and extensively studied from both an experimental and a theoretical point of view. In this thesis, we have followed a computational modelling approach to tackle a large variety of problems related to both the molecular mechanisms and the physiological implications of this often spectacular spatio-temporal organization. It is interesting to mention that this approach appears particularly well-adapted. An appropriate description of the detailed Ca^{2+} dynamics can indeed in most cases be obtained with a small number of variables (2 or 3 in most models). In consequence, the number of processes and parameters remains limited, which, among other advantages, allows the approach to be semi-quantitative. This greatly favours a fruitful collaboration with experimentalists. Moreover, experimental observations remain basically limited to the monitoring the cytosolic Ca^{2+} concentration under diverse conditions. Measurement of $InsP_3$ and ER Ca^{2+} indeed remains technically very difficult, if not impossible. Thus, another advantage of models, is to predict the temporal evolution of the other important messengers closely linked to cytosolic Ca^{2+}.

Computational modelling of Ca^{2+} dynamics requires the development of specific models. Although basic CICR models such as the one summarized in Table I.2 share many similarities with the classical Fitzugh-Nagumo equations, the analogy already disappears when diffusion is taken into account. As another example, the mechanism proposed to be responsible for the generation of complex Ca^{2+} oscillations (namely the self-modulation of the oscillator) is rather unusual for biochemical systems. There indeed, it is the interplay between two endogenous oscillatory mechanisms, or the external forcing of an oscillator, that most often leads to complex phenomena such as bursting or chaos. Let us still mention the frequency-encoding phenomenon. Although this is a classical concept in systems involving the reversible desensitization of a target-receptor, it needs to be revisited in the case of Ca^{2+} where oscillations are able to amplify the sensitivity of the pathway involved between the Ca^{2+} increases and the physiological response.

In this thesis, we have contributed to a better understanding of various current problems related to Ca^{2+} dynamics. Let us very briefly summarize these contributions, and mention at the same time the possible remaining open questions that need to be further investigated.

As far as oscillations are concerned, we have studied the effect of taking $InsP_3$ metabolism into account. This study was initially motivated by experimental observations related to the distinct effects of overexpressing one or the other of the 2 enzymes responsible for $InsP_3$ catabolism, one being Ca^{2+}-sensitive and the other one Ca^{2+}-insensitive. As quantitative data were available for these enzymes, we could provide a simple explanation for the apparent paradoxical experimental results. Moreover, this extended model suggested that the Ca^{2+}-stimulation of $InsP_3$ degradation could be the mechanism responsible for the complex Ca^{2+} oscillations in the form of bursting or chaos that had been reported in some cell types. These complex behaviours have been analyzed in the framework of the theory of dynamical systems.

As recent experimental observations suggested that Ca^{2+} oscillations could sometimes be accompanied by $InsP_3$ oscillations, we investigated if the small-amplitude $InsP_3$ oscillations observed in our model could be significant in this respect. This led us to suggest a simple experimental protocol allowing to test easily the significance of $InsP_3$ oscillations due to Ca^{2+}-stimulation of $InsP_3$ catabolism.

As to the possible future directions of research in the field of Ca^{2+} oscillations, it is quite sure that the specific effects of the various $InsP_3R$ isoforms need to be investigated. We have already performed some simple analysis in this direction. The latter suggests that type 2 $InsP_3R$ is the most robust oscillator, which agrees with the observation that the cell types which are very rich in this isoform display Ca^{2+} oscillations in a very large set of conditions. However, it makes no doubt that our phenomenological description of the dynamics of the 3 $InsP_3R$ subtypes is oversimplified. The development of a specific molecular model for each isoform is clearly an important task to be undertaken.

To my opinion, the most challeging problem related to Ca^{2+} dynamics is to make the link between the elementary Ca^{2+} signals (blips and puffs) on one hand and Ca^{2+} oscillations and waves on the other hand. We have shown here that we are able to reproduce semi-quantitatively most of the properties of these small-scale Ca^{2+} increases with a detailed stochastic model of a small group of $InsP_3Rs$. Our initial aim was to consider in a further step the coupling between a group of puff sites to generate propagating waves and, hopefully, periodic oscillaions. We must say that our tentatives remain up to now unsuccessfull. The problems are clearly related to the diffusion of cytosolic Ca^{2+} as the incorporation of realistic parameters values for this process can indeed not lead to a fast enough dissipation of the Ca^{2+} gradients. This is particularly interesting in view of the fact that, based on what he calls the 'approximation methods for stationary Ca^{2+} profiles', M. Falcke (2003a ; 2003b) was able to generate puffs and repetitive propagating waves in the same simulation system, just by changing the $InsP_3$ concentration. Another very interesting question in this respect is to understand how a regular periodicity can be generated by the small number of $InsP_3Rs$ (a few hundreds) present in a cell of about 10 μm diameter, such as an hepatocyte or an HeLa cell.

As far as Ca^{2+} wave propagation is concerned, we have shown that the apparent intercellular waves propagating among connected hepatocytes can best be described as phase waves. The phase shift between the adjacent cells can be explained by the observed gradient of sensitivity to the external agonist. Moreover, we predict that $InsP_3$ is the most probable molecular species travelling through gap junctions to coordinate Ca^{2+} signals. Although the multiplet of hepatocytes provides an excellent model system, the final aim of these studies is clearly to uncover the mechanism at the basis of Ca^{2+} wave propagation throughout the whole liver. Is this still a phase wave ? Does the diffusion of small amounts of $InsP_3$ through gap junctions still suffice to coordinate Ca^{2+} spiking on distances as long as a few centimeters ? An extended modelling approach is clearly required to answer these questions. To go a step further, it would also be interesting to extend this study of intercellular Ca^{2+} waves in the liver to the case of other tissues where these waves propagate from one cell type to the other, as for example in the brain. This rather new phenomenon would however require the development of innovative simulation techniques.

Our modelling approach of the fertilization Ca^{2+} waves in ascidian eggs has allowed us to make predictions about the nature of the ER inhomogeneity that characterizes a mature egg. Again, these results need to be extended to other eggs displaying other pacemakers and other types of fronts. A remarkable fact is that, based on this study, we were able to predict quantitatively the Ca^{2+}-sensitivity of the sperm factor (i.e. the species injected by the sperm into the egg, and responsible for the Ca^{2+} waves and the resulting resumption of the cell cycle).

Focussing finally on the physiological implications of these Ca^{2+} oscillations, we have shed light on 3 different possible advantages of Ca^{2+} oscillations. In the case of liver glycogenolysis, the model predicts that Ca^{2+} oscillations increase the sensitivity of the target system. The same mechanism had already been shown to occur in a totally different context, namely that of gene expression. As far as CaMKII is concerned, it looks as if the very unique mode of activation of this kinase by Ca^{2+} (based on intramolecular autophosphorylation) was designed to be sensitive to high frequency Ca^{2+} oscillations. Thus, in this case, there seems to be an adequation between Ca^{2+} dynamics and the enzymatic properties of the target protein to optimize the signalling pathway. Finally, our rather speculative approach of the link between Ca^{2+} oscillations and the cell cycle suggests that, in this case, the system would be sensitive to the number, rather than to the frequency, of the repetitive Ca^{2+} increases. Ca^{2+} oscillations would there serve to allow for an apparently prolonged Ca^{2+} increase, without damaging the cell. There are still many systems –such as secretion, gene expression or neuronal differentiation– where the oscillatory nature of the Ca^{2+} signal is known to play a fundamental role. For many of them, modelling could most probably help uncovering the key molecular mechanisms responsible for this frequency sensitivity, and thereby improve our understanding of these vital processes.

References

Allbritton N., Meyer T. and Stryer L. (1992) Range of messenger action of calcium ion and inositol 1,4,5-trisphosphate. *Science* 258, 1812-1815.

Allen V., Swigart P., Cheung R., Cockcroft S. and Katan M. (1997) Regulation of inositol lipid-specific phospholipase C δ by changes in Ca^{2+} ion concentration. *Biochem. J.* 327, 545-552.

Atri A., Amundson J., Clapham D. and Sneyd J. (1993) A single-pool model for intracellular Ca^{2+} oscillations and waves in the *Xenopus laevis* oocyte. *Biophys. J.* 65, 1727-1739.

Balla T., Sim S.S., Toshihiko I., Choi K.Y., Catt K. and Rhee S.G. (1991) Agonist-induced calcium signaling is impaired in fibroblasts overproducing inositol 1,3,4,5-tetrakisphosphate. *J. Biol. Chem.* 266: 24719-24726.

Baran I. (1994) Exit from mitosis induced by a calcium transient: the relation to the MPF and InsP3 dynamics. *BioSystems* 33, 203-214.

Baran I. (1996) Calcium and cell cycle progression: possible effects of external perturbations on cell proliferation. *Biophys. J.* 70, 1198-1213.

Bassani J., Bassani R. and Bers D. (1995) Calibration of indo-1 and resting intracellular $[Ca]_i$ in intact rabbit cardiac myocytes. *Biophys. J.* 68, 1453-1460.

Bayer K.U. and Schulman. H. (2001). Regulation of signal transduction by protein targeting: the case for CaMKII. *Biochem. Biophys. Res. Comm.* 289, 917-923.

Bayer K.U., De Koninck P. , Leonard A. , Hell J.W. , and Schulman H. (2001). Interaction with the NMDA receptor locks CaMKII in an active conformation. *Nature* 14, 801-805

Bayer, K.U., De Koninck P. and Schulman. H. (2002). Alternative splicing modulates the frequency-dependent response of CaMKII to Ca^{2+} oscillations. *EMBO* 21, 3590-3597.

Bergé, P., Y. Pomeau and C. Vidal. (1984) *Order within chaos: towards a deterministic approach to turbulence*. New York: Wiley.

Berridge, M.J. (1993). Inositol trisphosphate and calcium signalling. *Nature* 361, 315-325.

Berridge M.J. (1995) Capacitative Ca^{2+} entry. *Biochem. J.* 312, 1-11.

Berridge M.J., and Dupont G. (1995). Spatial and temporal signalling by calcium. *Curr. Opin. in Cell Biol.* 6, 267-274.

Berridge M. (1997). Elementary and global aspects of calcium signalling. *J. Physiol.* 499, 291-306.

Berridge M., Bootman M. and Lipp P. (1998) Calcium–a life and death signal. *Nature* 395, 645-648.

Berridge M.J., Lipp P. and Bootman M. (2000). The versatility and universality of calcium signalling. *Nature Mol. Cell Biol.* 1, 11-21.

Berridge M.J., Bootman M. and Roderick H. (2003) Calcium signalling: dynamics, homeostasis and remodelling. *Nat. Mol. Cell Biol.* 4, 517-529.

Bezprozvanny I., Watras J. and Ehrlich B. (1991) Bell-shaped calcium responses of $InsP_3$- and calcium-gated channels from endoplasmic reticulum of cerebellum. *Nature* 351, 751-754.

Bezprozvanny I. and Ehrlich B. (1994) Inositol 1,4,5-trisphosphate ($InsP_3$)-gated Ca channels from cerebellum: conduction properties for divalent cations and regulation by intraluminal calcium. *J. Gen. Physiol.* 104, 821-856.

Bezprozvanny I. and Ehrlich B. (1995) The inositol 1,4,5-trisphosphate receptor. *J. Membr. Biol.* 145, 205-216.

Biden T., Altin J., Karjalainen A. and Bygrave F. (1988) Stimulation of hepatic inositol 1,4,5-trisphosphate kinase activity by Ca^{2+}-dependent and -independent mechanisms. *Biochem. J.* 256, 697-701.

Bird G., Obie J. and Javie J. (1992) Sustained Ca^{2+} signalling in mouse lacrimal acinar cells due to photolysis of caged glycerophosphoryl-myo-inositol 4,5-bisphosphate. *J. Biol. Chem.* 267, 17722-17725.

Bird G. and Putney J. (1996) Effects of inositol 1,3,4,5-tetrakisphosphate on inositol-trisphosphate-activated Ca^{2+} signaling in mouse lacrimal acinar cells. *J. Biol. Chem.* 271, 6766-6770.

Blatter L. and Wier W. (1990) Intracellular diffusion, binding, and compartimentalization of the fluorescent calcium indicators indo-1 and fura-2. *Biophys. J.* 58, 1491-1499.

Bollen M., Keppens S. and Stalmans W. (1998). Specific features of glycogen metabolism in the liver. *Biochem. J.* 336, 19-31.

Bootman M., Niggli E., Berridge M.J. and Lipp P. (1997) Imaging the hierarchical Ca^{2+} signalling system in HeLa cells. *J. Physiol. Lond.* 499, 307-314.

Bootman M., Lipp P., and Berridge M.J. (2001). The organization and functions of local Ca^{2+} signals. *J. Cell Science* 114, 2213-2222.

Borghans J., Dupont G. and Goldbeter A. (1997) Complex intracellular oscillations. A theoretical exploration of possible mechanisms. *Biophys. Chem.* 66, 25-41.

Bradshaw J.M., Hudmon A. , and Schulman H. (2002). Chemical quench-flow kinetic studies indicate an intra-holoenzyme autophosphorylation mechanism for Ca^{2+}/calmodulin-dependent protein kinase II. *J. Biol. Chem.* 20991-20998.

Braet K., Cabooter L., Paemeleire K. and Leybaert L. (2004) Calcium signal communication in the central nervous system. *Biol. Cell* 96, 79-91.

Braun A., and Schulman H. (1995). The multifunctional calcium/calmodulin-dependent protein kinase: from form to function. *Annu. Rev. Physiol.* 57, 417-445.

Bugrim A., Fontanilla R., Eutenier B., Keizer J. and Nuccitelli R. (2003) Sperm initiates a Ca^{2+} wave in frog eggs that is more similar to Ca^{2+} waves initiated by IP_3 than by Ca^{2+}. *Biophys. J.* 84, 1580-1590.

Callamaras N., Marchant J., Sun X. and Parker I. (1998) Activation and co-ordination of $InsP_3$-mediated elementary Ca^{2+} events during global Ca^{2+} signals in *Xenopus* oocytes. *J. Physiol.* 509, 81-91.

Callamaras N. and Parker I. (1999) Radial localization of inositol 1,4,5-trisphosphate-sensitive Ca^{2+} release sites in *Xenopus* oocytes resolved by axial confocal linescan imaging. *J. Gen. Physiol.* 113, 199-213.

Capiod, T., J. Noel, L. Combettes and M. Claret. 1991. Cyclic AMP-evoked oscillations of intracellular [Ca^{2+}] in guinea-pig hepatocytes. *Biochem. J.* 275, 277-280.

Cardenas M. L. and Goldbeter A. (1996). The glucose induced switch between glycogen phosphorylase and glycogen synthase in the liver: outlines of theoretical approach. *J. Theor. Biol.* 182, 421-426.

Carroll M., Levasseur M., Wood C., Whitaker M., Jones K. and McDougall A. (2003) Exploring the mechanism of action of the sperm-triggered calcium-wave pacemaker in ascidian zygotes. *J. Cell Science* 116, 4997-5004.

Champeil P, Combettes L, Berthon B, Doucet E, Orlowski S, and Claret M. (1989) Fast kinetics of calcium release induced by myo-inositol trisphosphate in permeabilized rat hepatocytes. *J. Biol. Chem.* 264, 17665-17673.

Charles, A.C., Naus, C.C.G., Zhu, D.G., Kidder, Dirksen, E.R. and Sanderson, D. (1992) Intercellular calcium signaling via gap junctions in glioma cells. *J. Cell Biol.* 118, 195-201.

Chatton J.-Y., Liu H. and Stucki J. (1995) Simulatneous measurements of Ca^{2+} in the intracellular stores and the cytosol of hepatocytes during hormone-induced Ca^{2+} oscillations. *FEBS Lett.* 368, 165-168.

Chatton J.-Y., Cao Y. and Stucki J. (1998) Perturbation of myo-inositol-1,4,5-trisphosphate levels during agonist-induced Ca^{2+} oscillations. *Biophys. J.* 74, 523-531.

Chay, T.R. 1993. The mechanism of intracellular Ca^{2+} oscillation and electrical bursting in pancreatic β-cells. *Adv. Biophys.* 29, 75-103.

Chay, T., Y.S. Fan and Y.S. Lee. (1995) Bursting, spiking, chaos, fractals, and universality in biological rythms. *Int. J. Bif. Chaos* 5, 595-635.

Chay, T.R. (1997). Effects of extracellular calcium on electrical bursting and intracellular and luminal calcium oscillations in insulin secreting pancreatic beta-cells. *Biophys. J.* 73, 1673-1688.

Choi K., Kim H., Lee S. *et al.* (1990) Molecular cloning and expression of a complementary DNA for inositol 1,4,5-trisphosphate 3-kinase. *Science* 248, 64-66.

Chrisman T. D. and Jordan J. E. (1982). Purification of rat liver phosphorylase kinase. *J. Biol. Chem.* 257,10 798-10 804.

Clair C., Chalumeau C., Tordjmann T., Poggioli J., Erneux C., Dupont G. and Combettes L. (2001) Investigation of the roles of Ca^{2+} and $InsP_3$ diffusion in the coordination of Ca2+ signals between connected hepatocytes. *J. Cell Science* 114, 1999-2007.

Cohen P., Burchell A., Foulkes J. G., Cohen P. T. W., Vanaman T. C. and Nairn A. C. (1978). Identification of the Ca^{2+}-dependent modulator protein as the fourth subunit of rabbit skeletal muscle phosphorylase kinase. *FEBS Lett.* 92, 287-293.

Colbran R.J. (1993). Inactivation of Ca^{2+}/calmodulin-dependent protein kinase II by basal autophosphorylation. *J. Biol. Chem.* 268, 7163-7170.

Collas P., Chang T., Long C. and Robl J. (1995) Inactivation of histone H1 kinase by Ca^{2+} in rabbit oocytes. *Mol. Reprod.* 40, 253-258.

Combettes L, Tran D, Tordjmann T, Laurent M, Berthon B. and Claret M. (1994) Sequential activation of hormone-mediated Ca^{2+} signals in multicellular systems of rat hepatocytes. *Biochem. J.* 304, 585-594.

Combettes L., Cheek T. and Taylor C. (1996) Regulation of inositol trisphosphate receptors by luminal Ca^{2+} contributes to quantal Ca^{2+} mobilization. *EMBO J.* 15, 2086-2093.

Combettes L., Dupont G. and Parys J. (2004) New mechanisms and functions in Ca^{2+} signalling. *Biol. Cell* 96, 1-2.

Communi D., Vanweyenberg V. and Erneux C. (1994) Purification and biochemical properties of a high-molecular-mass inositol 1,4,5-trisphosphate 3-kinase isoenzyme in human platelets. *Biochem. J.* 298, 669-673.

Communi D., Vanweyenberg V.and Erneux C. (1997) D-myo-inositol 1,4,5-trisphosphate 3-kinase A is activated by receptor activation through a calcium:calmodulin-dependent protein kinase II phosphorylation mechanism. *EMBO J.* 16, 1943-1952.

Conigrave A., Patwardhan A., Broomhead L. and Roufogalis B. (1992) A purification strategy for inositol 1,4,5-trisphosphate 3-kinase from rat liver based upon heparin interaction chromatography. *Cell Signal.* 4, 303-321.

Coomber C. (1998). Site-selective autophosphorylation of Ca^{2+}/calmodulin-dependent protein kinase II as a synaptic encoding mechanism. *Neural. Comput.* 10, 1653-1678.

Cox L., Larman M., Saunders C., Hashimoto K., Swann K. and Lai F. (2002) Sperm phospholipase Cζ from humans and cynomolgus monkeys triggers Ca^{2+} oscillations, activation and development of mouse oocytes. *Reproduction* 124, 611-623.

Craske M., Takeo T., Gerasimenko O., Vaillant C., Torok K., Petersen O.H., and Tepikin A.V. (1999). Hormone-induced secretory and nuclear translocation of calmodulin: oscillations of calmodulin concentration with the nucleus as an integrator. *Proc Natl Acad Sci USA* 96, 4426-4431.

Cullen P., Comerford J. and Dawson A. (1988) Heparin inhibits the inositol 1,4,5-trisphosphate-induced Ca^{2+} release from rat liver microsomes. *FEBS Lett.* 228, 57-60.

Cuthbertson K. and Cobbold P. (1985) Phorbol ester and sperm activate mouse oocytes by inducing sustained oscillations in cell Ca^{2+}. *Nature* 316, 541-542.

Cuthbertson K. and Chay T. (1991) Modelling receptor-controlled intracellular calcium oscillators. *Cell Calcium* 12, 97-109.

Cyert M. and Kirschner M. (1988) Regulation of MPF activity in vitro. *Cell* 53, 185-195.

Damen J., Liu L., Rosten P., Humphries R., Jefferson A., Majerus P. and Krystal G. (1996) The 145-kDa protein induced to associate with Shc by multiple cytokines is an inositol tetraphosphate and phosphatidylinositol 3,4,5-trisphosphate 5-phosphatase. *Proc. Natl. Acad. Sci.* 93, 1689-1693.

D'Andrea P. and Vittur F. (1997) Propagation of intercellular Ca^{2+} waves in mechanically stimulated articular chondrocytes. *FEBS Lett.* 400, 58-64.

Dawson A.P. (1997) Calcium signalling : how do IP_3 receptor work ? *Curr. Biol.* 7, R544-R547.

De Koninck P., and H. Schulman (1998) Sensitivity of CaM kinase II to the frequency of Ca^{2+} oscillations. *Science* 279, 227-230.

Demer L., Wortham C., Dirksen E. and Sanderson M. (1993) Mechanical stimulation induces intercellular calcium signaling in bovine aortic endothelial cells. *Am. J. Physiol.* 264, H2094-H2102.

Depierre J. and Dallner G. (1975) Structural aspects of the membrane of the endoplasmic reticulum. *Biochim Biophys Acta* 415, 411-472.

De Smedt F., Missiaen L., Parys J., Vanweyenberg V., De Smedt H. and Erneux C. (1997) Isoprenylated human brain type I inositol 1,4,5-trisphosphate 5-phosphatase controls Ca^{2+} oscillations induced by ATP in Chinese hamster ovary cells. *J. Biol. Chem.* 272, 17367-17375.

De Young G. and Keizer J. (1992) A single pool inositol 1,4,5-trisphosphate-receptor-based model for agonist-stimulated oscillations in Ca^{2+} concentration. *Proc. Natl. Acad. Sci. USA* 89, 9895-9899.

Dixon, C.J., P.H. Cobbold and Green, A. (1993). Adenosine 5'-[ab-methylene] trisphosphate potentiates the oscillatory cytosolic Ca^{2+} responses of hepatocytes to ATP, but not to ADP. *Biochem. J.* 293, 757-760.

Dixon, C.J., P.H. Cobbol and Green, A (1995). Oscillations in cytosolic free Ca^{2+} induced by ADP and ATP in single rat hepatocytes display differential sensitivity to application of phorbol ester. *Biochem. J.* 309, 145-149.

Doedel, E.J. (1981). A program for the automatic bifurcation analysis of autonomous systems. *Congr. Num.* 30, 265-284.

Dolmetsch R., Xu K. and Lewis R. (1998) Calcium oscillations increase the efficiency and specificity of gene expression. *Nature* 392, 933-938.

Doorneweerd D., Tan A. and Nuttall F. (1982). Liver phosphorylase kinase: characterization of two interconvertible forms and partial purification of phosphorylase kinase a. *Mol. Cell. Biochem.* 47, 45-53.

Dosemeci A. and Albers R. (1996). A mechanism for synaptic frequency detection through autophosphorylation of CaM kinase II. *Biophys. J.* 70, 2493-2501.

Dufour J., Arias I., Turner T. (1997) Inositol 1,4,5-trisphosphate and calcium regulate the calcium channel function of the hepatic inositol 1,4,5-trisphosphate receptor. *J. Biol. Chem.* 272, 2675-2681.

Dumollard R. and Sardet C. (2001) Three different calcium wave pacemakers in ascidian eggs. *J. Cell Sci.* 114, 2471-2481.

Dumollard R., Carroll J., Dupont G. and Sardet C. (2002) Calcium wave pacemakers in eggs. *J. Cell Science* 115, 3557-3564.

Dupont G. and Goldbeter A. (1989) Theoretical insights into the origin of signal-induced calcium oscillations. In : *Cell to Cell signalling : From Experiments to Theoretical Models* (Goldbeter A., ed), pp. 461-474. Academic Press, London.

Dupont G. and Goldbeter A. (1992a) Oscillations and waves of cytosolic calcium: insights from theoretical models. *BioEssays* 14, 485-.493.

Dupont G. and Goldbeter A. (1992b). Protein phosporylation driven by intracellular calcium oscillations: a kinetic analysis. *Biophys. Chem.* 42, 257-270.

Dupont, G., A. Goldbeter. (1993). One-pool model for Ca^{2+} oscillations involving Ca^{2+} and inositol 1,4,5-trisphosphate as co-agonists for Ca^{2+} release. *Cell Calcium* 14, 311-322.

Dupont G. and Swillens S. (1996) Quantal release, incremental detection and long-period Ca^{2+} oscillations in a model based on regulatory Ca^{2+} binding sites along the permeation pathway. *Biophys. J.* 71, 1714-1722.

Dupont G., McGuinness O., Johnson M., Berridge M. and Borgese F. (1996) Phospholipase C in mouse oocytes: characterization of beta and gamma isoforms and their possible involvement in sperm-induced Ca^{2+} spiking. *Biochem. J.* 316, 583-591.

Dupont G. and Erneux C. (1997) Simulations of the effects of inositol 1,4,5-trisphosphate 3-kinase and 5-phosphatase activities on Ca^{2+} oscillations. *Cell Calcium* 22, 321-331.

Dupont G. (1998) Link between fertilization-induced Ca^{2+} oscillations and relief from metaphase II arrest in mammalian eggs: a model based on calmodulin-dependent kinase II activation. *Biophys. Chem.* 72, 153-167.

Dupont, G. and Goldbeter A. (1998). CaM kinase II as frequency decoder of Ca^{2+} oscillations. *BioEssays* 20, 607-610.

Dupont G. (1999) Spatio-temporal organisation of intracellular calcium signals: from experimental to theoretical aspects. *Comments Theor. Biol.* 5, 305-340.

Dupont G., Tordjmann T., Clair C., Swillens S., Claret M. and Combettes, L. (2000a) Mechanism of receptor-oriented intercellular calcium wave propagation in hepatocytes. *FASEB J.* 14, 279-289.

Dupont G., Swillens S., Clair C., Tordjmann T. and Combettes L. (2000b) Hierarchical organization of calcium signals in hepatocytes : from experiments to models. *Biochim. Biophys. Acta* 1498, 134-152.

Dupont G., Houart G. and De Koninck P. (2003a) Sensitivity of CaM kinase II to the frequency of Ca^{2+} oscillations: a simple model. *Cell Calcium* 34, 485-497.

Dupont G., Houart G. and Goldbeter A. (2003b) From simple to complex Ca^{2+} oscillations: regulatory mechanisms and theoretical models. In: *Undestanding Ca^{2+} dynamics: experiments and theory. M. Falcke and D. Malchow, eds.* Springer, Heidelberg.

Dupont G., Koukoui O., Clair C., Erneux C., Swillens S. and Combettes L. (2003c) Ca^{2+} oscillations in hepatocytes do not require the modulation of $InsP_3$ 3-kinase activity by Ca^{2+}. *FEBS Lett.* 534, 101-105.

Dupont G. and Dumollard R. (2004) Simulations of calcium waves in ascidian eggs: insights into the origin of the pacemaker sites and the possible nature of the sperm factor. *J. Cell Science* 117, 4313-4323.

Dyer J. and Michelangeli F. (2001) Inositol 1,4,5-trisphosphate receptor isoforms show similar Ca^{2+} release kinetics. *Cell Calcium* 30, 245-250.

Eberhard M. and Erne P. (1991) Calcium binding to fluorescent calcium indicators: calcium green, calcium orange and calcium crimson. *Biochem. Biophys. Res. Commun.* 180, 209-215.

Endo M., Tanaka M. and Ogawa Y. (1970) Calcium-induced release of calcium from the sarcoplasmic reticulum of single skinned cardiac cells. *J. Physiol. (London)* 249, 469-495.

Ermentrout B. (2002). Solving and analyzing dynamical systems using XPPAUT. In : *Computational Cell Biology. C. Fall, E. Marland, J. Wagner and J. Tyson, eds.* Springer, New-York.

Erneux C., Lemos M., Verjans B., Vanderhaegen P., Delvaux A., Dumont J.E. (1989) Soluble and particulate Ins1,4,5-P_3/Ins1,3,4,5-P_4 5-phosphatase in bovine brain. *Eur. J. Biochem.* 181, 317-322.

Erneux C. and Takazawa K. (1991) Intracellular control of inositol phosphates by their metabolizing enzymes. *Trends Pharmacol. Sci.* 12, 174-176.

Eshete F. and Fields R. (2001). Spike frequency decoding and autonomous activation of Ca^{2+}-calmodulin-dependent protein kinase II in dorsal root ganglion neurons. *J. Neurosci.* 21, 6694-6705.

Eugenin N., Gonzalez H., Saez C. and Saez J. (1998). Gap juctionnal communication coordinates vasopressin-induced glycogenolysis in rat hepatocytes. *Am. J. Physiol.* 274, G1109-G1116.

Fabiato A. and Fabiato F. (1975) Contractions induced by a calcium-triggered release of calcium from the sarcoplasmic reticulum of single skinned cardiac cells. *J. Physiol. (London)* 249, 469-495.

Falcke M., Hudson J., Camacho P. and Lechleiter J. (1999) Impact of mitochondrial Ca^{2+} cycling on pattern formation and stability. *Biophys. J.* 77, 37-44.

Falcke M. (2003a) On the role of stochastic channel behaviour in intracellular Ca^{2+} dynamics. *Biophys. J.* 84, 42-46.

Falcke M. (2003b) Buffers and oscillations in intracellular Ca^{2+} dynamics. *Biophys. J.* 84, 28-41.

Fall C. and Keizer J. (2002) Dynamic phenomena in cells. In : *Computational Cell Biology*. (Fall C., Marland S., Wagner J. and Tyson J., eds) pp 3-20. Springer, New-York.

Finch E., Turner T. and Goldin S. (1991) Calcium as coagonist of inositol 1,4,5-trisphosphate-induced calcium release. *Science* 252, 443-446.

Fink C., Slepchenko B. and Loew L. (1999) Determination of time-dependent inositol-1,4,5-trisphosphate concentrations during calcium release in a smooth muscle cell. *Biophys. J.* 77, 617-628.

Fink C., Slepchenko B., Moraru I., Watras J., Schaff J. and Loew L. (2000) An image-based model of calcium waves in differentiated neuroblastoma cells. *Biophys. J.* 79, 163-183.

Foltz. K., Partin J. and Lennarz W. (1993) Sea urchin egg receptor for sperm: sequence similarity of binding domain and hsp70. *Science* 259, 1421-1425.

Fontanilla R. and Nuccitelli (1998) Characterization of the sperm-induced calcium wave in *Xenopus* eggs using confocal microscopy. *Biophys. J.* 75, 2079-2087.

Foster P., Hogan S., Hansbro P. *et al.* (1994) The metabolism of D-myo-inositol 1,4,5-trisphosphate and D-myo-inositol 1,3,4,5-tetrakisphosphate by porcine skeletal muscle. *Eur. J. Biochem.* 222, 955-964.

Gabso M., Neher E. and Spira M. (1997) Low mobility of the Ca^{2+} buffers in axons of cultured *Aplysia* neurons. *Neuron* 18, 473-481.

Gall D., Baus E. and Dupont G. (2000) Activation of the liver glycogen phosphorylase by Ca^{2+} oscillations: a theoretical study. *J. Theor. Biol.* 207, 445-454.

Gautam A., Oi-Cheng N.G. and Boyer J.L. (1987) Isolated rat hepatocyte couplets in short-term culture: structural characteristics and plasma membrane reorganisation. *Hepatology* 7, 216-223.

Glotzer M., Murray A and Kirschner M. (1991) Cyclin is degraded by the ubiquitin pathway. *Nature* 349, 132-138.

Goldbeter A. and Lefever R. (1972) Dissipative structures for an allosteric model. Applications to glycolytic oscillations. *Biophys. J.* 12, 1302-1315.

Goldbeter A. and Nicolis G. (1976) An allosteric enzyme model with positive feedback applied to glycolytic oscillations. In: *Progress in Theoretical Biology* (Snell F. and Rosen R., eds) Academic Press, New-York, 4, 65-160.

Goldbeter A. and Segel L. (1977) Unified mechanism for relay and oscillations of cyclic AMP in *Dictyostelium discoideum*. *Proc. Natl. Acad. Sci. USA* 78, 6840-6844.

Goldbeter A. and Koshland D. Jr. (1981) An amplified sensitivity arising from covalent modification in biological systems. *Proc. Natl. Acad. Sci. USA* 87, 1461-1465.

Goldbeter A., Dupont G. and Berridge M. J. (1990) Minimal model for signal-induced Ca^{2+} oscillations and for their frequency encoding through protein phosphorylation. *Proc. Natl. Acad. Sci. U.S.A.* 87, 1461-1465.

Goldbeter A. (1991) A minimal cascade model for the mitotic oscillator involving cyclin and cdc2 kinase. *Proc. Natl. Acad. Sci. USA* 88, 9107-9111.

Goldbeter A. (1993) Modeling the mitotic oscillator driving the cell division cycle. *Comments Theor. Biol.* 3 ; 75-107.

Goldbeter A. (1996) *Biochemical oscillations and cellular rhythms. The molecular bases of periodic and chaotic behaviour*. Cambridge University Press, Cambridge.

Goldbeter A. and Guilmot J.-M. (1996) Thresholds and oscillations in enzymatic cascades. *J. Phys. Chem.* 100, 19174-19181.

Goldbeter A. (2002) Computational approaches to cellular rhythms. *Nature* 420, 238-245.

Goldbeter A. (2004) Computational biology : a propagating wave of interest. *Curr. Biol.* 14, R601-602.

Green, A.K., C.J. Dixon, A.G. MacLennan, P.H. Cobbold and Fisher, M.J. (1993). Adenine dinucleotide-mediated cytosolic free Ca^{2+} oscillations in single hepatocytes. *FEBS Lett.* 322, 197-200.

Green, A.K., P.H. Cobbold and Dixon C.J. (1994). Elevated intracellular cyclic AMP exerts different modulatory effects on cytosolic free Ca^{2+} oscillations induced by ADP and ATP in single rat hepatocytes. *Biochem. J.* 302, 949-955.

Gu X. and Spitzer N. (1995) Distinct aspects of neuronal differentiation encoded by frequency of spontaneous Ca^{2+} transients. *Nature* 375, 784-787.

Guillemette J., Caron A., Regimbald-Dumas Y., Arguin G., Mignery G., Boulay G. and Guillemette G. (2005) Expression of a truncated form of inositol 1,4,5-trisphosphate receptor type III in the cytosol of DT40 triple inositol 1,4,5-trisphosphate receptor-knockout cells. *Cell Calcium* 37, 97-104.

Haberichter T., Roux E., Marhl M. and Mazat J.-P (2002) The influence of different $InsP_3$ receptor isoforms on Ca^{2+} signaling in tracheal smooth muscle cells. *Bioelectrochemistry* 57: 129-138.

Hagar R., Burgstahler A., Nathanson M., and Ehrlich B. (1998) Type III $InsP_3$ receptor channel stays open in the presence of increased calcium. *Nature* 396, 81-84.

Hagar R. and Ehrlich B. (2000) Regulation of type III receptor by $InsP_3$ and ATP. *Biophys. J.* 79, 271-278.

Hajnoczky G., Robb-Gaspers L., Seitz M. and Thomas A. (1995) Decoding of cytosolic calcium oscillations in the mitochondria. *Cell* 82, 415-424.

Hajnoczky G. and Thomas A. (1997) Minimal requirements for calcium oscillations driven by the $InsP_3$ receptor. *EMBO J.* 16, 3533-3543.

Hannaert-Merah Z., Combettes L., Coquil J.-F., Swillens S., Mauger J.-P., Claret M. and Champeil P. (1995) Characterization of the co-agonist effects of strontium and calcium on *myo*-inositol trisphosphate-dependent ion fluxes in cerebellar microsomes. *Cell Calcium* 18, 390-399.

Hansen M. Boitano S. Dirksen E.R. and Sanderson M.J. (1993) Intercellular calcium signaling induced by extracellular adenosine 5'-triphosphate and mechanical stimulation in airway epithelial cells. *J. Cell Sci.* 106 , 995-1004.

Hansen M. Boitano S. Dirksen E.R. and Sanderson M.J. (1995) A role for phospholipase C activity but not ryanodine receptors in the initiation and propagation of intercellular calcium waves. *J. Cell Sci.* 106, 2583-2590.

Hanson P. and Schulman H. (1992). Inhibitory autophosphorylation of multifunctional Ca^{2+}/calmodulin-dependent protein kinase analyzed by site-directed mutagenesis. *J. Biol. Chem.* 267, 17216-17224.

Hanson P., Meyer T., Stryer L. and Schulman H. (1994). Dual role of calmodulin in autophosphorylation of multifunctional CaM kinase may underlie decoding of calcium signals. *Neuron* 12, 943-956.

Hardingham G. and Bading H. (2003). The Yin and Yang of NMDA receptor signaling. *Trends Neurosci.* 26, 81-89.

Harootunian A., Kao J., Paranjape S. and Tsien R. (1991) Generation of calcium oscillations in fibroblasts by positive feedback between calcium and IP_3. *Science* 251, 7-78.

Hattori M., Suzuki A., Higo T., Miyauchi H., Michikawa T., Nakamura T., Inoue T., and Mikoshiba K. (2004) Distinct roles of inositol 1,4,5-trisphosphate receptor types 1 and 3 in Ca^{2+} signalling. *J. Biol. Chem.* 279, 11967-11975.

Hofer A. and Schulz I. (1996) Quantification of intraluminal free [Ca] in the agonist-sensitive internal calcium store using compartimentalized fluorescent indicators : some considerations. *Cell Calcium* 20, 235-242.

Höfer T. (1999). Model of intercellular calcium oscillations in hepatocytes: synchronization of heterogeneous cells. *Biophys. J.* 77, 1244-1256.

Hirose K., Kadowski S., Tanabe M., Takeshima H. and Iino M. (1999) Spatiotemporal dynamics of inositol 1,4,5-trisphosphate that underlies complex mobilization patterns. *Science* 284: 1527-1530.

Holl R., Thorner M. , Mandell G., Sullivan J. , Sinha Y. and Leong D. (1988). Spontaneous oscillations of intracellular calcium and growth hormone secretion. *J. Biol. Chem.* 263, 9682-9685.

Holmes W. (2000) Models of calmodulin trapping and CaM kinase II activation in a dendritic spine. *J. Comput. Neurosc.* 8, 65-85.

Homa S., Carroll J. and Swann K. (1993) The role of calcium in mammalian oocyte maturation and egg activation. *Hum. Reprod.* 8, 1274-1281.

Houart G., Dupont G., Goldbeter A. (1999) Bursting, chaos and birhythmicity originating from self-modulation of the inositol 1,4,5-trisphosphate signal in a model for intracellular Ca^{2+} oscillations. *Bull. Math. Biol.* 61, 507-530.

Howell K., Skipwith A., Galione A., and Eckberg W. (2003) Phospholipase C-dependent Ca^{2+} release by worm and mammal sperm factors. *Biochem. Biophys. Res. Com.* 307, 47-51.

Hudmon A. and Schulman H. (2002a). Neuronal Ca^{2+}/calmodulin-dependent protein kinase II: the role of structure and autoregulation in cellular function. *Annu. Rev. Biochem.* 71, 473-510..

Hudmon A. and Schulman H. (2002b). Structure/function of the multifunctional Ca^{2+}/calmodulin-dependent protein kinase II. *Biochem. J.* 364, 593-611.

Hughes A. and Putney J. (1990) Inositol phosphate formation and its relationship to calcium signaling. *Env. Health Perspect.* 84, 141-147.

Hunding A. and Ipsen M. (2003) Simulation of waves in calcium models with 3D spherical geometry. *Math. Biosciences* 182, 45-66.

Ichas F., Jouaville L. and Mazat J.-P. (1997) Mitochondria are excitable organelles capable of generating and conveying electrical and calcium signals. *Cell* 89, 1145-1153.

Imredy J. and Yue D. (1992) Submicroscopic Ca^{2+} diffusion mediates inhibitory coupling between individual Ca^{2+} channels. *Neuron* 9, 197-207.

Inoue M., Iin H., Imagana I., Ogawa K. and Warashina A. (2003) $InsP_3$ receptor type 2 and oscillatory and monophasic Ca^{2+} transients in rat adrenal chromaffin cells. *Cell Calcium* 35, 59-70.

Irvine R. Inositol lipids in cell signalling. (1992) *Curr. Op. Cell Biol.* 4, 212-219.

Ishida A., Kitani T. and Fujisawa H. (1996) Evidence that autophosphorylation at Thr-286/Thr-287 is required for full activation of calmodulin-dependent protein kinase II. *Biochem. Biophys. Acta* 1311, 211-217.

Jacob R. (1990) Imaging cytoplasmic free calcium in histamine stimulated endothelial cells and in fMet-Leu-Phe simulated neutrophils. *Cell Calcium* 11, 241-249.

Jaffe L. (1983) Sources of calcium in egg activation: a review and hypothesis. *Dev. Biol.* 99, 265-276.

Jaffe L. (1993) Classes and mechanisms of calcium waves. *Cell Calcium* 14, 736-745.

Jellerette T., Kuraokawa M., Lee B., Malcuit C., Yoon S.Y., Smith J., Vermassen E., De Smedt H., Parys J. and Fissore R. (2004) Cell cycle-coupled Ca^{2+} oscillations in mouse zygotes and function of the inositol 1,4,5-trisphosphate receptor-1. *Dev. Biol.* 274, 94-109.

Jones K., Carroll J., Merriman J., Whittingham D. and Kono T. (1995) Repetitive sperm-induced Ca^{2+} transients in mouse oocytes are cell cycle dependent. *Development* 121, 3259-3266.

Jouaville L., Ichas F., Holmuhamedov E., Camacho P. and Lechleiter J. (1995) Synchronization of calcium wavess by mitochondrial substrates in *Xenopus* laevis oocytes. *Nature* 377, 438-441.

Jungermann K. and Kietzmann T. (1996) Zonation of parenchymal and non parenchymal metabolism in liver. *Annu. Rev. Nutr.* 16, 179-203.

Kaftan E., Ehrlich B., and Watras J. (1997) Inositol 1,4,5-trisphosphate ($InsP_3$) and calcium interact to increase the dynamic range of $InsP_3$ receptor-dependent calcium signaling. *J. Gen. Physiol.* 110: 529-538.

Kanaseki T., Ikeuchi Y.,Sugiura H. and Yamauchi T. (1991). Structural features of Ca^{2+}/calmodulin-dependent protein kinase II revealed by electron microscopy. *J. Cell Biol.* 115, 1049-1060.

Kasai H. and Augustine J. (1990) Cytosolic Ca^{2+} gradients triggering unidirectional fluid secretion from exocrine pancreas. *Nature* 348, 735-738.

Kasai H. and Petersen O.H. (1994) Spatial dynamics of second messengers: IP_3 and cAMP as long-range and associate messengers. *Trends Neurosci.* 17, 95-101.

Kargacin G. (1994) Calcium signaling in restricted diffusion spaces. *Biophys. J.* 67, 262-272.

Katayama E., Funahashi H., Michikawa T., Shiraishi T., Ikemoto T., Iino M. and Mikoshiba K. (1996) Native structure and arrangement of inositol 1,4,5-trisphosphate receptor molecules in bovine cerebellar Purkinje cells as studied by quick-freeze deepetch electron microscopy. *EMBO J.* 15, 4844-4851.

Kavanaugh W., Pot D., Chin S. *et al.* (1996) Multiple forms of an inositol polyphosphate 5-phosphatase form signaling complexes with Shc and Grb2. *Curr. Biol.* 6, 438-445.

Keizer, J. and De Young G. (1993). Effect of voltage-gated plasma membrane Ca^{2+} fluxes on IP_3-linked Ca^{2+} oscillations. *Cell Calcium* 14, 397-410.

Keener J. and Sneyd J. (1998) *Mathematical Physiology*. Springer-Verlag, New-York.

Khoo J.C. and Steinberg D. (1975). Stimulation of rat liver phosphorylase kinase by micromolar concentrations of Ca^{2+} *FEBS Lett.* 57, 68-72.

Klee C. and Vanaman T. (1982). Calmodulin. *Adv. Protein Chem.* 35, 213-321.

Kline D. and Kline J. (1992) Repetitive calcium transients and the role of calcium in exocytosis and cell cycle activation in the mouse egg. *Dev. Biol.* 149, 80-89.

Klingauf J. and Neher E. (1997) Modeling buffered Ca^{2+} diffusion near the membrane: implications for secretion in neuroendocrine cells. *Biophys. J.* 72, 674-690.

Kolodziej S.J., Hudmon A., Waxham M., and Stoops J. (2000). Three-dimensional reconstructions of calcium/calmodulin-dependent (CaM) kinase IIα and truncated CaM kinase IIα reveal a unique organization for its structural core and functional domains. *J. Biol. Chem.* 275, 14354-14359.

Kouchi Z., Fukami K., Shikano T., Oda S., Nakamura Y., Takenawa T. and Miyazaki S. (2004) Recombinant phospholipase C ζ has high Ca^{2+}-sensitivity and induces Ca^{2+} oscillations in mouse eggs. *J. Biol. Chem.* 279, 10408-10412.

Kraus-Friedmann N. and Feng L. (1996). The role of intracellular Ca^{2+} in the regulation of gluconeogenesis. *Metabolism* 45, 389-402.

Kuba K. and Takeshita S. (1981) Simulation of intracellular Ca^{2+} oscillations in a sympathetic neuron. *J. Theor. Biol.* 93, 1009-1031.

Kubiak J. (1989) Mouse oocytes gradually develop the capacity for activation during the metaphase II arrest. *Dev. Biol.* 136, 537-.545.

Kubiak J., Weber M., de Pennart H., Winston N. and Maro B. (1993) The metaphase II arrest in mouse oocytes is controlled through microtubule-dependent destruction of cyclin B in the presence of CSF. *EMBO J.* 12, 3773-3778.

Kubota Y. and Bower J. (2001) Transient versus asymptotic dynamics of CaM kinase II: possible roles of phosphatases. *J. Comput. Neuroscience* 11, 263-279.

Kummer, U., Olsen, L.F., Dixon, C.J., Green, A.K., Bornberg-Bauer, E. and Baier, G. (2000) Switching from simple to complex oscillations in calcium signaling. *Biophys. J.* 79, 1188-1195.

Kurokawa M., Sato K. and Fissore R. (2004) Mammalian fertilization: from sperm factor to phospholipase Cζ. *Biol. of the Cell* 96, 37-46.

Kushmerick M. and Podolsky R. (1969) Ionic mobility in muscle cells. *Science* 166, 1297-1298.

Kyozuka K., Deguchi R., Mohri T. and Miyazaki S. (1998) Injection of sperm extract mimics spatiotemporal dynamics of Ca^{2+} responses and progression of meiosis at fertilization of ascidian oocytes. *Development* 125, 4099-4105.

Laër L., Kloppstech M., Schöfl C., Sejnowski T., Brabant G. and Prank K. (2001) Noise enhanced hormonal signal transduction through intracellular calcium oscillations. *Biophys. Chem.* 91, 157-166.

Laxminarayan K., Matzaris M., Speed C., Mitchell C. (1993) Purification and characterization of a 43-kDa membrane-associated inositol polyphosphate 5-phosphatase from human placenta. *J. Biol. Chem.* 268, 4968-4974.

LeBeau A., Yule D., Groblewski G. and Sneyd J. (1999) Agonist-dependent phosphorylation of the inositol 1,4,5-trisphosphate receptor. *J. Gen. Physiol.* 113, 851-871.

Lechleiter J., Girard S., Peralta E. and Clapham D. (1991) Spiral calcium wave propagation and annihilation in *Xenopus laevis* oocytes. *Science* 252, 123-126.

Le Vine H., SahyouN.E., and Cuatrecasas P. (1986) Binding of calmodulin to the neuronal cytoskeletal protein kinase type II cooperatively stimulates autophosphorylation. *Proc. Natl. Acad. Sci. USA* 83, 2253-2257.

Lewis R. (2001) Calcium signaling mechanisms in T lymphocytes. *Annu. Rev. Immunol.* 19, 497-521.

Li G., Comte M., Wollheim C.and Cox A. (1989) Mode of activation of bovine brain inositol 1,4,5-trisphosphate 3-kinase by calmodulin and calcium. *Biochem. J.* 260, 771-775.

Lindqvist S., Sharp P., Johnson I., Satoh Y. and Williams MR. (1998) Acetylcholine-induced calcium signaling along the rat colonic crypt axis. *Gastroenterology* 115, 1131-1143.

Lisman J. and Zhabotinsky A. (2001). A model of synaptic memory: a CaMKII/PP1 switch that potentiates transmission by organizing an AMPA receptor anchoring assembly. *Neuron* 31, 191-201.

Lisman J., Schulman H. and Cline H. (2002). The molecular basis of CaMKII function in synaptic and behavioural memory. *Nat. Rev. Neurosci.* 3, 176-190.

Llinas R., Sugimori M. and Silver R. (1995) The concept of calcium concentration microdomains in synaptic transmission. *Neuropharmacology* 34, 1443-1451.

Llopis W.-H., Whitney M. ,Zlokarnik G. , and Tsien R. (1998) Cell-permeant caged $InsP_3$ ester shows that Ca^{2+} spike frequency can optimize gene expression. *Nature* 392, 936-941.

Loessberg-Stauffer P., Zhao H., Luby-Phelps K., Moss R., Star R. Muallem S. (1993) Gap-junction communication modulates $[Ca^{2+}]_i$ oscillations and enzyme secretion in pancreatic acini. *J. Biol. Chem.* 268, 19769-19775.

Lorca T., Abrieu A., Means A., Dorée M. (1994) Ca^{2+} is involved through type II calmodulin-dependent protein kinase in cyclin degradation and exit from metaphase. *Biochim. Biophys. Acta* 1223, 325-332.

Lorca T., Cruzalegui F., Fesquet D., Cavadore J., Méry J., Means A. and Dorée M. (1993) Calmodulin-dependent protein kinase II mediates inactivation of MPF and CSF upon fertilization of *Xenopus* eggs. *Nature* 366, 270-273.

McDougall A. and Sardet C. (1995) Function and characteristics of repetitive calcium waves associated with meiosis. *Current Biol.* 5, 318-328.

McDougall A., Levasseur M., O'Sullivan A. and Jones K. (2000) Cell cycle-dependent Ca^{2+} waves induced by a cytosolic sperm extract in mature ascidian oocytes mimic those observed at fertilization. *J. Cell Science* 113, 3453-3462.

Mailleux P., Takazawa K., Erneux C. and Vanderhaeghen J.-J. (1991) Inositol 1,4,5-trisphosphate 3-kinase distribution in the rat brain. High levels in the hippocampus CA1 pyramidal and cerebellar Purkinje cells suggest its involvement in some memory processes. *Brain Res.* 539, 203-210.

Mak D.-O., McBride S. and Foskett J.K. (1998) Inositol 1,4,5-trisphosphate activation of inositol trisphosphate receptor Ca^{2+} channel by ligand tuning Ca^{2+} inhibition. *Proc. Natl. Acad. Sci. USA* 95, 15821-15825.

Mak D.-O., McBride S., and Foskett J.K. (2001a) ATP regulation of recombinant type 3 inositol 1,4,5-trisphosphate receptor gating. *J. Gen. Physiol.* 117: 447-456.

Mak D.-O., McBride S., and Foskett J.K. (2001b) Regulation by Ca^{2+} and inositol 1,4,5-trisphosphate ($InsP_3$) of single recombinant type 3 $InsP_3$ receptor channels: Ca^{2+} activation uniquely distinguishes types 1 and 3 $InsP_3$ receptors . *J. Gen. Physiol.* 117: 447-456.

Malenka R. and Nicoll R. (1999) Long-term potentiation–a decade of progress ? *Science* 285, 1870-1874.

Malgaroli A. and Meldolesi J. (1991) $[Ca^{2+}]_i$ oscillations from internal stores sustain exocytic secretion from the chromaffin cells of the rat. *FEBS* 283, 169-172.

Marchant J., Callamaras N. and Parker I. (1999) Initiation of $InsP_3$-mediated Ca^{2+} waves in *Xenopus* oocytes. *EMBO J.* 18, 5285-5299.

Marhl M., Haberichter T., Brumen M. and Heinrich R. (2000) Complex Ca^{2+} oscillations and the role of mitochondria and cytosolic proteins. *Biosystems* 57, 75-86.

Marrero, I., A. Sanchez-Bueno, P.H. Cobbold and Dixon C. (1994) Taurolithocholate and thaurolithocholate 3-sulfate exert different effects on cytosolic free Ca^{2+} concentration in rat hepatocytes. *Biochem. J.* 300, 383-386.

Martiel J.-L. and Goldbeter A. (1987) A model based on receptor desensitization for cyclic AMP signaling in *Dictyostelium* cells. *Biophys. J.* 52, 807-828.

Meinke M., Bischop J. and Edstrom R. (1986) Zero-order ultrasensitivity in the regulation of glycogen phosphorylase. *Proc. Natl. Acad. Sci. U.S.A.* 83, 2865-2868.

Menniti F. and Putney J. (1990) Inositol 1,4,5-trisphosphate 3-kinase activity in high-speed supernatants from rat pancreatoma cells. *Biochem. J.* 274, 622-623.

Meyer T. and Stryer L. (1988) Molecular model for receptor-stimulated calcium spiking. *Proc. Natl. Acad. Sci. USA* 85, 5051-5055.

Meyer T., Holowka D. and Stryer L. (1988) Highly cooperative opening of calcium channels by inositol 1,4,5-trisphosphate. *Science* 240, 653-656.

Meyer T. and Stryer L. (1991) Calcium spiking *Annu. Rev. Biophysics Biophys. Chem.* 20, 153-174.

Meyer T., Hanson P., Stryer L., and Schulman H. (1992). Calmodulin trapping by calcium-calmodulin-dependent protein kinase. *Science* 256, 1199-1202.

Michelson S. and Schulman H. (1994). CaM kinase: a model for its activation dynamics. *J. Theor. Biol.* 171, 281-290.

Miller, S., and M. Kennedy. (1986). Regulation of brain type II Ca^{2+}/calmodulin-dependent protein kinase by autophosphorylation: a Ca^{2+}-triggered molecular switch. *Cell* 44: 861-870.

Mishra, J. and Bhalla, S. (2002) Simulations of inositol phosphate metabolism and its interaction with $InsP_3$-mediated calcium release. *Biophys. J.* 83, 1298-1316.

Missiaen L., Parys J., Sienaert I., Maes K., Kunzelmann K., Takahashi M., Tanzawa K. and De Smedt H. (1998) Functional properties of the type-3 $InsP_3$ receptor in 16HBE14o-bronchial mucosal cells. *J. Biol. Chem.* 273, 8983-8986.

Mitchell C., Connolly T., Majerus P. (1989) Identification and isolation of a 75-kDa inositol polyphosphate 5-phosphatase from human platelets. *J. Biol. Chem.* 264, 8873-8877.

Miyakawa T., Maeda A., Yamazawa T., Hirose K., Kurosaki T. and Iino M. (1999) Encoding of Ca^{2+} signals by differential expression of IP_3 receptor subtypes. *EMBO J.* 18, 1303-1308.

Miyakawa T., Mizushima A., Hirose K., Yamazawa T., Bezprozvanny I., Kurosaki T. and Iino M. (2001) Ca^{2+}-sensor region of $InsP_3$ receptor controls intracellular Ca^{2+} signaling. *EMBO J.* 20: 1674-1680.

Miyawaki A., Llopis J., Heim R., McCaffery J., Adams J., Ikura M. and Tsien R.Y. (1997) Fluorescent indicators for Ca^{2+} based on gree fluorescent proteins and calmodulin. *Nature* 388, 882-887.

Miyazaki S. (1988) Inositol 1,4,5-trisphosphate-induced calcium release and guanine nucleotide-binding protein-mediated periodic calcium rises in golden hamster eggs. *J. Cell Biol.* 106, 345-353.

Monck J., Robinson I., Escobar A., Vergara J. and Fernandez J. (1994) Pulsed laser imaging of rapid Ca^{2+} gradients in excitable cells. *Biophys. J.* 67, 505-514.

Montero M., Brini M., Marsault R., Alvarez J., Sitia R., Pozzan T. and Rizzuto R. (1995) Monitoring dynamic changes in free Ca^{2+} concentration in the endoplasmic reticulum of intact cells. *EMBO J.* 14, 5467-5475.

Montero M., Barrero M. and Alvarez J. (1997) Ca^{2+} microdomains control agonist-induced Ca^{2+} release in intact HeLa cells. *FASEB J.* 11, 881-885.

Moraru I., Kaftan E., Ehrlich B., and Watras J. 1999. Regulation of type 1 inositol 1,4,5-trisphosphate-gated calcium channels by $InsP_3$ and calcium. *J. Gen. Physiol.* 113, 837-849.

Morel J.-L., Fritz N., Lavie J.-L. and Mironneau J. (2003) Crucial role of type 2 inositol 1,4,5-trisphosphate receptors for acetylcholine-induced Ca^{2+} oscillations in vascular myocytes. *Arterioscler. Thromb. Vasc. Biol.* 23, 1567-1575.

Morin N., Abrieu A., Lorca T., Martin F. and Dorée M. (1994) The proteolysis-dependent metaphase to anaphase transition: calcium/calmodulin-dependent protein kinase II mediates onset of anaphase in extracts prepared from unfertilized *Xenopus* eggs. *EMBO J.* 13, 4343-4352.

Morita T., Tanimura A., Nezu A., Kurosaki T. and Tojyo Y. 2004. Functional analysis of the green fluorescent protein-tagged inositol 1,4,5-trisphosphate receptor type 3 in Ca^{2+} release and entry in DT40 B lymphocytes. *Biochem. J* : 382, 793-801.

Morris E.P. and Török K. (2001). Oligomeric structure of α-calmodulin-dependent protein kinase II. *J. Mol. Biol.* 308, 1-8.

Moses R. and Kline D. (1995) Calcium-independent, meiotic spindle-dependent metaphase-to-interphase transition in phorbol ester-treated mouse eggs. *Dev. Biol.* 171, 111-.122.

Motta P.M. (1988) *Biopathology of the liver. An ultrastructural approach.* (Motta, P.M. ed) Kluwer Academic Publishers, Dordrecht/Boston/London

Mukherji S., and Soderling T. (1994). Regulation of Ca^{2+}/calmodulin-dependent protein kinase II by inter- and intrasubunit-catalyzed autophosphorylation. *J. Biol. Chem.* 269, 13744-13747.

Murray J. (1989) *Mathematical Biology.* Springer, Berlin.

Murray A. and Hunt T. (1993) *The Cell Cycle: An Introduction.* Oxford University Press, Oxford.

Nadif Kasri N., Bultynck G., Smyth J., Szlufcik K., Parys J., Callewaert G., Missiaen L., Fissore R., Mikoshiba K. and De Smedt H. (2004) The N-terminal Ca^{2+}-independent calmodulin-binding site on the inositol 1,4,5-trisphosphate receptor is responsible for calmodulin inhibition, even though this inhibition requires Ca^{2+}. *Mol. Pharmacol.* 66, 276-284.

Naraghi M. and Neher E. (1997) Linearized buffered Ca^{2+} diffusion in microdomains and its implications for calculation of $[Ca^{2+}]$ at the mouth of a calcium channel. *J. Neurosci.* 17, 6961-6973.

Nash M., Young K., Challiss R., Nahorski S. (2001a) Single-cell imaging of graded $Ins(1,4,5)P_3$ production following G-protein-coupled-receptor activation. *Biochem. J.* 356: 137-142.

Nash M., Young K., Challiss R., Nahorski S. (2001b) Receptor-specific messenger oscillations. *Nature* 413: 381-382.

Nathanson M. and Burgstahler A. (1992) Coordination of hormone-induced calcium signals in isolated rat hepatocyte couplets. Demonstration with confocal microscopy. *Mol. Biol. Cell* 3, 113-121.

Nathanson M., Burgstahler A., Mennone A., Fallon M., Gonzalez C. and Saez J. (1995) Ca^{2+} waves are organized among hepatocytes in the intact organ. *Am. J. Physiol.* 32, G167-G171.

Nathanson MH and Schlosser SF. (1996) Calcium signaling mechanisms in liver in health and disease. *Prog. Liver Dis.* 14, 1-27.

Nedergaard M. (1994) Direct signaling from astrocytes to neurons in cultures of mammalian brain cells. *Science* 263, 1768-1771.

Neher E. (1986) Concentration profiles of intracellular calcium in the presence of a diffusible chelator. In : Heinemann U., Klee M., Neher E., Singer W. (eds) *Calcium Electrogenesis and Neuronal Functioning. Berlin* : Sringer, pp. 80-96.

Neher E. and Augustine G. (1992) Calcium gradients and buffers in bovine chromaffin cells. *J. Physiol. Lond.* 450, 273-301.

Neher E. (1995) The use of fura-2 for estimating Ca buffers and Ca fluxes. *Neuropharmacology* 34, 1423-1442.

Nicolis G. and Prigogine I. (1977) *Self-organization in Nonequilibrium Systems.* Wiley, New-York.

Okamoto H. and Ichikawa K. (2000). Switching characteristics of a model for biochemical-reaction networks describing autophosphorylation versus dephosphorylation of Ca^{2+}/calmodulin-dependent protein kinase II. *Biol. Cybern.* 82, 35-47.

Ozil J.-P. (1990) The parthenogenetic development of rabbit oocytes after repetitive pulsatile electrical stimulation. Development 109, 117-127.

Ozil J.-P. and Swann K. (1995) Stimulation of repetitive calcium transients in mouse eggs. *J. Physiol.* 483.2, 331-346.

Ozil J.-P. (1998) Role of calcium oscillations in mammalian egg activation : experimental approach. *Biophys. Chem.* 72, 141-152.

Parrington J., Swann K., Shevchenko V., Sesay A. and Lai F. (1996) Calcium oscillations in mammalian eggs triggered by a soluble sperm protein. *Nature* 379, 364-368.

Patterson R., Boehning D. and Snyder S. (2004) Inositol 1,4,5-trisphosphate receptors as signal integrators. *Annu. Rev. Biochem.* 73, 437-465.

Patton B., MilleS., and Kennedy M. (1990). Activation of type II calcium/calmodulin-dependent protein kinase by Ca^{2+}/calmodulin is inhibited by autophosphorylation of threonine within the calmodulin-binding domain. *J. Biol. Chem.* 265, 11204-11212.

Parker I., Choi J. and Yao Y. (1996) Elementary events of $InsP_3$-induced Ca^{2+} liberation in *Xenopus* oocytes: hot spots, puffs and blips. *Cell Calcium* 20, 105-121.

Parker I. and Yao Y. (1996) Ca^{2+} transients associated with openings of inositol trisphosphate-gated channels in *Xenopus* oocytes. *J. Physiol. Lond.* 491, 663-668.

Parys J. and Bezprozvanny I. (1995) The inositol trisphosphate receptor of *Xenopus* oocytes. *Cell Calcium* 18, 353-363.

Persechini A. and Stemmer P. (2002). Calmodulin is a limiting factor in the cell. *Trends Cardiovasc. Med.* 12, 32-37.

Petersen O.H. (2002). Calcium signal compartmentalization. *Biol. Res.* 35, 177-182.

Petrozzino J., Miller L. and Connor J. (1995) Micromolar Ca^{2+} transients in dendritic spines of hippocampal pyramidal neurons in brain slices. *Neuron* 14, 1223-1231.

Pipeleers D. (1987) The biosociology of pancreatic β cells. *Diabetologia* 30, 277-291.

Prank K., Laër L., von Zur Mühlen A., Brabant G. and Schöfl C. (1998). Decoding of intracellular calcium spikes train. *Europhys. Lett.* 42, 143-147.

Prigogine I. and Balescu R. (1956) Phénomènes cycliques dans la thermodynamique des processus irréversibles. *Bull. Cl. Sci. Acad. R. Belg.* XLII, 256-265.

Prigogine I., Lefever R., Goldbeter A. and Herschkowitz-Kaufman M. (1969) Symmetry-breaking instabilities in biological systems. *Nature* 223, 913-916.

Putney J., Takemura H., Hughes A., Horstman D. and Thastrup O. (1989) How do inositol phosphates regulate calcium signaling ? *FASEB J.* 3, 1899-1905.

Putney J., Broad L., Braun F., Lievremont J. and Bird G. (2001) Mechanisms of capacitative calcium entry. *J. Cell Science* 114, 2223-2229.

Raha S., Jones G. and Gear A. (1993) Sub-second oscillations of inositol 1,4,5-trisphosphate and inositol 1,3,4,5-tetrakisphosphate during platelet activation by ADP and thrombin: lack of correlation with calcium kinetics. *Biochem. J.* 292, 643-646.

Ramos-Franco J., Fill M., and Mignery G. (1998) Isoform-specific function of single inositol 1,4,5-trisphosphate receptor channels. *Biophys. J.* 75, 834-839.

Rapp P. and Berridge M.J. (1981) The control of transepithelial potential oscillations in the salivary gland of *Caliphora erythrocephala*. *J. Exp. Biol.* 93, 119-132.

Rapp P. E. (1987). Why are so many biological systems periodic ? *Progr. Neurobiol.* 29, 261-273.

Renard, D., J. Poggioli, B. Berthon, M. Claret. (1987) How far does phospholipase C depend on the cell calcium concentration ? *Biochem. J.* 243, 391-398.

Rhee S. and Choi K. (1992) Multiple forms of phospholipase C isozymes and their activation mechanisms. *Adv. Second Messenger Phosphoprotein Res.* 26, 35-61.

Rhee S.G. (2001) Regulation of phosphoinositide-specific phospholipase C. *Ann. Rev. of Biochemistry* 70, 281-312.

Rice A., Parrington J., Jones K. and Swann K. (2000) Mammalian sperm contain a Ca^{2+}-sensitive phospholipase C activity that can generate $InsP_3$ from PIP_2 associated with intracellular organelles. *Dev. Biol.* 228, 125-135.

Rich R.C., and Schulman H. (1998) Substrate-directed function of calmodulin in autophosphorylation of Ca^{2+}/calmodulin-dependent protein kinase II. *J. Biol. Chem.* 273, 28424-28429.

Richter J., Olsson I. and Anderson T. (1990) Correlation between spontaneous oscillations of cytosolic free Ca^{2+} and tumor necrosis factor-induced degranulation in adherent human neutrophils. *J. Biol. Chem.* 265, 14358-14363.

Rios E. and Stern M. (1997) Calcium in close quarters: microdomain feedback in excitation-contraction coupling and other cell biological phenomena. *Annu. Rev. Biophys. Biomol. Struct.* 26, 47-82.

Rizzuto R., Brini M., Murgia M. and Pozzan T. (1993) Microdomains with high Ca^{2+} close to IP_3-sensitive channels that are sensed by neighboring mitochondria. *Science* 262, 744-747.

Robb-Gaspers L. and Thomas A. (1995) Coordination of Ca^{2+} signaling by intercellular propagation of Ca^{2+} waves in the intact liver. *J. Biol. Chem.* 270, 8102-8107

Robb-Gaspers L., Rutter G., Burnett P., Hajnoczky G., Denton R. and Thomas A. (1998) Coupling between cytosolic and mitochondrial calcium oscillations: role in the regulation of hepatic metabolism. *Biochem. Biophys. Acta* 1366, 17-32.

Roegiers F., Djediat C., Dumollard R., Rouviere C. and Sardet C. (1999) Phases of cytoplasmic and cortical reorganizations of the ascidian zygote between fertilisation and first division. *Development* 126, 3101-3117.

Romond P.-C., Guilmot A. and Goldbeter A. (1994) The mitotic oscillator: temporal self-organization in a phosphorylation-dephosphorylation enzymatic cascade. *Ber. Bunsenges. Phys. Chem.* 98, 1152-1159.

Rongo, C. (2002) A fresh look at the role of CaMKII in hippocampal synaptic plasticity and memory. *BioEssays* 24: 223-233.

Rooney T., Renard D., Sass E. and Thomas A. (1991) Oscillatory cytosolic Ca^{2+} waves independent of stimulated inositol 1,4,5-trisphosphate formation in hepatocytes. *J. Biol. Chem.* 266, 12272-12282.

Rossier M., Capponi A., Vallotton M. (1987) Metabolism of inositol 1,4,5-trisphosphate in permeabilized rat aortic smooth muscle cells. *Biochem. J.* 145, 305-307.

Rorsman, P. and. Trube G. (1986). Calcium and delayed potassium currents in mouse pancreatic β-cells under voltage-clamp conditions. *J.Physiol. (London)* 374, 531-550.

Runft L. and Jaffe LA. (2000) Sperm extract injection into ascidian eggs signals Ca^{2+} release by the same pathway as fertilization. *Development* 127, 3227-3236.

Runft L., Jaffe L. and Mehlmann L. (2002) Egg activation at fertilization: where it all begins. *Dev. Biol.* 15, 237-254.

Russo G., Kyozuka K., Antonazzo L., Tostiand E. and Dale B. (1996) Maturation promoting factor in ascidian oocytes is regulated by different intracellular signals at meiosis I and II. *Development* 122, 1995-2003.

Sabatini, B.L., Maravall M. and K. Svoboda K.. (2001). Ca^{2+} signaling in dendritic spines *Curr. Opin. Neurobiol.* 11, 349-356.

Saez J., Connor J., Spray D. and Bennett M. (1989) Hepatocyte gap junctions are permeable to the second messenger, inositol 1,4,5-trisphosphate, and to calcium ions. *Proc. Natl. Acad. Sci. USA* 86, 2708-2712.

Sagata N., Watanabe N., Vanden Woude G. and Ikawa Y. (1989) The c-mos proto-oncogene product is a cytostatic factor responsible for meiotic arrest in vertebrate eggs. *Nature* 342, 512-518.

Sanderson M., Charles A., Boitano S. and Dirksen E. (1994) Mechanisms and function of intercellular calcium signaling. *Mol. Cell. Endocrinol.* 98, 173-187.

Sanderson M., Charles A., Dirksen E. (1995) Mechanical stimulation and intercellular communication increases intracellular Ca^{2+} in epithelial cells. *Cell Regulat.* 1, 585-596.

Sanderson M. (1996) Intercellular waves of communication. *News Physiol. Sci.* 11, 262-269.

Sardet C., Prodon F., Dumollard R., Chang P. and Chenevert J. (2002) Structure and function of the egg cortex from oogenesis through fertilization. *Dev. Biol.* 241, 1-23.

Saunders C., Larman M., Parrington J., Cox L., Royse J., Blaney L., Swann K. and Lai F. (2002) PLCζ: a sperm-specific trigger of oscillations in eggs and embryo development. *Development* 129, 3533-3544.

Schlosser S., Burgstahler A. and Nathanson M. (1996) Isolated rat hepatocytes can signal to other hepatocytes and bile duct cells by release of nucleotides. *Proc. Natl. Acad. Sci. USA* 93, 9948-9953.

Schulman H., Hanson P., and Meyer T. (1992) Decoding calcium signals by multifunctional CaM kinase. *Cell Calcium* 13, 401-411.

Schulman H. (1988) in : P .Greengard, G.A. Robison (Eds), *Advances in Second Messenger and Phosphoprotein Research*, Vol. 22, Raven Press, New York, p. 39.

Schuster, S., M. Marhl, and T. Höfer. (2002). Modelling of simple and complex calcium oscillations. *Eur. J. Biochem.* 269, 1333-1355.

Shears S. (1992) Metabolism of inositol phosphates. *Adv. in second messenger and phosphoprotein research* 26, 63-90.

Shen, P. and Larter R. (1995) Chaos in intracellular Ca^{2+} oscillations in a new model for non-excitable cells. *Cell Calcium.* 17, 225-232.

Sherman A., Keizer J. and Rinzel J. (1990) Domain model for Ca^{2+}-inactivation of Ca^{2+} channels at low channel density. *Biophys. J.* 58, 985-995.

Sims C., Allbritton N. (1998) Metabolism of inositol 1,4,5-trisphosphate and inositol 1,3,4,5-tetrakisphosphate by the oocytes of *Xenopus laevis*. *J. Biol. Chem.* 273, 4052-4058.

Singla S.I., Hudmon A., Goldberg J., Smith J. and Schulman H. (2001). Molecular characterization of calmodulin trapping by calcium/calmodulin-dependent protein kinase II. *J. Biol. Chem.* 276, 29353-29360.

Smith G., Wagner J. and Keizer J. (1996) Validity of the rapid buffering approximation near a point source of calcium ions. *Biophys. J.* 70, 2527-2539.

Sneyd J., Keizer J.and Sanderson M. (1995a). Mechanisms of calcium oscillations and waves: a quantitative analysis. *FASEB J.* 9, 1463-1472.

Sneyd J., Wetton B., Charles A., Sanderson M. (1995b) Intercellular calcium waves mediated by diffusion of inositol trisphosphate : a two-dimensional model. *Am. J. Phy.* 268, C1537-C1545.

Sneyd J., Wilkins M., Strahonja A., Sanderson M. (1998) Calcium waves and oscillations driven by an intercellular gradient of inositol (1,4,5)-trisphosphate. *Biophys. Chem.* 72, 101-109.

Sneyd J. and Dufour J.-F. (2002) A dynamic model of the type-2 inositol trisphosphate receptor. *Proc. Natl. Acad. Sci. USA* 19, 2398-2403.

Snow P., Yim D., Leibow J., Sainiand S. and Nuccitelli R. (1996) Fertilization stimulates an increase in inositol trisphosphate and inositol lipid levels in *Xenopus* eggs. *Dev. Biol.* 180, 108-118.

Soderling T., Chang B. and Brickey D. (2001) Cellular signaling through multifunctional Ca^{2+}/calmodulin -dependent protein kinase II. *J. Biol. Chem.* 276, 3719-3722.

Speed C., Little P., Hayman J. and Mitchell C. (1996) Underexpression of the 43 kDa inositol polyphosphate 5-phosphatase is associated with cellular transformation. *EMBO J.* 15, 4852-4861.

Speksnijder J., Corson D. and Jaffe L. (1989) Free calcium pulses following fertilization in the ascidian egg. *Dev. Biol.* 135, 182-190.

Spray D.C., Bai S., Burk R.D. and Saez, J.C. (1994) Regulation and function of liver gap junctions and their genes. *Prog Liver Dis.* 12, 1-18.

Stalmans W., Bollen M. and Mvumbi L. (1987). Control of glycogen synthesis in health and disease. *Diabetes/Metab. Rev.* 3, 127-161.

Stern M.D. (1992) Buffering of calcium in the vicinity of a channel pore. *Cell Calcium* 13, 183-192.

Stern M., Pizarro G. and Rios. (1997) Local control model of exciatation-contraction coupling in

skeletal muscle. *J. Gen. Physiol.* 110, 415-440.

Strausfeld U., Labbé J., Fesquet D., Cavadore J., Picard A., Sadhu K., Russell P. and Dorée M. (1991) Dephosphorylation and activation of a p34cdc2/cyclin B complex in vitro by human CDC25 protein. *Nature* 351, 242-245.

Stricker S. (1999) Comparative biology of calcium signalling during fertilization and egg activation in animals. *Dev. Biol.* 211, 157-176.

Strizhak, P., I.S. Magura, K.B. Yatsimirskii and Masyuk, A.I.. (1995) Return map approach to description of the deterministic chaos in cytosolic calcium oscillations. *J. Biol. Phys.* 21, 233-239.

Sugawara H., Kurosaki M., Takata M. and Kurosaki T. (1997) Genetic evidence for involvement of type 1, type 2 and type 3 inositol 1,4,5-trisphosphate receptors in signal transduction through the B-cell antigen receptor. *EMBO J.* 16, 3078-3088.

Sun X., Callamaras N., Marchant J. and Parker I. (1998) A continuum of $InsP_3$-mediated elementary Ca^{2+} signalling events in *Xenopus* oocytes. *J. Physiol.* 509, 67-80.

Swann K. and Ozil J.-P. (1994) Dynamics of the calcium signal that triggers mammalian egg activation *Int. Rev. Cytol.* 152, 183-222.

Swann K. (1996) Soluble sperm factors and Ca^{2+} release in eggs at fertilization. *Rev. Reprod.* 1, 33-39.

Swann K. and Parrington J. (1999) Mechanism of Ca^{2+} release at fertilization in mammals. *J. Exp. Zool.* 15, 267-75.

Swann K., Parrington J. and Jones K. (2001) Potential role of a sperm-derived phospholipase C in triggering the egg-activating Ca^{2+} signal at fertilization. *Reproduction* 122, 839-847.

Swanson C., Arkin A. and Ross J. (1997) An endogenous calcium oscillator may control early embryonic division. *Proc. Natl. Acad. Sci. USA* 94, 1194-1199.

Swatton J., Morris S., Cardy T. and Taylor C. (1999) Type 3 inositol trisphosphate receptors in RINm5F cells are biphasically regulated by cytosolic Ca^{2+} and mediate quantal Ca^{2+} mobilization. *Biochem. J.* 344, 55-60.

Swillens S., Combettes L. and Champeil P. (1994) Transient inositol 1,4,5-trisphosphate-induced Ca^{2+} release : a model based on regulatory Ca^{2+} binding sites along the permeation pathway. *Proc. Natl. Acad. Sci. USA* 91, 10074-10078.

Swillens S., Champeil P., Combettes L. and Dupont G. (1998) Stochastic simulation of a single inositol 1,4,5-trisphosphate-sensitive Ca^{2+} channel reveals repetitive openings during 'blip-like' Ca^{2+} transients. *Cell Calcium* 23, 291-302.

Swillens S., Dupont G., Combettes L. and Champeil P. (1999) From calcium blips to calcium puffs: theoretical analysis of the requirements for interchannel communication. *Proc. Natl. Acad. Sci. USA* 96, 13750-13755.

Takazawa K., Passareiro H., Dumont J., Erneux C. (1988) Ca^{2+}/calmodulin-sensitive inositol 1,4,5-trisphosphate 3-kinase in rat and bovine brain tissues. *Biochem. Biophys. Res. Commun.* 153, 632-641.

Takazawa K., Passareiro H., Dumont J., Erneux C. (1989) Purification of bovine brain inositol 1,4,5-trisphosphate 3-kinase isoenzyme. *Biochem. J.* 278, 883-886.

Takazawa K., Vandekerckhove J., Dumont J.E., Erneux C. (1990a) Cloning and expression in *Escherichia coli* of a rat brain cDNA encoding a Ca^{2+}/calmodulin-sensitive inositol 1,4,5-trisphosphate 3-kinase. *Biochem. J.* 272, 107-112.

Takazawa K., Lemos M., Delvaux A., Lejeune C., Dumont J.E., Erneux C. (1990b) Rat brain inositol 1,4,5-trisphosphate 3-kinase. Ca^{2+}-sensitivity, purification and antibody production. *Biochem. J.* 268: 213-217.

Takazawa K., Perret J., Dumont J., Erneux C. (1991a) Molecular cloning and expression of a human brain inositol 1,4,5-trisphosphate 3-kinase. *Biochem. Biophys. Res. Commun.* 174, 529-535.

Takazawa K., Perret J., Dumont J., Erneux C. (1991b) Molecular cloning and expression of a new putative inositol 1,4,5-trisphosphate 3-kinase. *Biochem. J.* 261, 483-488.

Tang Y. and H. Othmer H. (1995). Frequency encoding in excitable systems with applications to calcium oscillations. *Proc. Natl. Acad. Sci.* USA 92, 7869-7873.

Tang, Y., J.L. Stephenson and Othmer H.G. (1996) Simplification and analysis of models of calcium dynamics based on IP_3-sensitive calcium channel kinetics. *Biophys. J.* 70, 246-263.

Tanimura A. and Turner R. (1996) Calcium release in HSY cell conforms to a steady-state mechanism involving regulation of the inositol 1,4,5-trisphosphate receptor Ca^{2+} channel by luminal [Ca^{2+}]. *J. Cell Biol.* 132, 607-616.

Taylor C. (1998) Inositol trisphosphate receptors : Ca^{2+} modulated intracellular Ca^{2+} channels. *Biochim. Biophys. Acta* 1436, 19-33.

Taylor C., Genazzani A., and Morris S. (1999) Expression of inositol trisphosphate receptors. *Cell Calcium* 26, 237-251.

Taylor C. and Thorn P. (2001) Calcium signalling: IP_3 rises again...and again. *Curr. Biol.* 11, R352-R355.

Taylor C. and Laude A. (2002) $InsP_3$ receptors and their regulation by calmodulin and cytosolic Ca^{2+}. *Cell Calcium* 32, 321-334.

Tesarik J. (1994) Calcium in oocyte maturation. How the spermatozoon awakens the oocyte: lessons from intracytoplasmic sperm injection. Hum. Reprod. 9, 977-.978.

Thomas A. , Bird G, Hajnoczky G., Robb-Gaspers L. and Putney J. W. (1996). Spatial and temporal aspects of cellular calcium signalling. *FASEB J.* 10, 1505-1517.

Thomas D., Lipp P., Berridge M.J. and Bootman M. (1998) Hormone-evoked elementary Ca^{2+} signals are not stereotypic, but reflect activation of different size channel clusters and variable recruitment of channels within a cluster. *J. Biol. Chem.* 273, 27130-27136.

Thomas S., Brake B., Luzio J., Stanley K. and Banting G. (1994) Isolation and sequence of a full length cDNA encoding a novel rat inositol 1,4,5-trisphosphate 3-kinase. *Biochim. Biophys. Acta* 1220, 219-222.

Tordjmann T, Berthon B, Claret M. and Combettes L. (1997) Coordinated intercellular calcium waves induced by noradrenaline in rat hepatocytes: dual control by gap junctions and agonist. *EMBO J.* 16, 5398-5407.

Tordjmann T, Berthon B, Jaquemin E, Clair C, Stelly N, Guillon G, Claret M. and Combettes L. (1998) Receptor-oriented intercellular calcium waves mediated by a gradient in sensitivity to vasopressin in rat hepatocytes. *EMBO J.* 17, 4695-4703.

Tordjmann T., Clair C., Claret M. and Combettes L. (2000) Intercellular Calcium Signaling In "Non-Excitable" Cells. *In : Calcium: The Molecular Basis of Calcium Action in Biology and Medicine (Pochet, R., Donato, R., Haiech, J., Heizmann, C. and Gerke, V., Eds)* pp. 219-232, Kluwer. The Netherlands.

Tyson J. (1991) Modeling the cell division cycle: cdc2 and cyclin interactions. *Proc. Natl. Acad. Sci. USA* 88, 7328-7332.

Vandenheede J., Keppens S. and De Wulf H. (1977) Inactivation and reactivation of liver phopshorylase b kinase. *Biochim. Biophys. Acta* 481, 463-470.

Vanweyenberg V., Communi D., D'Santos C. and Erneux C. (1995) Tissue- and cell-specific expression of Ins(1,4,5)P_3 3-kinase isoenzymes. *Biochem. J.* 306, 429-435.

Venance L., Stella N., Glowinski J., Giaume C. (1997) Mechanism involved in initiation and propagation of receptor-induced intercellular calcium signaling in cultured rat astrocytes. *J. Neurosci.* 17, 1981-1992.

Verjans B., Lecocq R., Moreau C., Erneux C. (1992) Purification of bovine brain inositol 1,4,5-trisphosphate 5-phosphatase. *Eur. J. Biochem.* 204, 1083-1087.

Verjans B., De Smedt F., Lecocq R., Vanweyenberg V., Moreau C. and Erneux C. (1994a) Cloning and expression in *Escherichia coli* of a dog thyroid cDNA encoding a novel inositol 1,4,5-trisphosphate 5-phosphatase. *Biochem. J.* 300, 85-90.

Verjans B., Moreau C. and Erneux C. (1994b) The control of intracellular signal molecules at the level of their hydrolysis: the example of inositol 1,4,5-trisphosphate 5-phosphatase. *Mol. Cell. Endocrinol.* 98, 167-171.

Verkhratsky A. (2002). The endoplasmic reticulum and neuronal calcium signalling. *Cell Calcium* 32, 393-404.

Verlhac M.-H., Kubiak J., Clarke H. and Maro B. (1994) Microtubule and chromatin behavior follow MAP kinase activity but not MPF activity during meiosis in mouse oocytes. *Development* 120, 1017-1025.

Verlhac M.-H., Kubiak J., Weber M., Géraud G., Colledge W., Evans M. and Maro B. (1996) Mos is required for MAP kinase activation and is involved in microtubule organization during meiotic maturation in the mouse. *Development* 122, 815-822.

Vermassen E., Parys J.B., and Mauger J.-P. (2004) Subcellular distribution of the inositol 1,4,5-trisphosphate receptors : functional relevance and molecular determinants. *Biol. of the Cell* 96, 3-18.

Vincent C., Cheek T. and Johnson M. (1992) Cell cycle progression of parthenogenetically activated mouse oocytes to interphase is dependent on the level of internal calcium. *J. Cell Sci.* 103, 389-396.

Vitullo A. and Ozil J.-P. (1992) Repetitive calcium stimuli drive meiotic resumption and pronuclear development during mouse oocyte activation. *Dev. Biol.* 151, 128-136.

Wagner J., Li Y.-X., Pearson J. and Keizer J. (1998) Simulation of the fertilization Ca^{2+} wave in *Xenopus laevis* eggs. *Biophys. J.* 75, 2088-2097.

Wakui M., Osipchuk Y., Petersen O. (1990) Receptor-activated cytoplasmic Ca^{2+} spiking mediated by inositol trisphosphate is due to Ca^{2+}-induced Ca^{2+} release. *Cell* 63, 1025-1032.

Watanabe N., Hunt T., Ikawa Y. and Sagata N. (1991) Independent inactivation of MPF and cytostatic factor (Mos) upon fertilization of *Xenopus* eggs. *Nature* 352, 247-248.

Watras J., Bezprozvanny I. and Ehrlich B. (1991) Inositol 1,4,5-trisphosphate-gated channels in cerebellum: presence of multiple conductance states. *J. Neurosci.* 11, 3239-3245.

Whitaker M. and Patel R. (1990) Calcium and cell cycle control. *Development* 108, 525-542.

Wiesner T., Berk B. and Nerem R. (1996) A mathematical model of cytosolic calcium dynamics in human umbilical vein endothelial cells. *Am. J. Physiol.* 270, C1556-C1569.

Wilcox R., Nahorski R. (1994) Does Ins(1,3,4,5)P_4 play a role in Ca^{2+} signaling? *In: Signal-activated phospholipases. Ed: Liscovitch M.* p.189-212.

Wilkins M. and Sneyd J. (1998) Intercellular spiral waves of calcium. *J. Theor. Biol.* 191, 299-308.

Winston N., McGuinness O., Johnson M. and Maro B. (1995) The exit of mouse oocytes from meiotic M-phase requires an intact spindle during intracellular calcium release. *J. Cell Science* 108, 143-151.

Wojcikiewicz R.J.H. (1995) Type I, II, and III inositol 1,4,5-trisphosphate receptors are unequally susceptible to down-regulation and are expressed in markedly different proportions in different cell types. *J. Biol. Chem.* 270, 11678-11683.

Wojcikiewicz R. and Luo S. (1998) Differences among type I, II, and III inositol-1,4,5-trisphosphate receptors in ligand-binding affinity influence the sensitivity of calcium stores to inositol-1,4,5-trisphosphate. *Mol. Pharmacol.* 53, 656-662.

Woods N. M., Cuthbertson K. S. R. and Cobbold P. H. (1986). Repetitive transient rises in cytoplasmic free calcium in hormone-stimulated hepatocytes. *Nature* 319, 600-602.

Woods, N.M., Cuthbertson, K.S. and Cobbold, P.H. (1987) Phorbol-ester-induced alterations of free calcium ion transients in single rat hepatocytes. *Biochem J.* 246, 619-623.

Worley P., Baraban J., Supattapone S., Wilson V. and Snyder S. (1987) Characterization of inositol trisphosphate receptor binding in brain. *J. Biol. Chem.* 262, 12132-12136.

Xu Z., Lefevre L., Ducibella T., Schultz R. and Kopf G. (1996) Effects of calcium-BAPTA buffers and the calmodulin antagonist W-7 on mouse egg activation. *Dev. Biol.* 180, 594-604.

Xu C., Watras J. and Loew L. (2003) Kinetic analysis of receptor-activated phosphoinositide turnover. *J Cell Biol.* 161, 779-791.

Yao Y., Choi J. and Parker I. (1995) Quantal puffs of intracellular Ca^{2+} evoked by inositol trisphosphate in *Xenopus* oocytes *J. Physiol.* 482, 533-553.

Yule D., Stuenkel E. and Williams J. (1996) Intercellular calcium waves in rat pancreatic acini : mechanism of transmission. *Am. J. Physiol.* 271, C1285-1294.

Yule D., Straub S., and Bruce J. (2003) Modulation of Ca^{2+} oscillations by phosphorylation of $Ins(1,4,5)P_3$ receptors. *Biochem. Soc. Trans.* 31, 954-957.

Zhao M., Hollingworth S. and Baylor S. (1996) Properties of tri- and tetracarboxylate Ca^{2+} indicators in frog skeletal muscle fibers. *Biophys. J.* 70, 896-916.

Zhou Z. and Neher E. (1993) Mobile and immobile calcium buffers in bovine adrenal chromaffin cells. *J. Physiol. Lond.* 469, 245-273.

Zilberman Y., Howe L., Moore J., Hesketh T., Metcalfe J. (1987) Calcium regulates inositol 1,3,4,5-tetrakisphosphate production in lysed thymocytes and in intact cells stimulated with concanavalin A. *EMBO J.* 6, 957-962.